UC Davis

Title

Spectroscopic Signatures, Structural Data, and Reactivity of Divalent Group 14 Complexes Bonded to Metal Fragments

Permalink

https://escholarship.org/uc/item/1gq4r99f

Author

Phung, Alice Chi

Publication Date

2023

Peer reviewed|Thesis/dissertation

Spectroscopic Signatures, Structural Data, and Reactivity of Divalent Group 14 Complexes
Bonded to Metal Fragments

By

ALICE CHI PHUNG
DISSERTATION

Submitted in partial satisfaction of the requirements for the degree of

DOCTOR OF PHILOSOPHY

in

CHEMISTRY

in the

OFFICE OF GRADUATE STUDIES

of the

UNIVERSITY OF CALIFORNIA

DAVIS

Approved:

_____

PHILIP P. POWER

_____

LOUISE A. BERBEN

_____

MARIE C. HEFFERN

Committee in Charge

2023

Table of Contents

Acknowledgements

This PhD was not a solo effort, and so there are many individuals I must express my gratitude for.

Chief recognition must be given to Prof. Philip P. Power, without whom this thesis would not exist. The hours and resources required to complete this work were only possible because I was permitted to be in your lab and given the space to learn, make mistakes, and pursue my ideas.

Thanks are extended to my thesis committee members, Profs Louise A. Berben and Marie C. Heffern. To Prof. Berben, thank you for your part in my graduate studies milestones (Qualifying Exam, Third Year Seminar, and this thesis). To Prof. Heffern, thank you for your counsel and insight provided over the years.

Sincere acknowledgements are also dedicated to the steadfast presences during my time in graduate school:

My parents, Công Phùng and Trang Võ: cám ơn ba má vì sự ủng hộ và sự bình tĩnh mỗi lần con gọi thâm. Có lần con nói việc khó quá, thì ba má đã nói con có thể bỏ học và trở về được. Con đã biết con quá bướng bỉnh để bỏ học và cũng biết đó không phải là gì ai muốn, mà nghe ba má ủng hộ sự hạnh phúc của con đã giúp con vượt qua những thời kỳ khó khăn.

My brother, Lạc Phùng, and et. al, Eric Esparos and George Preno: thank you for your companionship and voice of reason.

Annie Tjahyadi (née Chapman): while I was writing this, you called me in tepid distress because you had spilled matcha tea on your pink dress, which I think aptly describes your role in my graduate journey and why I am thanking you now. Wir haben vielen Mal gescherzt, dass dieser Abschluss auch dir gehört.

Prof. Alexander M. Spokoyny: thank you for jumpstarting my journey in academia and your continued mentorship and support.

Drs. Kent Kirlikovali, Rafal Dziedzic, Alejandra Gonzalez, and Vinh Nguyen: thank you for answering my calls during odd hours, regardless of time zone, to answer questions I had about my chemistry. Additional thanks are extended to Kent and Rafal, for proof-reading my papers in winter 2022 and 2023.

Given the unique time period in which it took to complete this degree, the remainder of my acknowledgements are split before and after 2020.

Before 2020:
Power group members: Cary Stennett, Joshua Queen, Clifton Wagner, Robert Tureski, Vincent Wang, David Liptrot, Jade Pratt, Kelly Gullett, Skyler Osler, Thien Nguyen, Ella Schwirzke, and Beate Steller,
My friends: Chris Knell, Lucy Luong, and Nathan Phan,
all of whom helped me navigate the early days of graduate school and gave me reasons to stay in the program those first 4 years.

After 2020:
Power group members: Qihao Zhu, Wenxing Zou, and Connor McLoughlin,
My weekend crew: Sam Hartanto and Kevin Lee,
My friends: Ngan Ko (née Pham), Laarni Peralta, and Elizabeth Balderrama (née Lee),
My partner, Tyler Nguyen,
who all endured with me the strangeness of the COVID pandemic and inspired me to see this degree to the end.

Spectroscopic Signatures, Structural Data, and Reactivity of Divalent Group 14 Complexes Bonded to Metal Fragments

ABSTRACT: This dissertation focuses on the synthesis and characterization of ferriotetrylenes, which are complexes featuring a two-coordinate E(II) (E = Ge, Sn, or Pb) σ-bonded to $FeCp(CO)_2$ (Cp = η^5-C_5H_5) and a terphenyl group. The reactivity of the ferriotrylenes with ammonia is also described. Additionally, the synthesis and characterization of the biscarboranyl complexes (**bc**)Sn·THF, [(**bc**)Sn]₂KCl, and **bc**-CH=CH-**bc** (**bc** = 1,1′-bis(o-carborane) are also described. Single crystal X-ray crystallography was employed to establish the structural details of the solid-state structures. NMR spectroscopic studies (^{1}H, ^{11}B, ^{13}C, ^{119}Sn, ^{207}Pb) were employed for the spectroscopic characterization of the novel complexes and the characterization of the products of their reactions with ammonia. Spectroscopic methods were also used to determine the energetics of the reversible reaction with ammonia. New compounds were additionally characterized by UV-visible and infrared spectroscopy.

The ferriogermylene $Ar^{Me6}GeFeCp(CO)_2$ (Ar^{Me6} = −C_6H_3-(C_6H_2-2,4,6-CH_3)₂) was synthesized by salt metathesis of the terphenyl germanium chloride ($Ar^{Me6}GeCl$) with the potassium salt of the iron cyclopentadienyl dicarbonyl anion (K[$FeCp(CO)_2$]). In the solid state, $Ar^{Me6}GeFeCp(CO)_2$ can form one of three crystalline polymorphs in green, red, or dichroic red-green crystals. Regardless of polymorph, $Ar^{Me6}GeFeCp(CO)_2$ is spectroscopically and structurally similar to its more substituted derivative $Ar^{iPr4}GeFeCp(CO)_2$ (Ar^{iPr4} = −C_6H_3-(C_6H_3-2,6-iPr)₂). Additionally, it was shown to react with H_2O to afford the oxidative addition product $Ar^{Me6}Ge(OH)(H)FeCp(CO)_2$. The complexes $ArGeFeCp(CO)_2$ (Ar = Ar^{Me6} or Ar^{iPr4}) were shown to react with ammonia to afford the insertion products $ArGe(NH_2)(H)FeCp(CO)_2$ (Ar = Ar^{Me6} or Ar^{iPr4}).

ABSTRACT

Salt metathesis was also employed in the synthesis of the two tin derivatives $Ar^{Me6}SnFeCp(CO)_2$ and $Ar^{Me6}SnFeCp*(CO)_2$ ($Cp*$ = η^5-C_5Me_5). The compound $Ar^{Me6}SnFeCp(CO)(PMe_3)$ was produced through a phosphine-carbonyl exchange reaction. Spectroscopic and structural comparisons of these ferriostannylenes and the more substituted derivatives $ArSnFeCp(CO)_2$ (Ar = Ar^{iPr4} or Ar^{iPr6}) showed the effect of the substituents on the central Sn atom. Increasing the size of the alkyl substituents on the aryl groups (aryl = terphenyl or cyclopentadienyl) narrows the interligand angle at Sn and causes a corresponding bathochromic shift of the HOMO→LUMO transition in the UV-vis spectra. Changing a CO ligand on the Fe fragment to PMe_3 widens the interligand angle at Sn while causing a bathochromic shift of the HOMO→LUMO transition in the UV-vis spectrum.

The ferriostannylenes $ArSnFeCp(CO)_2$ (Ar = Ar^{Me6} or Ar^{iPr4}) were observed to react reversibly with ammonia. Visually, the reactions followed a similar color pattern to the reaction of the ferriogermylenes $ArGeFeCp(CO)_2$ (Ar = Ar^{Me6} or Ar^{iPr4}) with ammonia. Variable temperature ^{1}H NMR studies determined that the free energy of the reversible reaction of $Ar^{iPr4}SnFeCp(CO)_2$ with ammonia was essentially thermoneutral and are in good agreement with DFT calculations made by the Goicoechea research group on a phosphine system that displayed a related thermoneutral, reversible activation of ammonia. The ferrioplumbylenes $ArPbFeCp(CO)_2$ (Ar = Ar^{Me6} or Ar^{iPr4}) were synthesized in the same manner as the Ge and Sn congeners to complete the series. Spectroscopic and structural comparisons of the $ArEFeCp(CO)_2$ (E = Ge, Sn, or Pb; Ar = Ar^{Me6} or Ar^{iPr4}) series revealed a pattern that is reflected in the ferriotetrylene reactivities towards ammonia. The compound $Ar^{Me6}PbFeCp(CO)_2$ was inert in the presence of ammonia.

General Introduction

CHAPTER 1: General Introduction

The heavy group 14 carbene analogues :ER_2 (E = Si, Ge, Sn, Pb; R = alkyl, aryl, silyl, amido, alkoxo, thiolato, etc.) are of considerable importance in fundamental and applied chemistry.[1–3] Their syntheses, structures, and reactivity have been well studied.[1–4] The isolable tetrylenes feature a non-bonded lone pair and an empty *p*-orbital at the tetrel atom that can engage in synergistic reactions that can react with important small molecules such as H_2, NH_3, C_2H_4, CO, etc (**Figure 1**).[4,5] However, little attention has been given to the reactions of divalent tetrylenes that have a direct bond between the low valent group 14 element and a transition metal.
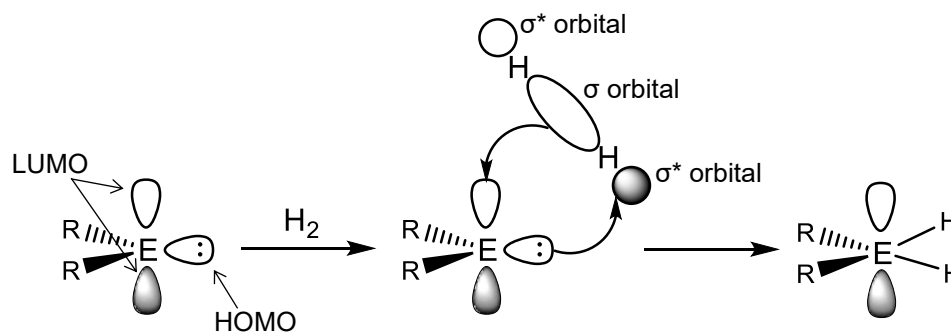
E = Ge, Sn, or Pb
R = alkyl, aryl, silyl, amido, alkoxo, thiolato, etc.[1,4,5]

Figure 1. Synergistic reactivity of tetrylene species as donor and acceptor, exhibiting transition metal-like behavior such as reacting with small molecules like H_2.[4–6]

The first report of metallotetrylenes, named for the bond between the transition metal and unsaturated tetrel atom, were the ferriogermylenes Mes*GeFe(CO)$_2$R (Mes* = –C_6H_2-2,4,6-^{t}Bu$_3$; R = Cp (η^5-C_5H_5) or Cp* (η^5-C_5Me_5)), synthesized in 1994 by Jutzi and Leue.[7] However, structural

characterization of these ferriogermylenes were not obtained. The first stable metallotetrylenes were isolated by Power and coworkers in 1996 and structurally characterized via X-ray crystallography.[8] The metallogermylenes,[8,9] metallostannylenes,[10] and metalloplumbylenes[11] synthesized soon thereafter were altogether found to have a relatively wide angle at the tetrel atom. The bent geometry is characteristic of the presence of a non-bonding lone pair at the tetrel atom.[4,5]

Since then, numerous other metallotetrylenes have been reported. The majority are derivatives of germanium or tin,[12–22] while metallosilylenes[23–26] and metalloplumbylenes[27–29] remain scarce. All these compounds are stabilized sterically via the use of a bulky ligand at the group 14 atom or by Lewis bases coordinating to E. Despite the growing library of characterized metallotetrylenes, their reactivity has received less attention. In contrast, there is ample precedent for transition metal-like reactivity by a heavy group 14 atom in other divalent species. The first such example was presented in 2005 by Power and coworkers with the activation of H_2 by the digermyne $Ar^{iPr4}Ge{\equiv}Ge\ Ar^{iPr4}$ ($Ar^{iPr4} = -C_6H_3\text{-}(C_6H_3\text{-}2,6\text{-}iPr)_2$).[30] Since then, other systems containing germanium or tin have been shown to react with small molecules such as H_2, NH_3, and CO under mild conditions.[31–37] Tetrylenes and metallotetrylenes differ only in the transition metal fragment in place of one of the stabilizing ligands, thereby sharing similar frontier orbitals on the central atom (**Figure 2a**). Thus, metallotetrylenes can be expected to also demonstrate transition metal-like behavior towards small molecules (**Figure 2b**).
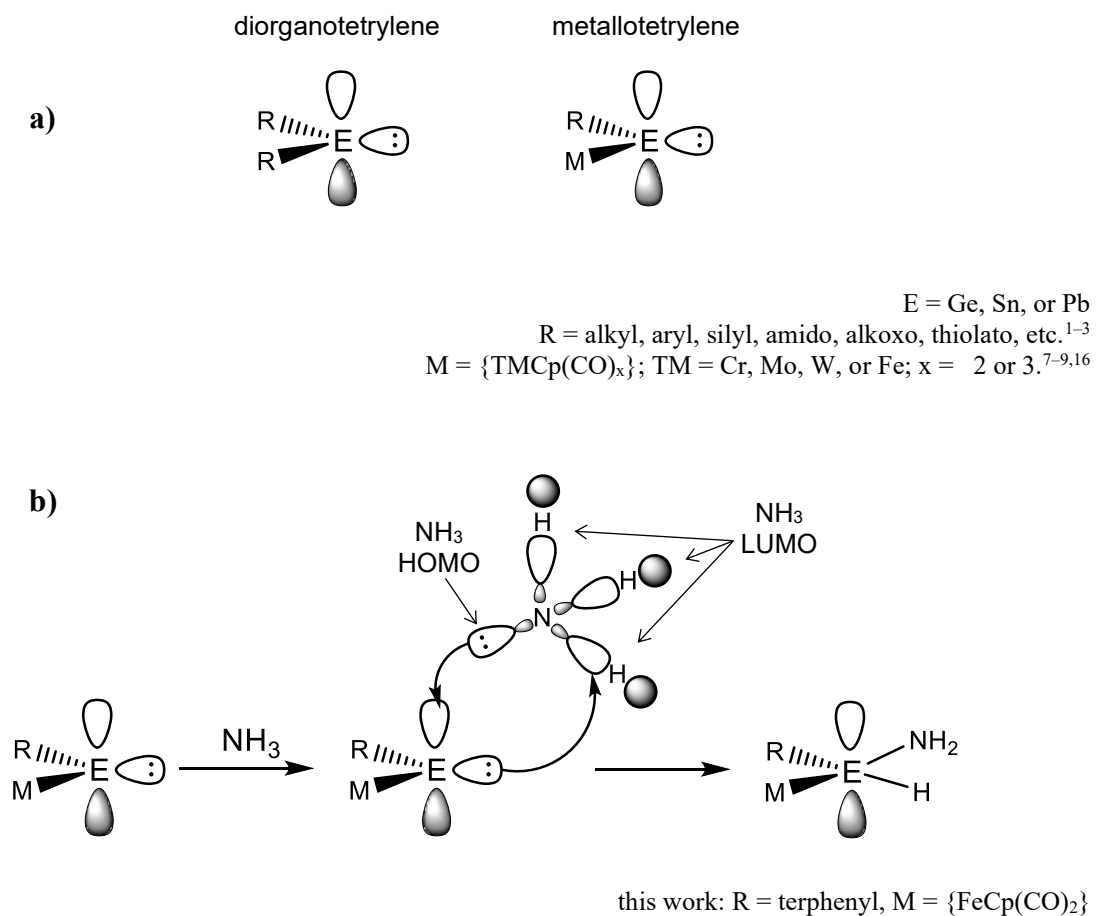
diorganotetrylene   metallotetrylene

a)

E = Ge, Sn, or Pb
R = alkyl, aryl, silyl, amido, alkoxo, thiolato, etc.[1–3]
M = {TMCp(CO)$_x$}; TM = Cr, Mo, W, or Fe; x = 2 or 3.[7–9,16]

b)

NH$_3$
HOMO

NH$_3$
LUMO

NH$_3$

this work: R = terphenyl, M = {FeCp(CO)$_2$}

Figure 2. **a)** Tetrylenes and metallotetrylenes have a bent geometry at the central tetrel atom, indicating a non-bonded lone pair and empty p-orbital operating as the HOMO and LUMO frontier orbitals, respectively. **b)** Proposed donor and acceptor behavior of metallotetrylenes towards NH$_3$, based on parallels with tetrelene species.

Reports of the early metallotetrylenes ArEMCp(CO)$_3$ (Ar = Ar^{iPr4} or Ar^{iPr6}; E = Ge, Sn, or Pb; M = Cr, Mo, or W) predominantly focus on the effect of the transition metal on the tetrel geometry and bonding.[9–11] In this dissertation, variations in the structural and spectroscopic properties of the ferrio-substituted complexes ArEFeCp(CO)$_2$ (Ar = Ar^{Me6} or Ar^{iPr6}; E = Ge, Sn, or Pb) are examined *vis-à-vis* their synthesis, spectroscopy, structure, and reactivity towards ammonia.

CHAPTER 2: Insertion Reactions of NH$_3$ and H$_2$O with Ferriogermylenes: Structural Isomerism and Polymorphism in a Metallogermylene.

The metallogermylenes ArGeFeCp(CO)$_2$ (Ar = Ar^{Me6} (**1**) or Ar^{iPr4} (**2**)[18]) were reacted with ammonia under mild conditions to give the insertion products ArGe(NH$_2$)(H)Cp(CO)$_2$ (Ar = Ar^{Me6} (**3**), Ar^{iPr4} (**4**)).[38] The Ge atom of **1** was additionally observed to insert into the H–OH bond of water to give Ar^{Me6}Ge(OH)(H)FeCp(CO)$_2$ (**5**). The hydroxy complex **5** was produced in the presence of adventitious water, despite the fact that the NH$_3$ was rigorously dried prior to use in order to generate spectroscopically clean samples of **3** and **4** for analysis. Observations gathered from the reactions of **1** and **2** with NH$_3$ were further used to aid in tracking the reaction progress of the ferriostannylenes ArSnFeCp(CO)$_2$ (Ar = Ar^{Me6} or Ar^{iPr4}) with ammonia (*vide infra*).
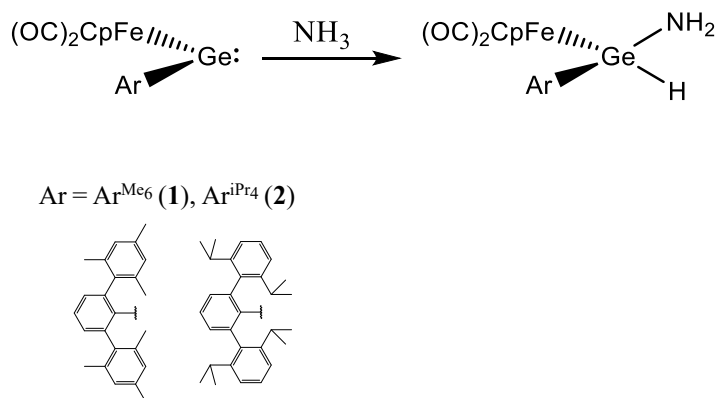

Figure 3. Reaction of **1** and **2** with NH$_3$.

Prior to this work, the only known investigation of the transition metal-like reactivity of metallotetrylenes was conducted by Tobita, et al. in 2015: The cationic germylene [Cp*(CO)$_3$WGe(IPr)][BAr$^F_4$] (IPr = 1,3-bis(2,6-diisopropylphenyl)imidazole-2-ylidene) (Ar^F = 3,5-(CF$_3$)$_2$C$_6$H$_3$), singly bonded to a tungsten atom and stabilized by an N-heterocyclic carbene

ligand, was shown to react with X–H (X = H, Si, B) bonds.[39] The reaction with dihydrogen proceeded to give the dihydrogermane product, while the insertion into Si–H and B-H bonds occurred reversibly and the substrates were regenerated upon gentle heating.[39]

Crystals of **1** were also observed to display polymorphism depending on crystal growth conditions.[38] The primary crystalline form of **1** are green blocks in the habit and unit cell typical of ferriotetrylenes of the series.[18] Microscopic examination of a bulk sample of green crystals of **1** revealed small amounts of red crystals which were initially believed to be impurities. Further inspection by X-ray crystallography revealed the red crystals were a polymorph of **1**. The red polymorphs could be intentionally obtained by concentrating a dark green solution of **1** in a warm water bath at ca. 40 °C then rapid cooling to ca. -32 °C. A red-green dichroic polymorph could be produced in the same way but with cooling to ca. -18 °C. X-ray structural comparisons of the three polymorphs reveal only a difference in the bending angle at the Ge atom, with the red and red-green polymorphs displaying comparatively narrower C-Ge-Fe angles. All polymorphs produced a green solution when re-dissolved in solvents.

CHAPTER 3: A Series of Ferriostannylenes with Differing Terphenyl Substituents

Three novel ferriostannylenes which differ from one another by the substituent on the tin atom were synthesized. $Ar^{Me6}SnFeCp(CO)_2$ (**6**) contains the least sterically encumbering terphenyl ligand in comparison to the previously reported ferriostannylenes ($Ar = Ar^{iPr4}$ and Ar^{iPr6}).[18] $Ar^{Me6}SnFeCp*(CO)_2$ (**7**) differs from **6** via the methyl-substituted cyclopentadienyl group (η^5-C_5Me_5) on iron while $Ar^{Me6}SnFeCp(PMe_3)(CO)$ (**8**) substitutes a CO group at the iron with a phosphine (**Figure 4**).
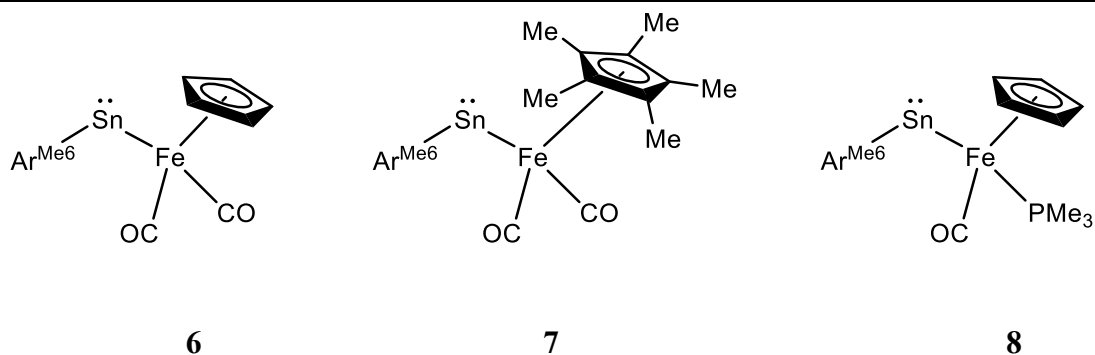
Figure 4. Ferriostannylenes **6-8**.

The majority of metallotetrylenes are Sn derivatives, with reports centered on the synthesis and characterization of the complexes rather than their chemistry.[10,15–18,21,40–42] Their spectroscopic and structural characteristics are additionally well-described. However, discussions on the substituent effect on the central Sn atom are rare.

Comparisons of the compounds ArSnFeCp(CO)$_2$ (Ar = Ar^{Me6} (**6**), Ar^{iPr4}, or Ar^{iPr6})[18] with different substituents show that an increase in the alkyl substituent size on the terphenyl group resulted in the following changes: a narrower C-Sn-Fe bond angle, an upfield shift of the ^{119}Sn NMR signal, and a bathochromic shift in the absorption of the UV-vis spectrum. Differences between **6** and **7** arise from the introduction of alkyl substituents on the Cp ring, which led to the same changes to those described in the comparisons of **6** with its more sterically encumbering derivatives. In comparison to compound **6**, compound **7** has a narrower C-Sn-Fe bond angle, an increased shielding of the tin atom in the ^{119}Sn NMR spectrum, and a comparatively red-shifted absorption in the UV-vis spectrum. Similar substituent effects on interligand angle and molecular stability were also noted in the diaryl tetrylenes EAr$_2$ (E = Ge, Sn, or Pb. Ar = Ar^{Me6}, Ar^{iPr4}, or Ar^{iPr6}).[43,44] Meanwhile, the ^{119}Sn NMR and IR spectra of **8** revealed that the phosphine-carbonyl exchange on the Fe atom caused a decrease in electron density on Sn but an increase in electron density on Fe,

while the UV-vis spectrum showed a lower HOMO→LUMO energy transition in comparison to

6, **7**, and ArSnFeCp(CO)$_2$ (Ar = Ar^{iPr4}, or Ar^{iPr6}).[18]

CHAPTER 4: Reversible Insertion of the Tin Atoms of the Ferriostannylenes ArSnFeCp(CO)$_2$ into the N–H bond of Ammonia, and Isolation and Reactivity of ArPbFeCp(CO)$_2$ with NH$_3$

Having established the reactivity of ferriogermylenes towards ammonia,[38] the reactivity of the other ferrio-substituted group 14 complexes with ammonia was subsequently explored. The Sn analogues ArSnFeCp(CO)$_2$ (Ar = Ar^{Me6} (**6**) or Ar^{iPr4} (**9**)[18]) displayed a reversible bond scission with ammonia that could be monitored visually via color changes associated with the reactions of **1** and **2** (green-colored starting material) to form **3** and **4** (orange-colored products). A VT ^{1}H NMR experiment of the reaction of **9** with NH$_3$ further confirmed the reversible nature of the ferriostannylene reaction with NH$_3$ by showing the Sn-N*H$_2$* amido singlet increasing in integration with a decrease in temperature, and vice versa, the amido singlet decreasing in integration with an increase in temperature. Calculations based on the VT NMR experiments indicate that the reaction is nearly thermoneutral at room temperature, which agrees with DFT calculations of a related reversible thermoneutral bond scission of NH$_3$ on the phosphorus center of a multicyclic constrained phosphine.[45]

Ferrioplumbylenes ArPbFeCp(CO)$_2$ (Ar = Ar^{Me6} (**11**) or Ar^{iPr4} (**12**)) were synthesized to complete the ferriotetrylene series. A comparison of the X-ray structural data of the ferriotetrylenes ArEFeCp(CO)$_2$ (E = Ge (**1** and **2**), Sn (**6** and **9**), or Pb (**12**)) reveals a narrowing of the C–E–Fe angle in the order Ge > Sn > Pb, with the Pb congener **12** showing the narrowest interligand angle of the ferriotetrylenes. Separately, a comparison of the UV-vis spectra of the ferriotetrylenes (Ge:

1 and **2**; Sn: **6** and **9**; Pb: **11** or **12**) shows that the absorption assigned to the n→p energy transition

of the tetrel atom experiences a red shift in the sequence Sn < Ge < Pb, which is in the same order

as the electronegativity value of the tetrel atom (Sn: 1.96, Ge: 2.01, Pb: 2.33).[46,47] However, the

UV-vis spectra of the six complexes also display a blue shift in the absorption assigned as the

π→π* transition of the aryl ligand following the sequence as the group 14 is descended, Ge > Sn

> Pb. Experimentally, the ferrioplumbylenes demonstrated the greatest molecular stability via the

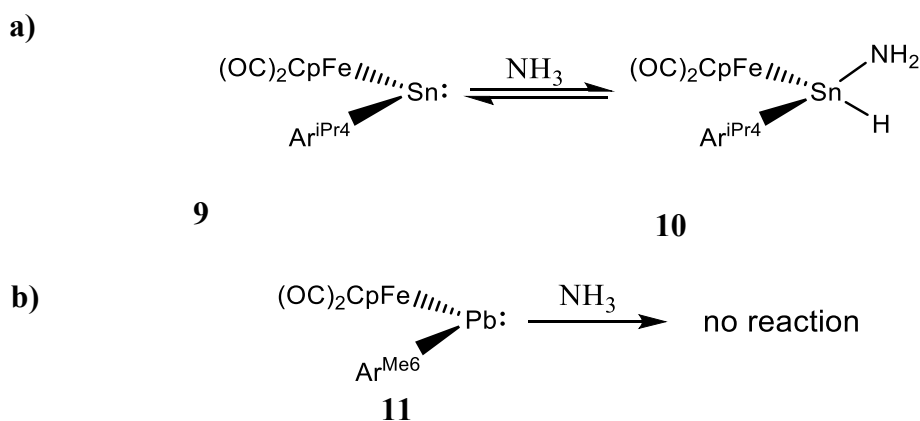lack of reactivity of **11** in a flushed atmosphere of NH_3 (**Figure 5b**).

a)

9
10

b)

11

Figure 5. **a)** Reaction of **9** with NH_3 to form **10**. b) Reaction of **11** with NH_3.

CHAPTER 5: Synthesis, Structure, Spectroscopy of the Biscarboranyl Stannylenes and a Dibiscarboranyl Ethene

The compound 1,1′-bis(ortho-carborane) (**H₂-bc**) comprises two icosahedral o-carborane cages

($C_2B_{10}H_{22}$) linked to one another through the C1 vertex. The electron deficiency of boron gives

rise to a delocalized electron system on the carborane cages.[48,49] The rigid structure and delocalized

electron system of **H₂-bc** makes it an interesting choice of metal-based ligand for organometallic complexes. The majority of **bc**-supported complexes feature a κ^2-C,C or κ^2-B,C bonded transition metal,[50–59] though biscarboranyl main group metal complexes are also known.[60–63]

Herein, two stannylenes bonded κ^2-C,C to the **bc** ligand are synthesized and characterized. The synthetic procedures are analogous, first activating the C-H vertices with potassium bis(trimethylsilyl) to generate K₂[**bc**] for a salt metathesis reaction with SnCl₂. Utilizing THF as the solvent for this reaction generated (**bc**)Sn·THF (**12**) while following the same synthetic procedure with a benzene/dichloromethane solvent mixture produced [(**bc**)Sn]₂KCl (**13**) (**Figure 6**). Compounds **12** and **13** are the first stannylenes supported by the **bc** ligand platform. The (**bc**)Sn moiety of **12** and **13** display structural similarities to other diorganostannylenes containing a cyclic C₄Sn moiety in geometry and bonding around the Sn atom.[64–77] Compound **12** displays a triplet of triplet signal in its ¹¹⁹Sn NMR spectrum, which arises from long-range nuclear spin-spin coupling between the ¹¹B and ¹¹⁹Sn nuclei.[78,79] Additionally, the ¹¹⁹Sn NMR signal for **12** appears at -137.31 ppm. This signal is downfield from the ¹¹⁹Sn NMR signals of diorganostannylene Sn(II)←THF compounds (-244.5 – -377.1 ppm)[65,66] due to the electron-withdrawing effect of the **bc** ligand on **12**. However, the ¹¹⁹Sn NMR signal for **12** is upfield from the ¹¹⁹Sn NMR signals of biscarboranyl stannanes (-21.22 – 53.10 ppm)[63] due to the THF ligand shielding the tin atom on **12**. The ¹¹⁹Sn signal of compound **13** could not be detected, despite numerous attempts with use of a wide variety of parameters, suggesting that the THF ligand in **12** may be stabilizing the electron environment at the Sn atom to enable detection of a signal.

In a procedure similar to the synthesis of **13**, when the reaction period of the C-H activation step is shortened from 24–48 hours to 9–12 hours, the mono-deprotonated species K[**H-bc**] is produced.

Addition of the K[**H-bc**]/benzene slurry to a dichloromethane solution of $SnCl_2$ causes a reaction with the solvent dichloromethane molecules to generate the **bc**-supported alkene (**bc**)CH=CH(**bc**) (**14**) (**Figure 6**). The alkene displays spectroscopic properties typical of other conjugated alkenes.

12 **13** **14**

○ = BH
○ = CH
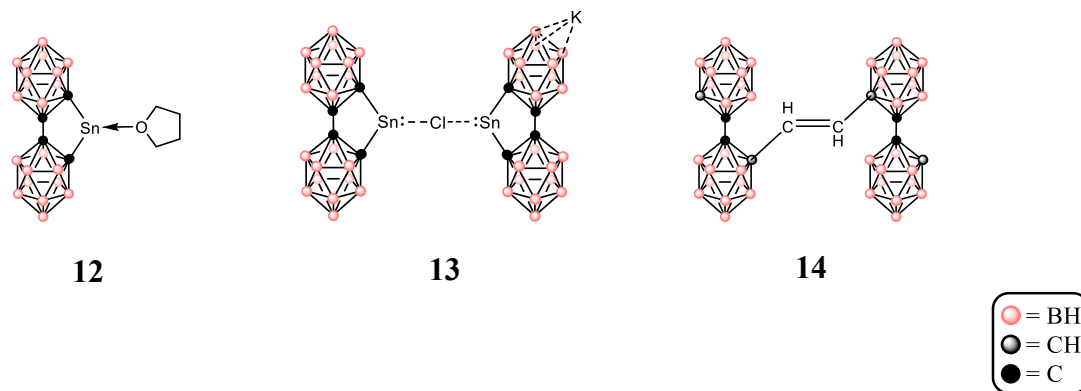● = C

Figure 6. Compounds **12-14**.

CHAPTER 1

ABSTRACT REFERENCES

(1)   Mizuhata, Y.; Sasamori, T.; Tokitoh, N. Stable Heavier Carbene Analogues. *Chem Rev* **2009**, *109*, 3479–3511.

(2)   Tokitoh, N.; Okazaki, R. Recent Topics in the Chemistry of Heavier Congeners of Carbenes. *Coord Chem Rev* **2000**, *210*, 251–277.

(3)   Chu, T.; Nikonov, G. I. Oxidative Addition and Reductive Elimination at Main-Group Element Centers. *Chem Rev* **2018**, *118*, 3608–3680.

(4)   Power, P. P. Reactions of Heavier Main-Group Compounds with Hydrogen, Ammonia, Ethylene and Related Small Molecules. *The Chemical Record* **2012**, *12*, 238–255.

(5)   Power, P. P. Main-Group Elements as Transition Metals. *Nature* **2010**, *463*, 171–177.

(6)   Power, P. P. Interaction of Multiple Bonded and Unsaturated Heavier Main Group Compounds with Hydrogen, Ammonia, Olefins, and Related Molecules. *Acc Chem Res* **2011**, *44*, 627–637.

(7)   Jutzi, P.; Leue, C. (Supermesityl)Chlorogermylene (Supermesityl = Mes* = 2,4,6-^{t}Bu$_3$C$_6$H$_2$): Synthesis and Derivatization to (Supermesityl)Ferriogermylenes. *Organometallics* **1994**, *13*, 2898–2899.

(8)   Simons, R. S.; Power, P. P. (η^5-C$_5$H$_5$)(CO)$_2$MoGeC$_6$H$_3$-2,6-Mes$_2$: A Transition-Metal Germylyne Complex. *J Am Chem Soc* **1996**, *118*, 11966–11967.

(9)   Pu, L.; Twamley, B.; Haubrich, S. T.; Olmstead, M. M.; Mork, B. V.; Simons, R. S.; Power, P. P. Triple Bonding to Germanium: Characterization of the Transition Metal Germylynes (η^5-C$_5$H$_5$)(CO)$_2$M≡Ge-C$_6$H$_3$-2,6-Mes$_2$ (M = Mo, W; Mes = −C$_6$H$_2$-2,4,6-Me$_3$) and (η^5-C$_5$H$_5$)(CO)$_2$M≡Ge-C$_6$H$_3$-2,6-Trip$_2$ (M = Cr, Mo, W; Trip = −C$_6$H$_2$-2,4,6-i-Pr$_3$) and the Related Single Bonded Metallogermylenes (η^5-C$_5$H$_5$)(CO)$_3$M-G̈e-C$_6$H$_3$-2,6-Trip$_2$ (M = Cr, W). *J Am Chem Soc* **2000**, *122*, 650–656.

(10)   Eichler, B. E.; Phillips, A. D.; Haubrich, S. T.; Mork, B. V.; Power, P. P. Synthesis, Structures, and Spectroscopy of the Metallostannylenes (η^5-C$_5$H$_5$)(CO)$_3$M−S̈n−C$_6$H$_3$-2,6-Ar$_2$ (M = Cr, Mo, W; Ar = C$_6$H$_2$-2,4,6-Me$_3$, C$_6$H$_2$-2,4,6-Pr$^i_3$). *Organometallics* **2002**, *21*, 5622–5627.

(11)   Pu, L.; Power, P. P.; Boltes, I.; Herbst-Irmer, R. Synthesis and Characterization of the Metalloplumbylenes (η^5-C$_5$H$_5$)(CO)$_3$M-P̈b-C$_6$H$_3$-2,6-Trip$_2$ (M = Cr, Mo, or W; Trip = −C$_6$H$_2$-2,4,6-i-Pr$_3$). *Organometallics* **2000**, *19*, 352–356.

(12)   Leung, W.-P.; Chiu, W.-K.; Mak, T. C. W. Synthesis and Structural Characterization of Metallogermylenes, Cp-Substituted Germylene, and a Germanium(II)-Borane Adduct from Pyridyl-1-Azaallyl Germanium(II) Chloride. *Organometallics* **2012**, *31*, 6966–6971.

(13)   Inomata, K.; Watanabe, T.; Tobita, H. Cationic Metallogermylene and Dicationic Dimetallodigermenes: Synthesis by Chloride Abstraction from *N*-Heterocyclic Carbene-Stabilized Chlorometallogermylenes. *J Am Chem Soc* **2014**, *136*, 14341–14344.

(14)   Handford, R. C.; Nesbit, M. A.; Smith, P. W.; Britt, R. D.; Tilley, T. D. Versatile Fe–Sn Bonding Interactions in a Metallostannylene System: Multiple Bonding and C–H Bond Activation. *J Am Chem Soc* **2022**, *144*, 358–367.

(15)   Liu, H.-J.; Guihaumé, J.; Davin, T.; Raynaud, C.; Eisenstein, O.; Tilley, T. D. 1,2-Hydrogen Migration to a Saturated Ruthenium Complex via Reversal of Electronic Properties for Tin in a Stannylene-to-Metallostannylene Conversion. *J Am Chem Soc* **2014**, *136*, 13991–13994.

(16)   Hayes, P. G.; Gribble, C. W.; Waterman, R.; Tilley, T. D. A Hydrogen-Substituted Osmium Stannylene Complex: Isomerization to a Metallostannylene Complex via an Unusual α-Hydrogen Migration from Tin to Osmium. *J Am Chem Soc* **2009**, *131*, 4606–4607.

(17)   Inoue, S.; Driess, M. Isolable Metallo-Germylene and Metallo-Stannylene σ-Complexes with Iron. *Organometallics* **2009**, *28*, 5032–5035.

(18)   Lei, H.; Guo, J.-D.; Fettinger, J. C.; Nagase, S.; Power, P. P. Synthesis, Characterization, and CO Elimination of Ferrio-Substituted Two-Coordinate Germylenes and Stannylenes. *Organometallics* **2011**, *30* (22), 6316–6322.

(19)   Filippou, A. C.; Philippopoulos, A. I.; Portius, P.; Neumann, D. U. Synthesis and Structure of the Germylyne Complexestrans-[X(Dppe)2W≡Ge(η^1-Cp*)] (X=Cl, Br, I) and Comparison of the W≡E Bonds (E=C, Ge) by Density Functional Calculations. *Angewandte Chemie International Edition* **2000**, *39*, 2778–2781.

(20)   Filippou, A. C.; Portius, P.; Philippopoulos, A. I.; Rohde, H. Triple Bonding to Tin: Synthesis and Characterization of the Stannylyne Complex Trans-[Cl(PMe$_3$)$_4$W≡Sn-C$_6$H$_3$-2,6-Mes$_2$]. *Angewandte Chemie International Edition* **2003**, *42*, 445–447.

(21)   Lebedev, Y. N.; Das, U.; Schnakenburg, G.; Filippou, A. C. Coordination Chemistry of [E(Idipp)]$^{2+}$ Ligands (E = Ge, Sn): Metal Germylidyne [Cp*(CO)$_2$W≡Ge(Idipp)]$^+$ and Metallotetrylene [Cp*(CO)$_3$W–E(Idipp)]$^+$ Cations. *Organometallics* **2017**, *36*, 1530–1540.

(22)   Tashita, S.; Watanabe, T.; Tobita, H. Synthesis of a Base-Stabilized (Chlorogermyl)Metallogermylene and Its Photochemical Conversion to a (Chlorogermyl)Germylyne Complex. *Chem Lett* **2013**, *42*, 43–44.

(23)   Filippou, A. C.; Chernov, O.; Stumpf, K. W.; Schnakenburg, G. Metal-Silicon Triple Bonds: The Molybdenum Silylidyne Complex [Cp(CO)$_2$Mo≡Si-R]. *Angewandte Chemie International Edition* **2010**, *49*, 3296–3300.

(24)   Filippou, A. C.; Chernov, O.; Schnakenburg, G. Metal-Silicon Triple Bonds: Nucleophilic Addition and Redox Reactions of the Silylidyne Complex [Cp(CO)2Mo≡Si-R]. *Angewandte Chemie International Edition* **2011**, *50*, 1122–1126.

(25) Filippou, A. C.; Chernov, O.; Schnakenburg, G. Chromium-Silicon Multiple Bonds: The Chemistry of Terminal N-Heterocyclic-Carbene-Stabilized Halosilylidyne Ligands. *Chemistry - A European Journal* **2011**, *17*, 13574–13583.

(26) El-Maradny, A.; Tobita, H.; Ogino, H. Photoreactions of Silyliron(II) Complexes Cp′Fe(CO)$_2$SiMe$_3$ (Cp′ = η^5-C$_5$H$_5$, η^5-C$_5$Me$_5$) with Di-*p*-Tolylgermane (*p*-Tol)$_2$GeH$_2$. *Chem Lett* **1996**, *25*, 83–84.

(27) Filippou, A. C.; Weidemann, N.; Schnakenburg, G.; Rohde, H.; Philippopoulos, A. I. Tungsten-Lead Triple Bonds: Syntheses, Structures, and Coordination Chemistry of the Plumbylidyne Complexestrans-[X(PMe$_3$)$_4$W≡Pb(2,6-Trip$_2$C$_6$H$_3$)]. *Angewandte Chemie International Edition* **2004**, *43*, 6512–6516.

(28) Seidel, N.; Jacob, K.; Fischer, A. K. Bis[2-((Dimethylamino)Methyl)Ferrocenyl]Lead, (FcN)$_2$Pb, as a Ligand: Synthesis and Characterization of the Heterotrimetallic Metalloplumbylene Compounds (FcN)$_2$PbM(CO)$_5$ (M = Cr, Mo, W). *Organometallics* **2001**, *20*, 578–581.

(29) Zhu, Q.; Fettinger, J. C.; Vasko, P.; Power, P. P. Interactions of a Diplumbyne with Dinuclear Transition Metal Carbonyls to Afford Metalloplumbylenes. *Organometallics* **2020**, *39*, 4629–4636.

(30) Spikes, G. H.; Fettinger, J. C.; Power, P. P. Facile Activation of Dihydrogen by an Unsaturated Heavier Main Group Compound. *J Am Chem Soc* **2005**, *127*, 12232–12233.

(31) Peng, Y.; Brynda, M.; Ellis, B. D.; Fettinger, J. C.; Rivard, E.; Power, P. P. Addition of H$_2$ to Distannynes under Ambient Conditions. *Chemical Communications* **2008**, 6042.

(32) Peng, Y.; Ellis, B. D.; Wang, X.; Power, P. P. Diarylstannylene Activation of Hydrogen or Ammonia with Arene Elimination. *J Am Chem Soc* **2008**, *130* (37), 12268–12269.

(33) Wang, X.; Zhu, Z.; Peng, Y.; Lei, H.; Fettinger, J. C.; Power, P. P. Room-Temperature Reaction of Carbon Monoxide with a Stable Diarylgermylene. *J Am Chem Soc* **2009**, *131*, 6912–6913.

(34) Peng, Y.; Ellis, B. D.; Wang, X.; Fettinger, J. C.; Power, P. P. Reversible Reactions of Ethylene with Distannynes Under Ambient Conditions. *Science (1979)* **2009**, *325*, 1668–1670.

(35) Peng, Y.; Guo, J.-D.; Ellis, B. D.; Zhu, Z.; Fettinger, J. C.; Nagase, S.; Power, P. P. Reaction of Hydrogen or Ammonia with Unsaturated Germanium or Tin Molecules under Ambient Conditions: Oxidative Addition versus Arene Elimination. *J Am Chem Soc* **2009**, *131* (44), 16272–16282.

(36) Brown, Z. D.; Power, P. P. Mechanisms of Reactions of Open-Shell, Heavier Group 14 Derivatives with Small Molecules: N−π* Back-Bonding in Isocyanide Complexes, C–H Activation under Ambient Conditions, CO Coupling, and Ancillary Molecular Interactions. *Inorg Chem* **2013**, *52*, 6248–6259.

(37) Wang, S.; Sherbow, T. J.; Berben, L. A.; Power, P. P. Reversible Coordination of H_2 by a Distannyne. *J Am Chem Soc* **2018**, *140*, 590–593.

(38) Phung, A. C.; Fettinger, J. C.; Power, P. P. Insertion Reactions of NH_3 and H_2O with the Ferriogermylenes $ArGeFeCp(CO)_2$ (Ar = Ar^{Me6} ($-C_6H_3$-$(C_6H_2$-2,4,6-$Me_3)_2)$) or Ar^{iPr4} ($-C_6H_3$-$(C_6H_3$-2,6-$^iPr_2)_2)$); Cp = η^5-C_5H_5): Structural Isomerism and Polymorphism in a Metallogermylene. *Organometallics* **2021**, *40* (20), 3472–3479.

(39) Inomata, K.; Watanabe, T.; Miyazaki, Y.; Tobita, H. Insertion of a Cationic Metallogermylene into E–H Bonds (E = H, B, Si). *J Am Chem Soc* **2015**, *137*, 11935–11937.

(40) Widemann, M.; Jeggle, S.; Auer, M.; Eichele, K.; Schubert, H.; Sindlinger, C. P.; Wesemann, L. Hydridotetrylene [Ar*EH] (E = Ge, Sn, Pb) Coordination at Tantalum, Tungsten, and Zirconium. *Chem Sci* **2022**, *13*, 3999–4009.

(41) Stewart, M. A.; Moore, C. E.; Ditri, T. B.; Labios, L. A.; Rheingold, A. L.; Figueroa, J. S. Electrophilic Functionalization of Well-Behaved Manganese Monoanions Supported by m-Terphenyl Isocyanides. *Chem. Commun.* **2011**, *47*, 406–408.

(42) Smith, P. W.; Handford, R. C.; Tilley, T. D. Heavy Tetrel Complexes of Ru Featuring Ru=E(R)X and Ru–E–R (E = Sn, Pb) Linkages. *Organometallics* **2019**, *38*, 4060–4065.

(43) McCrea-Hendrick, M. L.; Bursch, M.; Gullett, K. L.; Maurer, L. R.; Fettinger, J. C.; Grimme, S.; Power, P. P. Counterintuitive Interligand Angles in the Diaryls $E\{C_6H_3$-2,6-$(C_6H_2$-2,4,6-$^iPr_3)_2\}_2$ (E = Ge, Sn, or Pb) and Related Species: The Role of London Dispersion Forces. *Organometallics* **2018**, *37*, 2075–2085.

(44) Twamley, B.; Haubrich, S. T.; Power, P. P. Element Derivatives of Sterically Encumbering Terphenyl Ligands; 1999; pp 1–65.

(45) Abbenseth, J.; Townrow, O. P. E.; Goicoechea, J. M. Thermoneutral N–H Bond Activation of Ammonia by a Geometrically Constrained Phosphine. *Angewandte Chemie International Edition* **2021**, *60*, 23625–23629.

(46) Sanderson, R. T. Electronegativity and Bond Energy. *J Am Chem Soc* **1983**, *105*, 2259–2261.

(47) Mullay, J. Estimation of Atomic and Group Electronegativities. In *Electronegativity*; Springer-Verlag: Berlin/Heidelberg; pp 1–25.

(48) Grimes, R. N. *Carboranes*; Elsevier, 2016.

(49) Grimes, R. N. Carboranes in the Chemist's Toolbox. *Dalton Transactions* **2015**, *44* (13), 5939–5956.

(50) Jeans, R. J.; Chan, A. P. Y.; Riley, L. E.; Taylor, J.; Rosair, G. M.; Welch, A. J.; Sivaev, I. B. Arene–Ruthenium Complexes of 1,1′-Bis(*Ortho*-Carborane): Synthesis, Characterization, and Catalysis. *Inorg Chem* **2019**, *58* (17), 11751–11761.

(51) Sivaev, I. B.; Bregadze, V. I. 1,1′-Bis(Ortho-Carborane)-Based Transition Metal Complexes. *Coord Chem Rev* **2019**, *392*, 146–176.

(52) Chambrier, I.; Hughes, D. L.; Jeans, R. J.; Welch, A. J.; Budzelaar, P. H. M.; Bochmann, M. Do Gold(III) Complexes Form Hydrogen Bonds? An Exploration of Au^{III} Dicarboranyl Chemistry. *Chemistry – A European Journal* **2020**, *26*, 939–947.

(53) Martin, M. J.; Man, W. Y.; Rosair, G. M.; Welch, A. J. 1,1′-Bis(Ortho-Carborane) as a κ^2 Co-Ligand. *J Organomet Chem* **2015**, *798*, 36–40.

(54) Yao, Z.-J.; Zhang, Y.-Y.; Jin, G.-X. Pseudo-Aromatic Bis-o-Carborane Iridium and Rhodium Complexes. *J Organomet Chem* **2015**, *798*, 274–277.

(55) Kirlikovali, K. O.; Axtell, J. C.; Gonzalez, A.; Phung, A. C.; Khan, S. I.; Spokoyny, A. M. Luminescent Metal Complexes Featuring Photophysically Innocent Boron Cluster Ligands. *Chem Sci* **2016**, *7*, 5132–5138.

(56) Kirlikovali, K. O.; Axtell, J. C.; Anderson, K.; Djurovich, P. I.; Rheingold, A. L.; Spokoyny, A. M. Fine-Tuning Electronic Properties of Luminescent Pt(II) Complexes via Vertex-Differentiated Coordination of Sterically Invariant Carborane-Based Ligands. *Organometallics* **2018**, *37*, 3122–3131.

(57) Jeans, R. J.; Rosair, G. M.; Welch, A. J. *C,C′*-Ru to *C,B′*-Ru Isomerisation in Bis(Phosphine)Ru Complexes of [1,1′-Bis(*Ortho*-Carborane)]. *Chemical Communications* **2022**, *58*, 64–67.

(58) Owen, D. A.; Hawthorne, M. F. Novel Chelated Biscarborane Transition Metal Complexes Formed through Carbon-Metal σ Bonds. *J Am Chem Soc* **1970**, *92* (10), 3194–3196.

(59) Harwell, D. E.; McMillan, J.; Knobler, C. B.; Hawthorne, M. F. Structural Characterization of Representative d^7, d^8, and d^9 Transition Metal Complexes of Bis(*o*-Carborane). *Inorg Chem* **1997**, *36* (25), 5951–5955.

(60) Wong, Y. O.; Smith, M. D.; Peryshkov, D. v. Synthesis of the First Example of the 12-Vertex-*Closo*/12-Vertex-*Nido* Biscarborane Cluster by a Metal-Free B−H Activation at a Phosphorus(III) Center. *Chemistry - A European Journal* **2016**, *22*, 6764–6767.

(61) Wong, Y. O.; Smith, M. D.; Peryshkov, D. v. Reversible Water Activation Driven by Contraction and Expansion of a 12-Vertex-Closo-12-Vertex-Nido Biscarborane Cluster. *Chemical Communications* **2016**, *52* (86), 12710–12713.

(62) Yruegas, S.; Axtell, J. C.; Kirlikovali, K. O.; Spokoyny, A. M.; Martin, C. D. Synthesis of 9-Borafluorene Analogues Featuring a Three-Dimensional 1,1′-Bis(*o*-Carborane) Backbone. *Chemical Communications* **2019**, *55* (20), 2892–2895.

(63) Axtell, J. C.; Kirlikovali, K. O.; Dziedzic, R. M.; Gembicky, M.; Rheingold, A. L.; Spokoyny, A. M. Magnesium Reagents Featuring a 1,1′-Bis(*o*-carborane) Ligand Platform. *Eur J Inorg Chem* **2017**, *2017*, 4411–4416.

(64) Veith, M.; Belot, C.; Huch, V.; Zimmer, M. Influence of the Solvent on the Formation of New Tin(II) Methoxides Containing Thienyl Substituents: Crystal Structure and NMR Investigations. *Z Anorg Allg Chem* **2009**, *635*, 942–948.

(65) Huang, M.; Kireenko, M. M.; Lermontova, E. Kh.; Churakov, A. V.; Oprunenko, Y. F.; Zaitsev, K. V.; Sorokin, D.; Harms, K.; Sundermeyer, J.; Zaitseva, G. S.; Karlov, S. S. Novel Stannylenes Stabilized with Diethylenetriamido and Related Amido Ligands: Synthesis, Structure, and Chemical Properties. *Z Anorg Allg Chem* **2013**, *639*, 502–511.

(66) Arii, H.; Matsuo, M.; Nakadate, F.; Mochida, K.; Kawashima, T. Coordination of a Chiral Tin(Ii) Cation Bearing a Bis(Oxazoline) Ligand with Tetrahydrofuran Derivatives. *Dalton Transactions* **2012**, *41*, 11195.

(67) Eisler, D. J.; Chivers, T. Chalcogenide Derivatives of Imidotin Cage Complexes. *Chemistry - A European Journal* **2006**, *12*, 233–243.

(68) Clegg, W.; Harrington, R. W. CCDC 2055793: Experimental Crystal Structure Determination. *CSD Communication* **2021**.

(69) Iwamoto, T.; Masuda, H.; Ishida, S.; Kabuto, C.; Kira, M. Addition of Stable Nitroxide Radical to Stable Divalent Compounds of Heavier Group 14 Elements. *J Am Chem Soc* **2003**, *125*, 9300–9301.

(70) Yan, C.; Li, Z.; Xiao, X.; Wei, N.; Lu, Q.; Kira, M. Reversible Stannylenoid Formation from the Corresponding Stannylene and Cesium Fluoride. *Angewandte Chemie International Edition* **2016**, *55*, 14784–14787.

(71) Schäfer, A.; Saak, W.; Haase, D.; Müller, T. Persistent Dialkyl(Silyl)Stannylium Ions. *J Am Chem Soc* **2011**, *133*, 14562–14565.

(72) Kira, M.; Yauchibara, R.; Hirano, R.; Kabuto, C.; Sakurai, H. Chemistry of Organosilicon Compounds. 287. Synthesis and x-Ray Structure of the First Dicoordinate Dialkylstannylene That Is Monomeric in the Solid State. *J Am Chem Soc* **1991**, *113*, 7785–7787.

(73) Saito, M.; Shiratake, M.; Tajima, T.; Guo, J. D.; Nagase, S. Synthesis and Structure of the Dithienostannole Anion. *J Organomet Chem* **2009**, *694*, 4056–4061.

(74) Kavara, A.; Kampf, J. W.; Banaszak Holl, M. M. Direct Formation of Propargyltin Compounds via C−H Activation. *Organometallics* **2008**, *27*, 2896–2897.

(75) Kavara, A.; Kheir, M. M.; Kampf, J. W.; Banaszak Holl, M. M. Aryl Halide Radical Clocks as Probes of Stannylene/Aryl Halide C–H Activation Rates. *J Inorg Organomet Polym Mater* **2014**, *24*, 250–257.

(76) Izod, K.; McFarlane, W.; Tyson, B. V.; Carr, I.; Clegg, W.; Harrington, R. W. Stabilization of a Dialkylstannylene by Unusual B−H···Sn γ-Agostic-Type Interactions. A Structural, Spectroscopic, and DFT Study. *Organometallics* **2006**, *25*, 1135–1143.

(77)   Krebs, K. M.; Wiederkehr, J.; Schneider, J.; Schubert, H.; Eichele, K.; Wesemann, L. η^3 - Allyl Coordination at Tin(II)-Reactivity towards Alkynes and Benzonitrile. *Angewandte Chemie International Edition* **2015**, *54*, 5502–5506.

(78)   Wrackmeyer, B. Long-Range Nuclear Spin-Spin Coupling between ^{11}B and ^{13}C, ^{29}Si or ^{119}Sn: A Promising Tool for Structural Assignment. *Polyhedron* **1986**, *5*, 1709–1721.

(79)   Abragam, A. *The Principles of Nuclear Magnetism*; Oxford University Press: Oxford, 1961.

Insertion Reactions of NH_3 and H_2O with the Ferriogermylenes $ArGeFeCp(CO)_2$ (Ar = Ar^{Me6} (–C_6H_3-(C_6H_2-2,4,6-Me_3)$_2$) or Ar^{iPr4} (–C_6H_3-(C_6H_3-2,6-$^iPr_2$)$_2$); Cp = η^5-C_5H_5): Structural Isomerism and Polymorphism in a Metallogermylene

Alice C. Phung,[1] James C. Fettinger,[1] Philip P. Power[1]*

[1]Department of Chemistry, University of California, Davis, 1 Shields Avenue, Davis, California 95616

ABSTRACT: The ferriogermylenes $ArGeFeCp(CO)_2$ (Ar = –C_6H_3-(C_6H_2-2,4,6-Me_3)$_2$ (Ar^{Me6} (**1a**)), –C_6H_3-(C_6H_2-2,6-$^iPr_2$)$_2$ (Ar = Ar^{iPr4} (**1b**)) (Cp = η^5-C_5H_5) react with an excess of NH_3(l) to form the insertion products $ArGe(NH_2)(H)FeCp(CO)_2$ (Ar = Ar^{Me6} (**2a**) or Ar^{iPr4} (**2b**)). Similarly, ferriogermylene **1a** reacts with water to form the insertion product $Ar^{Me6}Ge(OH)(H)FeCp(CO)_2$ (**3**). Unusually, crystals of **1a** exist as three different polymorphs whose structures differ primarily in their C_{ipso}-Ge-Fe bond angles. Complexes **1-3** were characterized by NMR, UV-vis, IR spectroscopy, and X-ray crystallography.

2.1 INTRODUCTION

The syntheses, structures, and reactivity of heavy group 14 tetrylenes :ER_2 (E = Si, Ge, Sn, Pb; R = alkyl, aryl, silyl, amido, alkoxo, thiolato, etc.) have attracted wide interest.[1,2] The isolated tetrylenes feature bonds to two substituents as well as a non-bonded lone pair and an unoccupied p-orbital at the tetrel atom. Thus the tetrel atom can interact in a synergistic manner with important small molecules such as H_2, NH_3, C_2H_4, CO, etc.[3,4] Most of the chemical investigations thus far have featured tetrels bound to two organic substituents. However, the reactivity of the related divalent tetrelene molecules that feature a direct bond between the group 14 element and a transition metal have received much less attention.

CHAPTER 2

The first report of the synthesis of stable metallotetrylenes concerned the ferriogermylenes Mes*GeFe(CO)$_2$R (R = Cp, Cp*) (Mes* = C$_6$H$_2$-2,4,6-^{t}Bu$_3$, Cp* = η^5-C$_5$Me$_5$), reported in 1994 by Jutzi and Leue,[5] but these molecules were not structurally characterized however. Shortly thereafter, several other metallotetrylenes, the majority of which are derivatives of germanium or tin, were reported.[6–14] In contrast, metallosilylenes[15] and metalloplumbylenes[16] remain rare. These compounds were stabilized either by the use of a bulky ligand at the Group 14 atom or by additional Lewis bases coordinated to the tetrel atom. The metallotetrylenes feature a relatively wide angle at the tetrel atom that ranges from 106° to 118° and a bent geometry that is characteristic of the presence of a non-bonding lone pair at the tetrel atom. The related triple-bonded metallotetrylynes in which the coordination of E (E = Si, Ge, Sn, Pb) is linear or near linear were discovered serendipitously when molybdogermylenes were found to spontaneously dissociate CO during the reaction of NaMoCp(CO)$_3$ with Ar^{Me6}GeCl to yield Ar^{Me6}Ge≡MoCp(CO)$_2$.[17] Other routes to the metallogermylynes, including their Si, Sn, and Pb congeners, were reported by Filippou and coworkers[18–22], Tobita and coworkers[23], and more recently by our group[24] and by Wesemann and coworkers.[25]

Despite the growing library of well-characterized metallotetrylenes, investigations of their reactivity have lagged. Originally, the low-oxidation state digermynes ArGeGeAr and distannynes ArSnSnAr (Ar = Ar^{iPr4} or Ar^{iPr6} (–C$_6$H$_3$-(C$_6$H$_2$-2,4,6-^{i}Pr$_3$)$_2$)) were shown to react with small molecules such as H$_2$, NH$_3$, and CO under mild conditions[26–29] and they also displayed C-H activation reactions[30–36] due in part to their trans-bent structure and bis(metallanediyl) character. In a similar way, the diaryltetrylenes :EAr$_2$ (E = Ge, Sn) and the related carbenes also react with small molecules.[37–42] (**Figure 1**)

R = Ar^{Me6} or Ar^{iPr4}
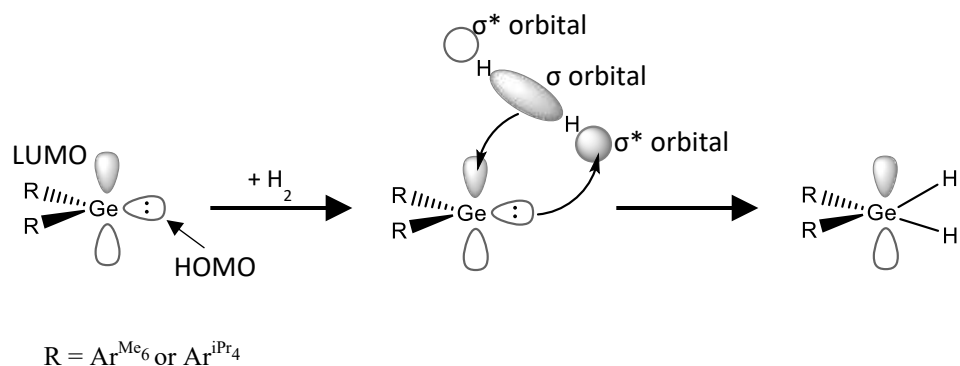
Figure 1. Synergistic reactivity of diorganogermylene species: behavior as donor and acceptor. Diaryltetrylgermylenes have been observed to display transition metal-like behavior and react with small molecules such as H_2.[39–42]

The only report of similar reactivity by metallotetrylenes was that by Tobita and coworkers in 2015 where the cationic tungstogermylene [(IPr)GeWCp*(CO)$_3$][BAr$^F_4$] (IPr = 1,3-bis(2,6-diisopropylphenyl)imidazole-2-ylidene) (Ar^F = 3,5-(CF$_3$)$_2$C$_6$H$_3$), stabilized by an N-heterocyclic carbene ligand, was shown to insert into dihydrogen to afford a tungstogermane, and into X-H (X = Si, B) bonds reversibly to afford a tungstogermylsilane and tungstogermylborane, respectively.[43] The authors reported that the cationic nature of the reported metallogermylene induces a lower HOMO-LUMO energy gap, in comparison to that in the neutral germylenes :GeAr$_2$ (Ar = Ar^{Me6} or Ar^{iPr4})[39].

In this work, we report that the neutral ferriogermylenes ArGeFeCp(CO)$_2$ (Ar = Ar^{Me6} (**1a**), Ar^{iPr4} (**1b**)) react with NH$_3$ and H$_2$O under mild conditions, to give the insertion products ArGe(NH$_2$)(H)FeCp(CO)$_2$ (Ar = Ar^{Me6} (**2a**), Ar^{iPr4} (**2b**)) and Ar^{Me6}Ge(OH)(H)FeCp(CO)$_2$ (**3**). In addition, we report that crystals of **1a** display polymorphism with the polymorphs displaying different interligand angles at the germanium atom.

CHAPTER 2

2.2 EXPERIMENTAL SECTION

General Procedures: All manipulations were carried out by using modified Schlenk techniques or in a Vacuum Atmospheres OMNI-Lab drybox under a N_2 or argon atmosphere. Solvents were dried over columns of activated alumina using a Grubbs type purification system (Glass Contour), stored over Na (THF) or K (hexanes, pentane, toluene) mirrors, and degassed via three freeze-pump-thaw cycles prior to use. The compounds ArGeCl (Ar = Ar^{Me6}, Ar^{iPr4})[44–46] and $K[FeCp(CO)_2]$[47] were synthesized according to literature procedures. The ^1H and $^{13}C\{^1H\}$ NMR spectra were recorded on Varian Inova 600 MHz or Bruker Avance III HD Nanobay 400 MHz spectrometers and were referenced to the residual solvent signals in C_6D_6 (δ 7.15 ppm). UV-Visible spectra were recorded using dilute hexane solutions in 3.5 mL quartz cuvettes using an Olis 17 Modernized Cary 14 UV-Vis/NIR spectrophotometer. Infrared spectra for **1a** and **3** were recorded as Nujol mulls between CsI windows on a PerkinElmer 1430 spectrophotometer. Infrared spectra for **2a** and **2b** were collected on a Bruker Tensor 27 ATRFTIR spectrometer. Melting points were determined on a Meltemp II apparatus in flame-sealed glass capillaries equipped with a partial immersion thermometer.

The ferriogermylene **1b** was synthesized according to a literature procedure.[10]

$Ar^{Me6}GeFeCp(CO)_2$ (1a): The synthesis of $Ar^{Me6}GeFeCp(CO)_2$ follows a modified version of a literature procedure for $Ar^{iPr4}GeFeCp(CO)_2$ (**1b**).[10] A solution of $Ar^{Me6}GeCl$ (3.5 g, 8.7 mmol)[45] in THF (30 mL) was added dropwise to a THF solution (ca. 40 mL) of $K[FeCp(CO)_2]$ (1.8 g, 8.7 mmol) at room temperature and stirred overnight. The solvent was removed under reduced pressure to afford a dark green-brown solid that was dissolved in toluene (ca. 50 mL). This solution was filtered through a Celite plug, and the deep green filtrate was concentrated to ca. 10 mL. Storage at ca. -18°C afforded dark green crystals of **1a**. Yield: 2.8 g (60%). Mp: 165-170°C. ^1H

NMR (400 MHz, C_6D_6, 20°C): δ 2.03 (s, 6H, p-C(CH_3)), δ 2.46 (s, 12H, o-C(CH_3)), δ 3.82 (s, 5H, η^5-C$_5H_5$), δ 6.68 (br s, 4H, flanking m-aromatic H), δ 7.13 (d, 2H, J_{HH} = 7.5Hz, central m-aromatic H), δ 7.45 (t, 1H, $^3J_{HH}$ = 7.5 Hz, central p-aromatic H). ^{13}C NMR (151 MHz, C_6D_6, 20°C): δ 20.56 (p-CH_3) δ 20.82 (o-CH_3), δ 85.43 (η^5-C$_5H_5$), δ 127.95, 127.99, 128.33, 129.06, 135.79, 136.72, 141.49 (Ar(C)), δ 176.96 (C_{ipso}-Ge), δ 212.12 (CO). UV-vis (hexane): λ_{max} (ε) 430 nm (1860 mol$^-$^{1} L cm^{-1}), 616 nm (427 mol^{-1} L cm^{-1}). IR (Nujol, cm^{-1}): v_{CO} 1980 (s), v_{CO} 1940 (s).

Ar^{Me6}Ge(NH$_2$)(H)FeCp(CO)$_2$ (2a): Anhydrous ammonia (ca. 40 mL, twice-dried over sodium) was condensed onto solid **1a** (0.5 g, 0.91 mmol) cooled in a dry ice/acetone bath to ca. -78°C, immediately giving a red solution. The solution was stirred for ca. 30 minutes at ca. -78°C. The cold bath was then removed to allow the solution to warm to room temperature with continued stirring. The resulting orange solid was left overnight at room temperature under ambient atmospheric pressure in an environment of ammonia and N_2. The orange solid was dissolved in ca. 40 mL toluene and concentrated to ca. 10 mL. Storage at ca. -18 °C gave orange-pink crystals of **2a**. Yield: 0.15 g (30%). Mp: 140-145°C. ^{1}H NMR: (400 MHz, C_6D_6, 20°C) δ 0.11 (br s, 2H, amide H), δ 2.14 (s, 6H, o-C(CH_3)), δ 2.20 (s, 6H, o-C(CH_3)), δ 2.31 (s, 6H, p-C(CH_3)), δ 3.80 (s, 5H, η^5-C$_5H_5$), δ 5.31 (t, 1H, Ge-H), δ 6.86 (m, 7H, aromatic H). ^{13}C NMR (151 MHz, C_6D_6, 20°C): δ 20.77 (p-CH_3) δ 21.39 (o-CH_3), δ 21.43 (o-CH_3), δ 83.79 (η^5-C$_5H_5$), δ 128.36, 128.75, 136.24, 136.37, 136.67, 139.89, 146.68 (Ar(C)), δ 214.93 (CO), δ 215.76 (CO), C_{ipso}-Ge signal not observed. UV-VIS (hexane): λ_{max} (ε) 304 nm (8000 mol^{-1} L cm^{-1}). IR (Nujol, cm^{-1}): v_{CO} 1989 (s), v_{CO} 1932 (s), v_{Ge-H}, 1608 (s), v_{NH2} 3399 (s), v_{NH2} 3317 (s).

Ar^{iPr4}Ge(NH$_2$)(H)FeCp(CO)$_2$ (2b): Anhydrous ammonia (ca. 40 mL, twice-dried over sodium) was condensed onto solid **1b** (0.6g, 0.93 mmol) cooled in a dry ice/acetone bath ca. -78°C. The neat reaction initially remained a colorless solution with green solids but slowly turned red-orange

with increasing addition of $NH_3(l)$. The solution was stirred for half an hour at ca. -78°C. The cold bath was then removed to allow the solution to warm to room temperature with stirring; the orange solid was observed to change to a light green color upon warming. The resulting pale green solid was left overnight at room temperature under ambient atmospheric pressure in an environment of ammonia and N_2. Dissolution of the green solid in hexanes regenerated an orange solution. Cooling the flask in a ca. -10°C cold bath gave pink-orange crystals of **2b**. Yield: 0.15 g (25%). Mp: 200-205°C. ^{1}H NMR (400 MHz, C_6D_6, 20°C) δ 0.13 (br s, 2H, amide H), δ 1.10 (ddd, $^3J_{HH}$ = 6.2, 4.4, 1.6 Hz, 12H, CH(CH_3)), δ 1.38 (d, $^3J_{HH}$ = 6.8 Hz, 6H, CH(CH_3)), δ 1.53 (d, 6H, CH(CH_3)), δ 3.06 (sept, $^3J_{HH}$ = 12.9 Hz, 2H, CH(CH$_3$)), δ 3.25 (sept, $^3J_{HH}$ = 12.9 Hz, 2H, CH(CH$_3$)), δ 3.87 (s, 5H, η^5-C$_5H_5$), δ 7.17-7.37 (m, 9H, aromatic H). ^{13}C NMR (151 MHz, C_6D_6, 20°C): δ 22.42 (CH(CH$_3$)$_2$) δ 22.83 (CH(CH$_3$)$_2$), δ 26.04 (CH(CH$_3$)$_2$), δ 26.16 (CH(CH$_3$)$_2$), δ 30.66 (CH(CH$_3$)$_2$), δ 84.19 (η^5-C_5H_5), δ 122.23, 122.77, 126.33, 128.24, 130.60, 140.58, 145.75, 147.00, 147.32 (Ar(C)), δ 215.26 (CO), δ 215.50 (CO), C_{ipso}-Ge signal not observed. UV-vis (hexane): λ_{max} (ε) 330 nm (21,000 mol$^-$^{1} L cm^{-1}). IR (Nujol, cm^{-1}): ν_{CO} 1992 (s), ν_{CO} 1941 (s), ν_{Ge-H} 1653 (s), ν_{NH2} 3689 (s), ν_{NH2} 3629 (s).

Ar^{Me6}Ge(OH)(H)FeCp(CO)$_2$ (3): Deionized H_2O (14 µL, 0.80 mmol) was added dropwise by syringe to a solution of **1a** (0.5 g, 0.89 mmol) in hexanes (ca. 40 mL) at room temperature and stirred overnight. The resulting red solution was concentrated to ca. 20 mL. Storage overnight at room temperature gave colorless crystals of **3**. Yield: 0.05 g (10%) Mp: 190-200°C. ^{1}H NMR: (400 MHz, C_6D_6, 20°C) δ 0.61 (d, $^3J_{HH}$ = 6.8 Hz, 1H, O-H), δ 2.14 (s, 6H, o-C(CH_3)), δ 2.25 (s, 6H, o-C(CH_3)), δ 2.36 (s, 6H, o-C(CH_3)), δ 3.84 (s, 5H, η^5-C$_5H_5$), δ 6.21 (d, $^3J_{HH}$ = 6.8, 1H, Ge-H), δ 6.83 (br s, 2H, flanking m-aromatic H), δ 6.89 (br s, 2H, flanking m-aromatic H), δ 6.92 (dd, 2H, J_{HH} = 7.6, 2.4 Hz, central m-aromatic H), δ 7.23 (t, 1H, $^3J_{HH}$ = 7.5 Hz, central p-aromatic H). ^{13}C NMR (151 MHz, C_6D_6, 20°C): δ 20.70 (p-CH$_3$) δ 21.23 (o-CH$_3$), δ 21.25 (o-CH$_3$), δ 83.85 (η^5-

C_5H_5), δ 127.94, 127.99, 128.51, 129.02, 136.40, 136.64, 136.72, 139.02, 146.30 (Ar(C)), δ 213.85 (CO), δ 215.35 (CO), C_{ipso}-Ge signal not observed. UV-vis (hexane): λ_{max} (ε) 295 nm (70,000 mol^{-1} L cm^{-1}). IR (Nujol, cm^{-1}): ν_{CO} 1995 (s), ν_{CO} 1934 (s), ν_{Ge-H} 1600 (s), ν_{Ge-OH} 3580 (s).

2.3 RESULTS AND DISCUSSION

Synthesis. Treatment of Ar^{Me6}GeCl^{44,46} with 1 equivalent of K[FeCp(CO)$_2$]^{47} gave, after workup and recrystallization from toluene, dark green crystals of the ferriogermylene Ar^{Me6}GeFeCp(CO)$_2$ (**1a**) in moderate yield. Microscopic examination of a bulk sample of green crystals of **1a** showed that it also included small amounts of red crystals, which were later identified as a polymorph of **1a** rather than an impurity or decomposition product. To intentionally obtain the red polymorph, a green solution of **1a** in toluene was concentrated *in vacuo* to under ca. 10 mL while warmed in a 40°C water bath followed by rapid cooling to ca. -32°C. The solution remained dark green, but the crystals grown from this super-saturated solution were red. Interestingly, super-concentration of a solution of **1a** in the same manner described above and storage at a warmer temperature of ca. -18°C gave a third polymorph of **1a**, observed under the microscope as red-green dichroic crystals. Both sets of polymorphs dissolve in hexanes or toluene to produce a green solution of the same color as the original green polymorph. The absorption spectra for the solutions of green, red, or dichroic polymorphs are indistinguishable. The X-ray structural data for the three polymorphs show unique unit cells but similar structures that differ mainly in the bending angle at the central germanium atom. The molecular structure of the dichroic polymorph of **1a** was not definitively determined because the peaks of residual electron density appear in a location that did not correspond to any sensible atomic position. These peaks are likely erroneous although the data are otherwise well behaved. (see the Supporting Information).
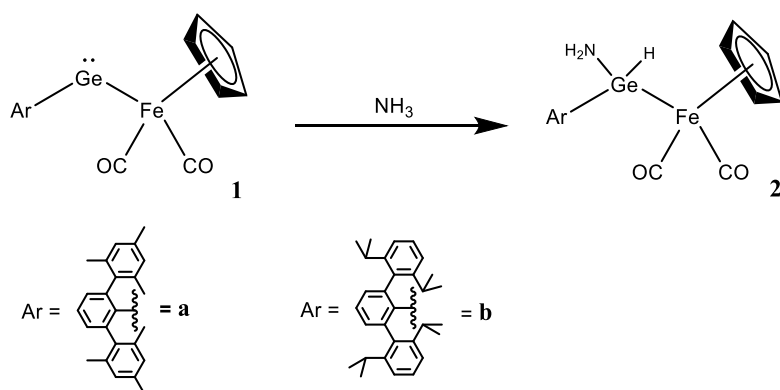
Scheme 1. The reaction of the neutral metallogermylene with NH_3.

The diarylgermylene $:Ge(Ar^{Me6})_2$ was shown earlier to insert into H-OR (R = H, Me bonds).[48] Similarly, investigation of the reactivity of ferriogermylene **1a** revealed that germanium inserts into the H–OH bond of adventitious water to form the germanium hydroxide $Ar^{Me6}Ge(OH)(H)FeCp(CO)_2$ (**3**). The NH_3 inserted products **2a** and **2b** could only be obtained cleanly by drying the ammonia twice over ca. 1 g Na(s) before the reaction. (Scheme 1)

The H_2O inserted product **3** was synthesized for spectroscopic analyses. (Scheme 2) Carrying out the reaction at a 1:1 ratio of **1a** to H_2O resulted in the formation of a white powder that ^1H NMR spectroscopy confirmed to be the arene $Ar^{Me6}H$. To prevent the elimination of the aryl ligand, a reaction containing a slight excess of **1a** (1.1 equivalents of **1a** to 1 equivalent of H_2O) was then carried out, which produced a red solution, from which colorless crystals of the germanium hydroxide $Ar^{Me6}Ge(OH)(H)FeCp(CO)_2$ (**3**) were grown.
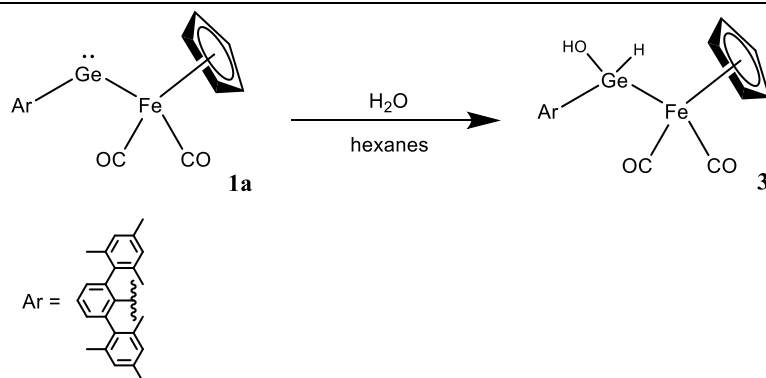
Scheme 2. The reaction of the neutral metallogermylene with H_2O.

Compounds **1a, 2ab,** and **3** were characterized by [^1]H NMR, [^13]C NMR, UV-vis, and IR spectroscopy.

Spectroscopy. The spectroscopic data for **1a** show similarities to the reported values of its more sterically crowded aryl-substituted analogues, $Ar^{Pri4}GeFeCp(CO)_2$ (**1b**) and $Ar^{Pri6}GeFeCp(CO)_2$[10] in the following ways: the [^1]H NMR spectrum of **1a** displays the signal of the cyclopentadienyl ring protons at 3.86 ppm (cf. the η^5-C_5H_5 protons of the ferriogermylenes **1b** and $Ar^{Pri6}GeFeCp(CO)_2$ appear at 3.84 ppm and 3.86 ppm, respectively); the UV-vis spectrum of **1a** has two absorptions at 430 and 616 nm, which are almost identical to the absorptions of **1b** and $Ar^{Pri6}GeFeCp(CO)_2$ at 430 and 620 nm;[10] and the IR spectrum of **1a** features two CO stretching frequencies at 1980 and 1940 cm^{-1}, which resemble the CO stretching frequencies of **1b** (1977 and 1917 cm^{-1}) and $Ar^{Pri6}GeFeCp(CO)_2$ (1984 and 1936 cm^{-1})[10]. The conclusion from these data is that the substitution on the aryl ligand has little effect on the electronic environment at the Fe atom.

In general, compounds **1a**, **1b**, and other reported metallogermylenes and metallostannylenes[6–8,10] show two bands in the UV-vis spectrum: a relatively intense band ($\varepsilon = 1860 – 2150$ mol^{-1} L cm^{-1}) in the 390 – 430 nm region corresponding to the $\pi \rightarrow \pi^*$ transition on the aryl ligand[49] and a less

intense band in the 580 – 620 nm region, tentatively assigned to to the n → p transition on the central germanium atom. This indicates that the identitiy of the transition metal (Fe, Cr, Mo, or W) does not have a large effect on the chromophores of these compounds. However, the cationic metallogermylene [(IPr)GeWCp*(CO)$_3$][BAr$^F_4$] of Tobita and coworkers[14] showed an absorption maximum at 671 nm, which was also assigned as the n → p (HOMO-LUMO) transition.[43] The shift towards the longer wavelength in [(IPr)GeWCp*(CO)$_3$][BAr$^F_4$] and the absence of a band in the 390 – 430 nm region, in comparison to **1a**, **1b**, and other neutral metallogermylenes, indicates that cationic character induces a shift to longer wavelengths.

The IR spectra of **1a** and **1b** show two CO stretching bands in the range 1980 – 1970 cm^{-1} and 1940 – 1910 cm^{-1}. This is in agreement with those observed for the ferriogermylenes Mes*GeFe(CO)$_2$R (R = Cp, Cp*)[5] and LGeFeCp(CO)$_2$ (L = CH{CMe(NAr}$_2$, Ar = 2,6-^{i}Pr$_2$C$_6$H$_3$).[8] The limits within which the ferriogermylene CO frequencies occur (2000 – 1910 cm^{-1}) is narrower than that of the metallogermylenes containing other transition metals (Cr, Mo, or W)[6,11,12,14] which show three major ν$_{CO}$ frequencies in the 2020 – 1880 cm^{-1} range. The fewer CO frequencies in **1a** and **1b** reflect a lower number of vibrational modes from fewer CO groups bound to the transition metal and the narrower range at higher wavenumbers indicates reduced backbonding into the π* orbitals of the carbonyls.

The non-bonding lone pair of electrons at the Ge atom together with the empty p-orbital perpendicular to the C-Ge-M (M = Fe, Cr, Mo, W) plane generate an interesting reactivity pattern resembling that of some transition metal complexes. This is shown by the insertion of [(IPr)GeWCp*(CO)$_3$][BAr$^F_4$] into H-H, Si-H, and B-H bonds.[43] Similarly, the ferriogermylenes **1a** and **1b** are both observed to insert into the N-H bond of NH$_3$. Condensation of an excess of NH$_3$ onto the ferriogermylenes ArGeFeCp(CO)$_2$ (Ar = Ar^{Me6} (**1a**), Ar^{iPr4} (**1b**)) gave a peach-

colored solid that, following workup and recrystallization from hexanes, gave colorless crystals of the amido germanium hydride $ArGe(NH_2)(H)FeCp(CO)_2$ (Ar = Ar^{Me6} (**2a**), Ar^{iPr4} (**2b**)).

The cyclopentadienyl ring protons of **2a** and **2b** (3.80 and 3.87 ppm, respectively) appear in the same region as those of the starting materials **1a** and **1b** (3.82 and 3.84 ppm, respectively). Additionally, the FT-IR spectra of the products show that the CO stretching frequencies of **2a** and **2b** (**2a:** 1989 and 1932 cm^{-1}, **2b**: 1992 and 1941 cm^{-1}) are in the same region as their corresponding starting materials. The addition of NH_3 to the germanium atom of the ferriogermylene has little or no effect on the CO stretching frequencies.

The germanium-bound -NH_2 resonances of **2a** and **2b** in their ^1H NMR spectra appear at 0.11 and 0.13 ppm. These resonances are shifted upfield in comparison to the -NH_2 resonances of the diarylgermylene amide $Ar_2Ge(NH_2)(H)$ (Ar = Ar^{Me6}: 0.37 ppm, Ar^{iPr4}: 0.37 ppm).[39] The Ge-H signals of **2a** and **2b** appear at 5.31 and 5.38 ppm, respectively, which are similarly upfield in comparison with their diarylgermylene counterparts $Ar_2Ge(NH_2)(H)$ (Ar = Ar^{Me6}: 5.47, Ar^{iPr4}: 5.84 ppm).[39] The increased shielding of the Ge-NH_2 and Ge-H protons observed in **2a** and **2b** suggest that the transition metal group {$FeCp(CO)_2$} acts as an electron donating group.

The FT-IR spectra of **2a** and **2b** each feature two stretching bands that correspond to the N-H stretching modes of the amide group (**2a**: 3399, 3317 cm^{-1}; **2b**: 3689, 3629 cm^{-1}). These amide stretching modes are weak yet distinct, similar to the IR spectra of their diarylgermylene analogues $Ar_2Ge(NH_2)(H)$ which also display weak N-H amide group stretching bands.[39] The data for **2a** are in agreement with the NH_2 stretching frequencies of $Ar^{Me6}_2Ge(NH_2)(H)$ (3397, 3323 cm^{-1})[39], while those of **2b** are at higher wavenumbers compared to its diarylgermylene analogue $Ar^{iPr4}_2Ge(NH_2)(H)$ (3381, 3313 cm^{-1}).[39] The germanium hydride frequencies of **2a** and **2b** (1608

cm^{-1} and 1653 cm^{-1}, respectively) are lower than their $Ar_2Ge(NH_2)(H)$ equivalents (Ar = Ar^{Me6}: 2110 cm^{-1} Ar^{iPr4}: 2080 cm^{-1})[39]. A similar shift towards lower wavenumbers is also seen in the Ge-H stretching frequency for **3** (1600 cm^{-1}) when compared to its diarylgermylene analogue (Ar^{Me6})$_2$Ge(OH)(H) (2150 cm^{-1}).[48] This shift in the Ge-H stretching mode towards lower wavenumbers, when compared to the Ge-H stretches seen in the diarylgermylene analogues, further confirms the ^{1}H NMR data that the {FeCp(CO)$_2$} moiety behaves as an electron donating group.

Compound **3** bears a resemblance to the insertion product (Ar^{Me6})$_2$Ge(OH)(H),[48] with the difference that a transition metal moiety replaces one of the aryl groups on the Ge atom. The ^{1}H NMR spectrum for **3** displays downfield shifted O-H and Ge-H protons (0.67 and 6.21 ppm, respectively) in comparison to the chemical shifts seen for (Ar^{Me6})$_2$Ge(OH)(H) (O-H: 0.47 ppm, Ge-H: 6.06 ppm).[48] However, the FT-IR spectrum of **3** shows that the hydroxyl and germanium hydride stretching frequencies (3580 and 3100 cm-1, respectively) have similar frequencies to their (Ar^{Me6})$_2$Ge(OH)(H) equivalents (O-H: 3600 cm^{-1}, Ge-H: 3000 cm^{-1}).[48]

The spectroscopic data for compound **3** also has similarities to the other insertion products **2a** and **2b**. The cyclopentadienyl ring protons of **3** (3.84 ppm) have a similar chemical shift to those of the amido germanium hydrides **2a** and **2b** (3.80 and 3.87 ppm, respectively). Likewise, the CO stretching frequencies for **3** (1995 and 1934 cm^{-1}) are similar to those of **2a** and **2b**. Both of these indicate that the electronegativity difference between the O and N atoms does not appear to have an effect on the electron density on the {FeCpCO$_2$} fragment. The UV-vis spectra of **2a**, **2b**, and **3** feature an absorption band in the near-UV region at 304 nm, 330 nm, and 295 nm, respectively. Both **2a** and **3**, which share the methyl-substituted aryl ligand, show a band at shorter wavelength

than the isopropyl-substituted insertion product **2b**, signifying that a substitution on the aryl ligand affects the electronic transition at the Ge atom.

X-Ray Crystal Structures. The metallogermylene **1a** forms three polymorphs: dark green blocks in the monoclinic space group $P2_1/c$, red blocks in the monoclinic space group $P2_1/c$ (Table S1), and dichroic red-green plates in the triclinic space group $P\bar{1}$ (Table S1). Crystals of the dark green polymorph grow more readily as the primary crystalline form, with the red polymorph being found in very small amounts in the crop of green crystals initially collected. The dichroic polymorph was produced from a crystal batch grown at ca. -18°C (*vide supra*). X-ray structural data for the three polymorphs show similar strucures and differ mainly in the interligand angle at germanium. All three polymorphs show that **1a** has a similar structure to that of the previously published **1b**,[10] in which a two-coordinate germanium is bound to a terphenyl group and an iron atom from the {FeCp(CO)$_2$} moiety. For the green polymorph of **1a**, the C1-Ge-Fe angle is 115.58(8)°, which is within range of other reported metallogermylenes (112.6°-117.8°)[6,10,14] and is similar to the C_{ipso}-Ge-C_{ipso} angle (114.4(2)°) of the analogous diaryl germylene :Ge(Ar^{Me6})$_2$.[45]

The red polymorph of **1a** has a C1-Ge-Fe angle of 109.45(9)°, which is ca. 6° narrower than that in the green polymorph, and also of other reported metallogermylenes (112.6°-117.8°),[6,10,14] as well as of the related diaryl :Ge(Ar^{Me6})$_2$ (114.4(2)°).[45] Otherwise, the Ge-C_{ipso} bond length (2.013(3) Å) and the Ge-Fe bond length (2.3901(6) Å) are essentially equal to those of the green polymorph (Ge-C_{ipso}: 2.003(3) Å, Ge-Fe: 2.3835(5) Å). In addition, the narrower C1-Ge-Fe angle of the red polymorph is within the same range seen for the NHC-Ge-M angles of the base-stabilized metallogermylenes LGeMCp(CO)$_2$ (L = CH{CMe(NAr)}$_2$, Ar = 2,6-^{i}Pr$_2$C$_6$H$_3$, M = Fe;[8] or L = {N(SiMe$_3$)C(Ph)C(SiMe$_3$)(C$_5$H$_4$N-2)}, M = Mo, W;[11] or L = {GeCl(Mes)$_2$}(I), Mes = mesityl, I = 1,3-diisopropyl-4,5-dimethylimidazol-2-ylidene, M = W[12]) (106.4°-110.8°).[8,11,12]

CHAPTER 2

The structural environment at the germanium atom for the dichroic and red polymorphs of **1a** are very similar and have C1-Ge-Fe angles near 110° which are narrower than the interligand angle 115.58(2)° in the green polymorph. However, the Ge-C$_{ipso}$ and Ge-Fe bond lengths in the red and dichroic polymorphs are essentially equal to those seen in the green polymorph.

Table 1. Selected Structural Data for **1-3**.

Compound	1a, green	1a, red	1a, dichroic	2a	2b	3
Ge-C1, Å	2.003(3)	2.013(3)	2.012(8)	1.9870(2)	1.992(3)	1.9929(15)
Ge-Fe, Å	2.3835(5)	2.3901(6)	2.3854(18)	2.4123(4)	2.3813(6)	2.4009(4)
C1-Ge-Fe, °	115.59(8)	109.48(9)	110.4(2)	115.5958(10)	120.69(9)	126.35(5)
Ge-H1, Å	-	-	-	1.5194(16)	1.5499(4)	1.4800(4)
Ge-N1, Å	-	-	-	1.8505(2)	1.757(4)	-
Ge-O1, Å	-	-	-	-	-	1.696(4)
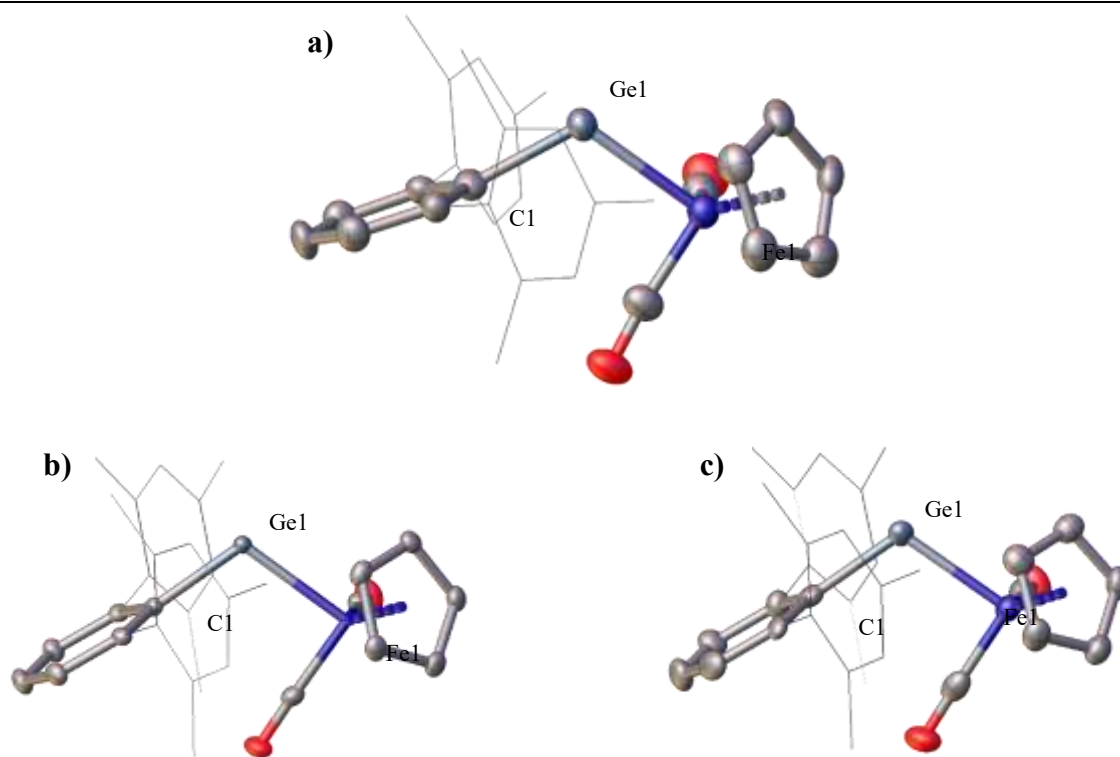
Figure 2. Thermal ellipsoid plot (50%) of **1a** (**a** (top): green polymorph, **b** (bottom left): red polymorph, **c** (bottom right): dichroic polymorph). H atoms are not shown and flanking phenyl

rings are shown as wire frames for clarity. **a)** Selected bond lengths (Å) and angles (deg): Ge1-Fe1 = 2.3835(5); Ge1-C1 = 2.003(3); C1-Ge1-Fe1 = 115.59(8). **b)** Selected bond lengths (Å) and angles (deg): Ge1-Fe1 = 2.3901(6); Ge1-C1 = 2.013(3); C1-Ge1-Fe1 = 109.48(9). **c)** Selected bond lengths (Å) and angles (deg): Ge1-Fe1 = 2.3854(18); Ge1-C1 = 2.012(8); C1-Ge1-Fe1 = 110.4(2).

The structures of all polymorphs of **1a** are similar to those of $Ar^{Me6}GeMoCp(CO)_3$[6] and $Ar^{Pri4}GeFeCp(CO)_2$[10]. All three structures feature an arylgermylene σ-bonded to an $M[Cp(CO)_n]$ group (M = Mo, Fe) and the ipso-carbon (C1) of the central aryl ring of the Ar^{Me6} ligand. The Ge-Fe bond distance in **1a** (green: 2.3835(5) Å, red: 2.3910(6) Å, dichroic: 2.3854(17) Å) is in agreement with the sum of the covalent radii of germanium (1.21 Å)[50] and iron (1.16 Å)[50] and is similar to that in the ferriogermylenes $Ar^{Pri4}GeFeCp(CO)_2$ (2.379(4) Å) and $Ar^{Pri6}GeFeCp(CO)_2$ (2.3747(8) Å).[10] For **1a** and its isopropyl-substituted analogue, **1b**, the bent geometry at the tetrel atom confirms the presence of a non-bonded tetrel lone pair[4,43].
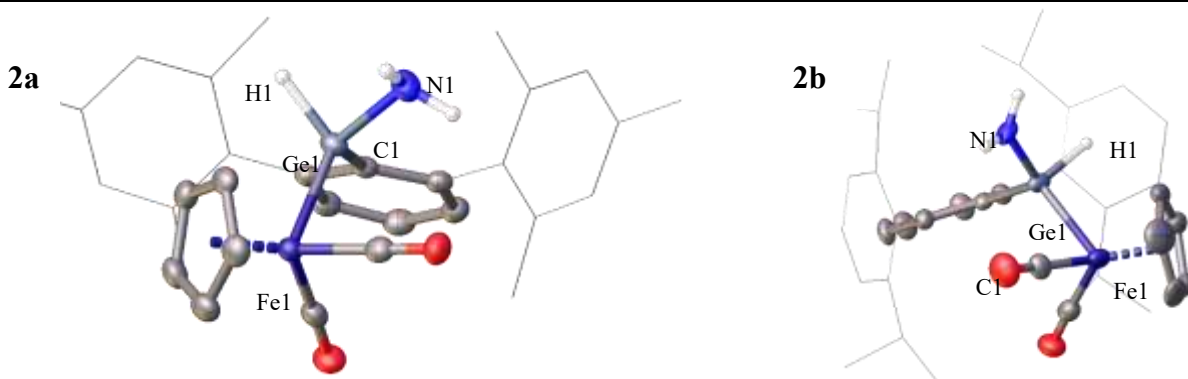
Figure 3. Thermal ellipsoid plots (50%) of **2a** (left) and **2b** (right). Carbon-bound H atoms and structural disorder are not shown for clarity. **2a** selected bond lengths (Å) and angles (deg): Ge1-Fe1 = 2.4123(4); Ge1-C1 = 1.9870(2); Ge1-N1 = 1.8505(2); Ge1-H1 = 1.5194(16); C1-Ge1-Fe1 = 115.5958(10). **2b** selected bond lengths (Å) and angles (deg): Ge1-Fe1 = 2.3813(6); Ge1-C1 = 1.992(3); Ge1-N1 = 1.757(4); Ge1-H1 = 1.5499(4); C1-Ge1-Fe1 = 120.69(9).

CHAPTER 2

Exposure of the ferriogermylenes **1a** and **1b** to an excess of ammonia resulted in the insertion of the Ge atom into the H—NH$_2$ bond to afford the amido germanium hydrides **2a** and **2b** as colorless crystals in the monoclinic, $P2_1/n$, and orthorhombic, $P2_12_12_1$, space groups, respectively. The insertion structures (Figure 3) feature a distorted tetrahedral coordination at the Ge atom. In **2b**, the amido and hydrogen groups bound to the central Ge atom are disordered over two sites at 50% occupancy each. The Ge-C1 (**2a**: 1.98706(2) and **2b**: 1.992(3) Å) and Ge-Fe (**2a**: 2.41237(4) and **2b**: 2.3813(6) Å) bond lengths remain almost unchanged following insertion, while the C1-Ge-Fe angle in **2a** and **2b** is wider (115.59(10)° and 120.69(9)°) than those in their respective precursors (109.45(9)° (**1a**, red), 110.0(2)° (**1a**, dichroic), 115.58(8)° (**1a**, green) and 115.27(6)° (**1b**)[10]).
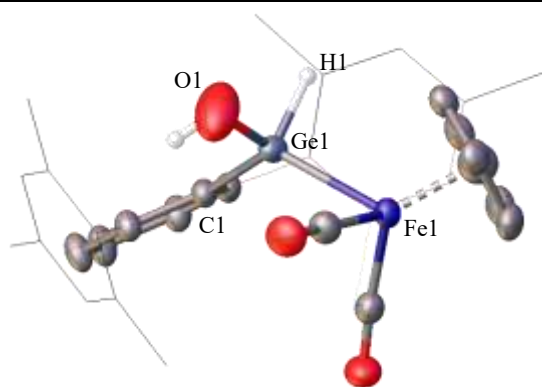
Figure 4. Thermal ellipsoid plots (50%) of **3**. Carbon-bound H atoms and structural disorder are not shown for clarity. **3** selected bond lengths (Å) and angles (deg): Ge1-Fe1 = 2.4009(4); Ge1-C1 = 1.9929(15); Ge1-O1 = 1.696(4); Ge1-H1 = 1.4800(4); C1-Ge1-Fe1 = 126.35(5).

The colorless crystals of **3** occur in the monoclinic space group $P2_1/c$ (Figure 4). As seen with **2a** and **2b**, the central Ge atom has a distorted tetrahedral coordination, whereas the Ge-Fe (2.4009(4) Å) and Ge-C1 (1.9929(15) Å) bond lengths remain unchanged from the starting material **1a**, and the C1-Ge-Fe angle widens from 109.45(9)° (**1a**, red), 110.0(2)° (**1a**, dichroic), or 115.58(8)° (**1a**, green) to 126.35(5)° (**3**). This general trend was also observed in the reaction of the

33

diarylgermylene :Ge(Ar^{Me6})$_2$ with H$_2$O, where the Ge-C$_{ipso}$ bond lengths remained unchanged while the interligand bond angle at the central Ge was observed to widen to 129.5(5)° from 114.2(2)° in its precursor.[48] Also like (Ar^{Me6})$_2$Ge(OH)(H), the hydrogen and hyroxide bound to the central Ge atom in **3** are disordered over two sites each with 50% occupancy. The interligand bridging angle in **3** is wider than that seen in the amido insertion products **2a** (115.5958(10) Å) and **2b** (120.69(9) Å).

2.4 CONCLUSION

The neutral ferriogermylenes ArGeFeCp(CO)$_2$ (Ar = Ar^{Me6} or Ar^{iPr4}) react with NH$_3$ and H$_2$O under mild conditions. Exposure to an excess of NH$_3$ produced the amido germanium hydrides and reaction with a deficiency of H$_2$O afford the germanium hydrido hydroxide. The ferriogermylene Ar^{Me6}GeFeCp(CO)$_2$ was observed to exist as three polymorphs with different bonding angles at germanium.

ASSOCIATED CONTENT

Supporting Information

Crystallographic data, photographs of polymorphs, video of polymorphs, and spectra (NMR, IR, UV-Vis).

Accession Codes

CCDC 2095118 (**1a, green**), 2101976 (**1a, red**), 2095126 (**2a**), 2095127 (**2b**), and 2095128 (**3**) contain the supplementary crystallographic data for this paper. These data can be obtained free of charge via www.ccdc.cam.ac.uk/data_request/cif, or by emailing data_request@ccdc.cam.ac.uk,

or by contacting The Cambridge Crystallographic Data Centre, 12 Union Road, Cambridge CB2 1EZ, UK; fax: +44 1223 336033.

AUTHOR INFORMATION

Corresponding Author

Philip P. Power – Department of Chemistry, University of California, Davis, California 95616, United States; orcid.org/0000-0002-6262-3209; Email: pppower@ucdavis.edu

Authors

Alice C. Phung – Department of Chemistry, University of California, Davis, California 95616, United States; https://orcid.org/0000-0002-0268-3971

James C. Fettinger - Department of Chemistry, University of California, Davis, California 95616, United States; orcid.org/0000-0002-6428-4909

Notes

The authors declare no competing financial interest.

2.5 REFERENCES

(1)   Mizuhata, Y.; Sasamori, T.; Tokitoh, N. Stable Heavier Carbene Analogues. *Chem. Rev.* **2009**, *109*, 3479–3511.

(2)   Hadlington, T. J.; Driess, M.; Jones, C. Low-Valent Group 14 Element Hydride Chemistry: Towards Catalysis. *Chem. Soc. Rev.* **2018**, *47*, 4176–4197.

(3)   Bourissou, D.; Guerret, O.; Gabbaï, F. P.; Bertrand, G. Stable Carbenes. *Chem. Rev.* **2000**, *100*, 39–92.

(4)   Power, P. P. Main-Group Elements as Transition Metals. *Nature* **2010**, *463*, 171–177.

(5)   Jutzi, P.; Leue, C. (Supermesityl)Chlorogermylene (Supermesityl = $^tBu_3C_6H_2$): Synthesis and Derivatization to (Super-Mesityl)Ferriogermylenes. *Organometallics* **1994**, *13*, 2898–2899.

(6)   Pu, L.; Twamley, B.; Haubrich, S. T.; Olmstead, M. M.; Mork, B. V.; Simons, R. S.; Power, P. P. Triple Bonding to Germanium: Characterization of the Transition Metal Germylynes (η^5-C_5H_5)(CO)$_2$M≡Ge-C_6H_3-2,6-Mes$_2$ (M = Mo, W; Mes = $-C_6H_2$-2,4,6-Me$_3$) and (η^5-C_5H_5)(CO)$_2$M≡Ge-C_6H_3-2,6-Trip$_2$ (M = Cr, Mo, W; Trip = $-C_6H_2$-2,4,6-$^iPr_3$) and the Related Single Bonded Metallogermylenes (η^5-C_5H_5)(CO)$_3$M-G̈e-C_6H_3-2,6-Trip$_2$ (M = Cr, W). *J. Am. Chem. Soc.* **2000**, *122*, 650–656.

(7)   Eichler, B. E.; Phillips, A. D.; Haubrich, S. T.; Mork, B. V.; Power, P. P. Synthesis, Structures, and Spectroscopy of the Metallostannylenes (η^5-C_5H_5)(CO)$_3$ M−S̈n−C_6H_3-2,6-Ar$_2$ (M = Cr, Mo, W; Ar = C_6H_2-2,4,6-Me$_3$, C_6H_2-2,4,6-Pr$^i_3$). *Organometallics* **2002**, *21* (25), 5622–5627.

(8)   Inoue, S.; Driess, M. Isolable Metallo-Germylene and Metallo-Stannylene σ-Complexes with Iron. *Organometallics* **2009**, *28*, 5032–5035.

(9)   Hayes, P. G.; Gribble, C. W.; Waterman, R.; Tilley, T. D. A Hydrogen-Substituted Osmium Stannylene Complex: Isomerization to a Metallostannylene Complex via an Unusual α-Hydrogen Migration from Tin to Osmium. *J. Am. Chem. Soc.* **2009**, *131*, 4606–4607.

(10)   Lei, H.; Guo, J.-D.; Fettinger, J. C.; Nagase, S.; Power, P. P. Synthesis, Characterization, and CO Elimination of Ferrio-Substituted Two-Coordinate Germylenes and Stannylenes. *Organometallics* **2011**, *30*, 6316–6322.

(11)   Leung, W.-P.; Chiu, W.-K.; Mak, T. C. W. Synthesis and Structural Characterization of Metallogermylenes, Cp-Substituted Germylene, and a Germanium(II)-Borane Adduct from Pyridyl-1-Azaallyl Germanium(II) Chloride. *Organometallics* **2012**, *31*, 6966–6971.

(12)   Tashita, S.; Watanabe, T.; Tobita, H. Synthesis of a Base-Stabilized (Chlorogermyl)Metallogermylene and Its Photochemical Conversion to a (Chlorogermyl)Germylyne Complex. *Chem. Lett.* **2013**, *42*, 43–44.

(13)   Liu, H.-J.; Guihaumé, J.; Davin, T.; Raynaud, C.; Eisenstein, O.; Tilley, T. D. 1,2-Hydrogen Migration to a Saturated Ruthenium Complex via Reversal of Electronic Properties for

Tin in a Stannylene-to-Metallostannylene Conversion. *J. Am. Chem. Soc.* **2014**, *136*, 13991–13994.

(14)   Inomata, K.; Watanabe, T.; Tobita, H. Cationic Metallogermylene and Dicationic Dimetallodigermenes: Synthesis by Chloride Abstraction from *N* -Heterocyclic Carbene-Stabilized Chlorometallogermylenes. *J. Am. Chem. Soc.* **2014**, *136*, 14341–14344.

(15)   Filippou, A. C.; Baars, B.; Chernov, O.; Lebedev, Y. N.; Schnakenburg, G. Silicon-Oxygen Double Bonds: A Stable Silanone with a Trigonal-Planar Coordinated Silicon Center. *Angew. Chem. Int. Ed.* **2014**, *53*, 565–570.

(16)   Pu, L.; Power, P. P.; Boltes, I.; Herbst-Irmer, R. Synthesis and Characterization of the Metalloplumbylenes $(\eta^5\text{-}C_5H_5)(CO)_3M\text{-}\breve{P}b\text{-}C_6H_3\text{-}2,6\text{-}Trip_2$ (M = Cr, Mo, or W; Trip = $-C_6H_2$ - 2,4,6-^{i}Pr$_3$). *Organometallics* **2000**, *19*, 352–356.

(17)   Simons, R. S.; Power, P. P. $(\eta^5\text{-}C_5H_5)(CO)_2$ MoGeC$_6$H$_3$-2,6-Mes$_2$: A Transition-Metal Germylyne Complex. *J. Am. Chem. Soc.* **1996**, *118*, 11966–11967.

(18)   Filippou, A. C.; Philippopoulos, A. I.; Portius, P.; Neumann, D. U. Synthesis and Structure of the Germylyne Complexes Trans-[X(Dppe)$_2$W≡Ge(η^1-Cp*)] (X=Cl, Br, I) and Comparison of the W≡E Bonds (E=C, Ge) by Density Functional Calculations. *Angew. Chem. Int. Ed.* **2000**, *39*, 2778–2781.

(19)   Filippou, A. C.; Portius, P.; Philippopoulos, A. I.; Rohde, H. Triple Bonding to Tin: Synthesis and Characterization of the Stannylyne Complex Trans-[Cl(PMe$_3$)$_4$W≡Sn-C$_6$H$_3$-2,6-Mes$_2$]. *Angew. Chem. Int. Ed.* **2003**, *42*, 445–447.

(20)   Filippou, A. C.; Weidemann, N.; Schnakenburg, G.; Rohde, H.; Philippopoulos, A. I. Tungsten-Lead Triple Bonds: Syntheses, Structures, and Coordination Chemistry of the Plumbylidyne Complexestrans-[X(PMe$_3$)$_4$W≡Pb(2,6-Trip$_2$C$_6$H$_3$)]. *Angew. Chem. Int. Ed.* **2004**, *43*, 6512–6516.

(21)   Filippou, A. C.; Chernov, O.; Stumpf, K. W.; Schnakenburg, G. Metal-Silicon Triple Bonds: The Molybdenum Silylidyne Complex [Cp(CO)$_2$Mo≡Si-R]. *Angewandte Chemie International Edition* **2010**, *49*, 3296–3300.

(22)   Lebedev, Y. N.; Das, U.; Schnakenburg, G.; Filippou, A. C. Coordination Chemistry of [E(Idipp)]$^{2+}$ Ligands (E = Ge, Sn): Metal Germylidyne [Cp*(CO)$_2$W≡Ge(Idipp)]$^+$ and Metallotetrylene [Cp*(CO)$_3$W–E(Idipp)]$^+$ Cations. *Organometallics* **2017**, *36*, 1530–1540.

(23)   Yoshimoto, T.; Hashimoto, H.; Hayakawa, N.; Matsuo, T.; Tobita, H. A Silylyne Tungsten Complex Having an Eind Group on Silicon: Its Dimer–Monomer Equilibrium and Cycloaddition Reactions with Carbodiimide and Diaryl Ketones. *Organometallics* **2016**, *35*, 3444–3447.

(24)   Queen, J. D.; Phung, A. C.; Caputo, C. A.; Fettinger, J. C.; Power, P. P. Metathetical Exchange between Metal–Metal Triple Bonds. *J. Am. Chem. Soc.* **2020**, *142*, 2233-2237.

(25)   Wesemann, L.; Widemann, M.; Eichele, K.; Schubert, H.; Sindlinger, C. P.; Klenner, S.; Pöttgen, R. Synthesis and Hydrogenation of Heavy Homologues of Rhodium Carbynes: [(Me₃P)₂(Ph₃P)Rh≡E-Ar*] (E = Sn, Pb). *Angew. Chem. Int. Ed.* **2021**, *60*, 5882-5889.

(26)   Spikes, G. H.; Fettinger, J. C.; Power, P. P. Facile Activation of Dihydrogen by an Unsaturated Heavier Main Group Compound. *J. Am. Chem. Soc.* **2005**, *127*, 12232–12233.

(27)   Peng, Y.; Brynda, M.; Ellis, B. D.; Fettinger, J. C.; Rivard, E.; Power, P. P. Addition of H₂ to Distannynes under Ambient Conditions. *Chem. Commun.* **2008**, No. 45, 6042.

(28)   Brown, Z. D.; Power, P. P. Mechanisms of Reactions of Open-Shell, Heavier Group 14 Derivatives with Small Molecules: N−π* Back-Bonding in Isocyanide Complexes, C–H Activation under Ambient Conditions, CO Coupling, and Ancillary Molecular Interactions. *Inorg. Chem.* **2013**, *52*, 6248–6259.

(29)   Wang, S.; Sherbow, T. J.; Berben, L. A.; Power, P. P. Reversible Coordination of H₂ by a Distannyne. *J. Am. Chem. Soc.* **2018**, *140*, 590–593.

(30)   Cui, C.; Olmstead, M. M.; Power, P. P. Reactivity of Ar'GeGeAr' (Ar' = C₆H₃-2,6-Dipp₂, Dipp = C₆H₃-2,6-*i*Pr₂) toward Alkynes: Isolation of a Stable Digermacyclobutadiene. *J. Am. Chem. Soc.* **2004**, *126*, 5062–5063.

(31)   Peng, Y.; Ellis, B. D.; Wang, X.; Fettinger, J. C.; Power, P. P. Reversible Reactions of Ethylene with Distannynes Under Ambient Conditions. *Science* **2009**, *325*, 1668–1670.

(32)   Summerscales, O. T.; Fettinger, J. C.; Power, P. P. C–H Activation of Cycloalkenes by Dimetallynes (M = Ge, Sn) under Ambient Conditions. *J. Am. Chem. Soc.* **2011**, *133*, 11960–11963.

(33)   Summerscales, O. T.; Caputo, C. A.; Knapp, C. E.; Fettinger, J. C.; Power, P. P. The Role of Group 14 Element Hydrides in the Activation of C–H Bonds in Cyclic Olefins. *J. Am. Chem. Soc.* **2012**, *134*, 14595–14603.

(34)   Sasamori, T.; Sugahara, T.; Agou, T.; Sugamata, K.; Guo, J.-D.; Nagase, S.; Tokitoh, N. Reaction of a Diaryldigermyne with Ethylene. *Chem. Sci.* **2015**, *6*, 5526–5530.

(35)   Guo, J.-D.; Sasamori, T. Activation of Small Molecules by Compounds That Contain Triple Bonds Between Heavier Group-14 Elements. *Chem. Asian J.* **2018**, *13*, 3800–3817.

(36)   Hanusch, F.; Groll, L.; Inoue, S. Recent Advances of Group 14 Dimetallenes and Dimetallynes in Bond Activation and Catalysis. *Chem. Sci.* **2020**, 2001-2015.

(37)   Kajiwara, T.; Takeda, N.; Sasamori, T.; Tokitoh, N. Unprecedented Insertion Reaction of a Silylene into a B–B Bond and Generation of a Novel Borylsilyl Anion by Boron–Metal Exchange Reaction of the Resultant Diborylsilane. *Chem. Commun.* **2004**, No. 19, 2218–2219.

(38)   Peng, Y.; Ellis, B. D.; Wang, X.; Power, P. P. Diarylstannylene Activation of Hydrogen or Ammonia with Arene Elimination. *J. Am. Chem. Soc.* **2008**, *130*, 12268–12269.

(39)   Peng, Y.; Guo, J.-D.; Ellis, B. D.; Zhu, Z.; Fettinger, J. C.; Nagase, S.; Power, P. P. Reaction of Hydrogen or Ammonia with Unsaturated Germanium or Tin Molecules under Ambient Conditions: Oxidative Addition versus Arene Elimination. *J. Am. Chem. Soc.* **2009**, *131*, 16272–16282.

(40)   Wang, X.; Zhu, Z.; Peng, Y.; Lei, H.; Fettinger, J. C.; Power, P. P. Room-Temperature Reaction of Carbon Monoxide with a Stable Diarylgermylene. *J. Am. Chem. Soc.* **2009**, *131*, 6912–6913.

(41)   Lai, T. Y.; Gullett, K. L.; Chen, C.-Y.; Fettinger, J. C.; Power, P. P. Reversible Complexation of Alkynes by a Germylene. *Organometallics* **2019**, *38*, 1421–1424.

(42)   Gullett, K. L.; Lai, T. Y.; Chen, C.-Y.; Fettinger, J. C.; Power, P. P. Reversible Binding of Ethylene and Propylene by Germylenes. *Organometallics* **2019**, *38*, 1425–1428.

(43)   Inomata, K.; Watanabe, T.; Miyazaki, Y.; Tobita, H. Insertion of a Cationic Metallogermylene into E–H Bonds (E = H, B, Si). *J. Am. Chem. Soc.* **2015**, *137*, 11935–11937.

(44)   Ruhlandt-Senge, K.; Ellison, J. J.; Wehmschulte, R. J.; Pauer, F.; Power, P. P. Isolation and Structural Characterization of Unsolvated Lithium Aryls. *J. Am. Chem. Soc.* **1993**, *115*, 11353–11357.

(45)   Simons, R. S.; Pu, L.; Olmstead, M. M.; Power, P. P. Synthesis and Characterization of the Monomeric Diaryls $M\{C_6H_3\text{-}2,6\text{-}Mes_2\}_2$ (M = Ge, Sn, or Pb; Mes = $2,4,6\text{-}Me_3C_6H_2-$) and Dimeric Aryl−Metal Chlorides $[M(Cl)\{C_6H_3\text{-}2,6\text{-}Mes_2\}]_2$ (M = Ge or Sn). *Organometallics* **1997**, *16*, 1920–1925.

(46)   Pu, L.; Olmstead, M. M.; Power, P. P.; Schiemenz, B. Synthesis and Characterization of the Monomeric Terphenyl−Metal Halides $Ge(Cl)\{C_6H_3\text{-}2,6\text{-}Trip_2\}$ (Trip = $C_6H_2\text{-}2,4,6\text{-}i\text{-}Pr_3$) and $Sn(I)\{C_6H_3\text{-}2,6\text{-}Trip_2\}$ and the Terphenyl−Metal Amide $Sn\{N(SiMe_3)_2\}\{C_6H_3\text{-}2,6\text{-}Trip_2}^{\dagger}$. *Organometallics* **1998**, *17*, 5602–5606.

(47)   Plotkin, J. S.; Shore, S. G. Convenient Preparation and Isolation of Pure Potassium Cyclopentadienyldicarbonylferrate, $K[(\eta^5\text{-}C_5H_5)Fe(CO)_2]$. *Inorg. Chem.* **1981**, *20*, 284–285.

(48)   Erickson, J. D.; Vasko, P.; Riparetti, R. D.; Fettinger, J. C.; Tuononen, H. M.; Power, P. P. Reactions of *m*-Terphenyl-Stabilized Germylene and Stannylene with Water and Methanol: Oxidative Addition versus Arene Elimination and Different Reaction Pathways for Alkyl- and Aryl-Substituted Species. *Organometallics* **2015**, *34*, 5785–5791.

(49)   Phillips, A. D.; Wright, R. J.; Olmstead, M. M.; Power, P. P. Synthesis and Characterization of $2,6\text{-}Dipp_2\text{-}H_3C_6SnSnC_6H_3\text{-}2,6\text{-}Dipp_2$ (Dipp = $C_6H_3\text{-}2,6\text{-}Pr^i_2$): A Tin Analogue of an Alkyne. *J. Am. Chem. Soc.* **2002**, *124*, 5930–5931.

(50)   Pyykkö, P.; Atsumi, M. Molecular Single-Bond Covalent Radii for Elements 1-118. *Chem. Eur. J.* **2009**, *15*, 186–197.

2.6 SUPPLEMENTARY INFORMATION

Table of Contents

X-ray Crystallography

Crystals of **1a**, **2ab**, and **3** were removed from a Schlenk flask under a stream of nitrogen and immediately covered with a layer of hydrocarbon oil. A suitable crystal was selected, attached to a glass fiber on a copper pin and quickly placed in the cold N_2 stream on the diffractometer. Data was collected at 100 K on a Bruker APEX DUO diffractometer with Mo Kα radiation ($\lambda = 0.71073$ Å). Absorption corrections were applied using SADABS.[S1] The crystal structures were solved by direct methods and refined by full matrix least-squares procedures in SHELXTL.[S2] All non-H atoms were refined anisotropically.

Table S1. Selected X-ray Crystallographic data for **1a**: green, red, and dichroic polymorphs

1a polymorph	green	red	dichroic
Formula		$C_{31}H_{30}FeGeO_2$	
Fw		562.99	
Color, habit	green, block	red, block	green & red, plate
Space group	$P2_1/c$	$P2_1/c$	$P\text{-}1$
A, å	15.7808(7)	16.2036(3)	8.915(3)
B, å	9.6448(4)	8.8948(2)	16.229(6)
C, å	16.9149(8)	37.0650(8)	18.739(7)
A, °	90	90	76.499(10)
B, °	90.657(2)	101.5790(10)	86.019(10)
Γ, °	90	90	89.859(11)
V, å³	2574.3(2)	5233.38(19)	2629.7(16)
Z	4	8	4
Crystal size, mm	0.149 × 0.113 × 0.039	0.383 × 0.192 × 0.183	0.233 × 0.203 × 0.075
D_{calc}, g cm⁻³	1.453	1.429	1.442
Abs. M, mm⁻¹	1.757	1.729	1.721
2θ, °	4.816 to 55.064	2.566 to 57.542	3.794 to 55.634
R(int)	0.0419	0.0497	0.2672
Obs. Reflns. [i>2σ(i)]	5928	13458	155382
Data/restraints/parameters	5928/0/322	13458/0/644	12237/0/643
R_1, obsd. Reflns.	0.0400	0.0503	0.1063

Table S2. Selected X-ray Crystallographic data for 2-3.

Compound	2a	2b	3
Formula	$C_{31}H_{33}FeGeNO_2$	$C_{37}H_{45}FeGeNO_2$	$C_{31}H_{32}FeGeO_3$
Fw	580.02	664.18	581.00
Color, habit	Colorless, block	Colorless, block	Colorless, block
Space group	$P2_1/n$	$P2_12_12_1$	$P2_1/c$
A, å	11.2499(2)	8.1224(4)	15.7736(14)
B, å	14.6309(2)	18.5737(9)	9.8287(9)
C, å	16.4228(3)	22.0779(11)	17.272(2)
A, °	90	90	90
B, °	96.4474(6)	90	90.304(10)
Γ, °	90	90	90
V, å³	2686.03(8)	3330.7(3)	2677.7(5)
Z	4	4	4
Crystal size, mm	0.357 × 0.257 × 0.168	0.365 × 0.269 × 0.241	0.558 × 0.48 × 0.408
D_{calc}, g cm⁻³	1.434	1.325	1.441
Abs. M, mm⁻¹	5.924	1.370	1.695
2θ, °	8.116 to 137.16	4.292 to 61.262	4.768 to 59.998
R(int)	0.0277	0.0378	0.0149
Obs. Reflns. [i>2σ(i)]	4902	10275	7798
Data/restraints/parameters	4902/0/457	10275/58/463	7798/8/350
R_1, obsd. Reflns.	0.0277	0.0378	0.0328

Figure S1. Photograph of **1a**, green polymorph

Figure S2. Photograph of **1a**, red polymorph.

Figure S3. Photograph of **1a**, red-green dichroic polymorph.

CHAPTER 2

NMR Spectra

Figure S4. ^{1}H NMR spectrum of **1a** in C$_6$D$_6$ at 298 K.

Figure S5. ^{13}C{^{1}H} NMR spectrum of **1a** in C$_6$D$_6$ at 298 K.

NMR Spectra

Figure S6. ^{1}H NMR spectrum of **2a** in C$_6$D$_6$ at 298 K.

Figure S7. ^{13}C{^{1}H} NMR spectrum of **2a** in C$_6$D$_6$ at 298 K.

NMR Spectra

Figure S8. ^{1}H NMR spectrum of **2b** in C$_6$D$_6$ at 298 K.

Figure S9. ^{13}C{^{1}H} NMR spectrum of **2b** in C$_6$D$_6$ at 298 K.

NMR Spectra

Figure S10. ^{1}H NMR spectrum of **3** in C_6D_6 at 298 K.
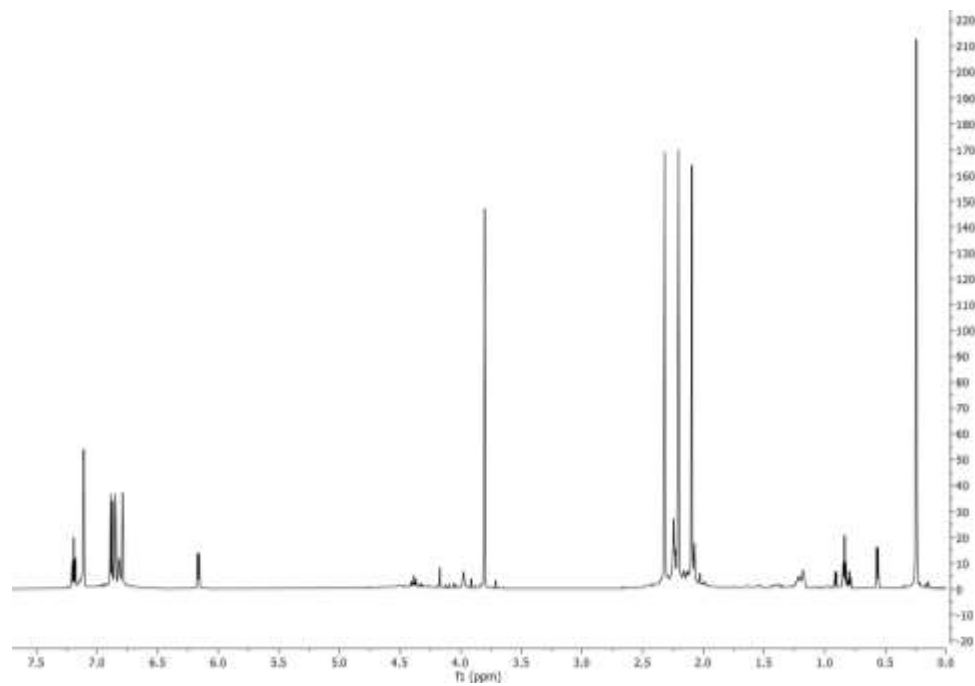
Figure S11. ^{13}C{^{1}H} NMR spectrum of **3** in C_6D_6 at 298 K.
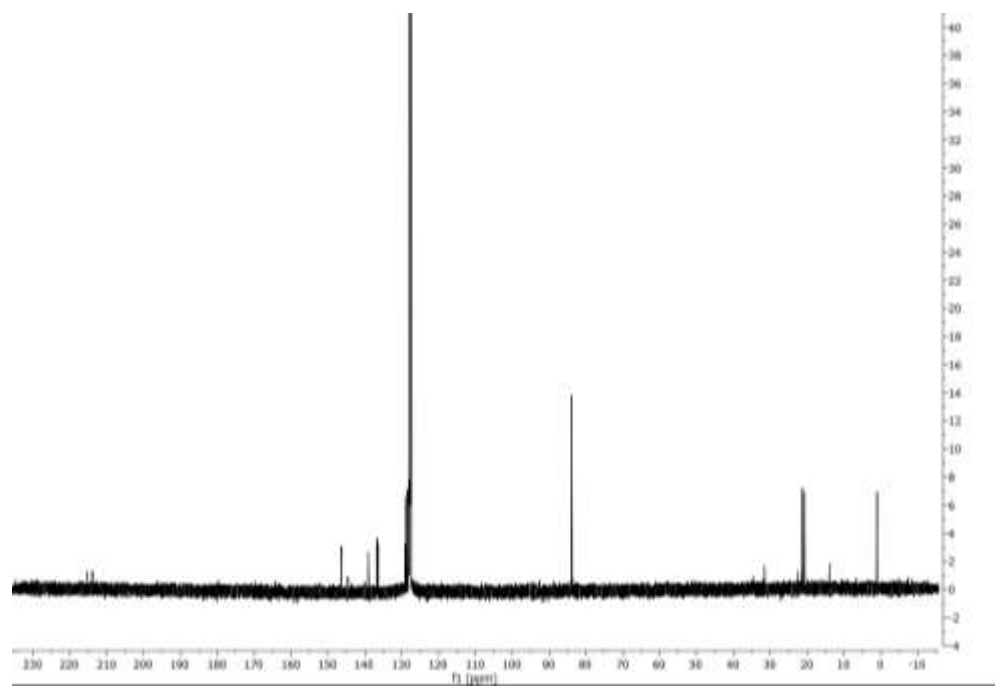
UV-vis Spectra

Figure S12. UV-vis spectrum of **1a** in hexanes at 298 K.

ArMe6GeFe(CO)2, 250 µM
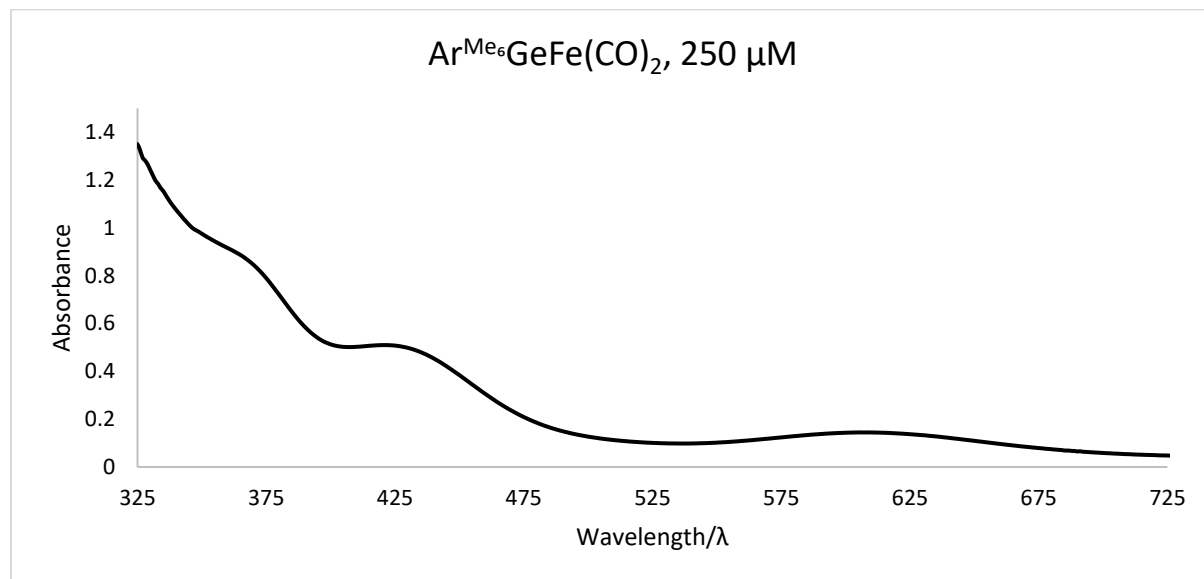
Figure S13. UV-vis spectrum of **2a** in hexanes at 298 K.

ArMe6Ge(NH2)(H)Fe(CO)2, 62 µM
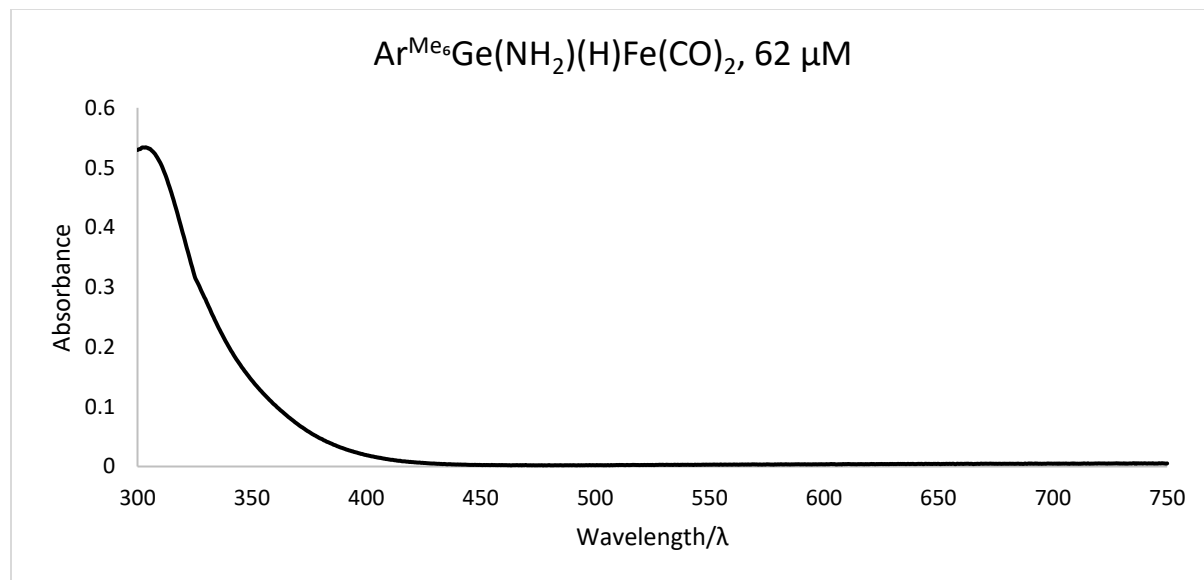
UV-vis Spectra

Figure S14. UV-vis spectrum of **2b** in hexanes at 298 K.
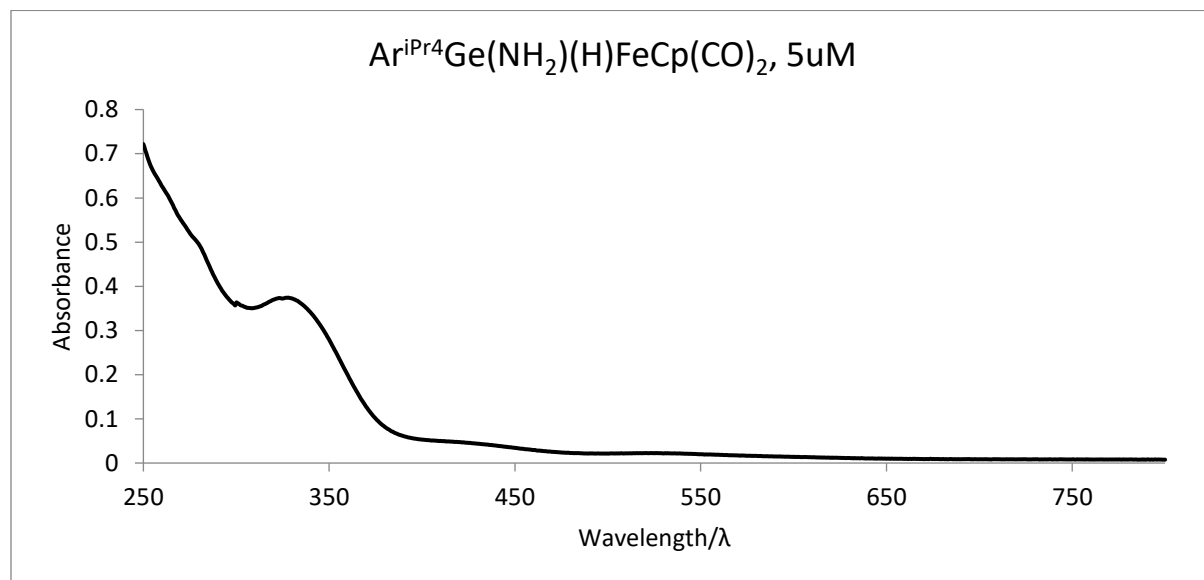
$Ar^{iPr4}Ge(NH_2)(H)FeCp(CO)_2$, 5uM

Figure S15. UV-vis spectrum of **3** in hexanes at 298 K.

$Ar^{Me6}Ge(OH)(H)Fe(CO)_2$, 1.4 uM
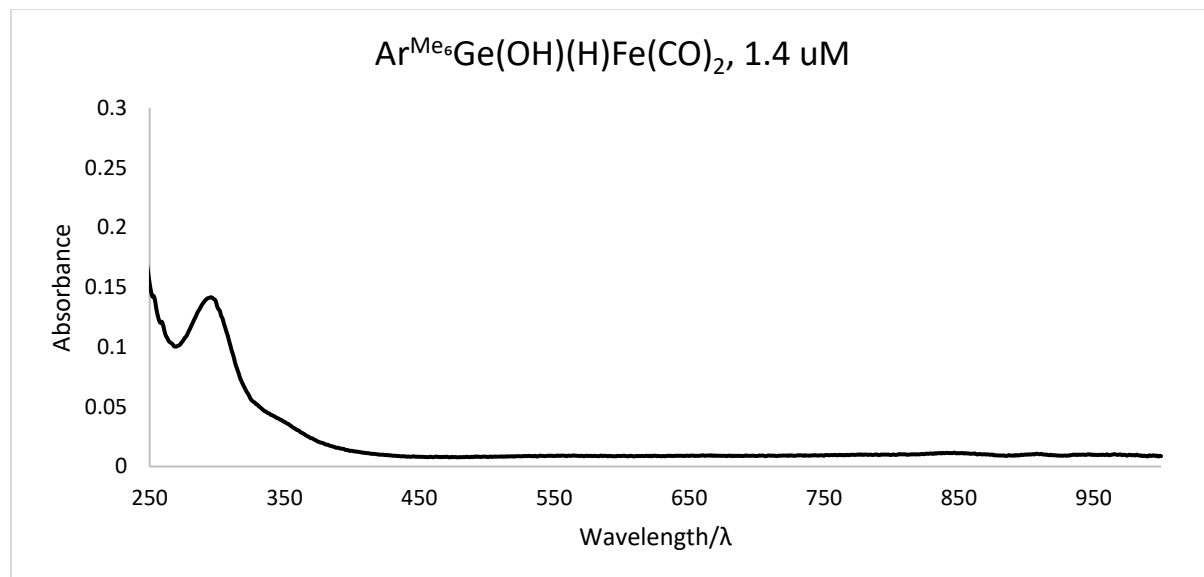
IR spectra

Figure S16. Infrared spectrum of **1a**
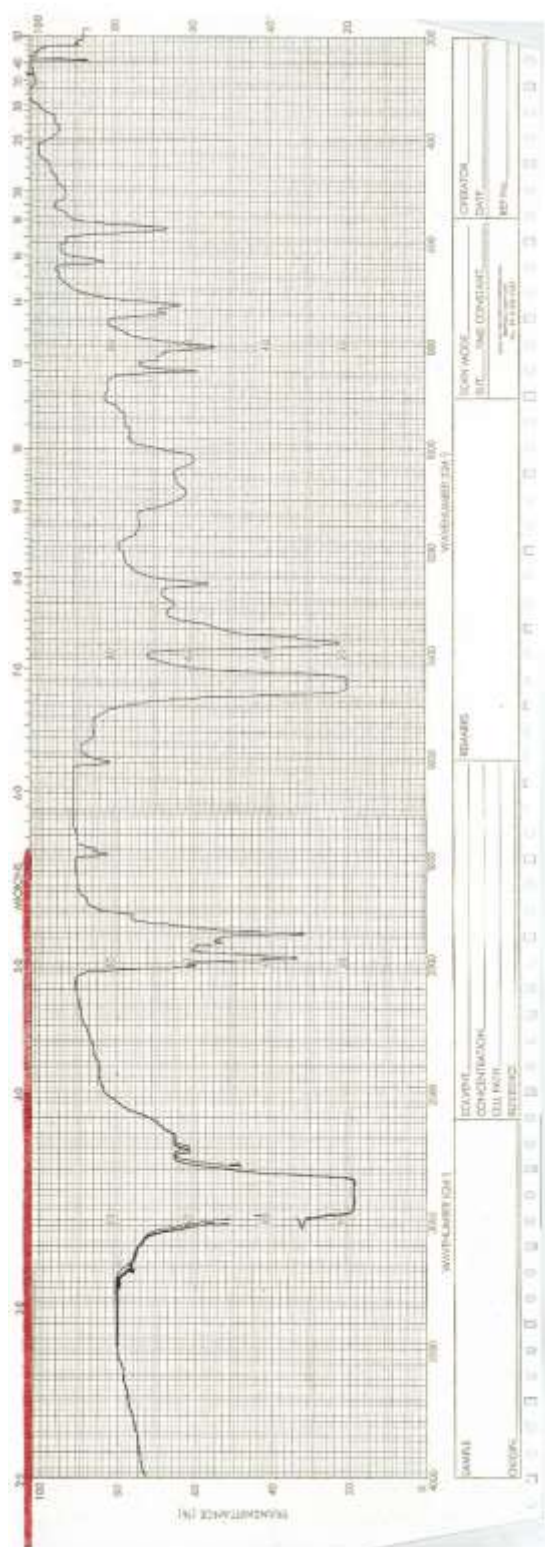
IR spectra
Figure S17. Infrared spectrum of **2a**
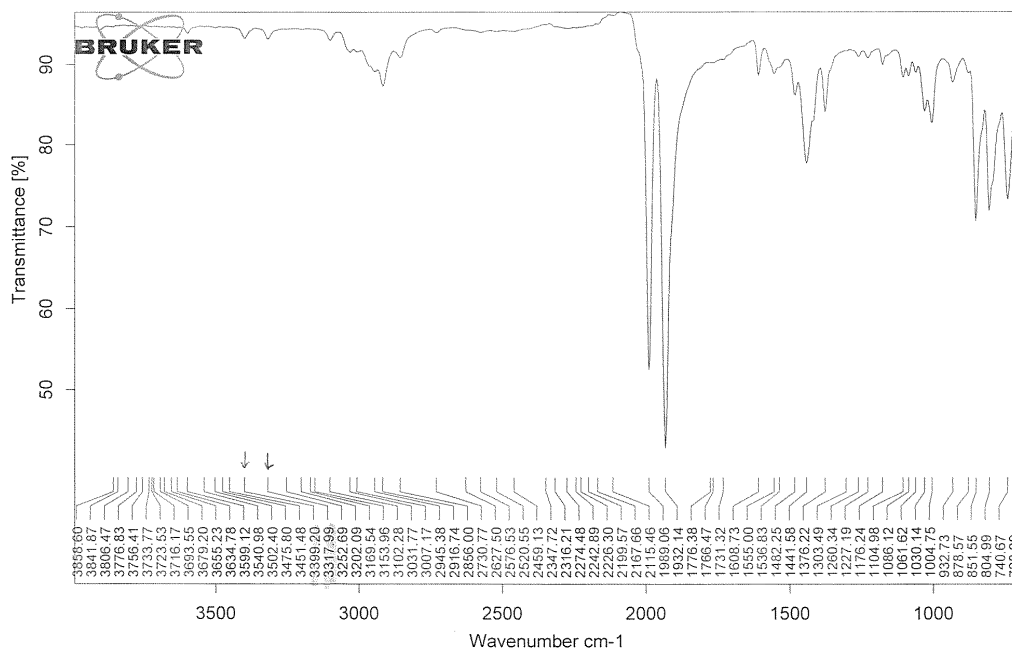
IR spectra
Figure S18. Infrared spectrum of **2b**
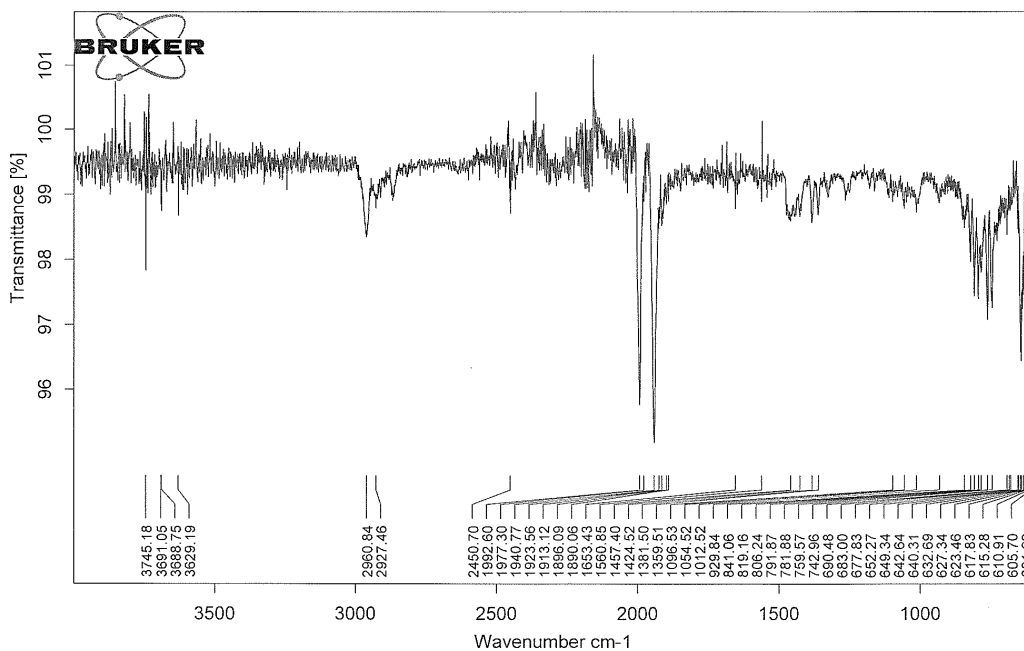
IR spectra
Figure S19. Infrared spectrum of **3**.
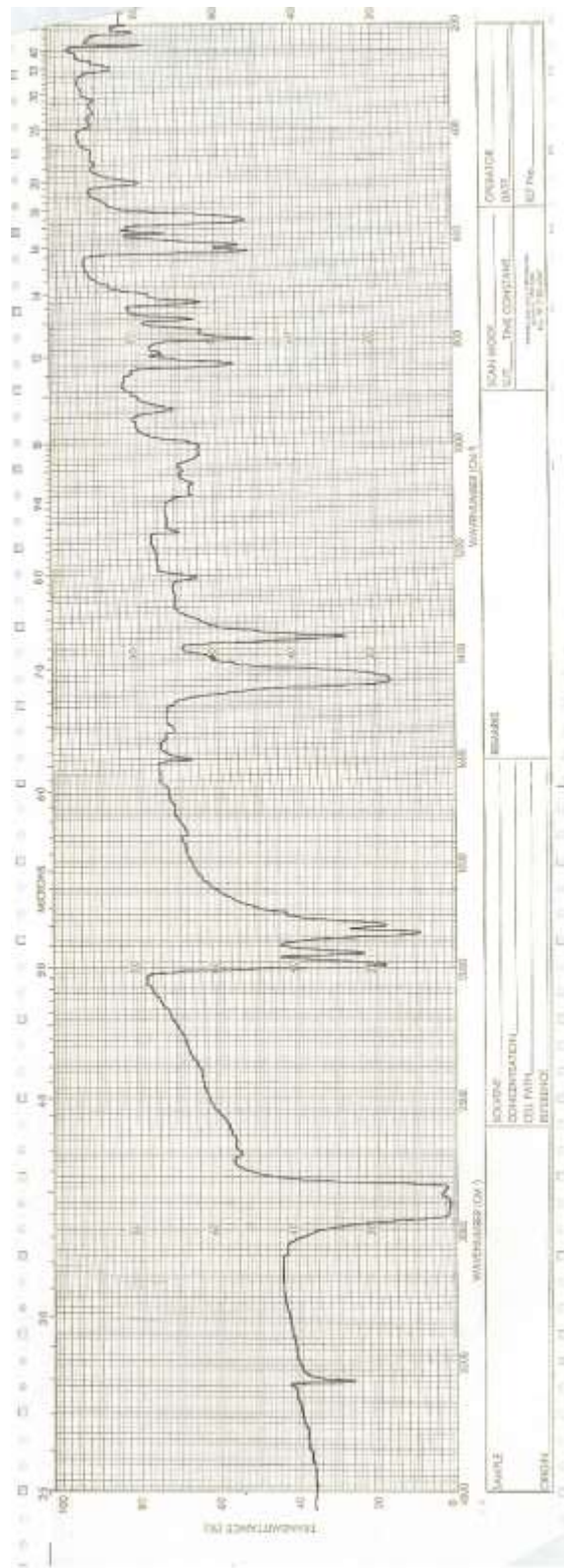
SI References

S1 Bruker, Bruker AXS Inc., Madison, Wisconsin, USA, **2001**

S2 G. M. Sheldrick, Acta Cryst. A 2015, 71, 3-8.

S3 Dolomanov, O. V.; Bourhis, L. J.; Gildea, R. J.; Howard, J. A. K.; Puschmann, H.; *OLEX2*: A complete structure solution, refinement and analysis program. J. Appl. Cryst, **2009**, *42*, 339-341.

A Series of Ferriostannylenes with Differing Terphenyl Substituents

Alice C. Phung,[1] James C. Fettinger,[1] Philip P. Power[1]*

[1]Department of Chemistry, University of California, 1 Shields Avenue, Davis, California 95616

ABSTRACT: A series of ferriostannylenes $Ar^{Me6}SnFeCp(CO)_2$ (Ar^{Me6} = $-C_6H_3$-(C_6H_2-2,4,6-$Me_3)_2$, Cp = η^5-C_5H_5) (**1**), $Ar^{Me6}SnFeCp^*(CO)_2$ (Cp* = η^5-C_5Me_5) (**2**), and $Ar^{Me6}SnFeCp(CO)(PMe_3)$ (**3**) were synthesized, in which they differ in their substituents on the transition metal fragment. The effects that these substituents have on their structures and the spectroscopic properties were examined by NMR, IR, UV-vis spectroscopy, and by X-ray crystallography. Compound **1** was compared to its more sterically crowded analogues $ArSnFeCp(CO)_2$ (Ar = Ar^{iPr4} or Ar^{iPr6}), with the structural data showing that the C-Sn-Fe angle narrows as the alkyl substituent size on the terphenyl ligand increases, contrary to steric expectations. Additionally, the spectroscopic data for **1** show that in comparison to its more sterically crowded analogues, it has a more shielded tin nucleus, a higher ν_{CO} frequency, and increased energy of its n→p transition. Compound **2** differs from **1** in that the Cp (η^5-C_5H_5) is changed to Cp* (η^5-C_5Me_5). Due to the increased alkyl substituent size of **2**, its structural and spectroscopic data in comparison to those of **1** observes a narrower C-Sn-Fe bond angle, lower ν_{CO} frequency, and a lowering of the energy of the n→p transition. In compound **3**, a carbonyl group at the Fe atom is replaced by the phosphine PMe_3. This ligand exchange causes **3** to experience a widening of the C-Sn-Fe bond angle, deshielding of the tin nucleus, lowering of the ν_{CO} frequency, and a greater lowering of the energy of the n→p transition than in **1**, **2** and $ArSnFeCp(CO)_2$ (Ar = Ar^{iPr4} or Ar^{iPr6}).

CHAPTER 3

3.1 INTRODUCTION

Metallotetrylenes feature a two-coordinate heavy group 14 metal atom such as Si,[1] Ge,[2–8] Sn,[3,8–15] or Pb[14,16–18] with a direct σ bond to a transition metal moiety. The majority of known metallotetrylenes are metallostannylenes, and the transition metals directly bonded to the tin atom are usually either members of group 6 (Cr, Mo, W)[8,9,13] or group 8 (Fe, Ru, Os).[3,10,12,14,15,19] The metallotetrylene structures have bent coordination geometry at the tetrel atom, indicating the presence of a nonbonded lone pair and an unoccupied p-orbital. The related triple-bonded metallostanylynes, in which the coordination of Sn is linear or near-linear, also feature a triple bond to a tungsten[20,21] or molybdenum atom.[22] An exception is the chloride substituted manganostannylene $ClSnMn(CO)_3(CNAr^{iPr4}_2)$ reported by Figueroa and coworkers featuring a σ bond between tin and manganese.[11]

Most reports focus on the details of the synthesis and characterization of the metallostannylene, which usually involves the main group metal–transition metal bond formation via a salt metathesis route.[3,9,14,15] The metallostannylenes obtained were generally well-characterized by spectroscopic (^1H, ^{13}C, and ^{119}Sn NMR and electronic) and X-ray crystal diffraction data. Other routes to metallostannylenes include reactions involving isomerization, H migration, and halide or hydride abstraction (**Figure 1**).[8,10,12,13,19] The triple-bonded Sn≡W cationic complexes were produced by dinitrogen elimination[20,21] or chloride abstraction,[21] and the Sn≡Mo neutral complexes by metathetical exchange.[22]

Figure 1. Routes to metallostannylenes. [3,8–10,12,13,15,19]

Salt metathesis.

3

$$ArSnCl + M'[MCp(CO)_x] \longrightarrow$$

M'Cl

Ar = Ar^{Me6}, Ar^{iPr4}, or Ar^{iPr6}
M' = Na or K
M = Cr, Mo, W; x = 3
Or M = Fe; x = 2
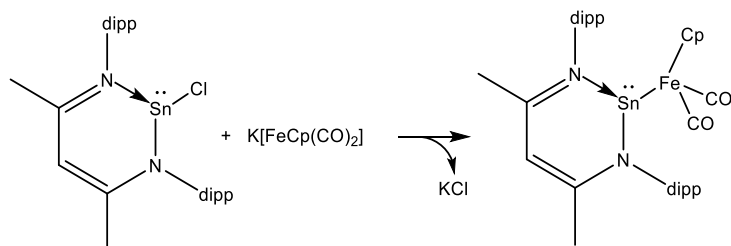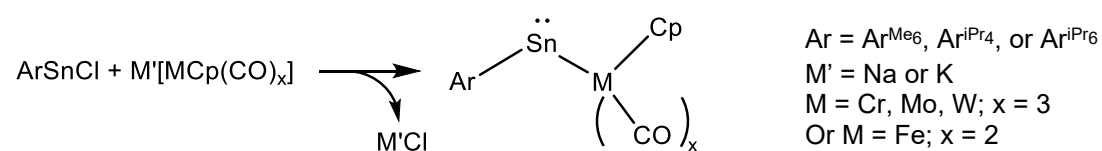
9,15

Deprotonation.

8

Isomerizaton/H-migration.

10

12

Chloride Abstraction.
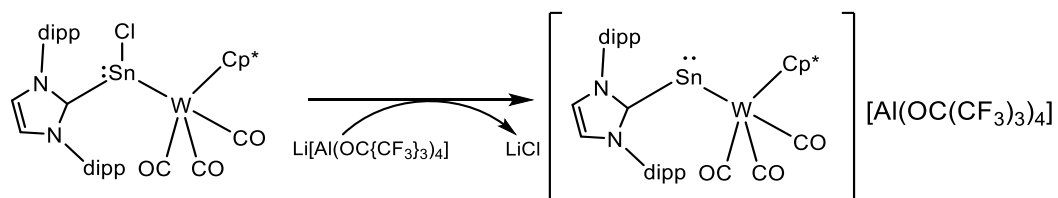
13
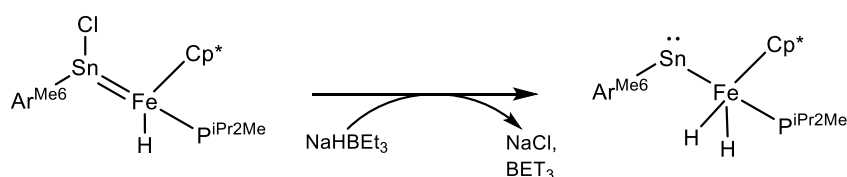
19

In addition to their syntheses, the reactivity of the metallotetrylenes has also been investigated.[1,7,10,12,15,19,23–27] However, there are few detailed investigations into how changing the substituents at the tetrel atom affects the spectroscopic properties of the complexes. Here, we report three new ferriostannylenes: $Ar^{Me6}SnFeCp(CO)_2$ (Ar^{Me6} = $-C_6H_3$-$(C_6H_2$-2,4,6-$Me_3)_2$, Cp = η^5-C_5H_5) (**1**), $Ar^{Me6}SnFeCp^*(CO)_2$ (Cp* = η^5-C_5Me_5) (**2**), and $Ar^{Me6}SnFeCp(CO)(PMe_3)$ (**3**).

3.2 EXPERIMENTAL SECTION

General Procedures: All manipulations were carried out by using modified Schlenk techniques or in a Vacuum Atmospheres OMNI-Lab drybox under a N_2 or argon atmosphere. Solvents were dried over columns of activated alumina using a Grubbs type purification system (Glass Contour),

stored over Na (THF, toluene) or K (hexanes) mirrors, and degassed via three freeze-pump-thaw cycles prior to use. The reagent trimethylphosphine (PMe$_3$) was purchased from Strem Chemicals and transferred to a J. Young's Schlenk tube prior to use. The compounds Ar^{Me6}SnCl[28–30] and K[FeCp(CO)$_2$][31] were synthesized according to literature procedures. The compound K[FeCp*(CO)$_2$] was synthesized by stirring a THF solution of {FeCp*(CO)$_2$}$_2$ over a potassium mirror for 1 month. The ^{1}H and ^{13}C{^{1}H} NMR spectra were recorded on Varian 600 MHz NMR or Bruker 400 MHz NMR spectrometers and were referenced to the residual solvent signals in C$_6$D$_6$ (^{1}H: δ 7.15 ppm, ^{13}C: δ 128.06 ppm).[32] The ^{31}P and ^{119}Sn NMR spectra were recorded on a Bruker Avance DRX 500 MHz spectrometer. UV-Visible spectra were recorded using dilute hexane solutions in 3.5 mL quartz cuvettes using an Olis 17 Modernized Cary 14 UV-Vis/NIR spectrophotometer. Infrared spectra for **1-3** were recorded as Nujol mulls between CsI windows on a PerkinElmer 1430 spectrophotometer. Melting points were determined in flame-sealed glass capillaries on a Meltemp II apparatus equipped with a partial immersion thermometer.

Ar^{Me6}SnFeCp(CO)$_2$ (1): A solution of Ar^{Me6}SnCl[28–30] (3.5 g, 7.5 mmol) in THF (ca. 30 mL) was added dropwise to a THF suspension (ca. 40 mL) of K[FeCp(CO)$_2$][31] (1.6 g, 7.5 mmol) at ca. 0 °C with stirring. The dark red solution was allowed to slowly warm to room temperature and stirred until the solution became dark green, ca. 1-3 days. The solvent was removed under reduced pressure to afford a dark green-brown solid that was redissolved in toluene (ca. 50 mL). The solution was filtered through a Celite/Florisil plug, and the deep green filtrate was concentrated to ca. 10 mL under reduced pressure. Storage at ca. -18 °C afforded dark green crystals of the product 1. Yield: 4.6 g (50%). Mp: 280-285 °C. ^{1}H NMR (600 MHz, C$_6$D$_6$, 20 °C): δ 1.98 (s, 6H, *p*-C(C*H*$_3$)), δ 2.41 (s, 12H, *o*-C(C*H*$_3$)), δ 3.66 (s, 5H, η^5-C$_5$*H*$_5$), δ 6.65 (br s, 4H, flanking *m*-aromatic *H*), δ 7.16 (d, 2H, J$_{HH}$ = 7.5Hz, central m-aromatic *H*), δ 7.42 (t, 1H, ^{3}J$_{HH}$ = 8.1 Hz, central *p*-

aromatic H). ^{13}C{^{1}H} NMR (151 MHz, C$_6$D$_6$, 20 °C): δ 20.56 (p-CH$_3$) δ 20.97 (o-CH$_3$), δ 85.25 (η^5-C$_5$H$_5$), δ 127.13, 129.58, 136.78, 136.96, 145.59 (Ar(C)), δ 187.73 (C_{ipso}-Sn), δ 210.6 (CO). ^{119}Sn NMR (149 MHz, C$_6$D$_6$, 20 °C): δ 2957. UV-vis (hexane): λ_{max} (ε) 370 nm (4800 mol^{-1} L cm^{-1}), 594 nm (790 mol^{-1} L cm^{-1}). IR (Nujol, cm^{-1}): ν_{CO} 2010 (s), ν_{CO} 1950 (s).

Ar^{Me6}SnFeCp*(CO)$_2$ (2): A solution of Ar^{Me6}SnCl$^{28-30}$ (0.023 g, 0.051 mmol) in THF (15 mL) was added dropwise to a THF suspension (ca. 10 mL) of K[FeCp*(CO)$_2$] (0.014 g, 0.051 mmol) at -78 °C. The solution was allowed to warm slowly to room temperature and stirred until the solution was dark green, ca. 3 days. The solvent was removed under reduced pressure to afford a dark green solid that was dissolved in toluene (ca. 50 mL). This solution was filtered through a Celite plug, and the deep green filtrate was concentrated to ca. 10 mL. Storage at ca. -18 °C afforded dark green crystals of **2**. Yield: 0.022 g (60%). Mp: 270-275 °C. ^{1}H NMR: (500 MHz, C$_7$D$_8$, 20 °C) δ 1.38 (s, 15H, η^5-C$_5$(CH$_3$)$_5$), δ 2.08 (s, 6H, p-C(CH$_3$)), δ 2.56 (s, 12H, o-C(CH$_3$)), δ 6.75 (br s, 4H, flanking m-aromatic H), δ 7.16 (d, 2H, J$_{HH}$ = 7.5Hz, central m-aromatic H), δ 7.46 (t, 1H, ^{3}J$_{HH}$ = 8.1 Hz, central p-aromatic H). UV-Vis (hexane): λ_{max} (ε) 384 nm (5500 mol^{-1} L cm^{-1}), λ_{max} (ε) 662 nm (0.2000 mol^{-1} L cm^{-1}). IR (Nujol, cm^{-1}): ν_{CO} 1990 (s), ν_{CO} 1945 (s).

Ar^{Me6}SnFeCp(CO)(PMe$_3$) (3): Pure, undiluted trimethylphosphine PMe$_3$ (0.1 mL, 1 mmol) was added dropwise by cannula to a solution of **1** (0.6 g, 0.1 mmol, ca. 2 drops) in hexanes (ca. 40 mL) at ca. 0 °C, which was then allowed to slowly warm to room temperature, and stirred overnight. The resulting red solution was concentrated to ca. 20 mL under reduced pressure. Storage at ca. -18 °C gave purple crystals of **3**. Yield: 0.4 g (60%). Mp: 265-270 °C. ^{1}H NMR: (500 MHz, C$_6$D$_6$, 20 °C) δ 0.53 (d, 9H, ^{2}J$_{HH}$ = 8.7 Hz, P(CH$_3$)$_3$), δ 1.99 (s, 6H, o-C(CH$_3$)), δ 2.46 (s, 6H, o-C(CH$_3$)), δ 2.61 (s, 6H, p-C(CH$_3$)), δ 3.61 (s, 5H, η^5-C$_5$H$_5$), δ 6.65 (s, 4H, flanking m-aromatic H), δ 7.13

(d, 2H, J_{HH} = 14.7 Hz, central m-aromatic *H*), δ 7.45 (t, 1H, $^3J_{HH}$ = 7.5 Hz, central *p*-aromatic *H*).

^{13}C NMR (151 MHz, C$_6$D$_6$, 20 °C): δ 20.33 (P(*C*H$_3$)$_3$), δ 20.56 (*p*-*C*H$_3$), δ 21.02 (*o*-*C*H$_3$), δ 21.97 (*o*-*C*H$_3$), δ 80.98 (η^5-*C*$_5$H$_5$), δ 127.66, 127.96, 128.16, 129.32, 136.36, 139.18 (Ar(*C*)), δ 166.86 (*C*$_{ipso}$-Sn), *C*O signal not observed. ^{31}P NMR (202 MHz, C$_6$D$_6$, 20 °C): δ 16.50. ^{119}Sn NMR (149 MHz, C$_6$D$_6$, 20 °C): δ 3762. UV-Vis (hexane): λ_{max} (ε) 350 nm (140 μmol^{-1} L cm^{-1}), λ_{max} (ε) 720 nm (1300 μmol^{-1} L cm^{-1}). IR (Nujol, cm^{-1}): ν_{CO} 1870 (s).

3.3 RESULTS AND DISCUSSION

Synthesis.

Scheme 1. Synthesis of compounds **1-3**.

R = η^5-C$_5$H$_5$ (**1**)

= η^5-C$_5$Me$_5$ (**2**)

1

3
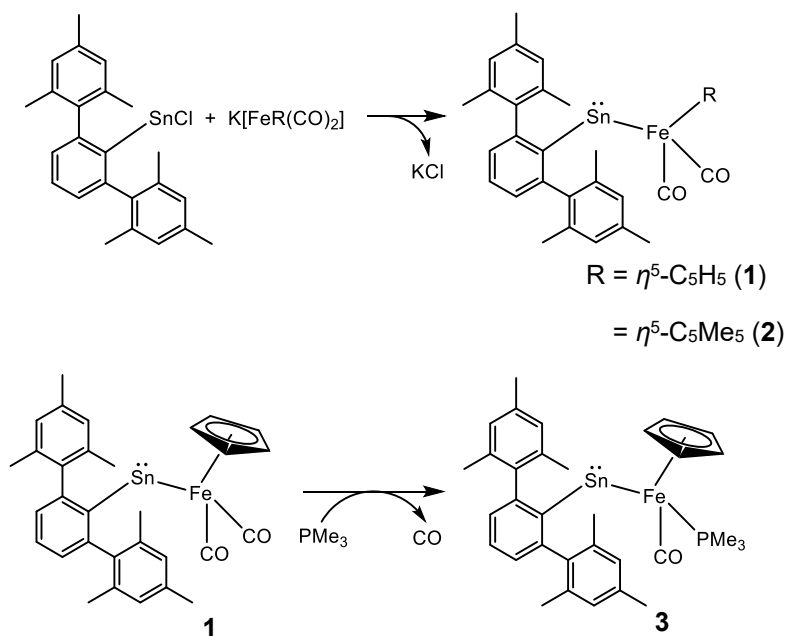
Compound **1** was synthesized via salt metathesis, similar to the majority of reported metallostannylenes (**Scheme 1**).[3,9,14] Treatment of 1 equiv of Ar^{Me6}SnCl[28,30] with 1 equiv of K[FeCp(CO)$_2$][31] in THF gave a dark green solution from which crystals of the ferriostannylene

CHAPTER 3

Ar^{Me6}SnFeCp(CO)$_2$ (**1**) were obtained in moderate yield after workup and recrystallization from hexanes.

The synthesis of the potassium salt K[FeCp*(CO)$_2$] for use in the synthesis of **2** proved more difficult than its Cp substituted counterpart. A high-yield synthesis of K[FeCp(CO)$_2$] was reported in 1981 by Plotkin and Shore and involves the use of the potassium ketyl radical to reduce the dimer {FeCp(CO)$_2$}$_2$.[31] Unfortunately, a similar ketyl route proved ineffective for the reduction of the bulkier {FeCp*(CO)$_2$}$_2$, and the unreduced dimer was recovered from the reaction mixture. Replacing the potassium ketyl with a sodium ketyl or KC$_8$ as reductants also proved ineffective. Ultimately, rapid stirring of 1 equiv of {FeCp*(CO)$_2$}$_2$ over an excess of potassium in the form of a metal mirror gave, after washing with toluene, K[FeCp*(CO)$_2$] as a pink powder. However, this route proved to be very inefficient since it involved stirring over the potassium mirror for ca. 1 month which afforded a 3% yield of the potassium salt.

The synthesis of **2** proceeded similarly to that of **1**. Treatment of 1 equiv of the aryl stannylene chloride Ar^{Me6}SnCl [28–30] with 1 equiv of the potassium salt K[FeCp*(CO)$_2$] gave green crystals of Ar^{Me6}SnFeCp*(CO)$_2$ (**2**) in low yield after workup and crystallization from toluene. Due to the difficulty involving the long reaction time and low yield in producing the [FeCp*(CO)$_2$]$^-$ anion, the quantity of pure crystals of **2** that were available were only sufficient for its characterization by ^{1}H NMR, UV-vis, IR spectroscopy, and X-ray crystallography. ^{13}C NMR and ^{119}Sn NMR spectra proved unobtainable due to the very low solubility of **2**.

Ferriostannylene **3** was achieved through a phosphine-carbonyl ligand exchange. Approximately 1 equiv of the voltile PMe$_3$(*l*) was added dropwise via cannula to a stirred hexanes solution

containing 1 equiv of **1**. Concentration of the green solution under reduced pressure of the hexanes solution gave purple-brown crystals of Ar^{Me6}SnFeCp(CO)(PMe$_3$) (**3**) in moderate yield.

Melting points of compounds **1-3** occur at high temperatures above 250°C, with the cooled samples appearing brown to black in color, suggesting decomposition.

NMR Spectroscopy. Comparison of the spectroscopic data for **1** to those of its more sterically crowded analogues ArSnFeCp(CO)$_2$ (Ar = Ar^{iPr4} or Ar^{iPr6})[15] revealed patterns that can be attributed to the bulk of the terphenyl ligand. The ^{119}Sn NMR spectra of the ferriostannylenes ArSnFeCp(CO)$_2$ (Ar = Ar^{Me6} (**1**), δ = 2957 ppm; Ar = Ar^{iPr4}, δ = 2951 ppm; Ar = Ar^{iPr6}, δ = 2915 ppm)[15] show that the tin signal shifts slightly upfield with increasing substituent bulk, indicating increased shielding of the tin nucleus.[33] The increase in electron donation to the Sn by its substituents can be explained by inductive effects, in which the influence from increasing electron donating effects with increasing alkyl substituent size is well-documented.[34,35] Additionally, the ^{1}H NMR spectra show a gradual downfield shift of the cyclopentadienyl protons resonance, with the singlet appearing at 3.66 ppm in **1** (Ar = Ar^{Me6}), at 3.78 ppm in Ar^{iPr4}SnFeCp(CO)$_2$ and at 3.80 ppm in Ar^{iPr6}SnFeCp(CO)$_2$.[15] The decreased shielding of the Cp group on the iron moiety can be attributed to an increased ionic character of the Fe–Cp bond in association with the increased π*-backbonding from the strong-field CO groups illustrated in the IR spectra (*vide infra*).

Compounds **1** and **2** differ only in the cyclopentadienyl group. An overlay of the ^{1}H NMR spectra of compounds **1** and **2** indicates a small downfield shift of the protons on the flanking phenyl rings of **2** while chemical shifts of the terphenyl ligand protons oriented away from the Cp ring remain unchanged. The deshielding of the ligand protons in closest proximity to the Cp* group in **2** is also

observed in the mesitylene protons of the metallogermylenes Mes*GeFe(CO)$_2$R (R = Cp or Cp*) (Mes* = C$_6$H$_2$-2,4,6-^{t}Bu$_3$).[36]

The signal corresponding to the terphenyl *o*-methyl group in both the ^{1}H (2.41 ppm) and ^{13}C (20.97 ppm) NMR spectra of **1** are split into two singlets of equal intensity in the respective spectra for **3** (^{1}H: 2.46 and 2.61 ppm; ^{13}C: 21.02 and 21.97 ppm), consistent with a lower symmetry arising from the phosphine-carbonyl ligand substitution. Moreover, the PMe$_3$ protons in **3** appear in the ^{1}H NMR spectrum as a doublet at 0.53 ppm due to ^{31}P coupling. The ^{31}P NMR signal of **3** appears at 16.50 ppm and the ^{119}Sn NMR signal is seen at 3762 ppm. Other organophosphine-substituted metallostannylenes feature a ^{31}P NMR signal shift in the range 41.16 – 76.2 ppm,[10,14,19] and metallostannylenes typically report a ^{119}Sn NMR signal in the range of 1982 – 2951ppm,[9,15,19] which places **3** significantly outside the reported ranges. As other phosphine-containing metallostannylenes are bonded to P^{i}Pr$_3$[10] or PMe^{i}Pr$_2$,[14,19] the upfield-shifted signal observed in the ^{31}P NMR signal of **3** can be attributed to the smaller PMe$_3$ lignad of **3**. Generally, decreased steric congestion at the phosphorus center has been shown to decrease the metal-phosphorus bond length, leading to a more shielded phosphorus nucleus.[37–43] The significantly more deshielded tin nucleus observed in the ^{119}Sn NMR spectrum of **3** can be attributed to the greater π*-backdonation to the CO group in **3** in comparison to ferriostannylenes **1**, **2**, and ArSnFeCp(CO)$_2$ (Ar = Ar^{iPr4} or Ar^{iPr6}),[15] observed in their respective IR spectra (*vide infra*), which subsequently shifts electron density away from the tin atom.

IR Spectroscopy. The IR spectrum of ArSnFeCp(CO)$_2$ show that the CO stretching bands shift to lower wavenumbers as the alkyl substituent size increases: from 2010 and 1950 cm^{-1} in **1**, to 1970 and 1921 cm^{-1} when Ar = Ar^{iPr4}, and 1967 and 1926 cm^{-1} when Ar = Ar^{iPr6}.[15] The shift to lower

frequencies suggests an increase in π^*-backbonding and a corresponding strengthening of the Fe–C bonds.[44]

The IR spectrum of **2** displays carbonyl stretching bands shifted to lower frequencies in comparison to **1** at 1990 and 1945 cm^{-1}. This difference is paralleled to a greater extent in the metallogermylenes Mes*GeFe(CO)$_2$R; from ν_{CO} bands at 2004 and 1950 cm^{-1} (R = Cp) to 1969 and 1920 cm^{-1} (R = Cp*).[36] The inductive effects of the methyl groups[34,35] cause an increase in electron density at the transition metal that is reflected in the strengthened Fe–C bond.

The IR spectrum of **3** displays a single CO stretching band at 1870 cm^{-1}, which appears at a lower wavenumber in comparison to the ν_{CO} of **1**, **2**, and ArSnFeCp(CO)$_2$ (Ar = Ar^{iPr4} or Ar^{iPr6}).[15] Given the weaker π-acceptor ability of PMe$_3$ in comparison to CO,[44] the lower frequency observed for **3** indicates that the single CO group bears the majority of the π^*-backdonation and contributes to a relatively stronger Fe–C bond than the other ferriostannylenes.

UV-vis Spectroscopy. Solutions of **3** are dark yellow to brown in color, in contrast to the typical dark green solutions shown by ferriostannylenes **1**, **2**, and ArSnFeCp(CO)$_2$ (Ar = Ar^{iPr4} or Ar^{iPr6})[15]. Despite this, the UV-vis spectra of **2** and **3** are similar to the reported spectra of the other ferriostannylenes, displaying a relatively intense band in the near UV region (384 nm and 350 nm, respectively) and a less intense band in the visible region (662 nm and 720 nm, respectively). The bands in the visible region correspond to an n→p transition and are more red-shifted than that of **1**. The bathochromic shift displayed by **2** is explained by the narrowing of the bending angle at Sn as displayed in its X-ray crystal structure. A direct relationship between narrower interligand

angles and absorptions at higher wavelengths, i.e. lower frequencies, are also observed in the diaryl stannylenes $Sn(Ar)_2$ ($Ar = Ar^{Me6}$, Ar^{iPr4}, or Ar^{iPr6}).[45]

Table 1. Selected spectroscopic data for $ArSnFeCp(CO)_2$ ($Ar = Ar^{iPr4}$ or Ar^{iPr6})[15] and **1-3**.

	$Ar^{iPr6}SnFe$ $Cp(CO)_2$ [15]	$Ar^{iPr4}SnFe$ $Cp(CO)_2$ [15]	1	2	3
C-Sn-Fe, (deg)	106.6(2)	112.65(9)	113.60(3)	111.05(15)	114.3(12) 116.88(9)
^{1}H NMR: $\delta_{Cp\ H}$ (ppm)	3.80	3.78	3.66	–	3.61
^{119}Sn: (ppm)	2915	2951	2957	–	3762
IR: νCO (cm^{-1})	1967 1926	1970 1921	2010 1950	1990 1945	1870
UV-vis: λ_{max} (n→p transition, nm)	608	608	598	662	720

Ferriostannylenes **1** and **2**, when compared against $ArSnFeCp(CO)_2$ ($Ar = Ar^{iPr4}$ or Ar^{iPr6}), have thus far have revealed a general tendency (**Table 1**): a sharper interligand angle in the X-ray crystal structure is accompanied by an upfield shift in the corresponding ^{119}Sn NMR signal, lower ν_{CO} frequencies in the IR spectrum, and a bathochromic shift of the n→p transition in the UV-vis spectrum. Although, the UV-vis absorptions for $Ar^{iPr4}SnFeCp(CO)_2$ and $Ar^{iPr6}SnFeCp(CO)_2$ are identical,[15] despite that the larger terphenyl ligand of Ar^{iPr6} causes a sharper interligand angle of 106.6(2)°.[15] The larger terphenyl ligand, Ar^{iPr6}, appears to narrow the interligand angle while the "extra" isopropyl substituent has no effect on the UV-vis spectrum, suggesting that there may be a limit in the ferriostannylenes in which a larger terphenyl ligand has no discernable effect on the HOMO-LUMO transition.

The X-ray crystal structure for **3** shows a wider C-Sn-Fe bond angle than that of **1**, and if earlier patterns are followed, there should be a hypsochromic shift in the n→p transition of **3**. However,

this absorption for **3** occurs at a markedly higher wavelength outside the 569 – 620 nm range in the other metallostannylenes.[9,15] This difference can be explained via Bent's Rule, in which the increased electropositivity of the Sn atom, exhibited by the more deshielded tin nucleus in the ^{119}Sn NMR spectrum of **3**, and the wider C-Sn-Fe angle are indicative of increased atomic *s* character in the tin atom.[46,47] The increase in atomic *s* character on the tin appears to affect a lowering of the energy of the n→p transition seen in the UV-vis spectrum of **3**.

X-ray Crystal Structures.

Table 2. Selected structural data for **1-3**.

	Ar[iPr6]SnFe Cp(CO)$_2$ [15]	Ar[iPr4]SnFe Cp(CO)$_2$ [15]	**1**	**2**	**3**
C$_{ipso}$–Sn, Å	2.444(7)	2.209(3)	2.2101(11)	2.088(5)	2.226(3)
Sn–Fe, Å	2.6031(17)	2.5633(6)	2.5854(3)	2.5609(11)	2.561(4) 2.5562(8)
Fe–Cp$_{centroid}$, Å	1.577(6)	1.671(6) 1.706(3)	1.7373(4)	1.738(3)	1.732(2) 1.729(10)
Fe–CO, Å	1.930(17) 1.739(10)	1.749(6) 1.732(4) 1.755(13)	1.767(3) 1.750(3)	1.766(8) 1.739(8)	1.730(6) 1.73(3)
C$_{ipso}$–Sn–Fe, deg	106.67(19)	112.65(9)	113.60(3)	111.05(15)	114.32(12) 116.88(9)
Fe–PMe$_3$, Å	-	-	-	-	2.1555(9) 2.1709(13)

The ferriostannylene **1** crystallizes from toluene as green blocks in the monoclinic space group *P*2$_1$/*c* that have identical values to those of its Ge congener Ar[Me6]GeFeCp(CO)$_2$.[24] The structure of **1** has a C$_{ipso}$-Sn-Fe angle of 113.60(3)°, which is within the range of other neutral

metallostannylenes (106.1(3)° – 118.76(5)°).[8,9,12–14,19] The green polymorph of the Ge congener

has a wider interligand angle (115.59(8)°), though its red and dichroic polymorphs are narrower

than **1** at 109.48(9)° and 110.4(2)°, respectively.[24] With the exception of the red and dichroic

polymorphs of the ferriogermylene, the interligand angle at the tetryl atom in tetrylenes have

generally been observed to be wider in the Ge complexes compared to the Sn congeners.[15,29,48]
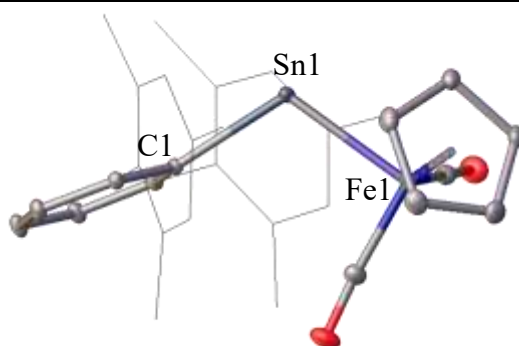
Figure 2. Thermal ellipsoid plot (50%) of **1**. Carbon-bound H atoms are not shown and flanking

phenyl rings are shown as wire frames for clarity. Selected bond lengths (Å) and angles (deg):

Sn1–C1 = 2.2101(11); Sn1–Fe1 = 2.5854(3); C1–Sn1–Fe1 = 113.60(3)°.

Compound **1** contains the least sterically encumbering ligand of the three ferriostannylenes in the

series and comparing the C_{ipso}-Sn-Fe angle of the three ferriostannylenes reveals a decreasing

interligand angle with increasing terphenyl size (Ar^{Me6} (**1**) = 113.60(3)°, Ar^{iPr4} = 112.65(9)°, Ar^{iPr6}

= 106.6(2)°)[15] (**Table 2**). This sterically counterintuitive trend was previously observed in the

interligand angles of the diaryl stannylenes :SnAr₂ (Ar = Ar^{Me6}: 114.7(2)°, Ar^{iPr4}: 117.56(8)°, Ar^{iPr6}:

107.61(9)°)[29,45,48,49] and was attributed to London dispersion effects arising from the H···H

attraction between the terphenyl ligands.[45,49] The X-ray crystal structures of the ferriostannylenes

show that the Cp or Cp* ring is oriented towards one of the flanking phenyl rings, further

suggesting that London dispersion effects play a role in determining the interligand angle of the ferriostannylenes (**Figure 3a**). X-ray crystal structures of the metallotetrylenes $Ar^{iPr6}SnMCp(CO)_3$ (M = Cr, Mo, W)[9] similarly show the cyclopentadienyl fragment oriented towards the large aryl ligand rather than away from it. The structures of the three ferriostannylenes show that the closest H⋯H distances between the alkyl substituent protons on the ligand and Cp ring protons are 3.20245(13) Å in **1**, 2.41579(12) Å in $Ar^{iPr4}SnFeCp(CO)_2$ (**Figure 3b**), and 2.8503(2) in $Ar^{iPr6}SnFeCp(CO)_2$.

a)

Ar^{Me6} Ar^{iPr4} Ar^{iPr6}
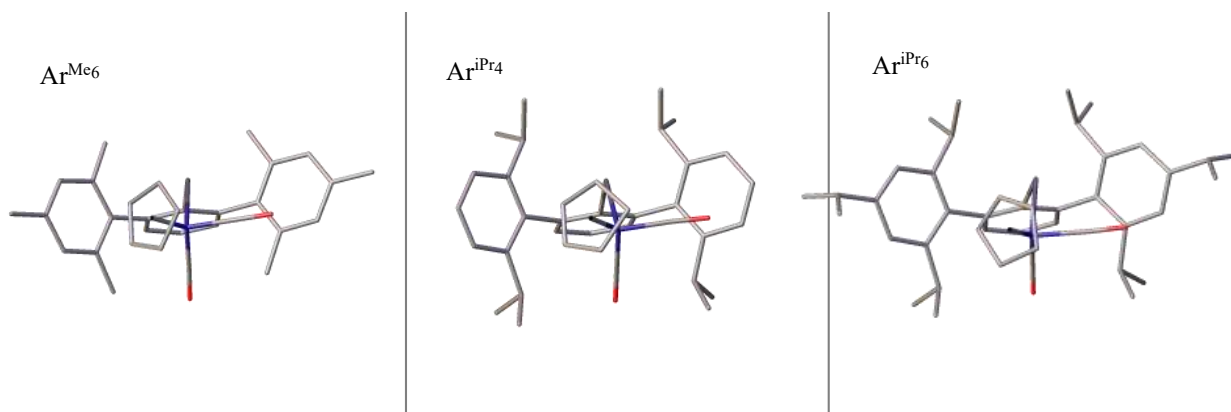
b)
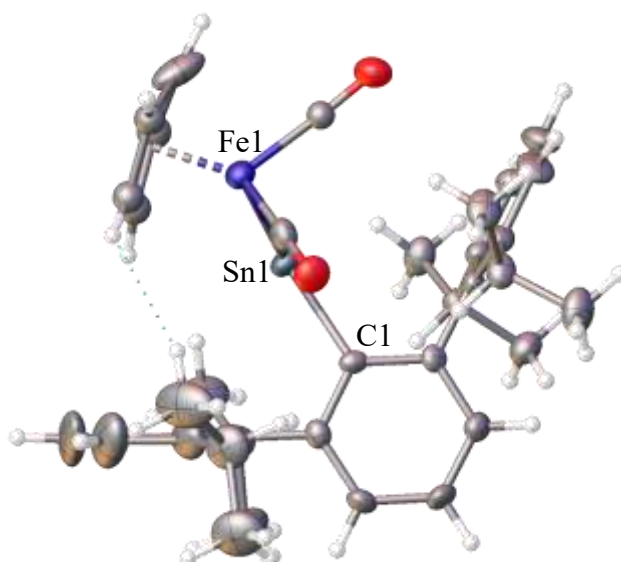
Figure 3. Above: **a)** Molecular graphics of **1** (left), $Ar^{iPr4}SnFeCp(CO)_2$ (center), and $Ar^{iPr6}SnFeCp(CO)_2$ (right) in the "tube" drawing style, showing the Cp fragment oriented towards a flanking phenyl ring. Carbon-bound H atoms and structural disorders are not shown for clarity. Below: **b)** Thermal ellipsoid plot (50%) of $Ar^{iPr4}SnFeCp(CO)_2$ showing the 'short' H···H contact (2.41579(12) Å).
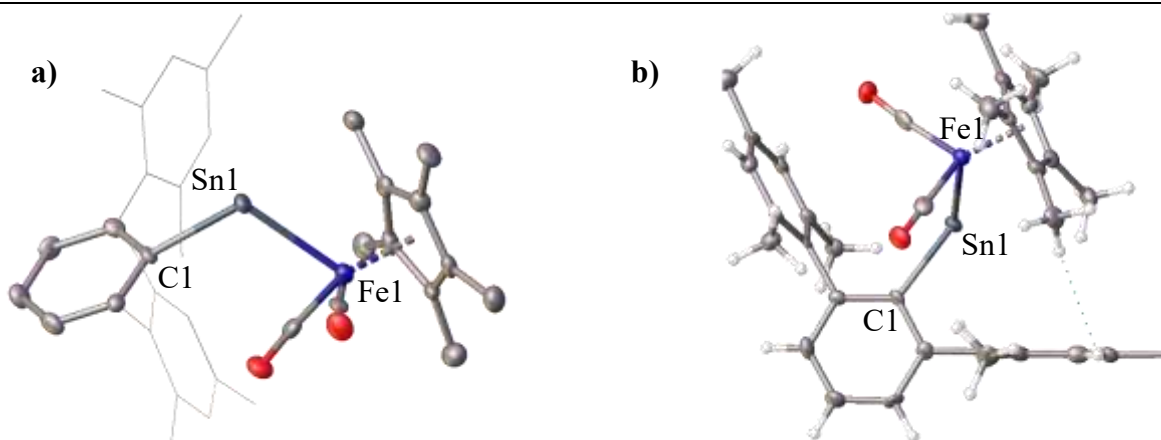
Figure 4. Thermal ellipsoid plots (50%) of **2**. **a)** "Side" view of **2**. Carbon-bound H atoms are not shown, and flanking phenyl rings are shown as wire frames for clarity. **b)** Rotated view of **2** showing the H···H contact = 2.6909(3) Å. Selected bond lengths (Å) and angles (deg): Sn1–C1 = 2.088(5); Sn1–Fe1 = 2.5609(11); C1–Sn1–Fe1 = 111.05(15)°.

The ferriostannylene **2** crystallizes as green blocks in the triclinic space group $P\bar{1}$. In comparison to **1**, compound **2** mainly differs in its slightly narrower C_{ipso}-Sn-Fe bond angle in comparison to that in **1** (**Table 2**). Though Cp* is a more electron-rich group than Cp,[50] the Sn–Fe and Fe–Cp*$_{centroid}$ distances remain similar to those of **1**, suggesting that attractive dispersion effects between the aryl groups take precedence over electronic effects. Unlike **1** and **2**, the

molybdostannylene pair $Ar^{iPr6}SnMo(\eta^5\text{-}C_5H_5)(CO)_3$ and $Ar^{iPr6}SnMo(\eta^5\text{-}1,3\text{-}Bu^t_2\text{-}C_5H_3)(CO)_3$ show that the interligand angle at tin increases from 110.14(10)° to 112.10(8)° as the number of Cp methyl substituents increases.[9] Additionally, the structure of $Ar^{iPr6}SnMo(\eta^5\text{-}1,3\text{-}Bu^t_2\text{-}C_5H_3)(CO)_3$ shows that the two *tert*-butyl groups are oriented away from the terphenyl ligand,[9] which suggests that despite the larger alkyl substituents on the Cp ring, reducing steric crowding takes precedence over increasing dispersion effects.
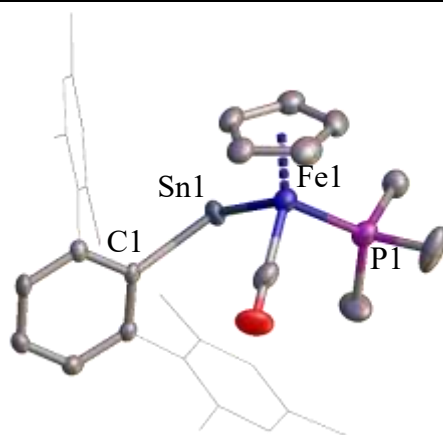
Figure 5. Thermal ellipsoid plot (50%) of **3**. Carbon-bound H atoms and structural disorder are not shown for clarity. Selected bond lengths (Å) and angles (deg): Sn1–C1 = 2.226(3); Sn1–Fe1 = 2.561(4), 2.5562(8); C1–Sn1–Fe1 = 114.3(12)°.

Compound **3** crystallizes as purple blocks in the triclinic space group $P\bar{1}$. The {FeCp(CO)(PMe₃)} fragment is disordered over two sites. The Fe–CO (1.730(6) and 1.73(3) Å) and Fe–PMe₃ (2.1555(9) and 2.1709(13) Å) bond distances are shorter than the sum of the covalent radii of Fe (1.16 Å), C (0.75 Å), and P (1.11 Å),[51] supporting the IR and ^{31}P NMR spectra which are consistent with increased backbonding into the π* orbital of CO and σ* orbital of PMe₃. The C_{ipso}-Sn-Fe bond angles in **3** are the widest of the three ferriostannylenes, at 114.3(12)° and 116.88(9)°. In general,

metallostannylenes containing an organophosphine on the transition metal atom display a larger interligand angle at tin. For example, $Ar^{Me6}SnRuCp*(H)_2(PMe^iPr_2)$ and $Ar^{Me6}SnFeCp*(H)_2(PMe^iPr_2)$ feature angles at the upper limits of the C_{ipso}-Sn-M range (106.1(3)° – 118.76(5)°)[8,9,12–14,19] at 117.98(10) and 118.76(5), respectively.[14,19] Compound **3** has a narrower interligand angle than those metallostannylenes likely due to the smaller organophosphine PMe_3 substituent in comparison to the PMe^iPr_2 ligand.[14,19] Both the crystal structures of $Ar^{Me6}SnRuCp*(H)_2(PMe^iPr_2)$ and $Ar^{Me6}SnFeCp*(H)_2(P^iPr_2Me)$ show the isopropyl substituents on the phosphorus atom oriented away from the terphenyl ligand, consistent with the more important role of steric effects in the metallostannylene structure.

3.4 CONCLUSION

Three new ferriostannylenes $ArSnFeCp(CO)_2$ with different terphenyl tin aryl substituents were synthesized. Comparisons of their spectroscopic and structural properties reveal gradual spectroscopic and structural changes which indicate increased stability arising from attractive dispersion C···H interaction. Complex **2** differs from **1** in that a methyl-substituted cyclopentadienyl group replaces the original Cp ligand. This has a similar effect to that of increasing the substituent bulk on the terphenyl ligands. Overall, a larger substituent bulk at the aryl groups results in a narrower angle at tin, which leads to increased electron density on the Sn and Fe atoms and a lower-energy n→p transition. Complex **3** differs from **1** through a phosphine-carbonyl exchange on the transition metal. Changing the ligand on the Fe atom from CO to PMe_3 yields a wider interligand the angle at the Sn center, but unlike the dispersion effects seen in **1**, **2**, and bulkier ferriostannylenes, spectroscopic analysis of **3** show that the wider angle is caused by the increasing *s* character on Sn.

CHAPTER 3

ASSOCIATED CONTENT

Supporting Information.

Crystallographic data and spectra (NMR, IR, UV–vis)

Accession Codes

CCDC 2258106 – 2258108 contain the supplementary crystallographic data for this paper. These data can be obtained free of charge via www.ccdc.cam.ac.uk/data_request/cif, or by emailing data_request@ccdc.cam.ac.uk, or by contacting The Cambridge Crystallographic Data Centre, 12 Union Road, Cambridge CB2 1EZ, UK; fax: +44 1223 336033.

AUTHOR INFORMATION

Corresponding Author

Philip P. Power – Department of Chemistry, University of California, Davis, California 95616, United States; orcid.org/0000-0002-6262-3209; Email: pppower@ucdavis.edu

Authors

Alice C. Phung – Department of Chemistry, University of California, Davis, California 95616, United States; https://orcid.org/0000-0002-0268-3971

James C. Fettinger - Department of Chemistry, University of California, Davis, California 95616, United States; https://orcid.org/0000-0002-6428-4909

CHAPTER 3

Author Contributions

The manuscript was written through contributions of all authors. All authors have given approval

to the final version of the manuscript.

PUBLICATION INFORMATION

This chapter was accepted in *Journal of Organometallic Chemistry* on August 26, 2023.

CHAPTER 3

3.5 REFERENCES

(1)   Liu, H.-J.; Landis, C.; Raynaud, C.; Eisenstein, O.; Tilley, T. D. Donor-Promoted 1,2-Hydrogen Migration from Silicon to a Saturated Ruthenium Center and Access to Silaoxiranyl and Silaiminyl Complexes. *J Am Chem Soc* **2015**, *137*, 9186–9194.

(2)   Pu, L.; Twamley, B.; Haubrich, S. T.; Olmstead, M. M.; Mork, B. V.; Simons, R. S.; Power, P. P. Triple Bonding to Germanium: Characterization of the Transition Metal Germylynes $(\eta^5\text{-}C_5H_5)(CO)_2M\text{:}Ge\text{-}C_6H_3\text{-}2,6\text{-}Mes_2$ (M = Mo, W; Mes = $-C_6H_2\text{-}2,4,6\text{-}Me_3$) and $(\eta^5\text{-}C_5H_5)(CO)_2M\text{:}Ge\text{-}C_6H_3\text{-}2,6\text{-}Trip_2$ (M = Cr, Mo, W; Trip = $-C_6H_2\text{-}2,4,6\text{-}i\text{-}Pr_3$) and the Related Single Bonded Metallogermylenes $(\eta^5\text{-}C_5H_5)(CO)_3M\text{-}\breve{G}e\text{-}C_6H_3\text{-}2,6\text{-}Trip_2$ (M = Cr, W). *J Am Chem Soc* **2000**, *122*, 650–656.

(3)   Inoue, S.; Driess, M. Isolable Metallo-Germylene and Metallo-Stannylene σ-Complexes with Iron. *Organometallics* **2009**, *28*, 5032–5035.

(4)   Leung, W.-P.; Chiu, W.-K.; Mak, T. C. W. Synthesis and Structural Characterization of Metallogermylenes, Cp-Substituted Germylene, and a Germanium(II)-Borane Adduct from Pyridyl-1-Azaallyl Germanium(II) Chloride. *Organometallics* **2012**, *31*, 6966–6971.

(5)   Tashita, S.; Watanabe, T.; Tobita, H. Synthesis of a Base-Stabilized (Chlorogermyl)Metallogermylene and Its Photochemical Conversion to a (Chlorogermyl)Germylyne Complex. *Chem Lett* **2013**, *42*, 43–44.

(6)   Inomata, K.; Watanabe, T.; Tobita, H. Cationic Metallogermylene and Dicationic Dimetallodigermenes: Synthesis by Chloride Abstraction from *N*-Heterocyclic Carbene-Stabilized Chlorometallogermylenes. *J Am Chem Soc* **2014**, *136*, 14341–14344.

(7)   Inomata, K.; Watanabe, T.; Miyazaki, Y.; Tobita, H. Insertion of a Cationic Metallogermylene into E–H Bonds (E = H, B, Si). *J Am Chem Soc* **2015**, *137*, 11935–11937.

(8)   Widemann, M.; Jeggle, S.; Auer, M.; Eichele, K.; Schubert, H.; Sindlinger, C. P.; Wesemann, L. Hydridotetrylene [Ar*EH] (E = Ge, Sn, Pb) Coordination at Tantalum, Tungsten, and Zirconium. *Chem Sci* **2022**, *13*, 3999–4009.

(9)   Eichler, B. E.; Phillips, A. D.; Haubrich, S. T.; Mork, B. V.; Power, P. P. Synthesis, Structures, and Spectroscopy of the Metallostannylenes $(\eta^5\text{-}C_5H_5)(CO)_3M\text{-}\breve{S}n\text{-}C_6H_3\text{-}2,6\text{-}Ar_2$ (M = Cr, Mo, W; Ar = $C_6H_2\text{-}2,4,6\text{-}Me_3$, $C_6H_2\text{-}2,4,6\text{-}Pr^i_3$). *Organometallics* **2002**, *21*, 5622–5627.

(10) Hayes, P. G.; Gribble, C. W.; Waterman, R.; Tilley, T. D. A Hydrogen-Substituted Osmium Stannylene Complex: Isomerization to a Metallostannylene Complex via an Unusual α-Hydrogen Migration from Tin to Osmium. *J Am Chem Soc* **2009**, *131*, 4606–4607.

(11)   Stewart, M. A.; Moore, C. E.; Ditri, T. B.; Labios, L. A.; Rheingold, A. L.; Figueroa, J. S. Electrophilic Functionalization of Well-Behaved Manganese Monoanions Supported by m-Terphenyl Isocyanides. *Chem. Commun.* **2011**, *47*, 406–408.

(12)   Liu, H.-J.; Guihaumé, J.; Davin, T.; Raynaud, C.; Eisenstein, O.; Tilley, T. D. 1,2-Hydrogen Migration to a Saturated Ruthenium Complex via Reversal of Electronic Properties for Tin in a Stannylene-to-Metallostannylene Conversion. *J Am Chem Soc* **2014**, *136*, 13991–13994.

(13)   Lebedev, Y. N.; Das, U.; Schnakenburg, G.; Filippou, A. C. Coordination Chemistry of $[E(Idipp)]^{2+}$ Ligands (E = Ge, Sn): Metal Germylidyne $[Cp^*(CO)_2W{\equiv}Ge(Idipp)]^+$ and Metallotetrylene $[Cp^*(CO)_3W{-}E(Idipp)]^+$ Cations. *Organometallics* **2017**, *36*, 1530–1540.

(14)   Smith, P. W.; Handford, R. C.; Tilley, T. D. Heavy Tetrel Complexes of Ru Featuring Ru${=}$E(R)X and Ru${-}$E${-}$R (E = Sn, Pb) Linkages. *Organometallics* **2019**, *38*, 4060–4065.

(15)   Lei, H.; Guo, J.-D.; Fettinger, J. C.; Nagase, S.; Power, P. P. Synthesis, Characterization, and CO Elimination of Ferrio-Substituted Two-Coordinate Germylenes and Stannylenes. *Organometallics* **2011**, *30* (22), 6316–6322.

(16)   Zhu, Q.; Fettinger, J. C.; Vasko, P.; Power, P. P. Interactions of a Diplumbyne with Dinuclear Transition Metal Carbonyls to Afford Metalloplumbylenes. *Organometallics* **2020**, *39*, 4629–4636.

(17)   Seidel, N.; Jacob, K.; Fischer, A. K. Bis[2-((Dimethylamino)Methyl)Ferrocenyl]Lead, $(FcN)_2Pb$, as a Ligand: Synthesis and Characterization of the Heterotrimetallic Metalloplumbylene Compounds $(FcN)_2PbM(CO)_5$ (M = Cr, Mo, W). *Organometallics* **2001**, *20*, 578–581.

(18)   Pu, L.; Power, P. P.; Boltes, I.; Herbst-Irmer, R. Synthesis and Characterization of the Metalloplumbylenes $(\eta^5\text{-}C_5H_5)(CO)_3M{-}\ddot{P}b{-}C_6H_3{-}2,6\text{-}Trip_2$ (M = Cr, Mo, or W; Trip = $-C_6H_2{-}2,4,6\text{-}i\text{-}Pr_3$). *Organometallics* **2000**, *19*, 352–356.

(19)   Handford, R. C.; Nesbit, M. A.; Smith, P. W.; Britt, R. D.; Tilley, T. D. Versatile Fe–Sn Bonding Interactions in a Metallostannylene System: Multiple Bonding and C–H Bond Activation. *J Am Chem Soc* **2022**, *144*, 358–367.

(20)   Filippou, A. C.; Portius, P.; Philippopoulos, A. I.; Rohde, H. Triple Bonding to Tin: Synthesis and Characterization of the Stannylyne Complex Trans-$[Cl(PMe_3)_4W{\equiv}Sn\text{-}C_6H_3\text{-}2,6\text{-}Mes_2]$. *Angewandte Chemie International Edition* **2003**, *42*, 445–447.

(21)   Filippou, A. C.; Philippopoulos, A. I.; Schnakenburg, G. Triple Bonding to Tin: Synthesis and Characterization of the Square-Pyramidal Stannylyne Complex Cation $[(Dppe)_2W{:}Sn{-}C_6H_3\text{-}2,6\text{-}Mes_2]^+$ (Dppe = $Ph_2PCH_2CH_2PPh_2$, Mes = $C_6H_2\text{-}2,4,6\text{-}Me_3$). *Organometallics* **2003**, *22*, 3339–3341.

(22)   Queen, J. D.; Phung, A. C.; Caputo, C. A.; Fettinger, J. C.; Power, P. P. Metathetical Exchange between Metal–Metal Triple Bonds. *J Am Chem Soc* **2020**, *142*, 2233–2237.

(23) El-Maradny, A.; Tobita, H.; Ogino, H. Photoreactions of Silyliron(II) Complexes Cp′Fe(CO)$_2$SiMe$_3$ (Cp′ = η^5-C$_5$H$_5$, η^5-C$_5$Me$_5$) with Di-*p*-Tolylgermane (*p*-Tol)$_2$GeH$_2$. *Chem Lett* **1996**, *25*, 83–84.

(24) Phung, A. C.; Fettinger, J. C.; Power, P. P. Insertion Reactions of NH$_3$ and H$_2$O with the Ferriogermylenes ArGeFeCp(CO)$_2$ (Ar = Ar^{Me6} (−C$_6$H$_3$-(C$_6$H$_2$-2,4,6-Me$_3$)$_2$) or Ar^{iPr4} (−C$_6$H$_3$-(C$_6$H$_3$-2,6-^{i}Pr$_2$)$_2$); Cp = η^5-C$_5$H$_5$): Structural Isomerism and Polymorphism in a Metallogermylene. *Organometallics* **2021**, *40*, 3472–3479.

(25) Filippou, A. C.; Chernov, O.; Schnakenburg, G. Metal-Silicon Triple Bonds: Nucleophilic Addition and Redox Reactions of the Silylidyne Complex [Cp(CO)2Mo≡Si-R]. *Angewandte Chemie International Edition* **2011**, *50*, 1122–1126.

(26) Ismail, M. L. bin; Liu, F.-Q.; Yim, W.-L.; Ganguly, R.; Li, Y.; So, C.-W. Reactivity of a Base-Stabilized Germanium(I) Dimer toward Group 9 Metal(I) Chloride and Dimanganese Decacarbonyl. *Inorg Chem* **2017**, *56*, 5402–5410.

(27) Liu, H.-J.; Ziegler, M. S.; Tilley, T. D. The Ruthenostannylene Complex [Cp*(IXy)H$_2$Ru-Sn-Trip]: Providing Access to Unusual Ru-Sn Bonded Stanna-Imine, Stannene, and Ketenylstannyl Complexes. *Angewandte Chemie International Edition* **2015**, *54*, 6622–6626.

(28) Ruhlandt-Senge, K.; Ellison, J. J.; Wehmschulte, R. J.; Pauer, F.; Power, P. P. Isolation and Structural Characterization of Unsolvated Lithium Aryls. *J Am Chem Soc* **1993**, *115*, 11353–11357.

(29) Simons, R. S.; Pu, L.; Olmstead, M. M.; Power, P. P. Synthesis and Characterization of the Monomeric Diaryls M{C$_6$H$_3$-2,6-Mes$_2$}$_2$ (M = Ge, Sn, or Pb; Mes = 2,4,6-Me$_3$C$_6$H$_2$−) and Dimeric Aryl−Metal Chlorides [M(Cl){C$_6$H$_3$-2,6-Mes$_2$}]$_2$ (M = Ge or Sn). *Organometallics* **1997**, *16*, 1920–1925.

(30) Pu, L.; Olmstead, M. M.; Power, P. P.; Schiemenz, B. Synthesis and Characterization of the Monomeric Terphenyl−Metal Halides Ge(Cl){C$_6$H$_3$-2,6-Trip$_2$} (Trip = C$_6$H$_2$-2,4,6-*i*-Pr$_3$) and Sn(I){C$_6$H$_3$-2,6-Trip$_2$} and the Terphenyl−Metal Amide Sn{N(SiMe$_3$)$_2$}{C$_6$H$_3$-2,6-Trip$_2$}. *Organometallics* **1998**, *17*, 5602–5606.

(31) Plotkin, J. S.; Shore, S. G. Convenient Preparation and Isolation of Pure Potassium Cyclopentadienyldicarbonylferrate, K[(η^5-C$_5$H$_5$)Fe(CO)$_2$]. *Inorg Chem* **1981**, *20*, 284–285.

(32) Fulmer, G. R.; Miller, A. J. M.; Sherden, N. H.; Gottlieb, H. E.; Nudelman, A.; Stoltz, B. M.; Bercaw, J. E.; Goldberg, K. I. NMR Chemical Shifts of Trace Impurities: Common Laboratory Solvents, Organics, and Gases in Deuterated Solvents Relevant to the Organometallic Chemist. *Organometallics* **2010**, *29*, 2176–2179.

(33) Wrackmeyer, B. 119Sn-NMR Parameters; 1985; pp 73–186.

(34) Stock, L. M. The Origin of the Inductive Effect. *J Chem Educ* **1972**, *49*, 400.

(35)   Schubert, W. M.; Murphy, R. B.; Robins, J. Electron Donor and Acceptor Properties of Alkyl Substituents. *Tetrahedron* **1962**, *17*, 199–214.

(36)   Jutzi, P.; Leue, C. (Supermesityl)Chlorogermylene (Supermesityl = Mes* = 2,4,6-^{t}Bu$_3$C$_6$H$_2$): Synthesis and Derivatization to (Supermesityl)Ferriogermylenes. *Organometallics* **1994**, *13*, 2898–2899.

(37)   Shaw, B. L. Some Steric, Conformational and Entropy Effects of Tertiary Phosphine Ligands. *J Organomet Chem* **1980**, *200*, 307–318.

(38)   Xiao, S.; Trogler, W. C.; Ellis, D. E.; Berkovitch-Yellin, Z. Nature of the Frontier Orbitals in Phosphine, Trimethylphosphine, and Trifluorophosphine. *J Am Chem Soc* **1983**, *105*, 7033–7037.

(39)   Tolman, C. A. Steric Effects of Phosphorus Ligands in Organometallic Chemistry and Homogeneous Catalysis. *Chem Rev* **1977**, *77*, 313–348.

(40)   Wang, S. P.; Richmond, M. G.; Schwartz, M. NMR Evidence for the Existence of a π-Accepting PMe$_3$ Ligand. Estimates of the Magnitude of π Effects of WL(CO)$_5$ Complexes. *J Am Chem Soc* **1992**, *114*, 7595–7596.

(41)   Krueger, S. T.; Poli, R.; Rheingold, A. L.; Staley, D. L. Synthesis, Molecular and Electronic Structure, and Properties of Mononuclear Trimethylphosphine-Containing Cyclopentadienyl Derivatives of Molybdenum(III) and Molybdenum(IV). Direct Evidence of Molybdenum(III)-Phosphorus π Back-Bonding. *Inorg Chem* **1989**, *28*, 4599–4607.

(42)   Song, S.; Alyea, E. C. Steric Effects of Bulky Phosphines on ^{95}Mo NMR Shieldings. *Can J Chem* **1996**, *74* (11), 2304–2320.

(43)   Bosque, R.; Sales, J. A QSPR Study of the ^{31}P NMR Chemical Shifts of Phosphines. *J Chem Inf Comput Sci* **2001**, *41*, 225–232.

(44)   Carbonyls, Phosphines, and Substitution. In *The Organometallic Chemistry of the Transition Metals*; John Wiley & Sons, Inc.: Hoboken, NJ, USA, 2014; pp 98–133.

(45)   McCrea-Hendrick, M. L.; Bursch, M.; Gullett, K. L.; Maurer, L. R.; Fettinger, J. C.; Grimme, S.; Power, P. P. Counterintuitive Interligand Angles in the Diaryls E{C$_6$H$_3$-2,6-(C$_6$H$_2$-2,4,6-^{i}Pr$_3$)$_2$}$_2$ (E = Ge, Sn, or Pb) and Related Species: The Role of London Dispersion Forces. *Organometallics* **2018**, *37*, 2075–2085.

(46)   Bent, H. A. An Appraisal of Valence-Bond Structures and Hybridization in Compounds of the First-Row Elements. *Chem Rev* **1961**, *61* (3), 275–311.

(47)   Alabugin, I. V.; Bresch, S.; Manoharan, M. Hybridization Trends for Main Group Elements and Expanding the Bent's Rule Beyond Carbon: More than Electronegativity. *J Phys Chem A* **2014**, *118*, 3663–3677.

(48) Spikes, G. H.; Peng, Y.; Fettinger, J. C.; Power, P. P. Synthesis and Characterization of the Monomeric Sterically Encumbered Diaryls E{C$_6$H$_3$-2,6-(C$_6$H$_3$-2,6-Pr$^i_2$)$_2$}$_2$ (E = Ge, Sn, or Pb). *Z Anorg Allg Chem* **2006**, *632*, 1005–1010.

(49) Pandey, K. K. Relativistic DFT Calculations of Structure and 119 Sn NMR Chemical Shifts for Bent M Sn C Bonding in Power's Metallostannylenes of Chromium, Molybdenum, Tungsten and Iron and Diaryl Stannylenes. *J Organomet Chem* **2016**, *815–816*, 23–34.

(50) Kuwabara, T.; Tezuka, R.; Ishikawa, M.; Yamazaki, T.; Kodama, S.; Ishii, Y. Ring Slippage and Dissociation of Pentamethylcyclopentadienyl Ligand in an (η^5-Cp*)Ir Complex with a κ^3-*O*, *C*, *O* Tridentate Calix[4]Arene Ligand under Mild Conditions. *Organometallics* **2018**, *37*, 1829–1832.

(51) Pyykkö, P.; Atsumi, M. Molecular Single-Bond Covalent Radii for Elements 1-118. *Chemistry - A European Journal* **2009**, *15*, 186–197.

CHAPTER 3

3.6 SUPPLEMENTARY INFORMATION

Table of Contents

X-ray Crystallography

Crystals of **1**, **2**, and **3** were removed from a Schlenk flask under a stream of nitrogen and immediately covered with a layer of hydrocarbon oil. A suitable crystal was selected, attached to a glass fiber on a copper pin and quickly placed in the cold N_2 stream on the diffractometer. Data was collected at 100 K on a Bruker APEX DUO diffractometer with Mo Kα radiation (λ = 0.71073 Å). Absorption corrections were applied using SADABS.[S1] The crystal structures were solved by direct methods and refined by full matrix least-squares procedures in SHELXTL.[S2] All non-H atoms were refined anisotropically.

Table S1. Selected X-ray Crystallographic data for **1-3**.

	1	2	3
Formula	$C_{31}H_{30}FeSNO_2$	$C_{72}H_{80}Co_2O_4Sn_2$	$C_{33}H_{39}OPFeSN$
Fw	609.09	1127.33	657.15
Color, habit	Green, block	Green, block	Violet, block
Space group	$P2_1/c$	$P\bar{1}$	$P\bar{1}$
A, å	15.7655(9)	8.7619(11)	10.7687(6)
B, å	9.9281(6)	10.5019(14)	11.7477(7)
C, å	16.8754(9)	18.102(2)	11.9054(7)
A, °	90	96.098(3)	84.5131(9)
B, °	90.7337(8)	93.090(3)	88.9830(9)
Γ, °	90	107.597(3)	89.5238(10)
V, å³	2641.1(3)	1572.3(4)	1498.95(15)
Z	4	1	2
Crystal size, mm	0.396 × 0.252 × 0.196	0.383 × 0.192 × 0.183	0.166 × 0.137 × 0.13
D_{calc}, g cm⁻³	1.532	1.191	1.456
Abs. M, mm⁻¹	1.521	1.085	1.394
2θ, °	4.76 to 61.126	2.272 to 51.446	4.654 to 55.08
R(int)	0.0149	0.0633	0.0346
Obs. Reflns. [i>2σ(i)]	8083	5733	6890
Data/restraints/parameters	8083/0/322	5733/0/372	6890/34/401
R_1, obsd. Reflns.	0.0184	0.0635	0.0462

CHAPTER 3

Photographs of Crystal Samples

Crystals of **1**, **2**, and **3** were removed from a Schlenk flask under a stream of nitrogen and immediately covered with a layer of hydrocarbon oil. The bulk crystal samples in oil were spread on a glass microscope slide and photographed through the lens of an optical microscope. The mounted crystals were photographed via camera on the Bruker APEX DUO diffractometer.

Figure S1. Bulk crystals of **1** at 298 K.
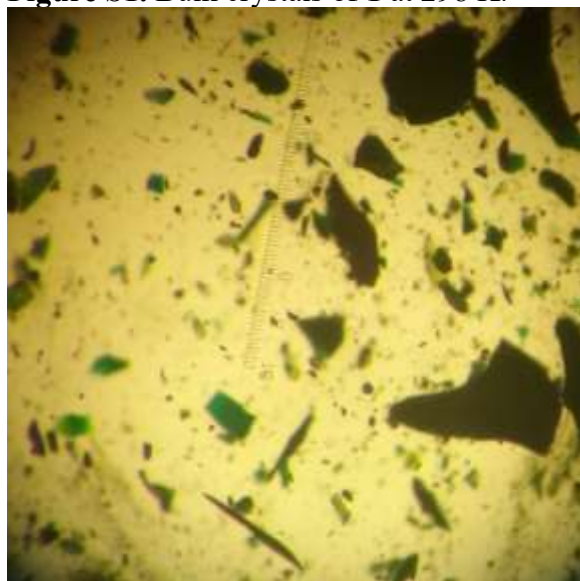
Figure S2. Mounted crystal of **1** at 100 K.

Figure S3. Crystals of **2** at 298 K.

Figure S4. Mounted crystal of **2** at 100 K.

Figure S5. Bulk crystals of **3** at 298 K.
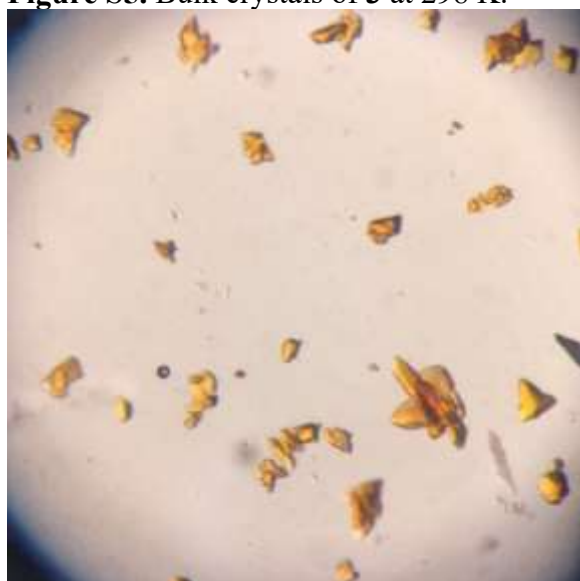
Figure S6. Mounted crystal of **3** at 100 K.

NMR Spectra

Figure S7. ^{1}H NMR spectrum of **1** in C_6D_6 at 298 K.
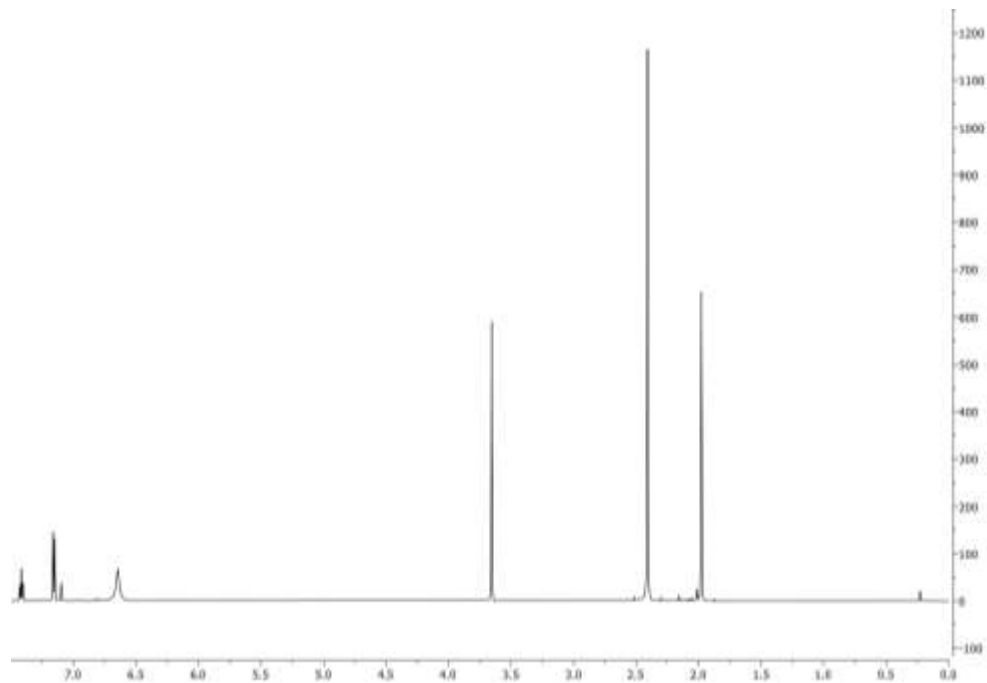
Figure S8. $^{13}C\{^1H\}$ NMR spectrum of **1a** in C_6D_6 at 298 K.
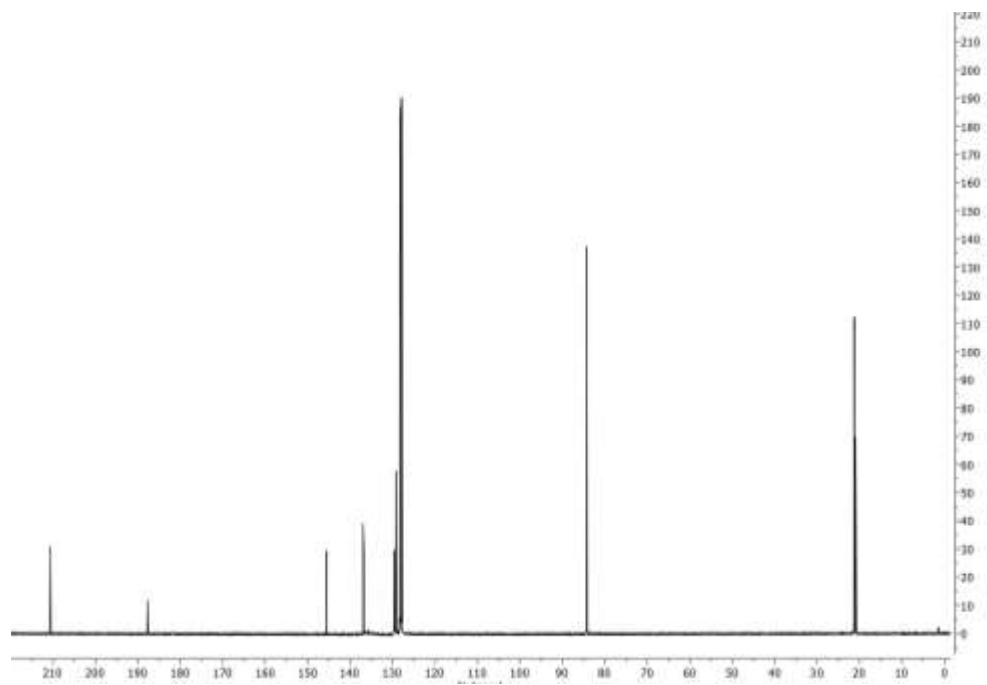
NMR Spectra

Figure S9. $^{119}Sn\{^1H\}$ NMR spectrum of **1** in C6D6 at 298 K.
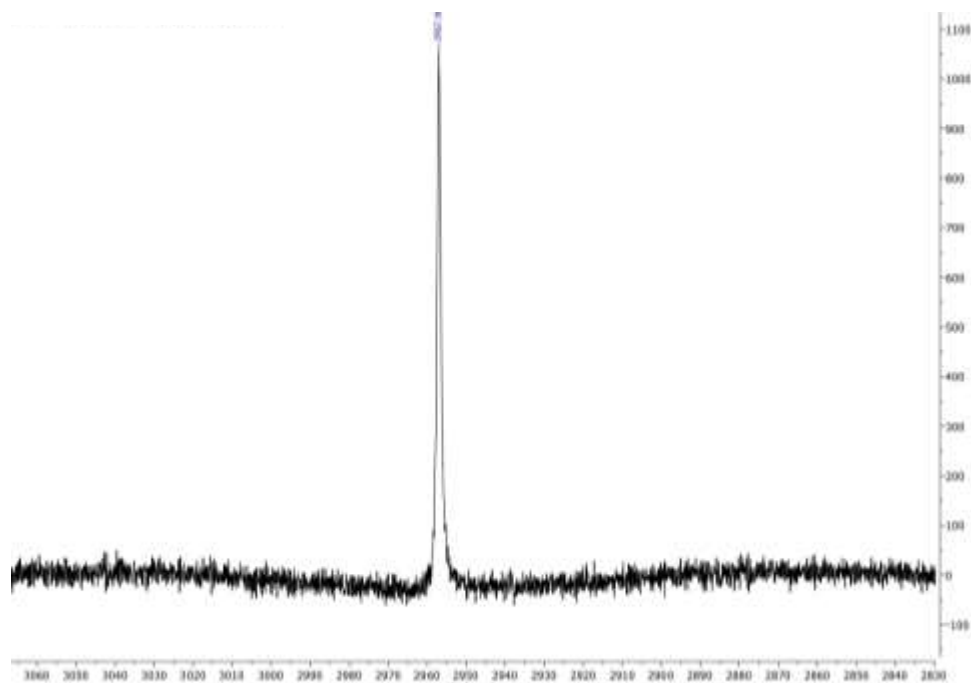
Figure S10. ^1H NMR spectrum of **2** in C_6D_6 at 298 K.
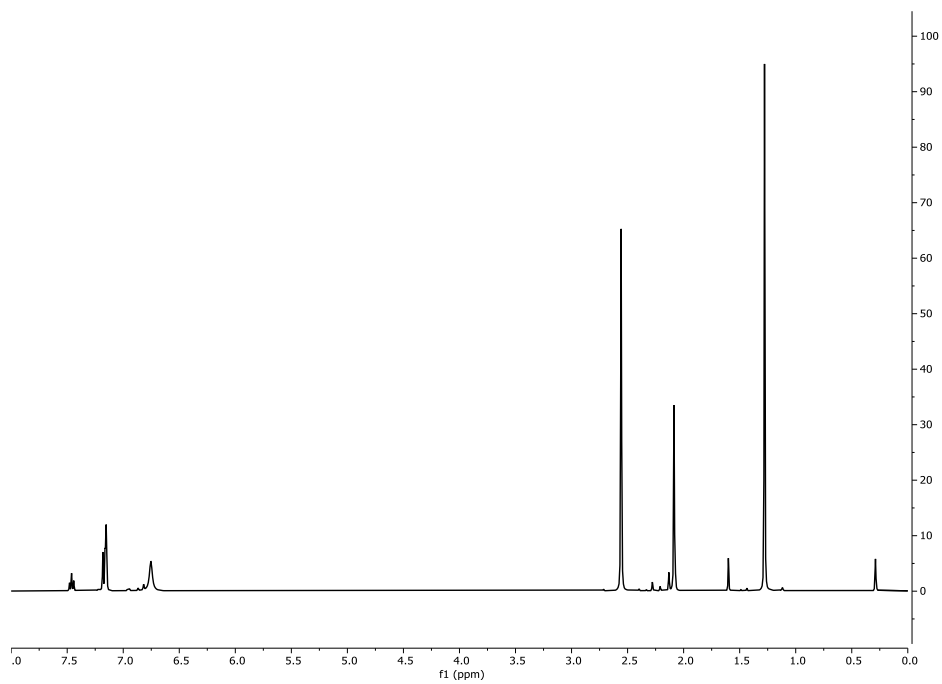
NMR Spectra

Figure S11. ^{1}H NMR spectrum of **3** in C$_6$D$_6$ at 298 K..
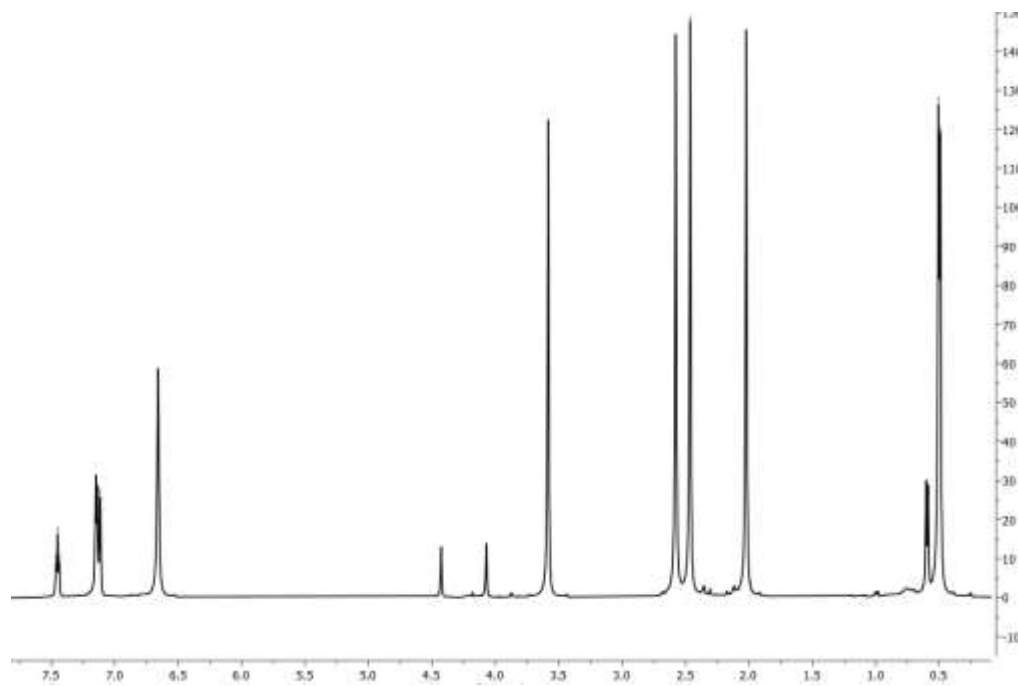
Figure S12. ^{13}C{^{1}H} NMR spectrum of **3** in C$_6$D$_6$ at 298 K.
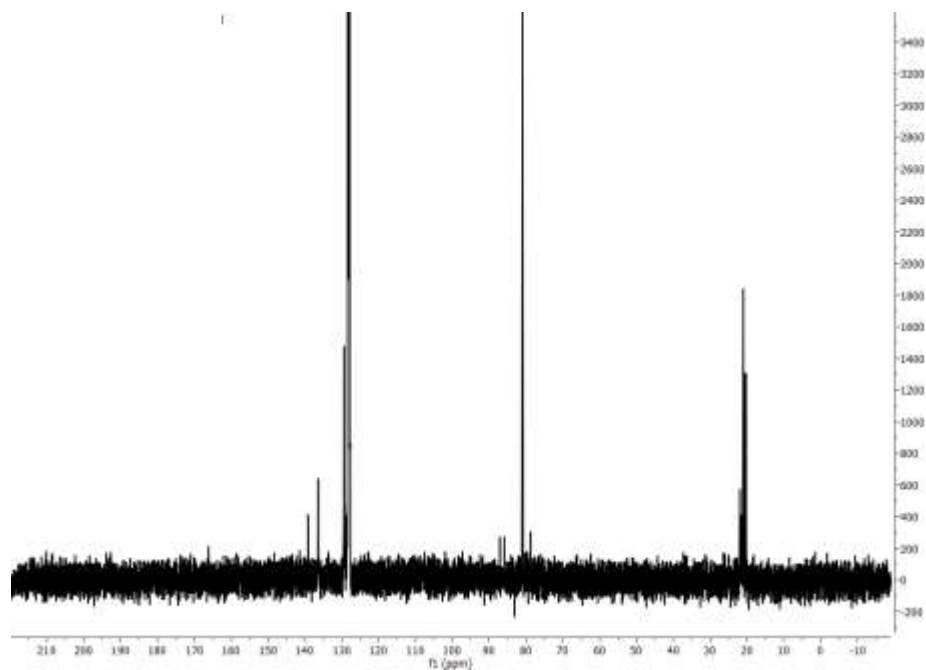
NMR Spectra

Figure S13. $^{31}P\{^1H\}$ NMR spectrum of **3** in C_6D_6 at 298 K.
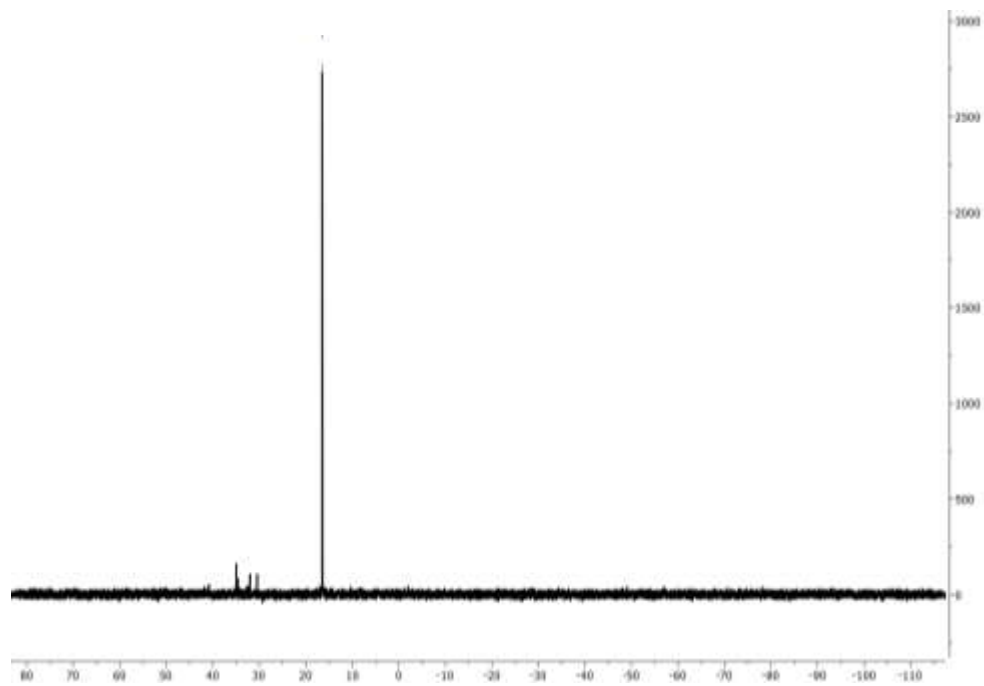
Figure S14. $^{119}Sn\{^1H\}$ NMR spectrum of **3** in C6D6 at 298 K.
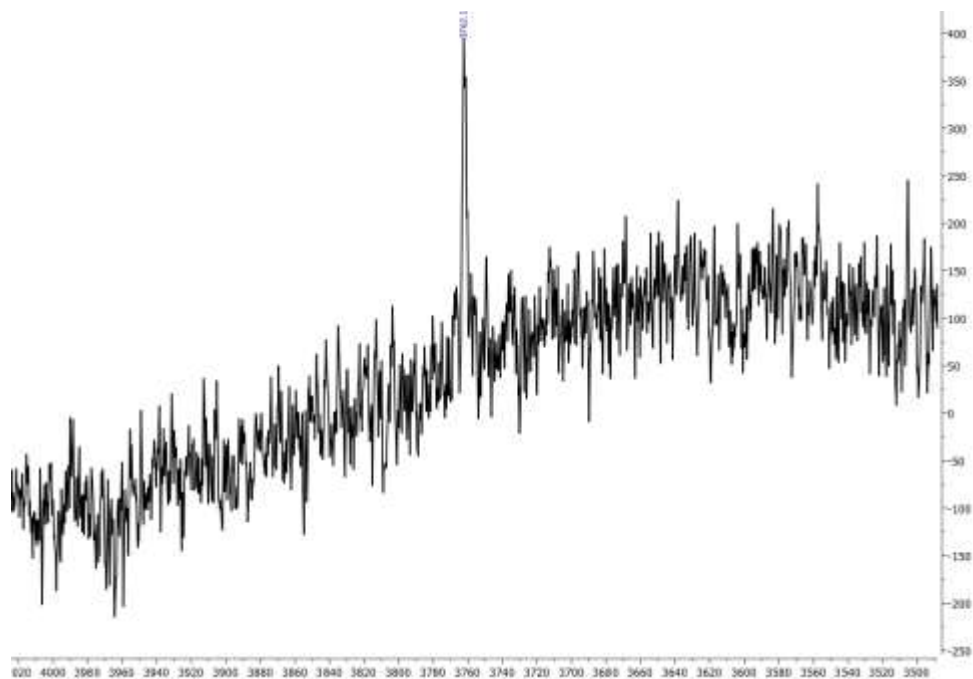
CHAPTER 3

UV-vis Spectra

Figure S15. UV-vis spectrum of **1** in hexanes at 298K.

$Ar^{Me_6}SnFeCp(CO)_2$, 90μM
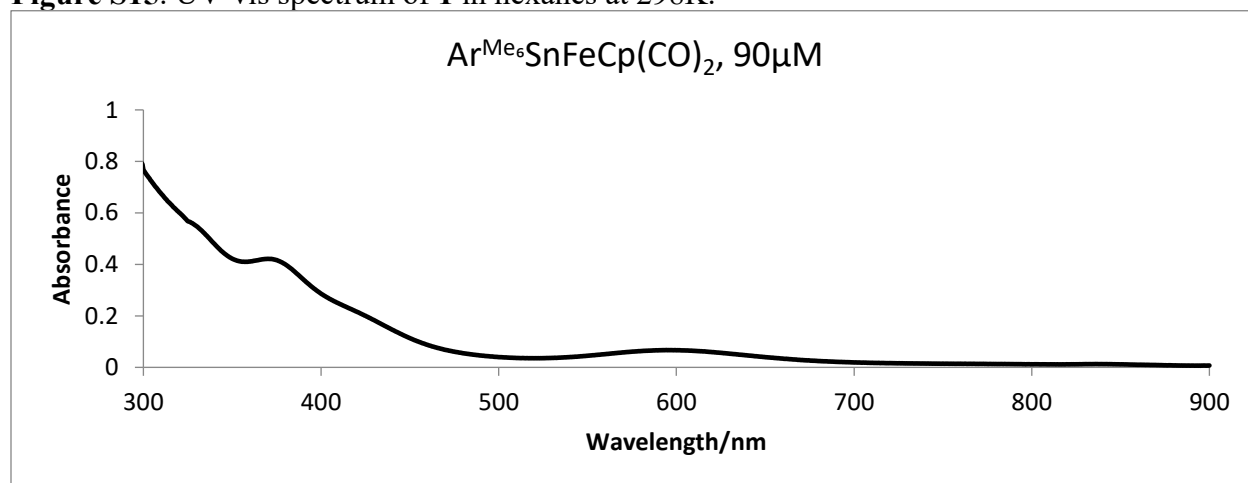
Figure S16. UV-vis spectrum of **2** in hexanes at 298K.

$Ar^{Me_6}SnFeCp^*(CO)_2$, 60 μM
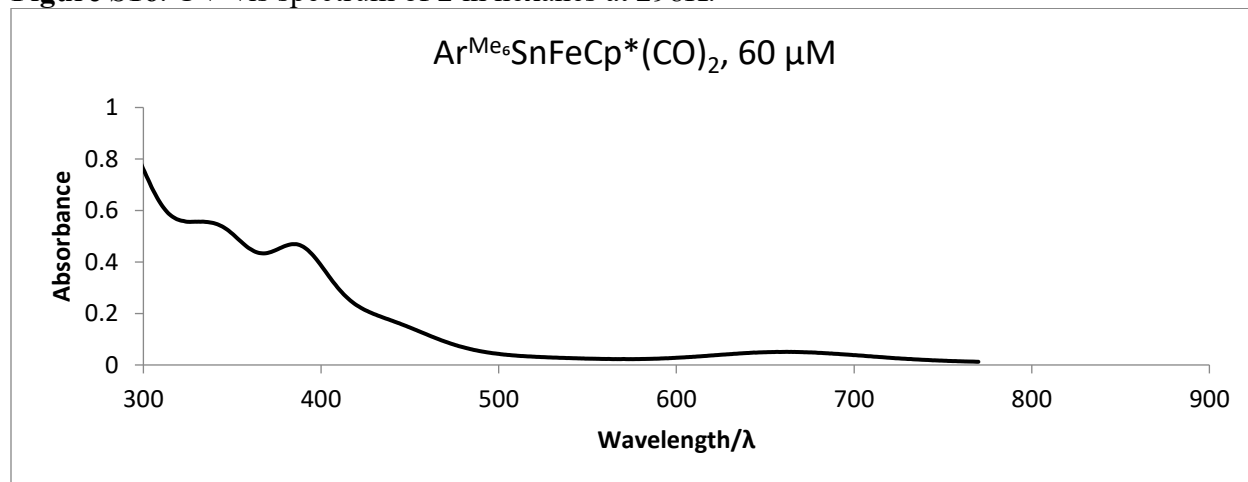
Figure S17. UV-vis spectrum of **3** in hexanes at 298K.
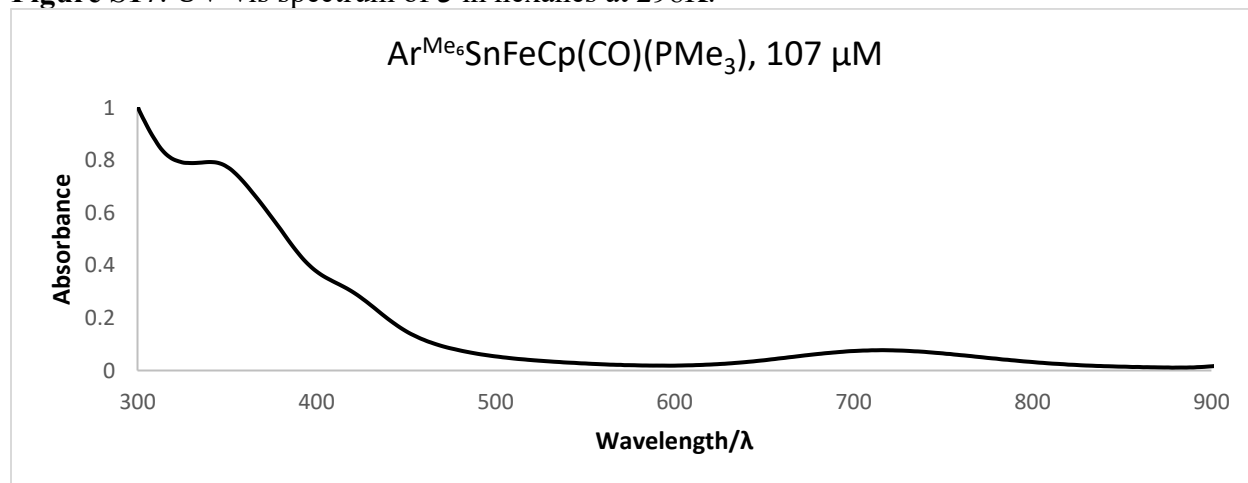
$Ar^{Me_6}SnFeCp(CO)(PMe_3)$, 107 μM

86

IR spectra

Figure S15. Infrared spectrum of **1**.

IR spectra
Figure S16. Infrared spectrum of **2**.
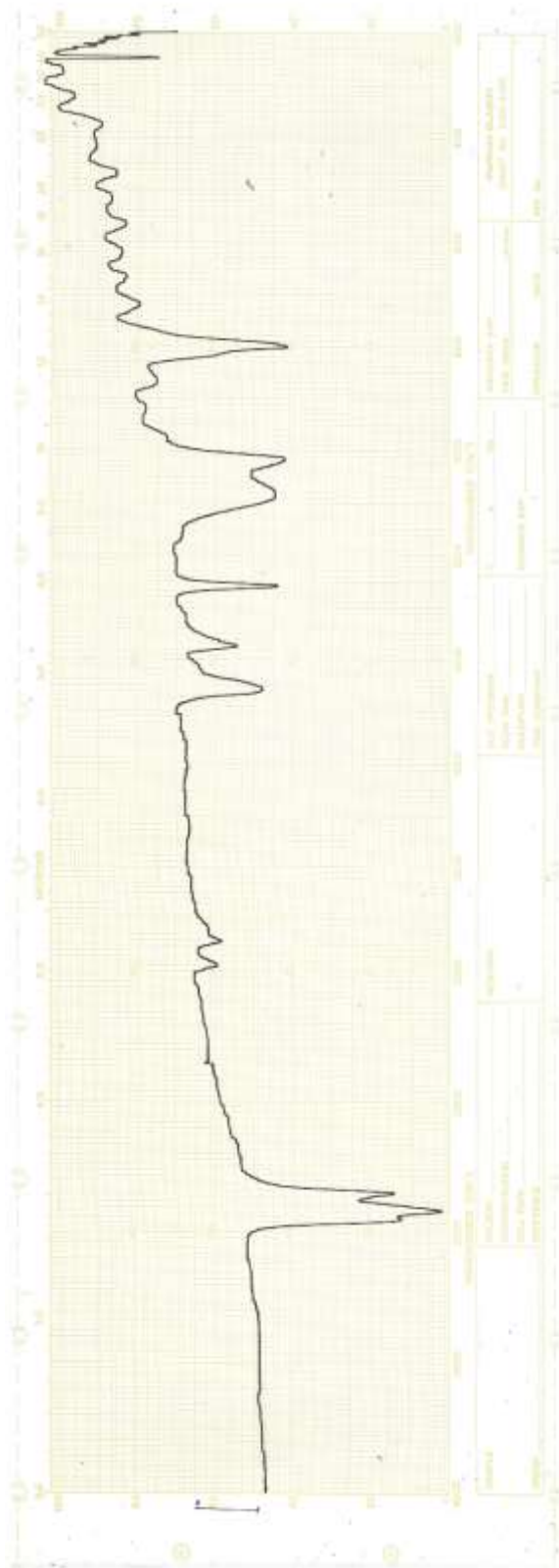
IR spectra
Figure S16. Infrared spectrum of **3**.
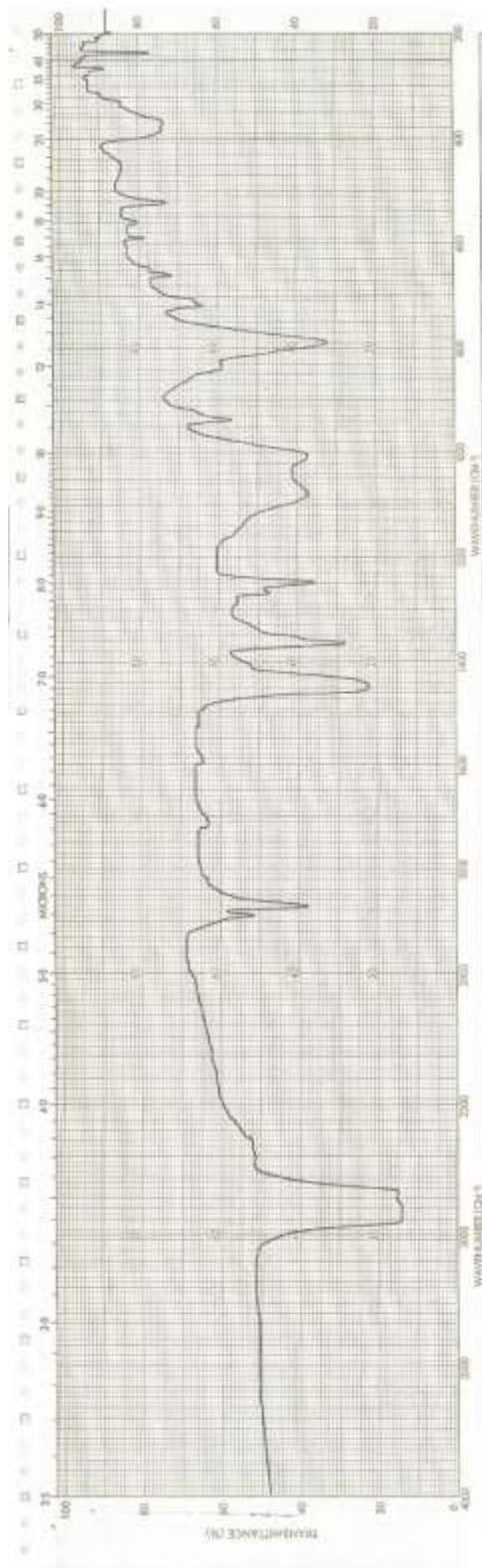
SI References

S1 Bruker, Bruker AXS Inc., Madison, Wisconsin, USA, **2001**

S2 G. M. Sheldrick, Acta Cryst. A 2015, 71, 3-8.

S3 Dolomanov, O. V.; Bourhis, L. J.; Gildea, R. J.; Howard, J. A. K.; Puschmann, H.; *OLEX2*: A complete structure solution, refinement and analysis program. J. Appl. Cryst, **2009**, *42*, 339-341.

Reversible Insertion of the Tin Atoms of the Ferriostannylenes ArSnFeCp(CO)$_2$ (Ar = Ar^{Me6} (−C$_6$H$_3$-(C$_6$H$_2$-2,4,6-Me$_3$)$_2$) or Ar^{iPr4} (−C$_6$H$_3$-(C$_6$H$_3$-2,6-^{i}Pr$_2$)$_2$)); Cp = η^5-C$_5$H$_5$) into the N–H bond of Ammonia, and Isolation and Reactivity of ArPbFeCp(CO)$_2$ with NH$_3$

Alice C. Phung,[1] Ella L. Schwirzke,[1] Derrick C. Kaseman,[1] James C. Fettinger,[1] Philip P. Power[1]*

[1]Department of Chemistry, University of California, 1 Shields Avenue, Davis, California 95616

ABSTRACT: The ferriostannylenes ArSnFeCp(CO)$_2$ (Ar = Ar^{Me6} (**1**) or Ar^{iPr4} (**2**)) and ferrioplumbylenes ArPbFeCp(CO)$_2$ (Ar = Ar^{Me6} (**3**) or Ar^{iPr4} (**4**)) were reacted with ammonia under both neat and solution-phase conditions. Compounds **1** and **2** displayed color changes attributable to a reversible insertion of the stannylene tin atom into an N–H bond. ^{1}H VT NMR spectroscopy corroborated the reversibility of **2** and NH$_3$ by showing the signal corresponding to the amido group decreasing in intensity with increasing temperature, and vice versa. A van't Hoff plot of the VT NMR data indicated that the free energy change of the reaction is $\Delta G = 0.04$ kcal mol^{-1} at 25 °C and 0.24 kcal mol^{-1} at 60 °C. Spectroscopic studies of **1-4** and their Ge analogues ArGeFeCp(CO)$_2$ (Ar = Ar^{Me6} or Ar^{iPr4}) display periodic trends. With an increased atomic number, the bending angles at the tetrel atom becomes narrower and the energy associated with the π→π* transition in the aryl ligand increases in the order Ge < Sn < Pb. However, the energy associated with the n→p transition on the tetrel atom decreases in the order Sn > Ge > Pb, which is the same order as the electronegativity values of the tetrel atom. Compounds **3** and **4** displayed great stability in the presence of air and wet acetone, and the ferrioplumbylene **3** displayed no reactivity towards ammonia.

CHAPTER 4

4.1 INTRODUCTION

The reactions of ammonia with low valent group 14 species have been shown to involve coordination of NH_3 to the group 14 element[1–5] or insertion of the main group metal into the N–H bond.[6–25] In 2021, the ferriogermylenes $ArGeFeCp(CO)_2$ (Ar = $-C_6H_3-(C_6H_2-2,4,6-Me_3)_2$ (Ar^{Me6}) and $-C_6H_3-(C_6H_2-2,6-^iPr_2)_2$ (Ar^{iPr4})) were reacted with neat ammonia to afford cleavage of the N–H bond with insertion of the germanium atom to afford $ArGe(NH_2)(H)FeCp(CO)_2$ (Ar = Ar^{Me6} and Ar^{iPr4}) (**Figure 1**).[22] These reactions proved to be irreversible however.

$Ar = Ar^{Me6}$ or Ar^{iPr4}

22

$Ar = Ar^{Me6}$ (**1**) or Ar^{iPr4} (**2**)

This work.

$Ar = Ar^{Me6}$ (**3**) or Ar^{iPr4} (**4**)

This work.
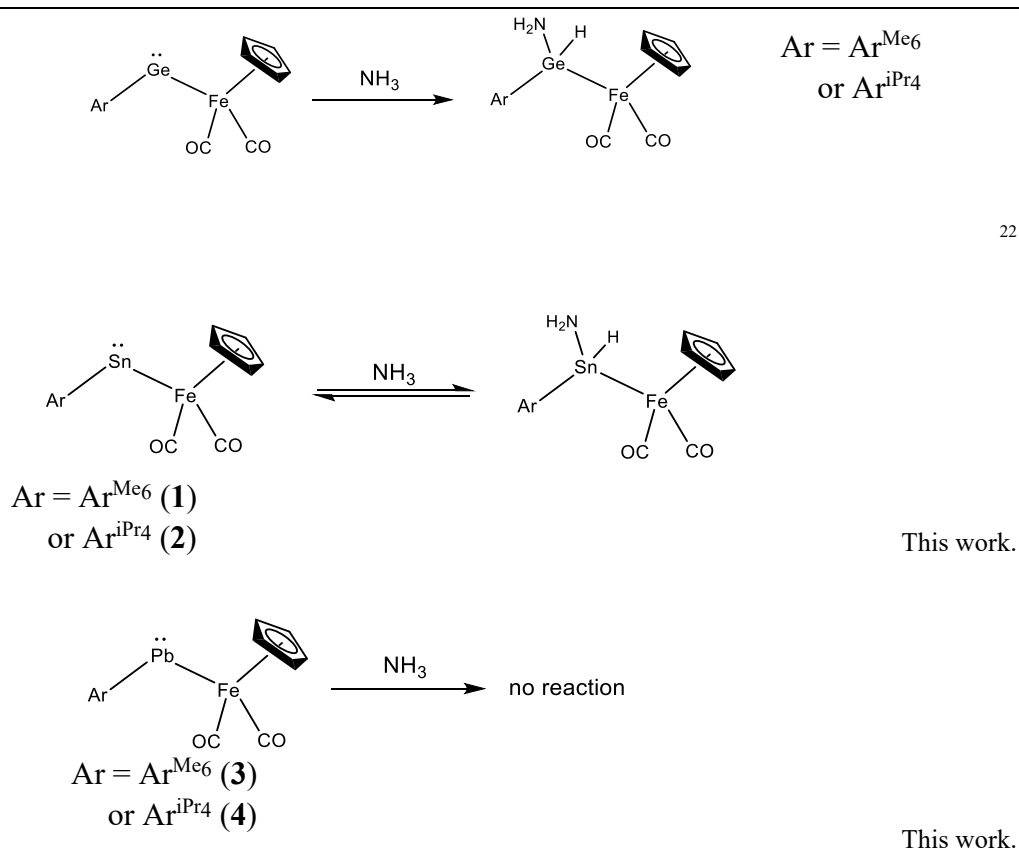
Figure 1. Reactions of $ArEFeCp(CO)_2$ with ammonia (E = Ge, Sn, or Pb; Ar = Ar^{Me6} or Ar^{iPr4}).

In this report, we extend these reactivity studies to include derivatives of tin and lead with an examination of the reactions of the ferriostannylenes $ArSnFeCp(CO)_2$ (Ar = Ar^{Me6} (**1**) or Ar^{iPr4} (**2**))

and ferrioplumbylenes ArPbFeCp(CO)$_2$ (Ar = Ar^{Me6} (**3**) or Ar^{iPr4} (**4**)). The reactions with ferriostannylenes **1** and **2** were found to be reversible and the thermodynamic parameters associated with the insertion were determined by VT NMR studies. In contrast, the ferrioplumbylenes **3** and **4** displayed no reaction with ammonia. A comparison of the spectroscopic properties of the ArEFeCp(CO)$_2$ series (E = Ge,[22] Sn,[23] or Pb; Ar = Ar^{Me6} or Ar^{iPr4}) is presented to investigate group 14 trends in the electronic nature of the ferriotetrylenes.

4.2 EXPERIMENTAL SECTION

General Procedures: All manipulations were carried out by using modified Schlenk techniques or in a Vacuum Atmospheres OMNI-Lab drybox under a N$_2$ or argon atmosphere. Solvents were dried over columns of activated alumina using a Grubbs type purification system (Glass Contour), stored over Na (toluene) or K (hexanes, diethyl ether) mirrors, and degassed via three freeze-pump-thaw cycles prior to use. The compounds ArSnFeCp(CO)$_2$ (Ar = Ar^{Me6} (**1**) or Ar^{iPr4} (**2**))[23], ArPbBr (Ar = Ar^{Me6} (**3**) or Ar^{iPr4} (**4**))[26–28], and K[FeCp(CO)$_2$][29] were synthesized according to literature procedures. Ammonia was twice-dried with sodium or a Na/K alloy, over approx. 36 hours and further dried by passage through a drying column containing CaO prior to use. The ^{1}H, ^{13}C{^{1}H}, ^{119}Sn{^{1}H}, and ^{207}Pb{^{1}H} NMR spectra were recorded on Bruker Avance DRX 500 MHz spectrometer and were referenced to the residual solvent signals in C$_6$D$_6$ (^{1}H: δ 7.15 ppm, ^{13}C: δ 128.06 ppm) or C$_7$D$_8$ (^{1}H: δ 2.09 ppm)[30]. UV-Visible spectra were recorded using dilute hexane solutions in 3.5 mL quartz cuvettes using an Olis 17 Modernized Cary 14 UV-Vis/NIR spectrophotometer. The infrared spectrum for **3** was recorded as Nujol mulls between CsI windows on a PerkinElmer 1430 spectrophotometer. The infrared spectrum for **4** was collected on a Bruker

CHAPTER 4

Tensor 27 ATRFTIR spectrometer. Melting points were determined in flame-sealed glass capillaries on a Meltemp II apparatus equipped with a partial immersion thermometer.

ArPbFeCp(CO)$_2$ (3: Ar^{Me6}, 4: Ar^{iPr4}): A solution of Ar^{Me6}PbBr (**3:** 2.2 g, 3.6 mmol) or Ar^{iPr4}PbBr (**4:** 0.8 g, 1.2 mmol) in diethyl ether (40 mL) was added dropwise to a diethyl ether (ca. 40 mL) suspension of K[FeCp(CO)$_2$] (**3:** 0.78 g, 3.6 mmol; **4:** 0.26 g, 1.2 mmol) cooled to ca. 0 °C. The resulting green solution was stirred overnight. The solvent was removed under reduced pressure to afford a green solid that was dissolved in a 1:1 toluene and hexanes mixture (ca. 50 mL). This solution was filtered through a Celite plug, and the green filtrate was concentrated to ca. 5 – 10 mL under reduced pressure until incipient crystallization. Storage at room temperature overnight produced dark green crystals of **3** or **4**.

3: Yield: 1.5 g (60%). Mp: 230-250 °C. ^{1}H NMR (500 MHz, C$_6$D$_6$, 20 °C): δ 2.04 (s, 6H, p-C(CH_3)), δ 2.45 (s, 12H, o-C(CH_3)), δ 3.52 (s, 5H, η^5-C$_5$H$_5$), δ 6.72 (s, 4H, flanking m-aromatic H), δ 7.60 (t, 1H, central p-aromatic H), δ 7.78 (d, 2H, J$_{HH}$ = 7.5Hz, central m-aromatic H). ^{13}C NMR (151 MHz, C$_6$D$_6$, 20 °C): δ 20.86 (p-CH_3) δ 83.41 (η^5-C$_5$H$_5$), δ 125.53, 130.29, 136.50, 137.02, 137.11 (Ar(C)), δ 146.98 (C_{ipso}-Pb), δ 195.83 (CO). ^{207}Pb NMR (149 MHz, C$_6$D$_6$, 20 °C): δ 11613. UV-vis (hexane): λ_{max} (ε) 330 nm (790 mol^{-1} L cm^{-1}), 630 nm (220 mol^{-1} L cm^{-1}). IR (Nujol, cm^{-1}): ν_{CO} 1970 (s), ν_{CO} 1921 (s).

4: Yield: 0.3 g (31%). Mp: 240-270°C. ^{1}H NMR: (500 MHz, C$_6$D$_6$, 20 °C) δ 1.12 (d, 12H, CH(CH_3)), δ 1.39 (d, 6H, CH(CH_3)), δ 2.89 (sept, ^{3}J$_{HH}$ = 12.9 Hz, 2H, CH(CH$_3$)), δ 3.37 (sept, ^{3}J$_{HH}$ = 12.9 Hz, 2H, CH(CH$_3$)), δ 3.59 (s, 5H, η^5-C$_5$H$_5$), δ 7.03-7.30 (m, 9H, aromatic H). ^{13}C NMR (151 MHz, C$_6$D$_6$, 20 °C): δ 22.95 (CH(CH_3)$_2$) δ 24.93 (CH(CH_3)$_2$), δ 25.04 (CH(CH_3)$_2$), δ 27.89 (CH(CH_3)$_2$), δ 31.22 (CH(CH$_3$)$_2$), δ 84.19 (η^5-C$_5$H$_5$), δ 123.45, 125.20, 132.01, 137.75,

138.93, 140.60, 141.66, 145.91, 147.44 (Ar(C)), δ 195.01 (CO) C_{ipso}-Pb signal not observed.

^{207}Pb NMR (149 MHz, C$_6$D$_6$, 20 °C): δ 11728.96. UV-VIS (hexane): λ_{max} (ε) 337 nm (4100

mol^{-1} L cm^{-1}), 634 nm (420 mol^{-1} L cm^{-1}). AT-FTIR: ν_{CO} 1961 (s), ν_{CO} 1916 (s).

Reaction of 1 or 2 with ammonia.

Solvent free: Anhydrous ammonia was condensed onto solid **1** (0.5 g, 0.82 mmol) or **2** (0.5 g, 0.72

mmol) in a Schlenk tube cooled in a dry ice/acetone bath to ca. -78°C, which gave a suspension of

a red-orange powder in colorless NH$_3$(l). The solution was stirred for ca. 60 minutes at ca. -78°C.

The cold bath was then removed to allow the solution to warm with continued stirring while the

excess NH$_3$ evaporated. The resulting orange solid was dried by overnight storage at room

temperature under N$_2$(g) at ambient atmospheric pressure. Dissolution of the orange solid in ca. 40

mL of hexanes gave a green solution that was concentrated until incipient crystallization, approx.

25 mL.

For **1**: The hexanes solution yielded a mixture of green crystals and orange-pink crystals. The

green crystals were determined by X-ray crystallography to be **1** and the orange-pink crystals

proved unsuitable for X-ray crystallography. The orange crystals could not be separated from

the green crystals, and a ^{1}H NMR spectrum of the green and orange-pink crystals mixture

displayed signals predominantly due to **1**.

For **2**: A mixture of green and colorless crystals were generated from the hexanes solution. The

green crystals were determined by X-ray crystallography to be **2** and the colorless crystals were

unsuitable for X-ray crystallography. A ^{1}H NMR spectrum of the dried crude solid showed a

mixture of **2** and Ar^{iPr4}Sn(NH$_2$)(H)FeCp(CO)$_2$. ^{1}H NMR: (500 MHz, C$_7$D$_8$, 20°C) δ 0.41 (br s,

2H, amide *H*), δ 1.08 (s, 18H, CH(C*H*$_3$)$_2$), δ 1.38 (s, 15H, CH(C*H*$_3$)$_2$), δ 3.39 (s, 4H, C*H*(CH$_3$)),

δ 3.91 (s, 5H, η^5-C$_5$H$_5$), δ 6.95 – 7.57 (br m, 9H, aromatic H).

In solution: In a 50 mL Schlenk flask, a deep green solution of **1** (0.1 g, 0.165 mmol, 30 mL) or

2 (0.12 g, 0.172 mmol, 10 mL) in a 1:1 toluene and hexanes mixture was frozen in a liquid nitrogen

bath. The headspace was evacuated and backfilled with ammonia gas (**1**: approx. 20 mL; **2**:

approx.. 40 mL). The frozen green solution was thawed with a room-temperature acetone bath to

afford an orange solution.

For **1**: Concentration to ca. 10 mL under reduced pressure and storage at ca. -32°C gave orange-

pink crystals. The crystals proved unsuitable for X-ray crystallographic studies. Dissolution of

these crystals in C$_6$D$_6$ gave a green solution. The ^{1}H NMR spectrum of the crystals

corresponded to compound **1**.

For **2**: Storage at ca. -32°C gave an orange solution with colorless crystals. The crystals proved

unsuitable for single crystal X-ray crystallographic studies. Reducing the pressure of the flask

to bring into the glove box for analysis caused the crystals to change to an ivory color. The ^{1}H

NMR spectrum of the crystals showed Ar^{iPr4}H and cyclopentadiene.

Reaction in a J-Young's Tube: Approximately 0.014 g of **2** (0.02 mmol) was dissolved in ca. 1

mL of C$_7$D$_8$ in a J-Young's tube at room temperature. The solution was frozen in a liquid nitrogen

bath and the headspace was evacuated and backfilled with a few drops of dried ammonia. The J-

Young's tube was sealed under slightly reduced pressure and the solution was allowed to slowly

come to room temperature prior to collecting ^{1}H NMR spectra. The ^{1}H NMR spectrum at 300 K

showed signals due to the insertion product Ar^{iPr4}Sn(NH$_2$)(H)FeCp(CO)$_2$: (500 MHz, C$_7$D$_8$, 25°C)

δ 0.39 (br s, 2H, amide H), δ 1.09 (d, $^2J_{HH}$ = 6.8 Hz, 12H, CH(CH_3)$_2$), δ 1.38 (d, $^2J_{HH}$ = 6.8 Hz,

12H, CH(CH_3)$_2$), δ 3.41 (s, 4H, CH(CH$_3$)), δ 3.87 (s, 5H, η^5-C$_5$H$_5$), δ 6.95 – 7.45 (br m, aromatic

H). ^{13}C{^{1}H} NMR: (151 MHz, C$_7$D$_8$, 20°C) δ 24.38 (CH(CH$_3$)$_2$) δ 27.64 (CH(CH$_3$)$_2$), δ 31.75

(CH(CH$_3$)$_2$), δ 85.29 (η^5-C_5H$_5$), δ 124.46, 126.55, 130.97, 141.17, 147.17, 148.62 (Ar(C)), δ 216.26

(CO), C$_{ipso}$-Sn signal not observed. ^{119}Sn{H} NMR: (186 MHz, C$_7$D$_8$, 20°C) δ 389.2.

Reaction of 3 with ammonia:

Solvent-free: Anhydrous ammonia was condensed onto solid **3** (90 mg, 0.13 mmol) cooled in a

dry ice/acetone bath to ca. -78°C to give a suspension of a green powder in colorless NH$_3$(l). The

solution was stirred for ca. 3 hours at ca. -78°C. The cold bath was then removed and stirring

continued while the excess NH$_3$ evaporated. The resulting green solid (unreacted **3**) was stored

overnight at room temperature to dry under N$_2$(g) at ambient atmospheric pressure.

In solution: In a 50 mL Schlenk flask, a deep green solution of **3** (80 mg, 0.12 mmol) in a 1:1

toluene and hexanes mixture (10 mL) was frozen in a liquid nitrogen bath. The headspace was

evacuated and backfilled with ammonia gas. The frozen solution was thawed in a room-

temperature acetone bath to afford a green solution. The solution was allowed to warm to room

temperature and was stirred under NH$_3$(g) at ambient atmospheric pressure for ca. 24 hours.

Removing the solvent gave a green solid of **3**.

4.3 RESULTS AND DISCUSSION

Ferriostannylene reactions with ammonia. The solvent-free reaction of the ferriostannylenes **1**

and **2** with ammonia proceeded analogously to the reaction of the ferriogermylenes

ArGeFeCp(CO)$_2$ (Ar = Ar^{Me6} or Ar^{iPr4}) with ammonia,[22] with the ferriostannylenes generating an

orange solution and precipitate in the same way as the germanium derivatives. In the previous

work with the germanium analogues, the orange products were was identified spectroscopically and crystallographically as the amido germanium hydride $ArGe(NH_2)(H)FeCp(CO)_2$ (Ar = Ar^{Me6} or Ar^{iPr4}).[22]

Addition of hexanes to the orange solid produced in the reaction of **1** with $NH_3(l)$ gave a green solution that generated a mixture of green and orange-pink crystals (**Figure S1b**). The green crystals were confirmed by X-ray crystallography to be the starting material **1**. The peach-colored crystals under the microscope appeared similar in color and habit to the crystals of $Ar^{Me6}Ge(NH_2)(H)FeCp(CO)_2$. However, these crystals proved unsuitable for X-ray crystallographic studies (**Figure S1c**). Dissolution of the orange solid in C_6D_6 produced a green solution and ^1H NMR analysis showed only starting material **1**. Considering the absence of a signal in the ^1H NMR spectrum that can be assigned as amide protons, as well as the observed behavior of the product to give a green solution from an orange solid, the product of the reaction appears to revert to **1** upon dissolution in solvent (**Figure S3**).

The orange powder produced from the reaction of **2** with $NH_3(l)$ was observed to spontaneously convert to a green-colored solid under reduced pressure, despite increasing the drying time for the crude orange product to 24 hours. A ^1H NMR analysis of the pale green powder displayed the addition of a broad singlet at 0.41 ppm, which falls within the range of $SnNH_2$ protons in amido tin complexes (0.38 – 0.93 ppm).[7,10] Furthermore, the broad lineshape of the singlet at 0.41 ppm is similar to the broad signal of the N-H_2 protons signal of the germanium derivatives $ArGe(NH_2)(H)FeCp(CO)_2$ (Ar = Ar^{Me} or Ar^{iPr4}).[22] Integrating the cyclopentadienyl proton singlet at 3.91 ppm to 5H gives a relative intensity of 2H for the broad singlet. However, the relative intensity of the signals for the isopropyl methyl protons exceeds the expected value of 24H. The

relative intensities of the ^{1}H NMR signals signifies that the light green powder is a mixture of **2** and an insertion product, and the similarity of the singlet at 0.41 ppm to known amido germanium derivatives[10,22] suggests that the insertion product is likely $Ar^{iPr4}Sn(NH_2)(H)FeCp(CO)_2$.

Based on the temperature-dependent color changes observed in the solution-phase reaction of **2** with ammonia (*vide infra*), the reaction was performed in a J-Young's tube for VT ^{1}H NMR analysis. Prior to adding $NH_3(g)$ to the NMR sample, the ^{119}Sn NMR spectrum displayed a signal at 2959 ppm corresponding to **2** in C_7D_8. After adding dried $NH_3(g)$, the singlet at 2959 ppm disappeared and a new singlet at 389 ppm was observed. This signal lies downfield of the ^{119}Sn signals reported for the amido tin hydrides $[ArSn(\mu\text{-}NH_2)]_2$ (Ar = Ar^{Me6}, δ = 313 ppm; Ar^{iPr4}, δ = 280 ppm)[7,9,10] and may be due to the Sn atom bonding to a more electronegative Fe atom (in comparison to another ipso-carbon of an aryl group) thereby causing an increase in the deshielding effect on tin. The ^{1}H NMR spectrum at 300 K after adding dried $NH_3(g)$ revealed a broad singlet at 0.39 ppm, which is in the same region as the $Sn\text{-}NH_2$ proton signals of $[ArSn(\mu\text{-}NH_2)]_2$ (Ar = Ar^{Me6}, Ar^{iPr4}, or Ar^{iPr6}) (0.38 – 0.93 ppm).[7,9,10] The singlet at 0.39 ppm also has a relative intensity of 2H in comparison to the isopropyl methyl proton signals (24H) and cyclopentadienyl proton singlet (5H), lending additional support to the assignment of the signal to the $N\text{-}H_2$ protons. A signal that could reasonably be assigned as the Sn-H signal was not observed. The upfield shifted ^{119}Sn NMR spectrum at 300 K signifies a conversion of the starting material $Ar^{iPr4}SnFeCp(CO)_2$ to a four-coordinate product, while the ^{1}H NMR spectrum of this the reaction indicates that this product is $Ar^{iPr4}Sn(NH_2)(H)FeCp(CO)_2$.

The ^{1}H NMR spectra of the sample were obtained at 320 K and 340 K in C_7D_8. With increasing temperature, the singlet assigned to the amide protons was observed to shift upfield, broaden, and

decrease in intensity relative to the signal of the Cp protons. The upfield migration and broadening of the amide proton singlet with changing temperatures is similar to that observed for temperature-dependent amide proton exchange.[31,32] However, the majority of the amide proton exchange NMR studies reported in the literature occur within proteins[31–37] or intramolecularly.[38] While the behavior of the singlet corresponding to the $Sn-NH_2$ protons could be the result of an intermolecular exchange, the decrease in integration of the amido protons singlet with increase in temperature indicates a more likely instance of a temperature-dependent reversible process.

As the temperature decreased, the singlet assigned to the $N-H_2$ protons was observed to shift downfield to its original location at 0.39 ppm at 300 K and increase in intensity in the process. A van't Hoff plot was constructed from the variable temperature ^1H NMR spectra (cf. **Figures S9 and S16**). The ΔH and ΔS values that were calculated from the van't Hoff plot are -1.6 kcal mol^{-1} and -5.5 × 10^{-3} kcal mol^{-1} K^{-1}, respectively. The free energy of the reaction ΔG is thus 0.04 kcal mol^{-1} at 25 °C and 0.24 kcal mol^{-1} at 60 °C. These values are in good agreement with the free energy of the reaction reported for the reversible activation of ammonia by the constrained high energy multicyclic phosphine, 7-phenyl-7H-[1,3,2]benzodiazaphospholo[2,1-b][1,3,2]benzothiazaphosphole, with the computations indicating an essentially thermoneutral reaction ΔG_{DFT} = -0.4 kcal mol^{-1} at room temperature and slightly endergonic reaction ΔG_{DFT} = 0.6 kcal mol^{-1} at 60 °C.[24]

The reactions of **1** or **2** with ammonia were also carried out in a 1:1 hexanes and toluene mixture and observed to produce an orange solution upon addition of ammonia. The flask containing the product of **2** with $NH_3(g)$, when removed from the ca. -32 °C storage, was observed to change in color to green as the flask slowly warmed. However, when the flask was returned to storage at ca.

CHAPTER 4

-32 °C, the solution was later observed to have returned to an orange color. These observations illustrate the temperature dependence of the reversible reaction of **2** with NH$_3$(*g*) in solution-phase conditions.

The crystals were harvested at low-temperatures ca. -30 °C and quickly placed under a 90 K cold stream for crystallographic data collection. Early collection data initially gave a well-defined diffraction pattern, but after ca. 30 minutes this deteriorated in quality as the crystals changed into an amorphous opaque block, from which no satisfactory structure solution could be obtained.

Ferrioplumbylene synthesis and characterization. Treatment of 1 equiv of ArPbBr[26,28] with 1 equiv of K[FeCp(CO)$_2$][29] gave, after workup and recrystallization from a 1:1 toluene and hexanes mixture, dark green crystals of the ferrioplumbylene ArPbFeCp(CO)$_2$ (Ar = Ar^{Me6} (**3**) or Ar^{iPr4} (**4**)) in moderate yield. (**Equation 1**) Salt metathesis is the most common route to these group 14 element-transition metal species,[22,23,39–42] although the most recently reported ferrioplumbylene was synthesized via the metathesis of the diplumbyne Ar^{iPr6}Pb≡Pb Ar^{iPr6} with the dinuclear iron carbonyl (Fe(CO)$_5$)$_2$.[43]

$$\text{ArPbBr} + \text{K[FeCp(CO)}_2\text{]} \xrightarrow{\text{Et}_2\text{O, 25 °C}} \text{ArPbFeCp(CO)}_2 + \text{KBr}$$

$$Ar = Ar^{Me6} \text{ (\textbf{3})}$$
$$= Ar^{iPr4} \text{ (\textbf{4})}$$
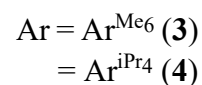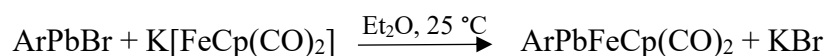
Equation 1. Synthesis of compounds **3** and **4**.

The ferrioplumbylenes **3** and **4** displayed remarkable stability. Exposing the green crystals to air and dissolution in wet acetone gave a green solution that showed no signs of decomposition for up

to 30 minutes. Compounds **3** and **4** were characterized by ^{1}H, ^{13}C, ^{207}Pb NMR, UV-vis, and IR spectroscopy. Attempts to grow crystals of compound **3** suitable for X-ray crystallography were unsuccessful. Nonetheless for **4**, the larger ligand enabled the formation of crystals that were suitable for X-ray crystallography.[44]

Table 1. Selected Structural and Spectroscopic Data for ArEFeCp(CO)$_2$. (E = Ge, Sn, or Pb; Ar = Ar^{Me6} or Ar^{iPr4})

ArEFeCp(CO)$_2$	E = Ge[22,23] Ar = Ar^{Me6}, Ar^{iPr4}	E = Sn[23] Ar = Ar^{Me6}, Ar^{iPr4}	E = Pb Ar = Ar^{Me6} (**3**), Ar^{iPr4} (**4**)
C$_{ipso}$-E-Fe, deg	115.59(8) 115.27(6)	113.60(3) 112.65(9)	n/a 111.09(16)
^{1}H NMR: δ_{Cp}, ppm	3.82 3.84	3.66 3.78	3.52 3.59
UV-vis: λ_{max} $\pi \rightarrow \pi^*$ transition, nm	430 428	384 382	330 337
UV-vis: λ_{max} n$\rightarrow$p transition, nm	616 620	594 608	630 634
IR: ν_{CO}, cm^{-1}	1980 & 1940 1977 & 1917	2010 & 1950 1970 & 1921	1970 & 1921 1961 & 1916

A comparison of the ferriotetrylenes ArEFeCp(CO)$_2$ (E = Ge, Sn, or Pb; Ar = Ar^{Me6} or Ar^{iPr4}) (**Table 1**) shows that interligand angle at the tetrel atom narrows with increasing atomic number, Ge > Sn > Pb. The cyclopentadienyl group proton signals in the ^{1}H NMR spectra and the absorptions assigned to the $\pi \rightarrow \pi^*$ transition on the aryl ligand[22,23,45] in the UV-vis spectra also observe spectroscopic shifts in the order Ge > Sn > Pb. Thus, for a larger tetrel atom, the interligand angle is observed to sharpen, the cyclopentadienyl group protons experience increased shielding,

and the $\pi \rightarrow \pi^*$ transition on the aryl ligand shifts towards higher energies. Dissimilarly, the v_{CO} bands in the IR spectra and the absorptions assigned to the n→p transition of the tetrel atom in the UV-vis spectra[40,46] feature a pattern in the sequence Sn < Ge < Pb that correlates to their electronegativites values on the Sanderson scale (Sn: 1.96, Ge: 2.01, Pb: 2.33).[47,48] Thus, as the electronegativity of the tetrel atom increases, the CO stretching frequencies observe a shift towards lower wavenumbers and the n→p transition experiences a lowering of the energy transition.

Within the context of other metallopumblylenes, $Ar^{iPr6}PbMCp(CO)_2$ (M = Cr, Mo, or W), the difference in electronegativities among the transition metals (Fe: 1.83, Cr: 1.66, Mo: 2.16, W: 2.36)[47,48] account for the observed spectroscopic differences. The Cp protons of **3** and **4** appear more downfield than those of the Mo and W analogues (M = Cr, δ_{Cp} = 3.55 ppm; M = Mo, δ_{Cp} = 4.05 ppm; M = W, δ_{Cp} = 4.07 ppm)[41] and is consistent with the greater metal-ligand interaction for the molybdenum and tungsten complexes.[40] Moreover, the ^{207}Pb NMR spectra for **3** and **4** display signals at 11613 and 11729 ppm, respectively, significantly more downfield than the ^{207}Pb signals of $Ar^{iPr6}PbMCp(CO)_2$ (M = Cr, Mo, or W) which appear in the 9374 – 9659 ppm region.[41] Lastly, the CO stretching bands of **3** and **4** appear at higher frequencies than those of $Ar^{iPr6}PbMCp(CO)_2$ (M = Cr, Mo, or W) (v_{CO} = 1962 – 1825 cm^{-1})[41] indicating weaker Fe–C bonds than M–C bonds (M = Mo, Cr, or W).
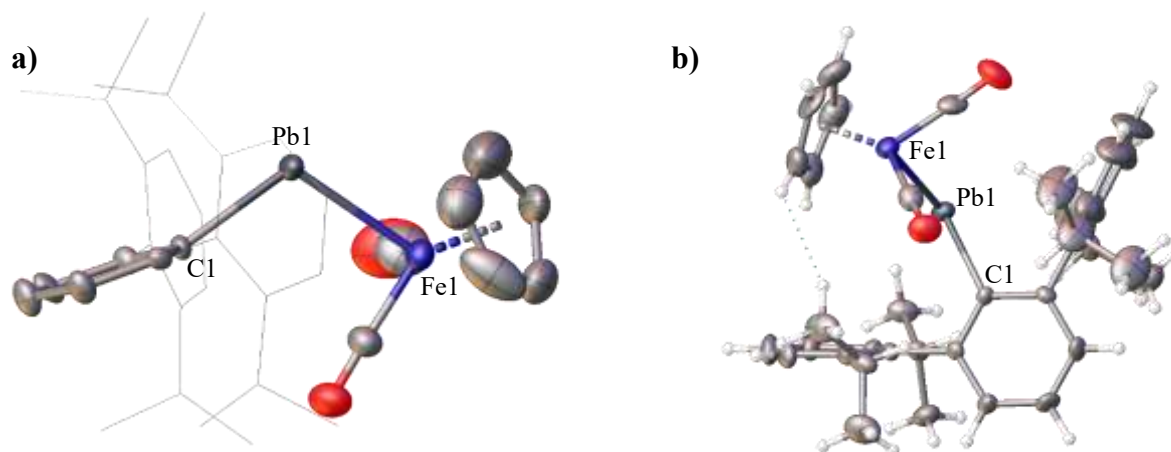
Figure 2. Thermal ellipsoid plots (50%) of **4**. **a)** "Side" view of **4**. Carbon-bound H atoms and structural disorder are not shown and flanking phenyl rings are shown as wire frames for clarity. **b)** Rotated view of **2** showing the H···H contact = 2.4937(1) Å. Selected bond lengths (Å) and angles (deg): Pb1–C1 = 2.321(6); Pb1–Fe1 = 2.6388(11); C1–Pb1–Fe1 = 111.09(16)°.

The C-Pb-Fe bond in **4** (111.09(16)°) is within the range of the metalloplumbylenes Ar^{iPr6}PbMCp(CO)$_3$ (M = Mo, Cr, W), Ar^{iPr6}PbMn(CO)$_5$, and (PbAr^{iPr6})$_2$Fe(CO)$_4$ (108.6(2)° – 113.58(9)°).[41,43] However, the ruthenoplumbylene Ar^{iPr6}PbRuCp*(P^{i}Pr$_2$Me)(H)$_2$ (119.28(9)°) and the heterotrimetallic metalloplumbylenes (FcN)$_2$PbM(CO)$_5$ (Fc = bis[2-((dimethylamino)methyl)ferrocenyl], M = Cr, Mo, W) (127.23(7)° – 133.51(7)°) report wider angles at the Pb atom, since these species contain sterically encumbering or sterically constraining ligands on either side of the Pb atom.[42,49]

Ferrioplumbylene reaction with ammonia. The solvent-free and solution-phase reactions of the ferrioplumbylene **3** proceeded in a similar way to that of **1** and **2**. Stirring this solution for long periods of time, from 3 – 24 hours, did not yield any observable changes. Elimination of the excess ammonia produced a green powder that, when dissolved in C$_6$D$_6$, gave a dark green solution that

^{1}H NMR analysis confirmed to be the starting material **3**. Given the inactivity of **3** towards $NH_3(l)$, the general pattern of increased stability with increasing terphenyl size,[44] and the stability exhibited by both **3** and **4** to the air and dissolved in and wet acetone, a reaction with ammonia was not attempted for ferrioplumbylene **4**.

4.4 CONCLUSION

Ferriostannylenes **1** and **2**, which differ in the size of the terphenyl group, react reversibly with ammonia. The reactions were conducted with NH_3 as a neat reagent, with condensed $NH_3(l)$ functioning as both solvent and reactant. In the neat-phase reactions, the reaction between **1** and NH_3 displayed reversibility upon addition of solvent to the product, and the reversibility between **2** and NH_3 was observed to occur under reduced pressure. The reactions were also performed with **1** or **2** dissolved in a 1:1 toluene and hexanes solution, stirring under an atmosphere of $NH_3(g)$. Ferriostannylene **2** displayed a temperature-dependence of the reversibility in the solution-phase, so the reaction of **2** and $NH_3(g)$ was examined via a ^{1}H VT NMR-scale reaction, which showed conversion to the amido tin hydride and allowed the thermodynamic parameters of the reaction to be determined. A van't Hoff plot of the 1H VT NMR data gave ΔH and ΔS values of -1.6 kcal mol^{-1} and -5.5×10^{-3} kcal mol^{-1} K^{-1}, respectively. Thus, the free energy of the reaction ΔG is 0.04 kcal mol^{-1} at 25 °C and 0.24 kcal mol^{-1} at 60 °C. The ferrioplumbylenes **3** and **4** were also synthesized to observe their reactivity with ammonia but were observed to be generally inert regardless of reaction conditions.

CHAPTER 4

ASSOCIATED CONTENT

Supporting Information.

Crystallographic data and spectra (NMR, IR, UV–vis).

Accession Codes.

CCDC 2248739 contain the supplementary crystallographic data for this paper. These data can be obtained free of charge via www.ccdc.cam.ac.uk/data_request/cif, or by emailing data_request@ccdc.cam.ac.uk, or by contacting The Cambridge Crystallographic Data Centre, 12 Union Road, Cambridge CB2 1EZ, UK; fax: +44 1223 336033.

AUTHOR INFORMATION

Corresponding Author

Philip P. Power – Department of Chemistry, University of California, Davis, California 95616, United States; orcid.org/0000-0002-6262-3209; Email: pppower@ucdavis.edu

Authors

Alice C. Phung – Department of Chemistry, University of California, Davis, California 95616, United States; https://orcid.org/0000-0002-0268-3971

Ella L. Schwirzke – Department of Chemistry, University of California, Davis, California 95616, United States

Derrick C. Kaseman – Department of Chemistry, University of California, Davis, California 95616, United States; https://orcid.org/0000-0003-2076-1264

James C. Fettinger – Department of Chemistry, University of California, Davis, California 95616, United States; https://orcid.org/0000-0002-6428-4909

Author Contributions

All authors have given approval to the final version of the manuscript.

Notes

The authors declare no competing financial interest.

CHAPTER 4

4.6 REFERENCES

(1)   Blaschette, A.; Hippel, I.; Krahl, J.; Wieland, E.; Jones, P. G.; Sebald, A. Polysulfonylamine. *J Organomet Chem* **1992**, *437*, 279–297.

(2)   Weinert, C. S.; Fanwick, P. E.; Rothwell, I. P. Novel Germanium(II) Binaphthoxide Complexes: Synthesis and Crystal Structure of (R,R)-[Ge{OC$_{20}$H$_{10}$(OSiMe$_3$)-2′-(SiMe$_3$)$_2$-3,3′}$_2$] and (R)-[Ge{O$_2$C$_{20}$H$_{10}$(SiMe$_2$Ph)$_2$-3,3′}{NH$_3$}]; Catalytic Function of Ge[N(SiMe$_3$)$_2$]$_2$ for the Mono-Silylation of 3,3′-Disubstituted-1,1′-Bi-2,2′-Naphthols. *Journal of the Chemical Society, Dalton Transactions* **2002**, No. 15, 2948–2950.

(3)   Wetherby, A. E.; Goeller, L. R.; DiPasquale, A. G.; Rheingold, A. L.; Weinert, C. S. Metal-Dependent Reactions of Bulky Metal(II) Amides M[N(SiMe$_3$)$_2$]$_2$ with 3,3′-Disubstituted Binaphthols (HO)$_2$C$_{20}$H$_{10}$(SiR$_3$)$_2$ -3,3′: Selective Conversion of One Equivalent −OH Group to a Silyl Ether −OSiMe$_3$. *Inorg Chem* **2008**, *47*, 2162–2170.

(4)   Green, R. A.; Moore, C.; Rheingold, A. L.; Weinert, C. S. Formation and Structures of Germanium(II) Aryloxo/Oxo Clusters. *Inorg Chem* **2009**, *48*, 7510–7512.

(5)   Kowalke, J.; Brendler, E.; Wagler, J. Valinate and SiMe$_2$ – An Interesting Couple in Pentacoordinate Si-Complexes: Templated Generation of the Dipeptide Val-Val and Formation of an Organosilicon-Ammonia-Adduct. *J Organomet Chem* **2021**, *956*, 122126.

(6)   Power, P. P. Interaction of Multiple Bonded and Unsaturated Heavier Main Group Compounds with Hydrogen, Ammonia, Olefins, and Related Molecules. *Acc Chem Res* **2011**, *44*, 627–637.

(7)   Stanciu, C.; Hino, S. S.; Stender, M.; Richards, A. F.; Olmstead, M. M.; Power, P. P. Synthesis and Characterization of Ge(II), Sn(II), and Pb(II) Monoamides with −NH$_2$ Ligands. *Inorg Chem* **2005**, *44* (8), 2774–2780.

(8)   Frey, G. D.; Lavallo, V.; Donnadieu, B.; Schoeller, W. W.; Bertrand, G. Facile Splitting of Hydrogen and Ammonia by Nucleophilic Activation at a Single Carbon Center. *Science (1979)* **2007**, *316* (5823), 439–441.

(9)   Peng, Y.; Ellis, B. D.; Wang, X.; Power, P. P. Diarylstannylene Activation of Hydrogen or Ammonia with Arene Elimination. *J Am Chem Soc* **2008**, *130*, 12268–12269.

(10)   Peng, Y.; Guo, J.-D.; Ellis, B. D.; Zhu, Z.; Fettinger, J. C.; Nagase, S.; Power, P. P. Reaction of Hydrogen or Ammonia with Unsaturated Germanium or Tin Molecules under Ambient Conditions: Oxidative Addition versus Arene Elimination. *J Am Chem Soc* **2009**, *131*, 16272–16282.

(11)   Jana, A.; Objartel, I.; Roesky, H. W.; Stalke, D. Cleavage of a N−H Bond of Ammonia at Room Temperature by a Germylene. *Inorg Chem* **2009**, *48*, 798–800.

(12) Jana, A.; Schulzke, C.; Roesky, H. W. Oxidative Addition of Ammonia at a Silicon(II) Center and an Unprecedented Hydrogenation Reaction of Compounds with Low-Valent Group 14 Elements Using Ammonia Borane. *J Am Chem Soc* **2009**, *131*, 4600–4601.

(13) Meltzer, A.; Inoue, S.; Präsang, C.; Driess, M. Steering S−H and N−H Bond Activation by a Stable N-Heterocyclic Silylene: Different Addition of H_2S, NH_3, and Organoamines on a Silicon(II) Ligand versus Its Si(II)→$Ni(CO)_3$ Complex. *J Am Chem Soc* **2010**, *132*, 3038–3046.

(14) Präsang, C.; Stoelzel, M.; Inoue, S.; Meltzer, A.; Driess, M. Metal-Free Activation of EH_3 (E=P, As) by an Ylide-like Silylene and Formation of a Donor-Stabilized Arsasilene with a HSi=AsH Subunit. *Angewandte Chemie International Edition* **2010**, *49*, 10002–10005.

(15) Wang, W.; Inoue, S.; Yao, S.; Driess, M. Reactivity of N-Heterocyclic Germylene Toward Ammonia and Water. *Organometallics* **2011**, *30*, 6490–6494.

(16) Alberto, M. E.; Russo, N.; Sicilia, E. EH_3 (E=N, P, As) and H_2 Activation with N-Heterocyclic Silylene and Germylene Homologues. *Chemistry - A European Journal* **2013**, *19*, 7835–7846.

(17) Usher, M.; Protchenko, A. v.; Rit, A.; Campos, J.; Kolychev, E. L.; Tirfoin, R.; Aldridge, S. A Systematic Study of Structure and E−H Bond Activation Chemistry by Sterically Encumbered Germylene Complexes. *Chemistry - A European Journal* **2016**, *22*, 11685–11698.

(18) Protchenko, A. v.; Bates, J. I.; Saleh, L. M. A.; Blake, M. P.; Schwarz, A. D.; Kolychev, E. L.; Thompson, A. L.; Jones, C.; Mountford, P.; Aldridge, S. Enabling and Probing Oxidative Addition and Reductive Elimination at a Group 14 Metal Center: Cleavage and Functionalization of E–H Bonds by a Bis(Boryl)Stannylene. *J Am Chem Soc* **2016**, *138*, 4555–4564.

(19) Wendel, D.; Szilvási, T.; Henschel, D.; Altmann, P. J.; Jandl, C.; Inoue, S.; Rieger, B. Precise Activation of Ammonia and Carbon Dioxide by an Iminodisilene. *Angewandte Chemie International Edition* **2018**, *57*, 14575–14579.

(20) Reiter, D.; Frisch, P.; Wendel, D.; Hörmann, F. M.; Inoue, S. Oxidation Reactions of a Versatile, Two-Coordinate, Acyclic Iminosiloxysilylene. *Dalton Transactions* **2020**, *49*, 7060–7068.

(21) Do, D. C. H.; Protchenko, A. v.; Fuentes, M. Á.; Hicks, J.; Vasko, P.; Aldridge, S. N–H Cleavage *vs.* Werner Complex Formation: Reactivity of Cationic Group 14 Tetrelenes towards Amines. *Chemical Communications* **2020**, *56*, 4684–4687.

(22) Phung, A. C.; Fettinger, J. C.; Power, P. P. Insertion Reactions of NH_3 and H_2O with the Ferriogermylenes ArGeFeCp(CO)$_2$ (Ar = Ar^{Me6} ($-C_6H_3$-(C_6H_2-2,4,6-Me_3)$_2$) or Ar^{iPr4} ($-C_6H_3$-(C_6H_3-2,6-$^iPr_2$)$_2$); Cp = η^5-C_5H_5): Structural Isomerism and Polymorphism in a Metallogermylene. *Organometallics* **2021**, *40*, 3472–3479.

(23) Lei, H.; Guo, J.-D.; Fettinger, J. C.; Nagase, S.; Power, P. P. Synthesis, Characterization, and CO Elimination of Ferrio-Substituted Two-Coordinate Germylenes and Stannylenes. *Organometallics* **2011**, *30*, 6316–6322.

(24) Abbenseth, J.; Townrow, O. P. E.; Goicoechea, J. M. Thermoneutral N−H Bond Activation of Ammonia by a Geometrically Constrained Phosphine. *Angewandte Chemie International Edition* **2021**, *60*, 23625–23629.

(25) Spikes, G. H.; Fettinger, J. C.; Power, P. P. Facile Activation of Dihydrogen by an Unsaturated Heavier Main Group Compound. *J Am Chem Soc* **2005**, *127*, 12232–12233.

(26) Ruhlandt-Senge, K.; Ellison, J. J.; Wehmschulte, R. J.; Pauer, F.; Power, P. P. Isolation and Structural Characterization of Unsolvated Lithium Aryls. *J Am Chem Soc* **1993**, *115*, 11353–11357.

(27) Simons, R. S.; Pu, L.; Olmstead, M. M.; Power, P. P. Synthesis and Characterization of the Monomeric Diaryls $M\{C_6H_3$-2,6-$Mes_2\}_2$ (M = Ge, Sn, or Pb; Mes = 2,4,6-$Me_3C_6H_2$−) and Dimeric Aryl−Metal Chlorides $[M(Cl)\{C_6H_3$-2,6-$Mes_2\}]_2$ (M = Ge or Sn). *Organometallics* **1997**, *16*, 1920–1925.

(28) Pu, L.; Olmstead, M. M.; Power, P. P.; Schiemenz, B. Synthesis and Characterization of the Monomeric Terphenyl−Metal Halides $Ge(Cl)\{C_6H_3$-2,6-$Trip_2\}$ (Trip = C_6H_2-2,4,6-i-Pr_3) and $Sn(I)\{C_6H_3$-2,6-$Trip_2\}$ and the Terphenyl−Metal Amide $Sn\{N(SiMe_3)_2\}\{C_6H_3$-2,6-$Trip_2\}$. *Organometallics* **1998**, *17*, 5602–5606.

(29) Plotkin, J. S.; Shore, S. G. Convenient Preparation and Isolation of Pure Potassium Cyclopentadienyldicarbonylferrate, $K[(\eta^5$-$C_5H_5)Fe(CO)_2]$. *Inorg Chem* **1981**, *20*, 284–285.

(30) Fulmer, G. R.; Miller, A. J. M.; Sherden, N. H.; Gottlieb, H. E.; Nudelman, A.; Stoltz, B. M.; Bercaw, J. E.; Goldberg, K. I. NMR Chemical Shifts of Trace Impurities: Common Laboratory Solvents, Organics, and Gases in Deuterated Solvents Relevant to the Organometallic Chemist. *Organometallics* **2010**, *29*, 2176–2179.

(31) Trainor, K.; Palumbo, J. A.; MacKenzie, D. W. S.; Meiering, E. M. Temperature Dependence of NMR Chemical Shifts: Tracking and Statistical Analysis. *Protein Science* **2020**, *29*, 306–314.

(32) Baxter, N. J.; Williamson, M. P. Temperature Dependence of [1]H Chemical Shifts in Proteins. *J Biomol NMR* **1997**, *9*, 359–369.

(33) Kim, P. S. Amide Proton Exchange as a Probe of Protein Folding Pathways. *Methods Enzymol* **1986**, *131*, 136–156.

(34) Perrett, S.; Clarke, J.; Hounslow, A. M.; Fersht, A. R. Relationship between Equilibrium Amide Proton Exchange Behavior and the Folding Pathway of Barnase. *Biochemistry* **1995**, *34*, 9288–9298.

(35) Green, A. R.; Li, K.; Lockard, B.; Young, R. P.; Mueller, L. J.; Larive, C. K. Investigation of the Amide Proton Solvent Exchange Properties of Glycosaminoglycan Oligosaccharides. *J Phys Chem B* **2019**, *123*, 4653–4662.

(36) Roder, H.; Wagner, G.; Wuethrich, K. Individual Amide Proton Exchange Rates in Thermally Unfolded Basic Pancreatic Trypsin Inhibitor. *Biochemistry* **1985**, *24*, 7407–7411.

(37) Ohnishi, M.; Urry, D. W. Temperature Dependence of Amide Proton Chemical Shifts: The Secondary Structures of Gramicidin S and Valinomycin. *Biochem Biophys Res Commun* **1969**, *36*, 194–202.

(38) Westerhausen, M. Dynamic Behavior and Structures of Alkaline Earth Metal Bis[Bis(Trialkylsilyl)Amides and -Phosphanides]. *Trends in Organometallic Chemistry* **1997**, *2*, 89–105.

(39) Inoue, S.; Driess, M. Isolable Metallo-Germylene and Metallo-Stannylene σ-Complexes with Iron. *Organometallics* **2009**, *28*, 5032–5035.

(40) Eichler, B. E.; Phillips, A. D.; Haubrich, S. T.; Mork, B. V.; Power, P. P. Synthesis, Structures, and Spectroscopy of the Metallostannylenes $(\eta^5\text{-}C_5H_5)(CO)_3M\text{–}\breve{S}n\text{–}C_6H_3\text{-}2,6\text{-}Ar_2$ (M = Cr, Mo, W; Ar = $C_6H_2\text{-}2,4,6\text{-}Me_3$, $C_6H_2\text{-}2,4,6\text{-}Pr^i_3$). *Organometallics* **2002**, *21*, 5622–5627.

(41) Pu, L.; Power, P. P.; Boltes, I.; Herbst-Irmer, R. Synthesis and Characterization of the Metalloplumbylenes $(\eta^5\text{-}C_5H_5)(CO)_3M\text{-}\breve{P}b\text{-}C_6H_3\text{-}2,6\text{-}Trip_2$ (M = Cr, Mo, or W; Trip = $-C_6H_2\text{-}2,4,6\text{-}i\text{-}Pr_3$). *Organometallics* **2000**, *19*, 352–356.

(42) Smith, P. W.; Handford, R. C.; Tilley, T. D. Heavy Tetrel Complexes of Ru Featuring Ru=E(R)X and Ru–E–R (E = Sn, Pb) Linkages. *Organometallics* **2019**, *38*, 4060–4065.

(43) Zhu, Q.; Fettinger, J. C.; Vasko, P.; Power, P. P. Interactions of a Diplumbyne with Dinuclear Transition Metal Carbonyls to Afford Metalloplumbylenes. *Organometallics* **2020**, *39*, 4629–4636.

(44) Twamley, B.; Haubrich, S. T.; Power, P. P. Element Derivatives of Sterically Encumbering Terphenyl Ligands; 1999; pp 1–65.

(45) Phillips, A. D.; Wright, R. J.; Olmstead, M. M.; Power, P. P. Synthesis and Characterization of 2,6-Dipp$_2$-H$_3$C$_6$SnSnC$_6$H$_3$-2,6-Dipp$_2$ (Dipp = C$_6$H$_3$-2,6-Pr$^i_2$): A Tin Analogue of an Alkyne. *J Am Chem Soc* **2002**, *124*, 5930–5931.

(46) Merrill, W. A.; Rivard, E.; DeRopp, J. S.; Wang, X.; Ellis, B. D.; Fettinger, J. C.; Wrackmeyer, B.; Power, P. P. Synthesis and Characterization of the M(II) (M = Ge, Sn, or Pb) Phosphinidene Dimers {M(μ-PAr′)}$_2$ (Ar′ = C$_6$H$_3$-2,6-(C$_6$H$_3$-2,6-Pr$^i_2$)$_2$). *Inorg Chem* **2010**, *49*, 8481–8486.

(47) Sanderson, R. T. Electronegativity and Bond Energy. *J Am Chem Soc* **1983**, *105*, 2259–2261.

(48)   Mullay, J. Estimation of Atomic and Group Electronegativities. In *Electronegativity*; Springer-Verlag: Berlin/Heidelberg; pp 1–25.

(49)   Seidel, N.; Jacob, K.; Fischer, A. K. Bis[2-((Dimethylamino)Methyl)Ferrocenyl]Lead, (FcN)$_2$Pb, as a Ligand: Synthesis and Characterization of the Heterotrimetallic Metalloplumbylene Compounds (FcN)$_2$PbM(CO)$_5$ (M = Cr, Mo, W). *Organometallics* **2001**, *20*, 578–581.

4.7 SUPPLEMENTARY INFORMATION

Table of Contents

X-ray Crystallography

Crystals of **4** were removed from a Schlenk flask under a stream of nitrogen and immediately covered with a layer of hydrocarbon oil. A suitable crystal was selected, attached to a glass fiber on a copper pin and quickly placed in the cold N_2 stream on the diffractometer. Data was collected at 100 K on a Bruker APEX DUO diffractometer with Mo Kα radiation (λ = 0.71073 Å). Absorption corrections were applied using SADABS.[S1] The crystal structures were solved by direct methods and refined by full matrix least-squares procedures in SHELXTL.[S2] All non-H atoms were refined anisotropically.

Table S1. Selected X-ray Crystallographic data for **4**.

	4
Formula	$C_{37}h_{42}feo_2pb$
Fw	781.74
Color, habit	Green rod
Space group	$P2_12_12_1$
A, å	8.3897(4)
B, å	18.0566(8)
C, å	21.6854(9)
A, °	90
B, °	90
Γ, °	90
V, å³	3285.1(3)
Z	4
Crystal size, mm	0.293 x 0.084 x 0.060
D$_{calc}$, mg cm^{-3}	1.581
Abs. M, mm^{-1}	5.590
2θ, °	2.191 to 27.486
R(int)	0.0335
Obs. Reflns. [i>2σ(i)]	6799
Data/restraints/parameters	7520 / 24 / 432
R_1, obsd. Reflns.	0.0392

Images

Figure S1. Images of the solvent-free reactions of **1** and NH$_3$(*l*).
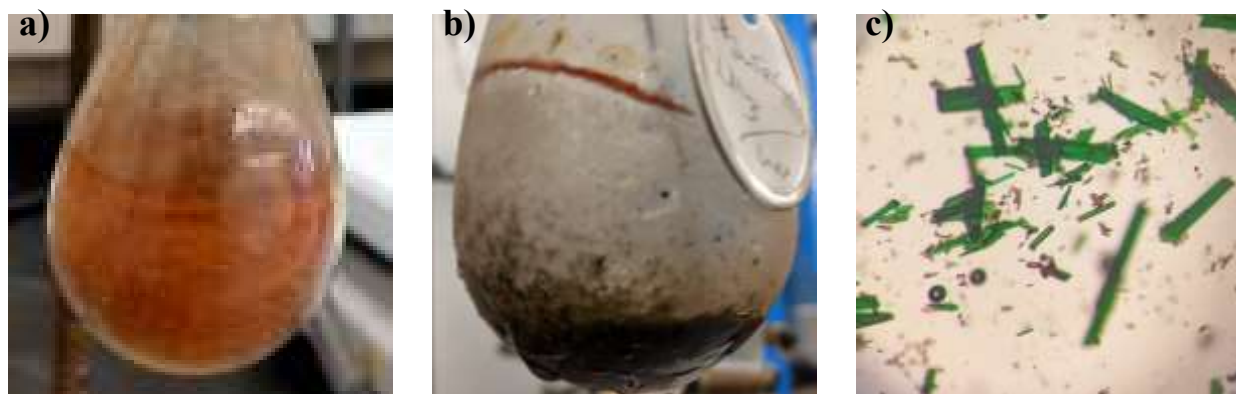
a) The product of the reaction of **1** with NH$_3$ is an orange powder.
b) Dissolving the orange powder in hexanes gave a green solution, which when concentrated, gave a mixture of red and green crystals.
c) Microscope photograph of the green and pink-orange crystals from the flask.

Figure S2. Images of the solvent-free reactions of **2** and NH$_3$(*l*).
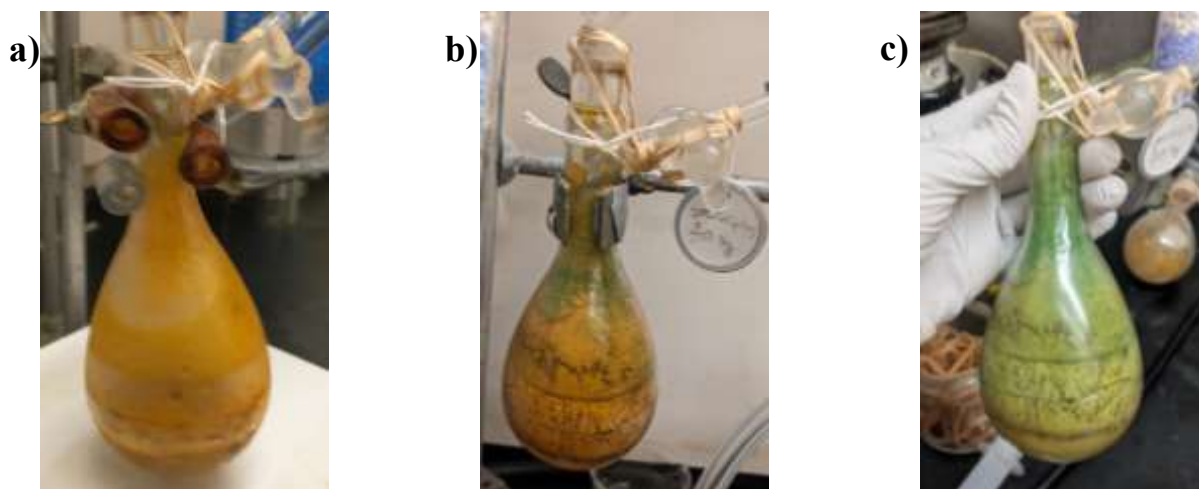
a) The resulting orange powder following condensation of NH$_3$(*l*) onto green crystals of **2**.
b) Removing excess ammonia and drying the product in an atmosphere of N$_2$(*g*) left a mix of orange and light green powder.
c) Placing the dried orange powder under reduced pressure removed the orange color and left a light green powder that was analyzed by ^{1}H NMR.

NMR Spectra

Figure S3. Overlay of the ^{1}H NMR spectra of **1+NH₃** (green, C₇D₈, 298 K) and **1** (red, C₆D₆, 298 K).
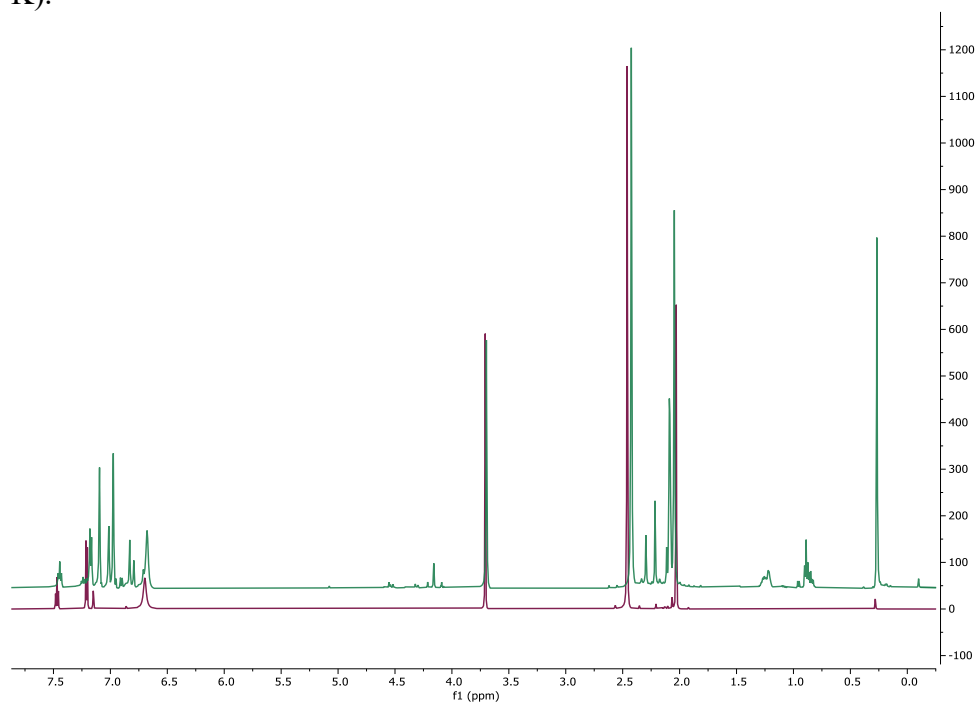
Note: δ = 0.88 & 1.55 ppm: residual *n*-hexanes

Figure S4. ^{1}H NMR spectrum of **2+NH₃** (solvent free reaction) in C₇D₈ at 298K.
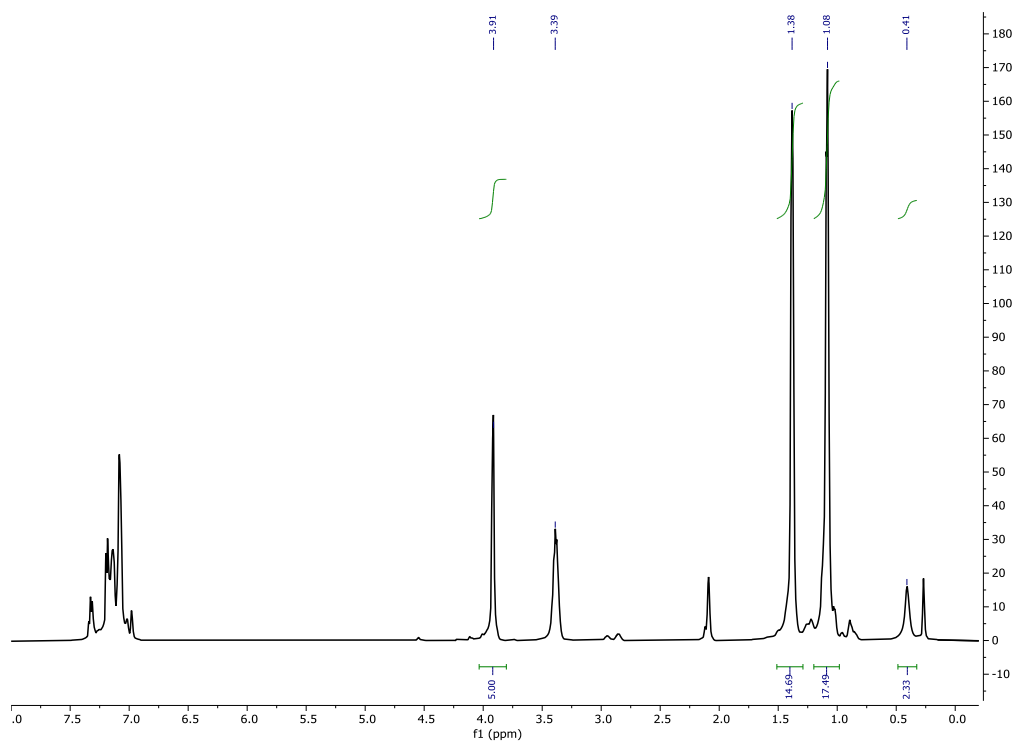
NMR Spectra

Figure S5. ^{1}H NMR spectrum of **2** in C$_7$D$_8$ at 298 K.
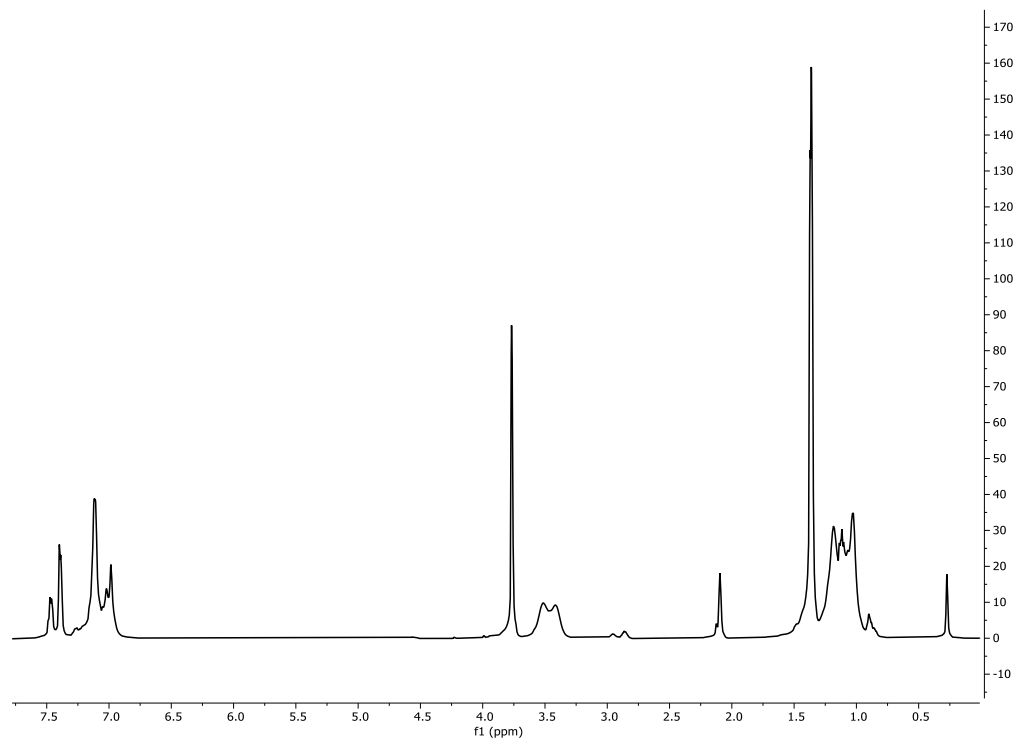
Figure S6. ^{1}H NMR spectrum of **2+NH$_3$** in C$_7$D$_8$ at 298 K.
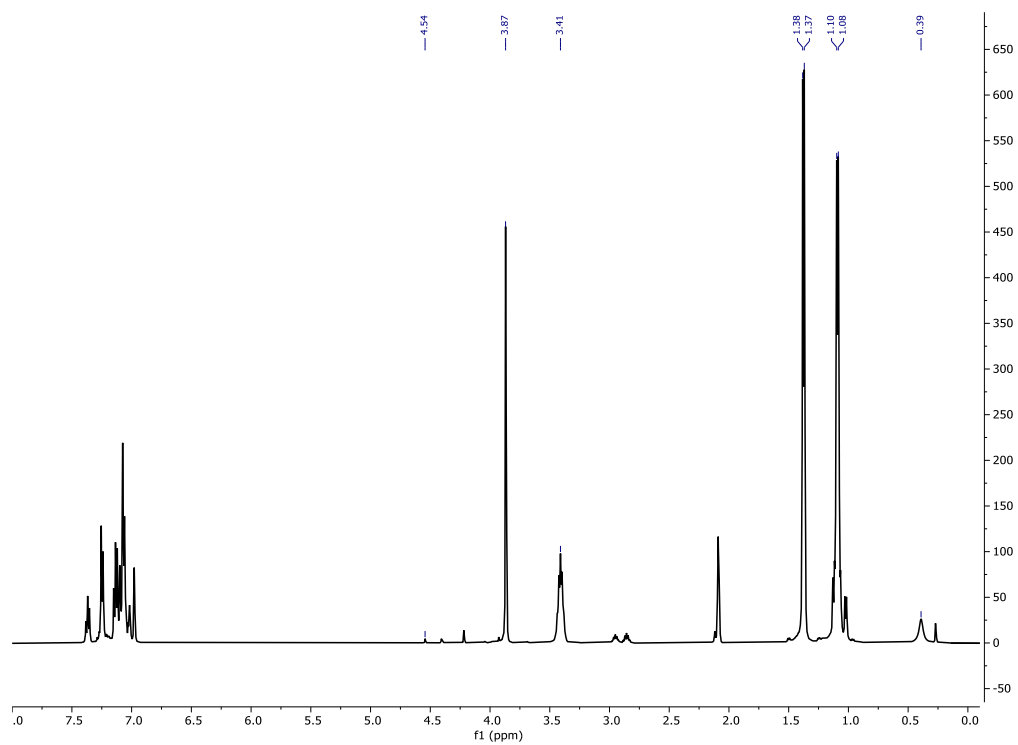
NMR Spectra

Figure S7. $^{119}Sn\{_1H\}$ NMR spectrum of **2** in C_7D_8 at 298 K.
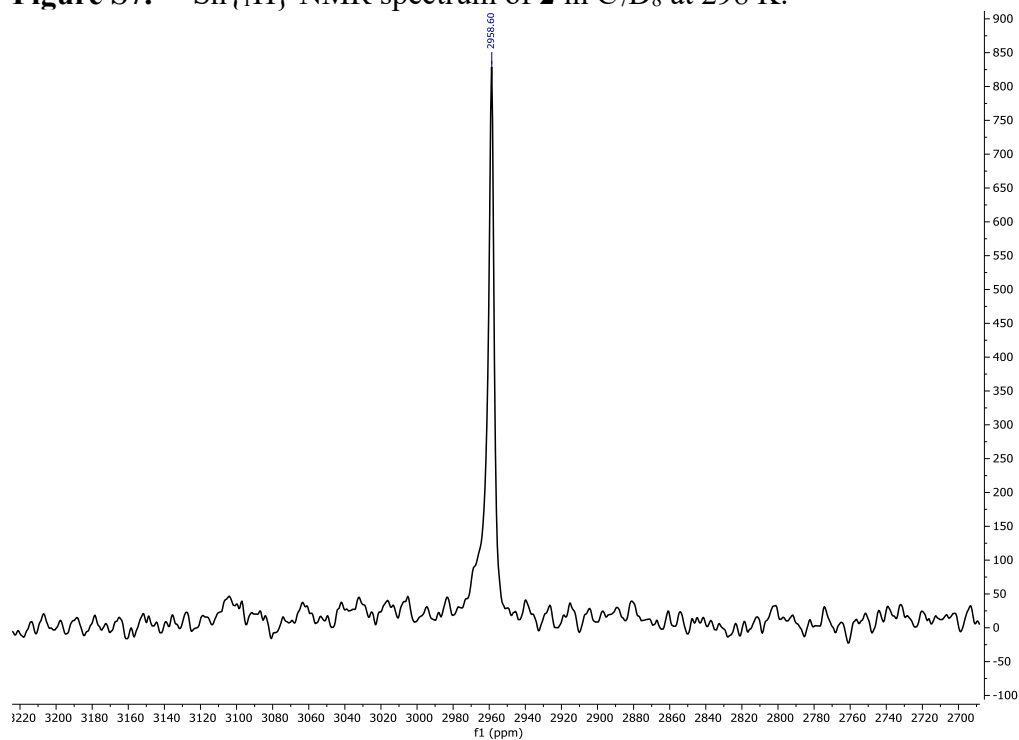
Figure S8. $^{119}Sn\{^1H\}$ NMR spectrum of **2+NH₃** in C_7D_8 at 298 K.
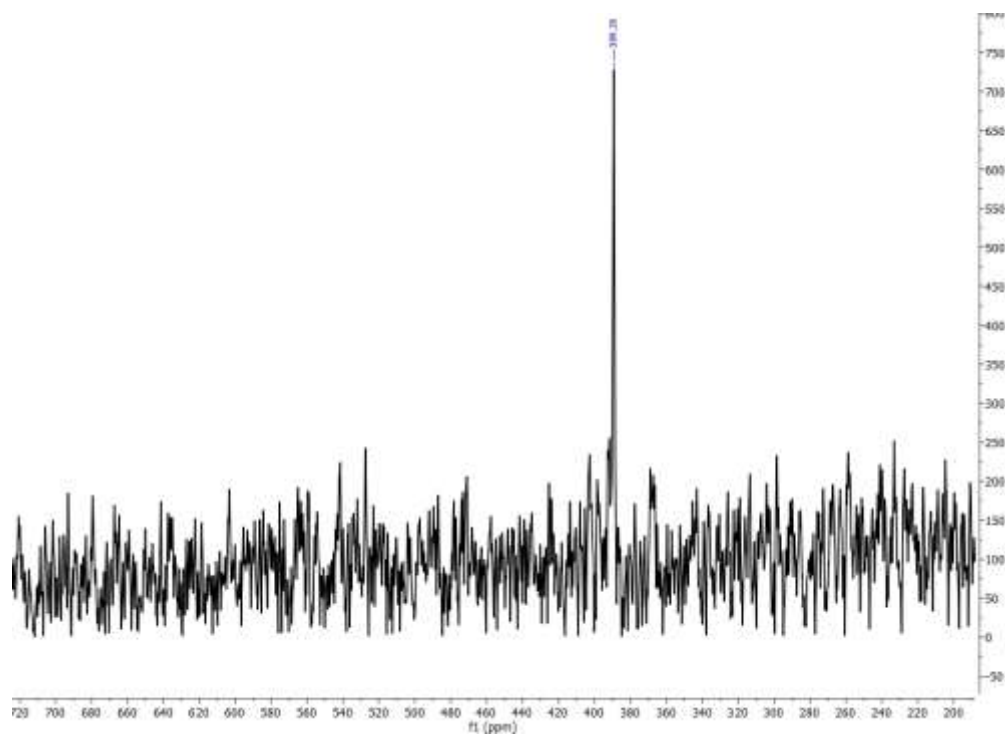
NMR Spectra

Figure S9. $^{13}C\{^1H\}$ NMR spectrum of **2·NH₃** in C_7D_8 at 298 K.
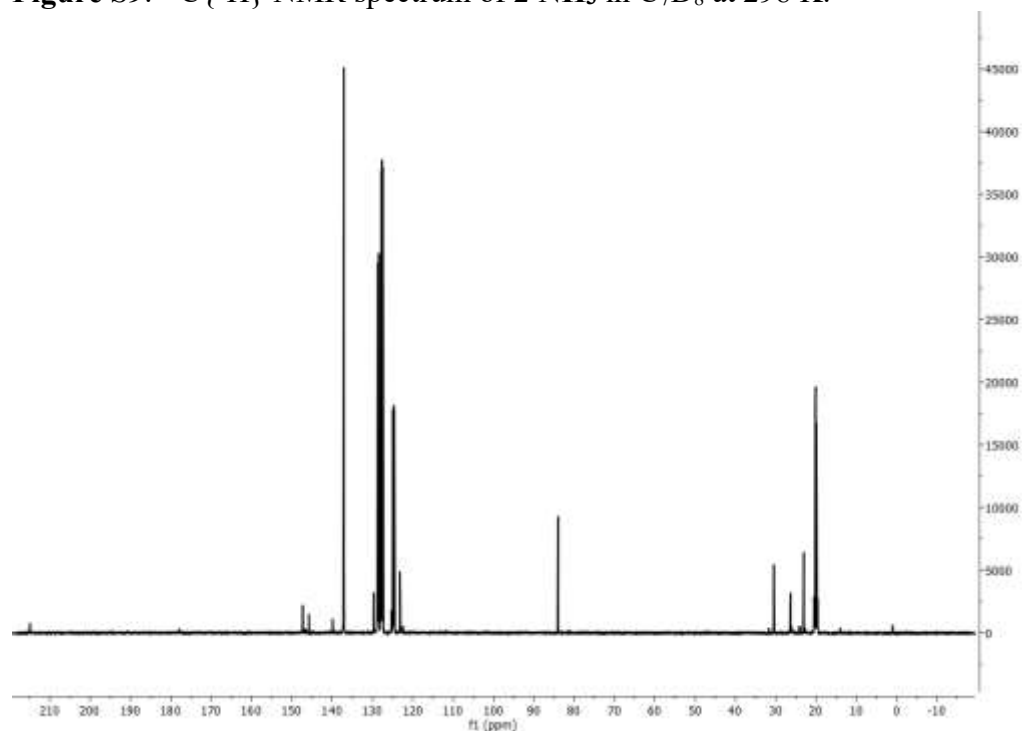
NMR Spectra

Figure S10. ^{1}H NMR spectra of the NMR-scale reaction of **2** with $NH_3(g)$ in C_7D_8 from 340 to 260 K at 10 K intervals: zoomed in at 1.5 – -0.8 ppm.
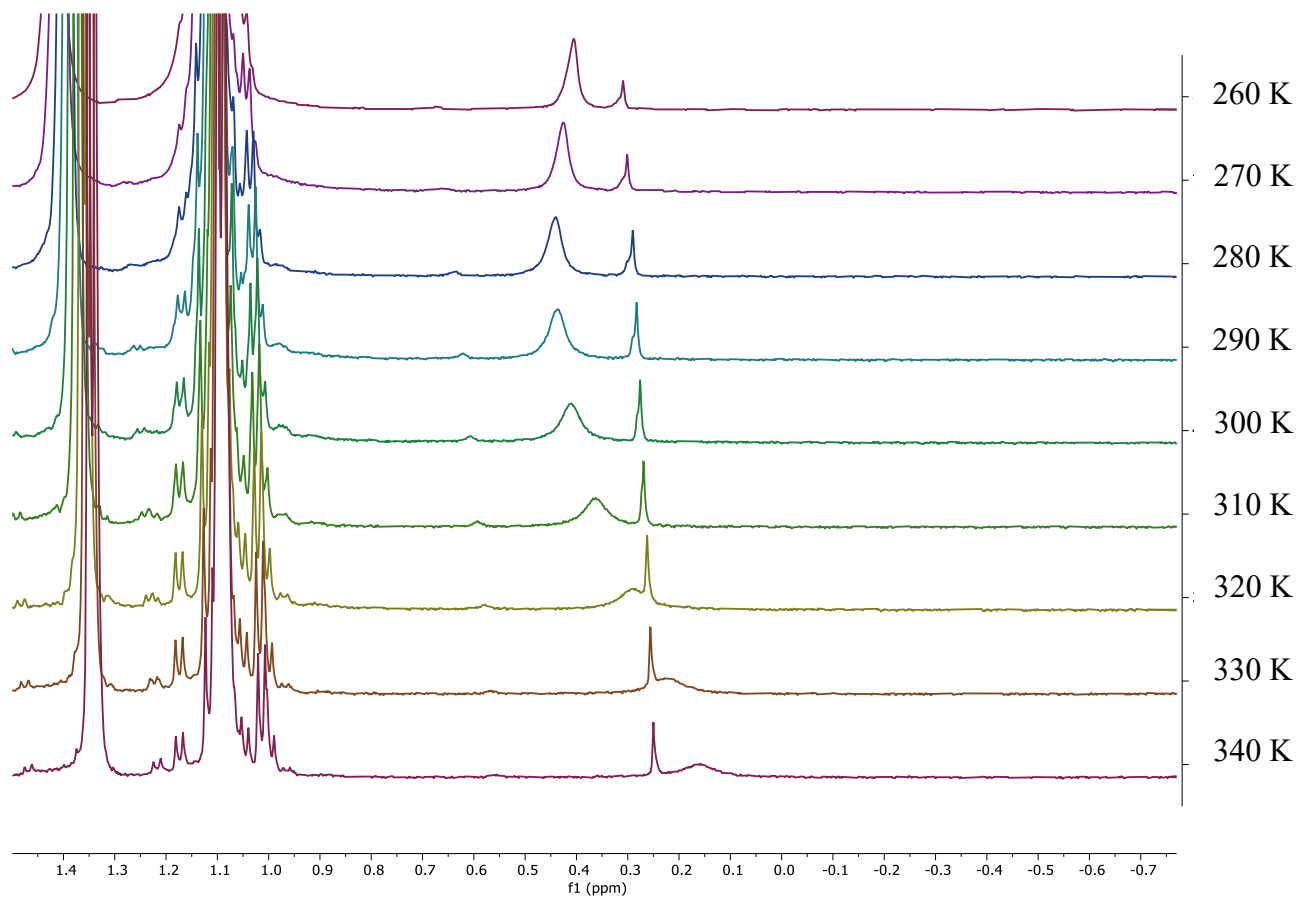
NMR Spectra

Figure S11. ^{1}H NMR spectrum of **3** in C$_6$D$_6$ at 298 K.
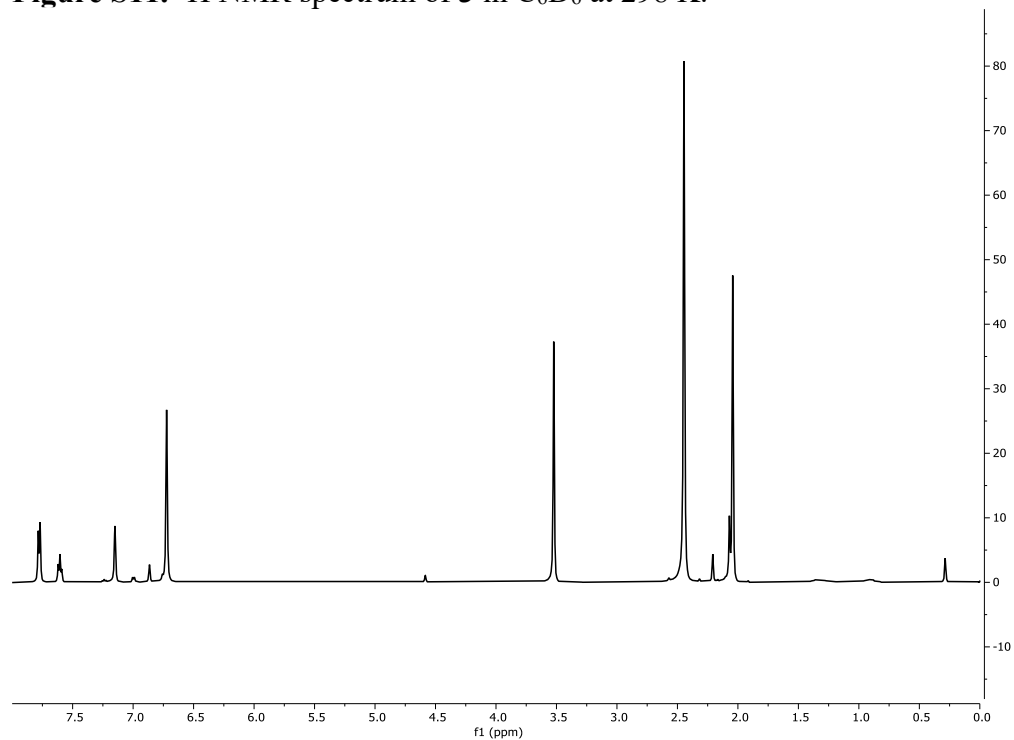
Figure S12. ^{1}H NMR spectrum of **4** in C$_6$D$_6$ at 298 K.

NMR Spectra

Figure S13. ^{13}C NMR spectrum of **3** in C_6D_6 at 298 K.

Figure S14. ^{13}C NMR spectrum of **4** in C_6D_6 at 298 K.
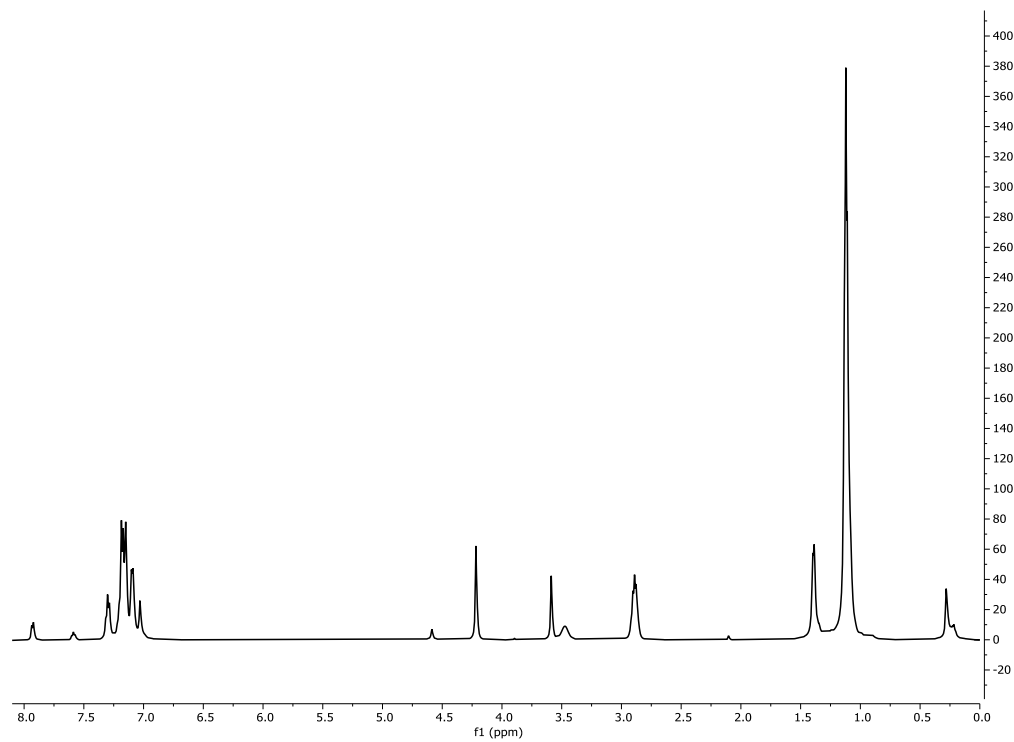
NMR Spectra
Figure S15. ^{207}Pb NMR spectrum of 3 in C_6D_6 at 298 K.
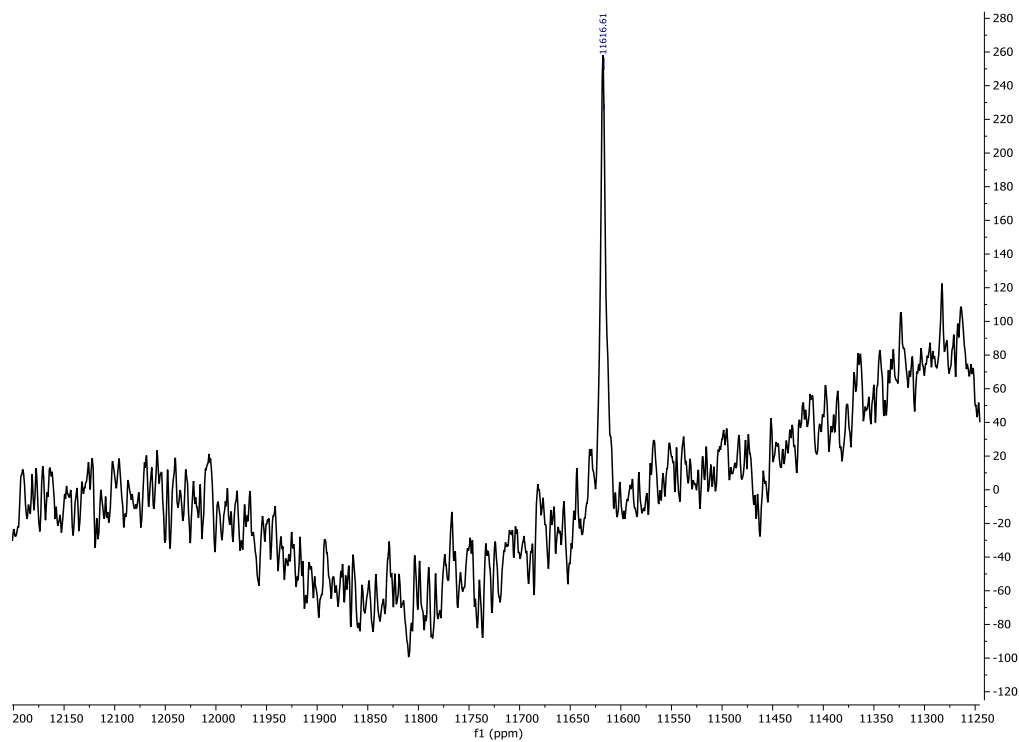
Figure S16. ^{207}Pb NMR spectrum of 4 in C_6D_6 at 298 K.
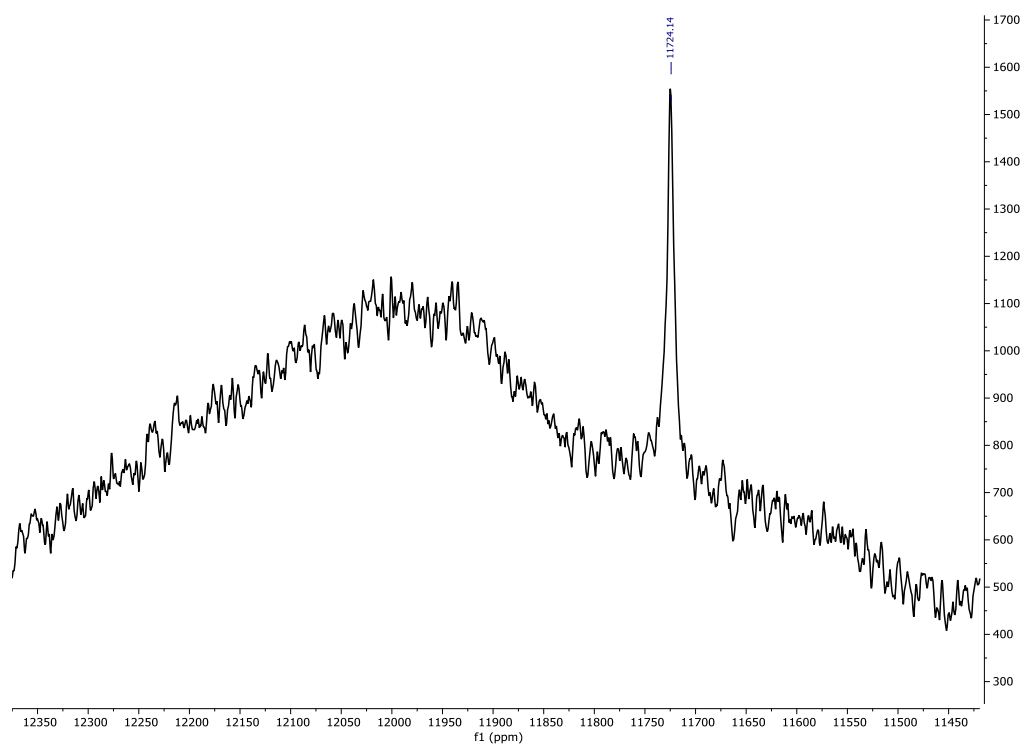
van't Hoff Plot

^{1}H NMR spectra were collected once per minute as the temperature was gradually decreased from 340 K to 260 K at a rate of 1 K per minute. The equilibrium constant K was determined by setting the concentration of the starting material **2** (Ar^{iPr4}SnFeCp(CO)$_2$) = 1 and the concentration of the insertion product (Ar^{iPr4}Sn(NH$_2$)(H)FeCp(CO)$_2$) = area under the amide proton singlet. An excess of NH$_3$(g) relative to **2** was assumed.

Figure S17. van't Hoff Plot of the variable temperature reaction of **2** with NH$_3$(g).
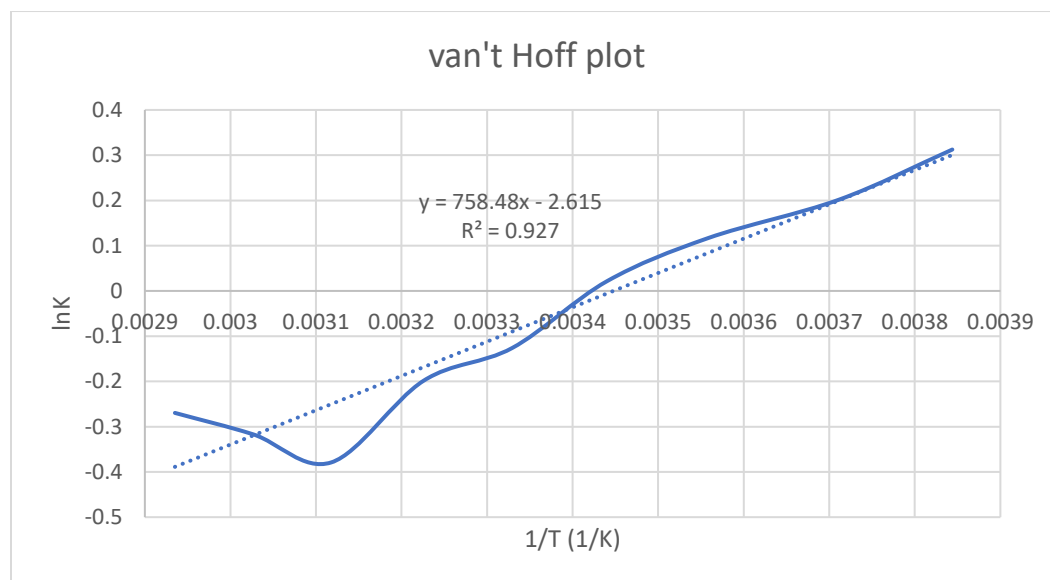
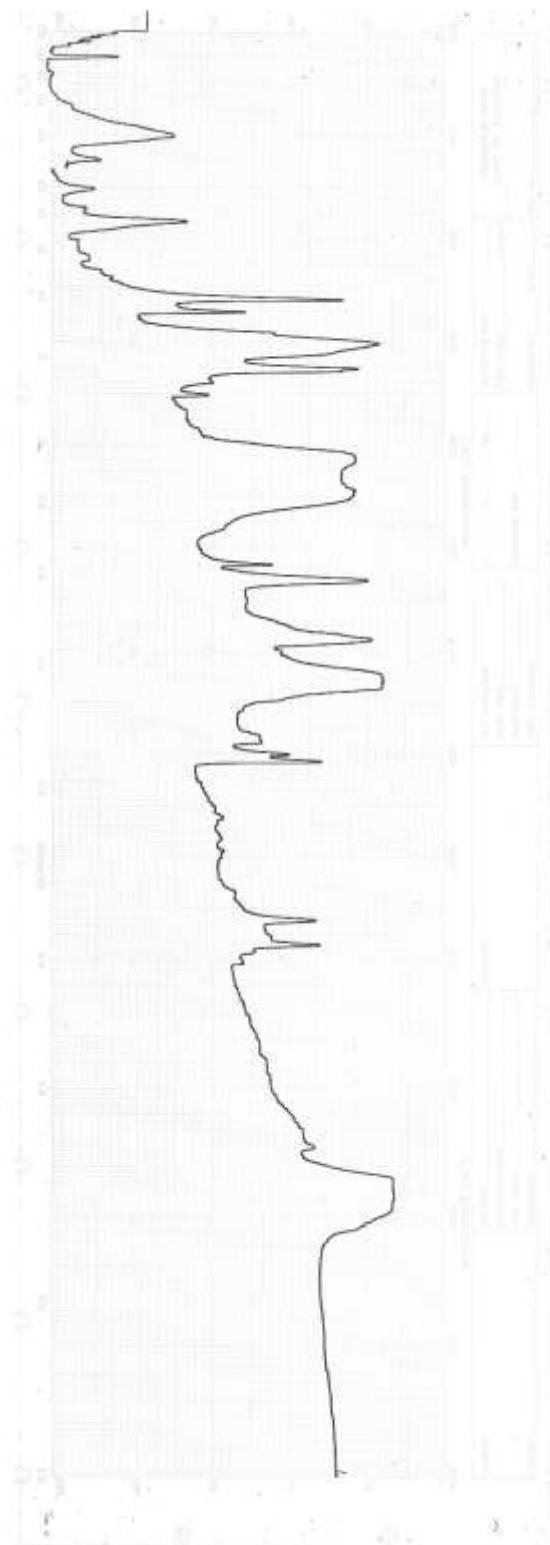**Table S2**. Calculated thermodynamics based on the van't Hoff plot **Fig. S16**.

R (J mol^{-1} K^{-1})	$-\Delta H/R$	$\Delta S/R$
8.314	758.48	-2.615

	ΔH	ΔS
J	-6306.00272	-21.7411
Kcal	-1.50717082	-0.00519625

UV-vis Spectra

Figure S18. UV-vis spectrum of **3** in hexanes at 298 K.

$Ar^{Me_6}PbFe(CO)_2$, 286 µM
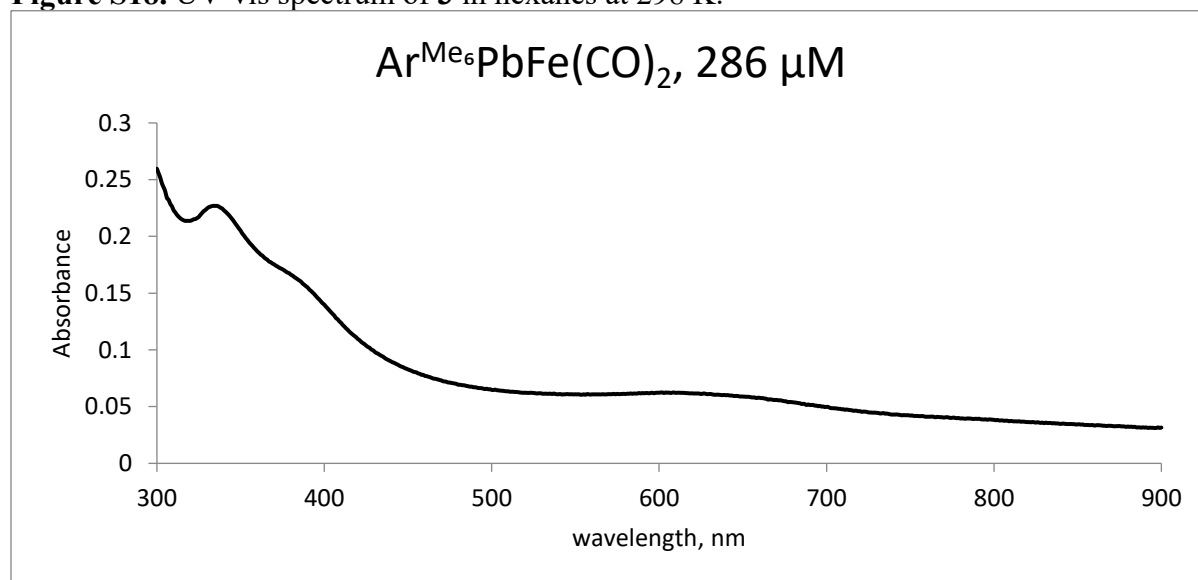
Figure S19. UV-vis spectrum of **4** in hexanes at 298 K.

$Ar^{iPr_4}PbFeCp(CO)_2$, 40.9 µM
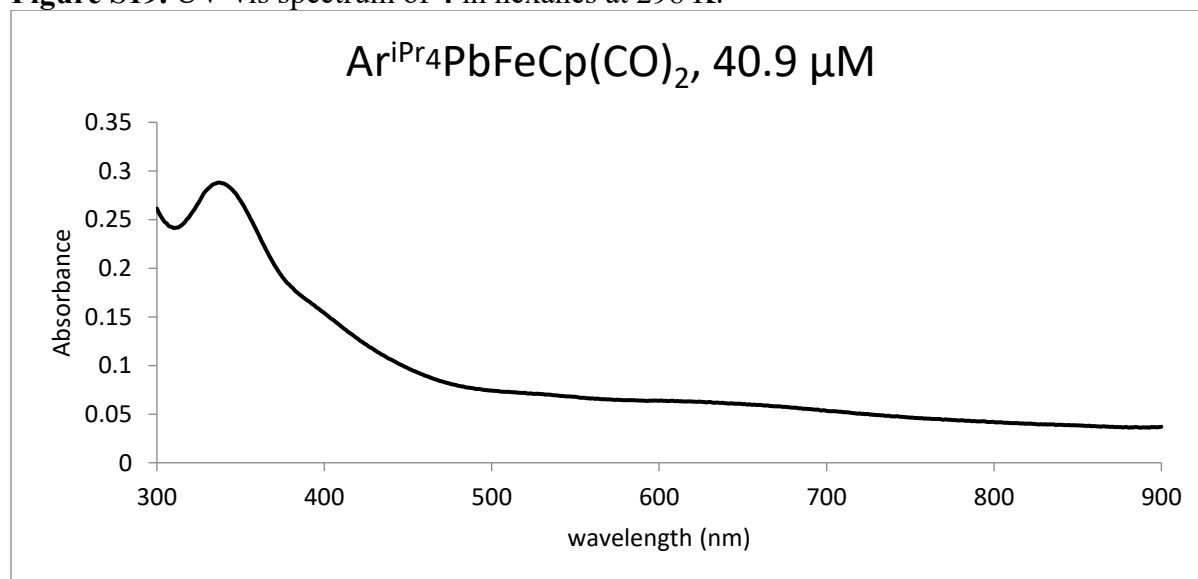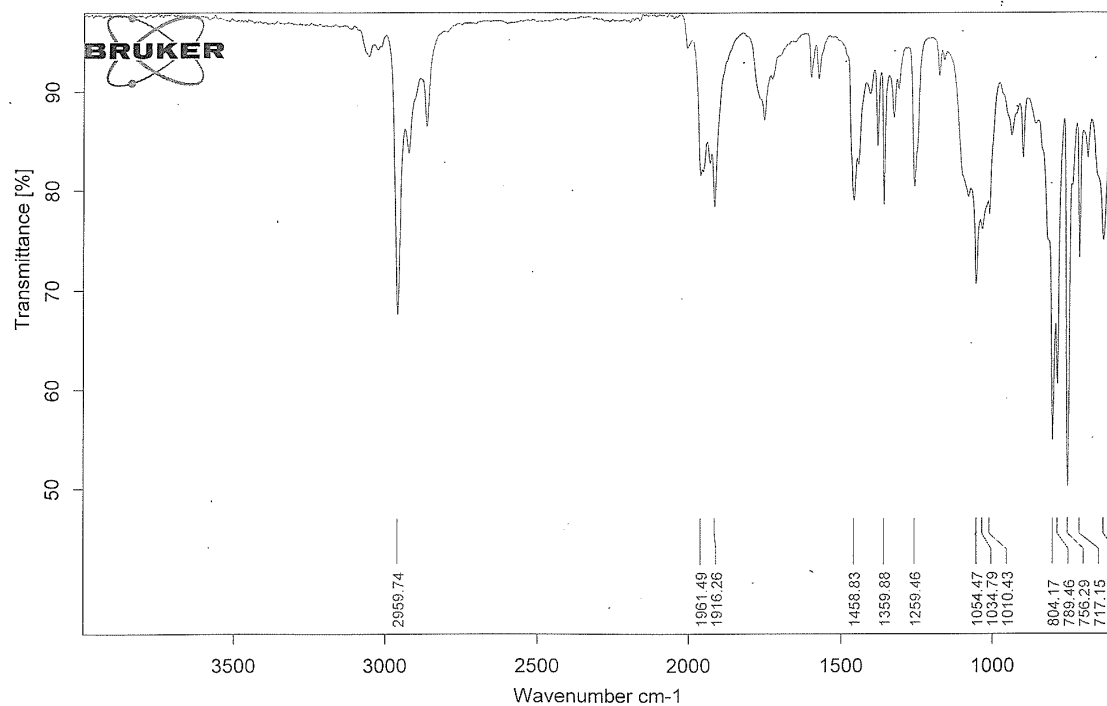
IR Spectra

Figure S20. IR spectrum of **3**.

IR Spectra

Figure S21. IR spectrum of **4**.

SI References

S1 Bruker, Bruker AXS Inc., Madison, Wisconsin, USA, **2001**

S2 G. M. Sheldrick, Acta Cryst. A 2015, 71, 3-8.

S3 Dolomanov, O. V.; Bourhis, L. J.; Gildea, R. J.; Howard, J. A. K.; Puschmann, H.; *OLEX2*: A complete structure solution, refinement and analysis program. J. Appl. Cryst, **2009**, *42*, 339-341

Synthesis, Structure, Spectroscopy of the Biscarboranyl Stannylenes (bc)Sn·THF and [(bc)Sn]₂KCl (bc = 1,1′(*ortho*-biscarborane)) and Dibiscarboranyl Ethene (bc)CH=CH(bc)

Alice C. Phung,[1] James C. Fettinger,[1] Philip P. Power[1]*

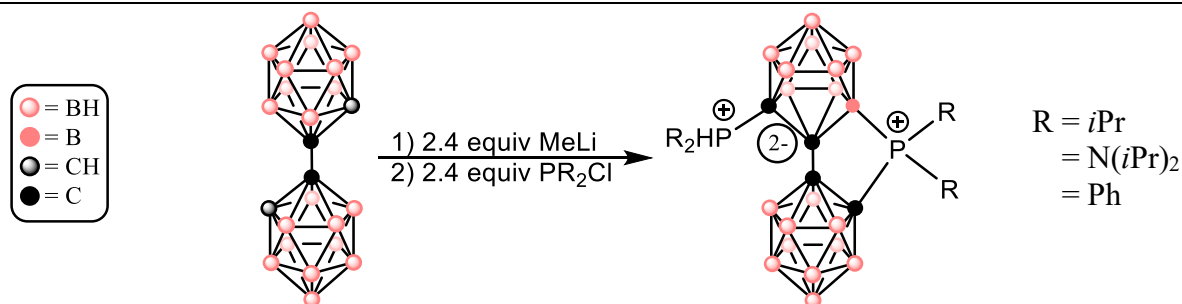[1]Department of Chemistry, University of California, 1 Shields Avenue, Davis, California 95616

ABSTRACT: Two compounds containing a Sn(II) atom supported by a bidentate biscarborane ligand have been synthesized via salt metathesis. The synthetic procedures for **(bc)Sn·THF** (**bc** = 1,1′ (*ortho*-carborane) (**1**) and [(**bc**)Sn]₂KCl (**2**) involved the reaction of K₂[**bc**] with SnCl₂ in either a THF solution (**1**) or in a benzene/dichloromethane solvent mixture (**2**). Using the same solvent conditions as those for **2** but using a shorter reaction time gave a dibiscarboranyl ethene (**3**). The products were characterized by ^{1}H, ^{13}C, ^{11}B, ^{119}Sn NMR, UV-vis, and IR spectroscopy, and by X-ray crystallography. The diffraction data for **1** and **2** show that the Sn atom has a trigonal pyramid environment and is constrained by the **bc** ligand in a planar five-membered C₄Sn heterocycle. The ^{119}Sn NMR spectrum of **1** displays a triplet of triplet signal, which appears unusual due to the absence of a Sn-H signal in the ^{1}H NMR, IR spectrum, and X-ray crystallographic data. However, a comparison of other organotin compounds featuring a Sn atom bonded to carboranes reveal similar multiplets in their ^{119}Sn NMR spectra, likely arising from long-range nuclear spin-spin coupling between the carboranyl ^{11}B and ^{119}Sn nuclei. Compound **3** displays structural and spectroscopic characteristics typical of conjugated alkenes.
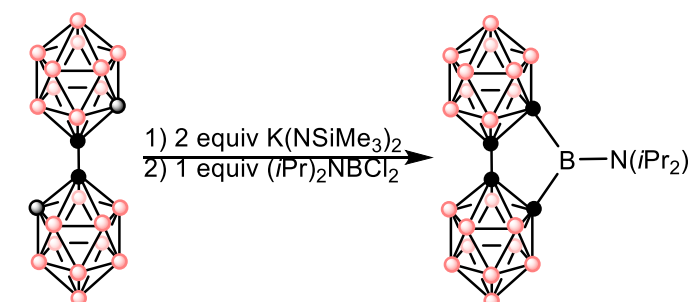
CHAPTER 5

5.1 INTRODUCTION

The charge-neutral compound 1,1'-bis(*ortho*-carborane) (**H₂-bc**), often described as a three-dimensional aromatic analogue of biphenyl, is an interesting ligand for the support of stannylenes due to its steric bulk and strong κ^2-binding that can form strained five-membered metallacycles.[1–3] The majority of **bc** ligand metal complexes feature a transition metal that is κ^2-C,C or κ^2-B,C-bonded to the **bc** ligand and stabilized by an aryl or alkyl group[3–11] or another **bc** ligand.[3,12,13] In these cases, the central transition metal is constrained to a square planar or tetrahedral geometry due to the rigid nature of the **bc** ligand scaffold. Additionally, there are reports of deboronated **bc**-based transition metal complexes incorporating the transition metal atom into the **bc** cage.[3,14–16]

In contrast, there are relatively few main group metal complexes stabilized by a **bc** ligand,[17–22] and the synthesis of these complexes has required activation of the C-H vertices of **H₂-bc**. Since the boron-bonded hydrogens are hyridic while the carbon-bonded hydrogens are protic,[1,2] lithiation is a common route for the C-H activation of **H₂-bc**. The phosphorus complex *closo*-(C₂B₁₀H₁₀)(PR₂)-*nido*-(C₂B₁₀H₉)(PHR₂) (R = *i*Pr, N(*i*Pr)₂, or Ph) describes the activation of **H₂-bc** by lithiation to produce the dilithio salt.[18] Alternatively, the synthesis for the 9-borafluorene three-dimensional analogue (**bc**)B(N(*i*Pr)₂) generates the dipotassium salt of **bc** via potassium bis(trimethylsilyl)amide prior to a salt metathesis reaction with (*i*Pr₂)NBCl₂.[19] Currently, the only known **bc** complex containing a heavy group 14 metal is the Sn(IV) complex, (**bc**)SnMe₂, synthesized via reaction of the Grignard intermediate (**bc**)Mg(DME)₂ (DME = 1,2-dimethoxyethane) with SnMe₂Cl₂ (**Figure 1**).[20]

= BH
= B
= CH
= C

1) 2.4 equiv MeLi
2) 2.4 equiv PR$_2$Cl

R$_2$HP ⊕ (2-) ⊕ P R / R

R = iPr
= N(iPr)$_2$
= Ph

Wong, Y. O.; Smith, M. D; Peryshkov, D. V. *Chem Eur J*, **2016**, 22, 6764 – 6767.[18]

1) 2 equiv K(NSiMe$_3$)$_2$
2) 1 equiv (iPr)$_2$NBCl$_2$

B—N(iPr$_2$)

Yruegas, S.; Axtell, J. C.; Kirlikovali, K. O.; Spokoyny, A. M.; Martin, C. D. *Chem Comm* **2019**, *55*, 2892–2895.[19]

1) 1 equiv Mg(nBu)$_2$
2 equiv DME
2) 1 equiv Me$_2$SnCl$_2$

Me / Sn / Me
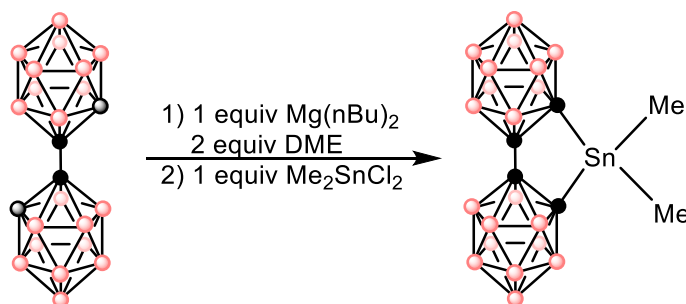
Axtell, J. C.; Kirlikovali, K. O.; Dziedzic, R. M.; Gembicky, M.; Rheingold, A. L.; Spokoyny, A. M. *Eur J Inorg Chem*, **2017**, *2017*, 4411–4416.[20]

Figure 1. Synthetic routes of other **bc**-supported main-group metal complexes.

Unlike the rarity of bis-carboranyl group 14 complexes, several *ortho-* and *meta*-carboranes containing B–Sn and C–Sn bonds are known.[23,24] The earliest reports in 1965 concerned the trialkylcarboranyl tin complexes (C$_2$B$_{10}$H$_{10}$)(SnR$_3$)$_2$, (R = alkyl), with each carbon vertex of the carborane cage bonded to a Sn(IV) atom, although structural data was not provided.[25] The first isolable carboranyl tin structures were the organotin complexes [*o*-C$_2$B$_{10}$H$_{10}$(CH$_2$NMe$_2$)SnR$_2$Br (R = Me or Ph; X = Cl or Br) which feature a Sn(IV) bonded to a carbon vertex and stabilized by a

Lewis basic –CH$_2$NMe$_2$ chelating group (**Table 2, ref 24**).[26] In general, the majority of the tin-carborane complexes are achieved through an initial lithiation step in the stannylation of the C-H vertices of the carboranes cages.[16,23–38]

Monomeric, homoleptic stannylenes of the formula SnR$_2$ are usually supported by bulky organic or related ligands such as alkyl, aryl, silyl, amido, alkoxo, thiolato, etc.[39–41] Given the bulkiness and rigidity of **H$_2$-bc**, the compound may be a suitable platform to support a stannylene, as biscarborane-supported stannylenes are not known prior to this work. Herein, we present the synthesis and characterization of complexes containing a 1,1′-bis(*o*-carboranyl) stannylene (**bc**)Sn moiety. These compounds were obtained by first deprotonating **H$_2$-bc** via KHMDS to create the potassium salt, K$_2$[**bc**],[9] which was then added to a SnCl$_2$ solution. The reaction of K$_2$[**bc**] with SnCl$_2$ in a THF solution gives the THF-coordinated (**bc**)Sn·THF (**1**) while a benzene/dichloromethane mixture affords [(**bc**)Sn]$_2$KCl (**2**). Shortening the reaction tme of the dipotassium salt from 24 hours to 9 hours prior to addition to a dichloromethane solution of SnCl$_2$ produced the alkene (**bc**)CH=CH(**bc**) (**3**) (**Scheme 1**), presumably through a coupling reaction between the mono-deprotonated K[**H-bc**] salt and CH$_2$Cl$_2$ solvent molecules. X-ray crystallography, ^{1}H NMR, ^{11}B NMR, ^{13}C NMR, and UV-vis spectroscopy show that the (**bc**)Sn moiety in complexes **1** and **2** confer structural and spectroscopic similarities between the two. Compound **1** was further characterized by ^{119}Sn NMR spectroscopy. Characterization by X-ray crystallography, ^{1}H, ^{11}B, ^{13}C NMR, UV-vis, and IR spectroscopy of compound **3** confirms its conjugated alkene structure.

131
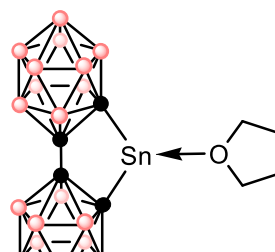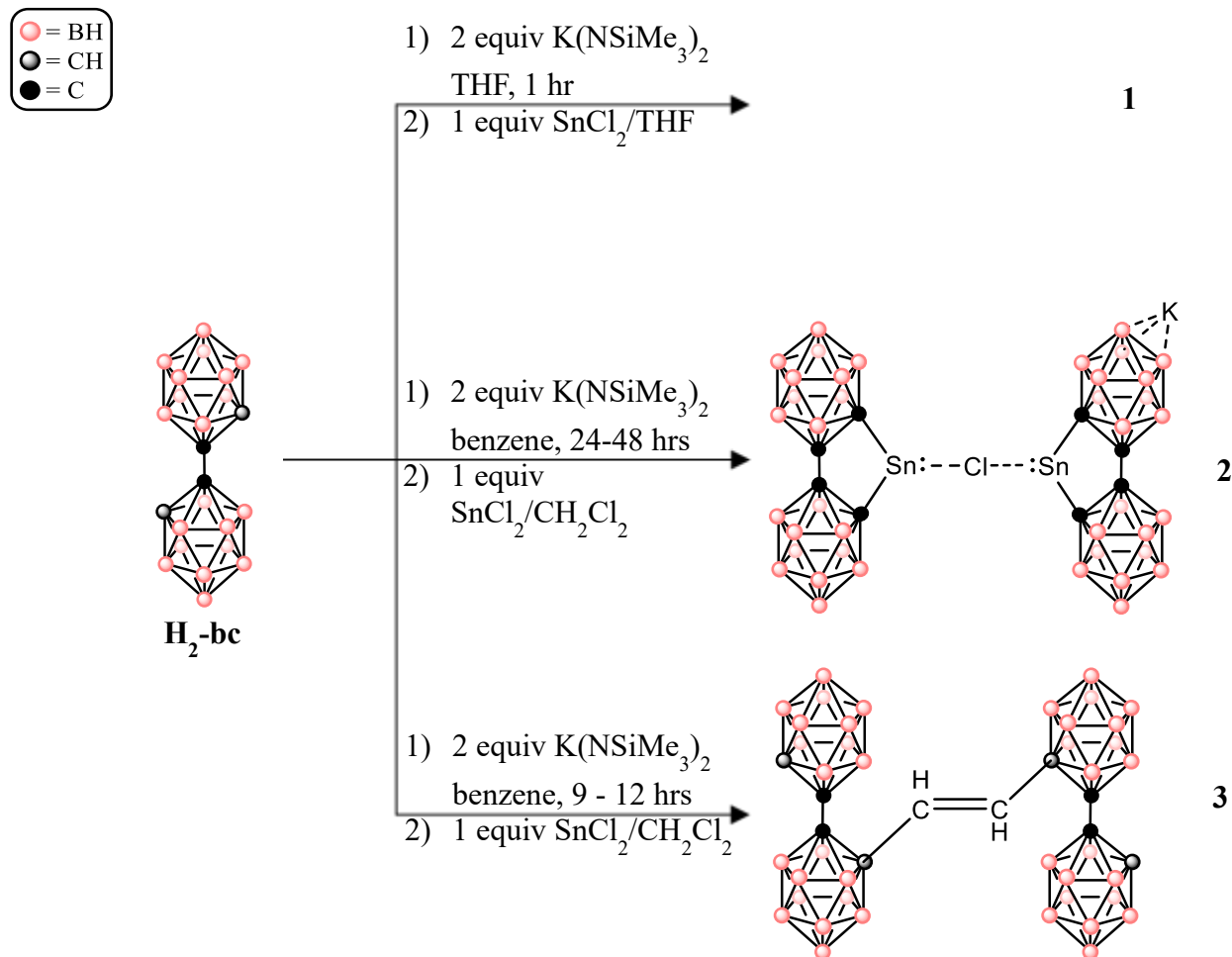
Scheme 1. The syntheses of **1-3**.

5.2 EXPERIMENTAL SECTION

General Procedures: All manipulations were carried out by using modified Schlenk techniques under a N_2 atmosphere. Solvents were dried over columns of activated alumina using a Grubbs type purification system (Glass Contour), stored over Na (THF, toluene) mirrors, K (diethyl ether, hexanes) mirrors, or 3Å molecular sieves (dichloromethane) and degassed via three freeze-pump-thaw cycles prior to use. Potassium bis(trimethylsilyl)amide (KHMDS) was purchased from Sigma-Aldrich and washed three times with hexanes prior to use. The compound **H₂-bc** was

synthesized according to literature procedures.[10,42] The ^{1}H, ^{11}B{1H}, ^{13}C{^{1}H}, and ^{119}Sn{^{1}H}

NMR spectra were recorded on a Bruker Avance DRX 500 MHz spectrometer and the ^{1}H and

^{13}C{^{1}H} spectra were referenced to the residual solvent signals in C_6D_6 (^{1}H: δ 7.15 ppm, ^{13}C: δ

128.06 ppm).[43] UV-Visible spectra were recorded using dilute hexane solutions in 3.5 mL quartz

cuvettes using an Olis 17 Modernized Cary 14 UV-Vis/NIR spectrophotometer. Infrared spectra

for **1** and **2** were recorded as Nujol mulls between CsI windows on a PerkinElmer 1430

spectrophotometer. The infrared spectrum for **3** was collected on a Bruker Tensor 27 ATRFTIR

spectrometer. Melting points were determined on a Meltemp II apparatus in flame-sealed glass

capillaries equipped with a partial immersion thermometer.

(bc)SnTHF (1): THF (ca. 50 mL) was added to a flask containing H$_2$-**bc** (0.50 g, 1.75 mmol) and

KHMDS (0.69 g, 3.5 mmol) and stirred at room temperature for 1 hour. The resulting K$_2$[**bc**]

solution was then added to a room temperature THF suspension of SnCl$_2$ (0.33 g, 1.75 mmol). The

solution was stirred overnight to afford a pale pink solution. The THF was removed under reduced

pressure and the resulting dark pink solid was re-dissolved in ca. 40 mL warm toluene. Filtration

through a Celite plug gave a pale-yellow solution. The toluene was removed under reduced

pressure and the solid was re-dissolved in dichloromethane. Concentration of the dichloromethane

solution to ca. 10 mL and storage at ca. -18 °C gave pale yellow crystals of 1. Yield: 0.57 g (70%).

Mp: 250 – 260 °C. ^{1}H NMR (500 MHz, C_6D_6, 20 °C): δ 1.40 (m, 4H, THF C*H*$_2$(3,4)) δ 1.41 – 3.40

(m, B*H*), δ 3.55 (m, 4H, THF C*H*$_2$(2,5)). ^{11}B{^{1}H} NMR (160.5 MHz, C_6D_6, 20 °C) δ -11.47 (5B),

δ -9.33 (6B), δ -8.12 (5B), δ 1.27 (2B), δ 0.59 (2B). ^{13}C{^{1}H} NMR (151 MHz, C_6D_6, 20 °C): δ

24.95 (THF *C*H$_2$(3,4), δ 62.91 (**bc** *C*) δ 69.99 (THF *C*H$_2$(2,5)), δ 71.81 (**bc** *C*). ^{119}Sn NMR (149

MHz, C_6D_6, 20 °C): δ -137.31 ($^2J_{119Sn-11B}$ = 1487 Hz). UV-Vis (toluene): λ_{max} (ε) 280 nm (15 000 mol^{-1} L cm^{-1}) 345 nm (9600 mol^{-1} L cm^{-1}).

[(bc)Sn]₂KCl (2): Benzene (ca. 50 mL) was added to a flask containing H₂-**bc** (0.50 g, 1.75 mmol) and KHMDS (0.69 g, 3.5mmol) and stirred at room temperature until a tan-colored solution was achieved (approx. 24-48 hours). The K_2[**bc**] solution was then added directly to a room temperature dichloromethane solution of $SnCl_2$ (0.33 g, 1.75 mmol). The solution was stirred overnight to yield a pale pink solution. The solvent was removed under reduced pressure and the orange solid was re-dissolved in warm toluene and separated from the light gray solid by filtration. Toluene was removed under reduced pressure and the solid was re-dissolved in dichloromethane. Pale yellow crystals of 2 were grown from a concentrated dichloromethane solution (ca. 10 mL) stored at room temperature overnight. Yield: 0.39 g (50%). Mp: 240 °C. ^{1}H NMR (600 MHz, C_6D_6, 20°C): δ 1.50 – 3.50 (m, B*H*). ^{11}B{^{1}H} NMR (160.5 MHz, C_6D_6, 20 °C) δ -11.47 (5B) δ -9.33 (6B), δ -8.12 (5B), δ 1.27 (2B), δ 0.59 (2B). ^{13}C{^{1}H} NMR (151 MHz, C_6D_6, 20 °C): δ 62.91 (**bc** *C*), δ 71.62 (**bc** C). ^{119}Sn NMR signal not observed. UV-Vis (toluene): λ_{max} (ε) 280 nm (3700 mol^{-1} L cm^{-1}) 345 nm (820 mol^{-1} L cm^{-1}).

(bc)₂(CH)₂ (3): Benzene (ca. 50 mL) was added to a flask containing H₂-**bc** (0.50 g, 1.75 mmol) and KHMDS (0.69 g, 3.5mmol) and stirred at room temperature for 9-12 hours. The pale-yellow slurry was then added directly to a room temperature dichloromethane solution of $SnCl_2$ (0.33 g, 1.75 mmol). The solution was stirred overnight until all $SnCl_2$ solids were solubilized, affording a pale yellow-orange solution. The solvent was removed under reduced pressure and the orange solid was re-dissolved in warm toluene to filter off the white solid. Toluene was removed under reduced pressure and the product was re-dissolved in ca. 10 mL benzene. Concentration of the benzene solution of the product to ca. 1 mL and storage overnight at room temperature gave yellow-orange

crystals of 3. Yield: 0.27 g (50%). Mp: 260 – 270 °C. ^{1}H NMR (500 MHz, C$_6$D$_6$, 20 °C): δ 1.40 –

3.50 (m, BH), δ 3.78 (s, 2H, cage CH), δ 5.44 (s, 1H, olefinic CH), δ 6.10 (s, 1H, C=CH). ^{11}B{^{1}H}

NMR (160.5 MHz, C$_6$D$_6$, 20 °C) δ -11.47 (8B), δ -9.33 (11B), δ -8.04 (9B), δ -6.37 (2B), δ 1.27

(5B), δ 0.56 (5B). ^{13}C{^{1}H} NMR (151 MHz, C$_6$D$_6$, 20 °C): δ 2.65 (olefinic CH), δ 62.91 (**bc** C) δ

71.82 (**bc** C). UV-Vis (toluene): λ_{max} (ε) 284 nm (780 mol^{-1} L cm^{-1}), 334 nm (290 mol^{-1} cm^{-1}). AT-

FTIR: $\nu_{=CH}$ 3063 (s), $\nu_{=CH}$ 1254.13 (s), $\nu_{=CH}$ 1069.56 (s), $\nu_{=CH}$ 716.55 (s).

5.3 RESULTS AND DISCUSSION

Synthesis. C-H activation typically involves alkyl lithium reagents to create a reactive C–Li bond.

Working with the biscarborane system presents an interesting synthetic challenge, as both the

hydridic B-H and protic C-H vertices of **H$_2$-bc** are potentially susceptible to lithiation,[44,45] with

the lack of selectivity previously noted to lead to isomers [10] or cage-opened products.[17,18,46]

Peryshkov and co-workers in 2016 had intended to synthesize an "independently C-substituted

biscarborane cluster" and bind a phosphorus atom to the **bc** ligand through the carbon vertices in

κ^1-mode.[18] However, addition of a dialkylphosphine chloride to the Li$_2$[**bc**]/THF solution gave an

asymmetric scaffold, with one of the carborane cages of the **bc** molecule undergoing a cage-

opening reaction to produce the *closo*-(C$_2$B$_{10}$H$_{10}$)-*nido*-(C$_2$B$_{10}$H$_9$) backbone.[18] *Nido*-carboranyl

species are a known decomposition product of **H$_2$-bc** in the presence of a strong base or

nucleophile.[44,47–49]

Synthetic methods for selective **bc** vertex-activation were first reported in 2018 with the

(**bc**)Pt(dtb-bpy) (dtb-bpy = 4,4′-di-*tert*-butyl-2,2′-bipyridine) isomers.[9] The κ^2-C,C-bound isomer

was generated by reacting **H$_2$-bc** with 2 equiv of the non-nucleophilic and mild base potassium

bis(trimethylsilyl)amide (KHMDS) and the κ^2-B,C-bound isomer was generated by reacting **H$_2$-**

bc stepwise with 1 equiv KHMDS and 1 equiv MeLi.[9] This method of selectively activating the

CHAPTER 5

C-H vertices without forming deboronated *nido*-carboranyl side products via a non-nucleophilic, mild base was utilized to generate compounds **1-3**.

Initially, following the procedure of Spokoyny and coworkers[9] produced a tan-colored THF solution of K$_2$[**bc**] which was added to a THF suspension of 1 equiv of SnCl$_2$ and resulted in the isolation of compound **1**. Recrystallization from dichloromethane gave pale yellow crystals of **1**. X-ray crystallographic data revealed a THF molecule bound to the central Sn atom, suggesting that the THF solvent aids in the stabilization of the complex for isolation. The synthesis was repeated with different solvents in order to obtain a THF-free biscarboranyl stannylene.

The synthesis of **2** proceeded similarly to that of **1** but with the difference that the THF solvent was replaced with a benzene/dichloromethane mixture (**Scheme 1**). Generating K$_2$[**bc**] in a benzene solution required increased time due to the low solubility of the dipotassium salt in benzene in comparison to in THF. Once a benzene solution assumed the same tan color as the K$_2$[**bc**]/THF solution, approx. 24-48 hours at room temperature, addition to a rapidly stirring dichloromethane solution of 1 equiv of SnCl$_2$ gave, after workup and recrystallization in the same manner as **1**, light orange crystals of **2**.

Compound 3 was synthesized by a procedure similar to that of 2, with the only procedural difference being the amount of time the benzene solution was allowed to stir (Scheme 1). Stirring 1 equiv of H$_2$-**bc** with 2 equiv of KHMDS in benzene for approx. 9-12 hours afforded an ivory-colored to pale-yellow solution which was then added to a rapidly stirring dichloromethane solution of 1 equiv of SnCl$_2$. Workup and recrystallization from benzene gave pale-orange crystals of 3. The additional carbon atoms to afford the C=C bridging fragment are from the dichloromethane solvent. Given the pale color of the K$_2$[**bc**] benzene solution observed with the

shortened reaction time, it is likely that the KHMDS had activated only one C-H vertex prior to addition to the $SnCl_2/CH_2Cl_2$ solution. This mono-activated K[H-**bc**] proceeded to react with the solvent molecules to afford a C=C bond. The reaction was repeated without $SnCl_2$, but compound 3 was not generated, suggesting that $SnCl_2$ is required to create the bridging alkene, possibly via a coupling mechanism similar to the Stille reaction.[50]

X-ray Crystal Structures.

Table 1. Selected structural data for **1-3**.

Compound	1	2	3
$C_{cage} - Sn$, Å	2.272(3), 2.279(4)	Sn1: 2.276(3), 2.309(3) Sn2: 2.288(4), 2.289(3)	–
$Sn - O$ or $Sn - Cl$, Å	2.249(3)	Sn1: 2.5868(8) Sn2: 2.5874(8)	–
$C_{cage} - Sn - C_{cage}$, deg	83.05(12)	Sn1: 81.69(11) Sn2: 81.86(12)	–
$C - Sn - THF$ or $C - Sn - Cl$, deg	90.95(12), 93.12(12)	Sn1: 88.27(7), 94.11(7) Sn2: 92.62(7), 90.91(7)	–
$C = C$, Å	–	–	1.319(4)
$C_{cage} - C_{olefin}$, Å	–	–	1.488(3)
$C_{cage} - C_{olefin} - C_{olefin}$, deg	–	–	123.1(1)

Due to the rigid nature of the **bc** ligand, the stannylenes in **1** and **2** are constrained to a five-membered C_4Sn cycle. The sum of the angles of the stannocycles equal 533.45° in **1** and 538.55° and 538.96° in **2**, indicating an essentially planar C_4Sn cyclic moiety. The C–C bond that links the

carborane cages together in **1** and **2** is in the range 1.532(5) Å – 1.542(4) Å, which is slightly shorter than the C–C bond of the **H₂-bc** precursor (1.602(2)).[51] Additionally, the Sn–C bonds of **1** and **2** are 2.272(3) – 2.309(3) Å (**Table 1**), slightly longer than the sum of the covalent radii of Sn (1.40 Å) and C (0.75 Å).[52] The shortened C_{cage}–C_{cage} bond and the minor elongation of the Sn–C single bond likely function to relieve strain to accommodate the larger Sn atom into the planar heterocycle. This constrained framework has also forced a narrow sub-90° angle at the central Sn atom at 83.05(12)° in **1** and 81.69° and 81.86° in **2** (**Table 1**), enabling a C-Sn-C bond angle narrower than other 5-membered organotin heterocycles (82.9(9)° – 93.8(2)°).[53–64]
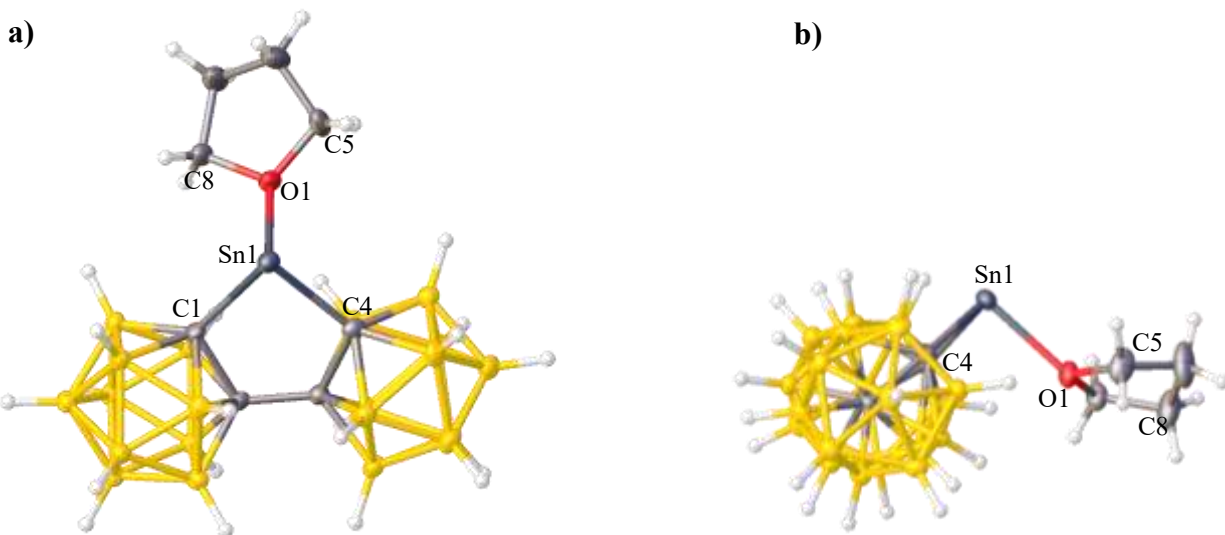
Figure 2. Thermal ellipsoid plot (50%) of **1**. CH₂Cl₂ solvent molecules are not shown for clarity. **a)** "Top" view of **2**. **b)** "Side" view of **2**. Selected bond lengths (Å) and angles (deg): C1-Sn1 = 2.272(3), C4-Sn1 = 2.279(4), O1-Sn1 = 2.249(3), C1-Sn1-C4 = 83.05(12), C1-Sn1-O1 = 90.95(12), C4-Sn1-O1 = 93.12(12).

Compound **1** co-crystallizes with two dichloromethane molecules and shows that a THF molecule is coordinated to the κ^2-C,C bonded Sn atom. The Sn–O$_{THF}$ distance of 2.239(3) Å is within the range of other Sn–O$_{THF}$ distances in THF-coordinated Sn(II) complexes (2.261(14) – 2.422(6) Å),[65–68] consistent with a dative Sn←O interaction. Additionally, the THF molecule is bonded to the Sn atom at approximately perpendicular to the C$_4$Sn plane, with C-Sn-O$_{THF}$ angles at 90.95(12)° and 93.12(12)° (**Figure 2b**). In total, the sum of the angles around the tin atom equals 267.12(12)° and indicates a highly pyramidalized geometry. The coordination geometry at Sn is typical of other THF-coordinated Sn complexes, which report C-Sn-O$_{THF}$ angles of 84.8(3) – 94.6(6)°.[65–68]
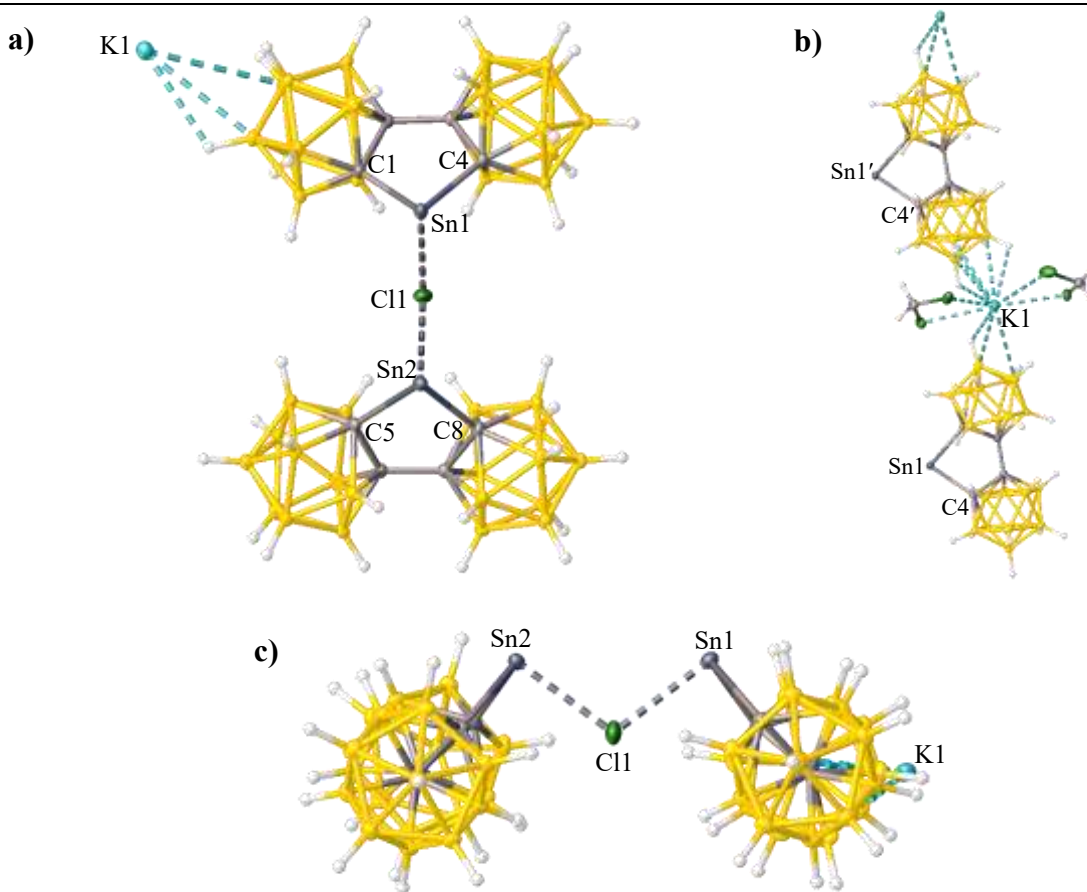
Figure 3. Thermal ellipsoid plot (50%) of **2**. **a)** View of **2** to show coordination positions of K1 and Cl1. The CH$_2$Cl$_2$ solvent molecules are not shown for clarity. **b)** Expanded view of **2** to show

coordination of K1. **c)** View of **2** to show coordination of Cl1. CH_2Cl_2 solvent molecules are not shown for clarity. Selected bond lengths (Å) and angles (deg): C1-Sn1 = 2.276(3), C4-Sn1 = 2.309(3), C5-Sn2 = 2.288(4), C8-Sn2 = 2.289(3), Cl1-Sn1 = 2.5868(8), Cl1-Sn2 = 2.5874(8), C1-Sn1-C4= 81.69(11), C5-Sn2-C8 = 81.86(12), Sn1-Cl1-Sn2 = 106.98(3), C1-Sn1-Cl1 = 88.27(7), C4-Sn1-Cl1 = 94.11(7), C5-Sn2-Cl1 = 92.62(7), C8-Sn2-Cl1 = 90.91(7).

Compound **2** co-crystallizes with two dichloromethane molecules as well as the K^+ ion from $K_2[bc]$ and Cl^- ion from $SnCl_2$ in the previous step of the synthesis. The K^+ ion appears as a counterion coordinated to the B-H vertices of the **bc** cage (**Figure 3b**) and the Cl^- ion forms a Sn-Cl-Sn bridging fragment between two (**bc**)Sn moieties (**Figure 3c**). The counteranion charge to the K+ cation should be delocalized over the biscarborane cages.[1,3] Organotin complexes containing a Sn-Cl-Sn fragment typically report bridging Sn-Cl bond distances in the range of 2.540(2) – 2.967(1) Å,[69–78] and this fragment of compound **2** features Sn-Cl bond distances of 2.5868(8) and 2.5874(8) Å, which are at the lower end of the above range. The relatively short Sn–Cl distances in **2** indicate a strong interaction between the two ions, although whether this is a consequence of the rigid structure or electron-withdrawing influence of the **bc** ligand is not apparent.
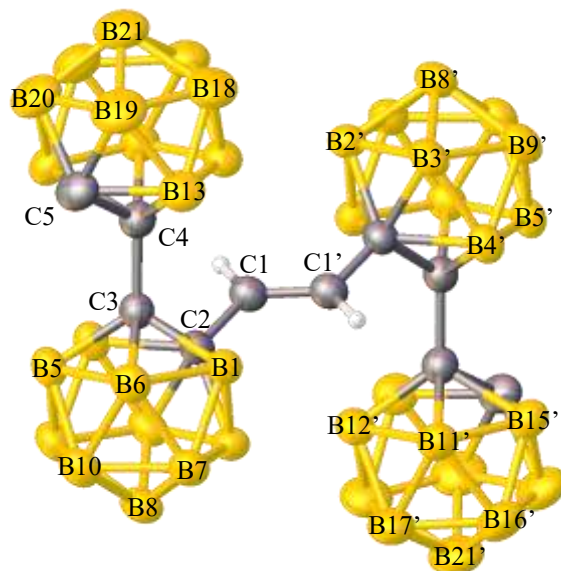
Figure 4. Thermal ellipsoid plot (50%) of **3**. Cage-bonded H atoms are not shown for clarity. Selected bond lengths (Å) and angles (deg): C1-C1'= 1.319(4), C1-C2= 1.488(3), C3-C4 = 1.533(3), C2-C1-C1'= 123.1(2).

Structural data for compound **3** shows an inversion center which imposes a *trans* configuration around the central C1–C1′ bond (**Figure 4**). The C1–C1′ bond distance (1.319(4) Å) and C2-C1-C1′ bond angle (123.1(2)°) are consistent with the presence of a C=C double bond.[67] Overall, compound **3** has C_{2h} symmetry. A series of dicarboranyl ethenes R($C_2B_{10}H_{10}$)CH=CH($C_2B_{10}H_{10}$)R (R = Ph or C_6H_4Me-*p*) analogous to compound **3** similarly contain a trans C=C double bond. [46] More recently, carborane clusters linked via a phenyl group have also been reported, generally containing the formula ($C_2B_{10}H_{11}$)-Ph-($C_2B_{10}H_{11}$).[79–81] To the best of our knowledge, compound **3** is the first dibiscarboranyl ethene in the literature.

Spectroscopy. Compounds 1-3 were characterized by ^{1}H NMR, ^{11}B NMR, ^{13}C NMR, UV-vis, IR spectroscopy, and X-ray crystallography. Compound **1** was also characterized by ^{119}Sn NMR spectroscopy.

The ^{1}H NMR spectrum for **1** displays the coordinated THF proton signals at 1.40 and 3.55 ppm, which is in the same range as those of other THF-coordinated Sn(II) complexes ($\delta_{CH_2(3,4)} = 1.3 - 1.8$; $\delta_{CH_2(2,5)} = 3.5 - 3.7$)[65–68] as well as signals due to free THF in C_6D_6 ($\delta_{CH_2(3,4)} = 1.43$; $\delta_{CH_2(2,5)} = 3.57$).[43]

The ^{119}Sn NMR spectrum for **1** displays a signal at -137.31 ppm. Related (**bc**)Sn compounds report ^{119}Sn signals further downfield than compound **1**, with (**bc**)SnMe$_2$ at -21.22 ppm in d^8-THF and the methyl-substituted derivative (**Mebc**)SnMe$_2$ (**Mebc** = 8,8′,9,9′,10,10′,12,12′-octamethyl-1,1′-bis(o-carborane)) at 9.20 ppm in d^8-THF and 53.10 ppm in C_6D_6 (**Table 2**).[20] A decrease in coordination environment around the Sn atom usually results in a downfield shift of the ^{119}Sn resonance.[82] Nonetheless, 3-coordinate **1** displays an upfield shift in comparison to the 4-coordinate (**bc**)SnMe$_2$ and (**Mebc**)SnMe$_2$. The three-coordinate, THF-bonded complexes Sn[OC(C$_4$H$_3$S)$_3$]$_2$(THF)[65] and [Sn(box)(THF)]$^+$ (box = 1,1-bis[(4S)-4-phenyl-1,3-oxazolin-2-yl]ethane)[67] report ^{119}Sn NMR signals upfield of the chemical shifts of **1** at -244.5 and -377.1 ppm, respectively. As the signal for **1** is observed between its tetra-coordinated analogues and Sn(II)←THF derivatives, THF coordination aids in shielding the tin atom, leading to a more shielded Sn atom than (**bc**)SnMe$_2$ and (**Mebc**)SnMe$_2$, while the electron-withdrawing effect of the **bc** ligand causes a deshielding on Sn relative to other Sn(II)←THF complexes.

The triplet of triplets which occurs in the ^{119}Sn NMR spectrum of compound **1** is unusual given the absence of a Sn–H signal in its ^{1}H NMR and IR spectra, and X-ray structural data. Additionally,
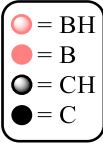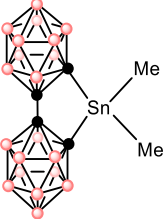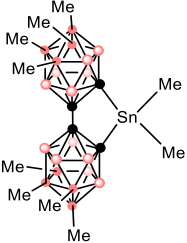
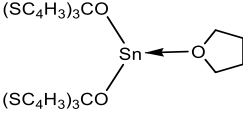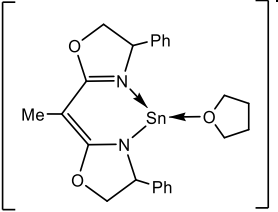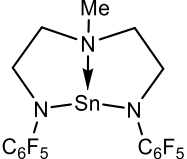^{119}Sn NMR signals for Sn(II)←THF complexes often appear as singlets in the spectrum (**Table 2**).[65–67] However, multivalent Sn complexes bonded to electron-withdrawing groups and supported by a Sn←X (X = N or P) dative bond report multiplets in their ^{119}Sn NMR spectra (**Table 2**).[26–28,66] The carboranyl-tin complexes by Gielen and coworkers report 1:2:3:4:3:2:1 septets in their corresponding ^{119}Sn NMR spectra at -166.3 ppm and -166.2 ppm, with coupling constants of 1268 Hz and 1271 Hz[28] similar to the coupling constant for the ^{119}Sn NMR signal of **1** (1487 Hz). In addition, carboranyl tin complexes supported by a Sn←X dative bond (X = N or P) typically observe doublets in the ^{119}Sn NMR spectrum, depending on both the identity of the X atom and coordination about Sn.[26–28,30,82–84] The splitting patterns which appear in the ^{119}Sn NMR spectra of compound **1** and carboranyl tin coordination complexes presumably arise from long-range nuclear spin-spin coupling between the carboranyl boron and tin nuclei.[85,86] The quadrupolar relaxation rate of the ^{11}B nucleus ($I = \frac{3}{2}$) is known to influence the appearance of the resonances of nuclei with spin $I = \frac{1}{2}$, such as ^{119}Sn.[85–87] Specific to compound **1**, the four boron atoms bonded to the tin-bound carbon atom (B3, B6, B7, and B11) exist in two different chemical environments due to the C_{2v} symmetry of the o-carborane cage (**Figure 5**), likely causing the triplet of triplets displayed in the ^{119}Sn spectrum of **1**.
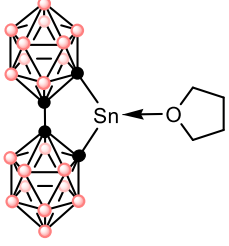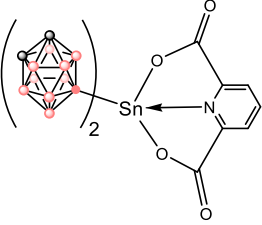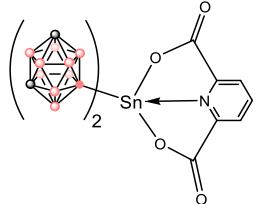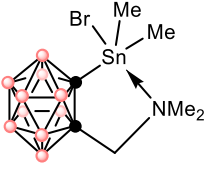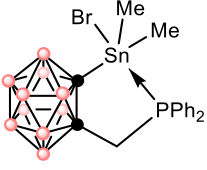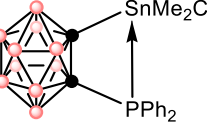
Despite numerous attempts to record spectra, with use of a wide variety of parameters, the ^{119}Sn NMR signal for compound **2** could not be detected. Problems in obtaining the ^{119}Sn data were also encountered for the dianions $K_2[Ar^{iPr6}SnSnAr^{iPr6}]$, which was hypothesized to be caused by the unsymmetric electron environment at the Sn atoms, which may cause rapid relaxation through the high anisotropy of the chemical shift tensor.[78,88] The THF ligand in **1** appears to stabilize the electron environment at the Sn atom to facilitate detection of a signal. In addition, though the ^{11}B

NMR spectra of **1** and **2** are both proton-decoupled, the spectrum for **2** displays tin satellites at -14 and -5 ppm (See SI, **Figure S5**) that are absent in the spectrum for **1**. This difference can also be attributed to the coordination of THF to the ^{119}Sn nucleus in **1** but not **2**.

Table 2. The ^{119}Sn NMR chemical shifts for **1** and selected compounds.

	^{119}Sn δ (ppm)/ (Solvent)	J_{119sn} (Hz)	Reference
O = BH, ● = B, ◉ = CH, ● = C	-21.22 (s) / (d^8-THF)	-	20
	9.20 (s) / (d^8-THF) 53.10 (s) / (C$_6$D$_6$)	-	20
(SC$_4$H$_3$)$_3$CO — Sn ← O, (SC$_4$H$_3$)$_3$CO	-244.5 (s) / (CDCl$_3$)	-	65
	-377.1 (s) / (d^8-THF)	-	67
	-127 (quint) / (CDCl$_3$)	412.5	66

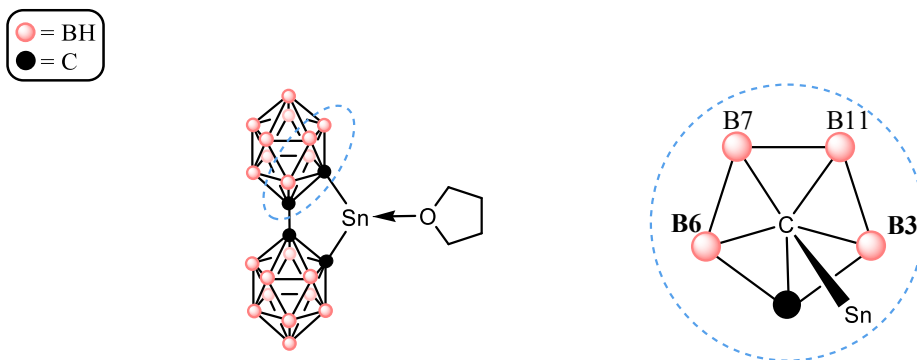|	Chemical shift / Solvent	Value	Ref.
	-137 (tt) / (C₆D₆)	1487	this work
	-166.3 (sept) / (n.r.)	1268	28
	-166.2 (sept) / (n.r.)	1271	28
	-118.63 (n.r.) / (CDCl₃)	(n.r.)	26
	-30.2 (d) / (CDCl₃)	320.3	27
	108.3 (d) / (CDCl₃)	72.6	27

n.r.: not reported.

Figure 5. Left: The tin-bonded carbon vertex face is marked with a blue circle. Right: "Front" view of the blue-circled face, showing the two chemical environments of B3/B6 (**bolded**) versus B7/B11.

The UV-vis spectrum of **1** displays two absorptions in the near-UV region at 280 nm and 345 nm. These absorptions persist in **2**, appearing also at 280 nm and 345 nm regardless of whether a THF or K ion is coordinated to Sn. The similar absorptions in the UV-vis spectra for **1** and **2** suggests that compounds **1** and **2** exist as the same compound in the solution phase. The relatively intense absorptions at 280 nm and similarly at 284 nm in the UV-vis spectrum for **3** can be tentatively assigned to an energy transfer on the bis-carborane ligand. The near-UV vis region of the absorption bands of **1** and **2** suggests a high energy HOMO→LUMO transition of the (**bc**)Sn compounds.

Compound **3** exhibits spectroscopic features characteristic of alkenes. The olefin protons appear at 5.43 and 6.10 ppm in the ^{1}H NMR spectrum and the olefin carbon at 2.65 ppm in the ^{13}C NMR spectrum, at the high frequency shifts indicative of more conjugated alkenes.[89] The UV-vis spectrum of **3** displays a shoulder at 334 nm, corresponding to an olefin π→π* transition at a relatively longer wavelength for alkenes groups, further confirming a conjugated alkene.[89]

Interestingly, a $v_{C=C}$ stretching frequency in the IR spectrum within the characteristic 1680 – 1640 cm^{-1} region is not observed.

5.4 CONCLUSION

The syntheses for **1-3** proceeded in a similar way to each other with only simple modifications in solvents or reaction time. In THF solvent, the synthetic procedure gave the THF-coordinated **1**, while using a stepwise benzene and dichloromethane solvent mixture gave **2**. Shortening the reaction period of the step that generates the dipotassium salt from 24-48 hours to 9-12 hours gave the alkene **3**. Compound **1** exists as a Lewis acid-base pair with THF, as displayed in the X-ray structural data. Furthermore, the **bc** ligand platform confers interesting spectroscopic characteristics in the ^{119}Sn NMR spectrum that is unusual for Sn(II)-THF complexes but usual for organotin complexes featuring electron-withdrawing ligands like carboranes. X-ray structural data for **2** show the Sn atom contains a similar structural motif to that of **1**. Compound **3** is the first example of a dibiscarborane-supported alkene.

ASSOCIATED CONTENT

Supporting Information.

Crystallographic data and spectra (NMR, IR, UV–vis)

Accession Codes.

CCDC 2248737-2248739 contain the supplementary crystallographic data for this paper. These data can be obtained free of charge via www.ccdc.cam.ac.uk/data_request/cif, or by

emailing data_request@ccdc.cam.ac.uk, or by contacting The Cambridge Crystallographic Data Centre, 12 Union Road, Cambridge CB2 1EZ, UK; fax: +44 1223 336033.

AUTHOR INFORMATION

Corresponding Author

Philip P. Power – Department of Chemistry, University of California, Davis, California 95616, United States; orcid.org/0000-0002-6262-3209; Email: pppower@ucdavis.edu

Authors

Alice C. Phung – Department of Chemistry, University of California, Davis, California 95616, United States; https://orcid.org/0000-0002-0268-3971

James C. Fettinger - Department of Chemistry, University of California, Davis, California 95616, United States; orcid.org/0000-0002-6428-4909

Author Contributions

The manuscript was written through contributions of all authors. All authors have given approval to the final version of the manuscript.

Notes

The authors declare no competing financial interest.

CHAPTER 5

ACKNOWLEDGMENT

PUBLICATION INFORMATION

CHAPTER 5

5.5 REFERENCES

(1)   Grimes, R. N. *Carboranes*; Elsevier, 2016.

(2)   Grimes, R. N. Carboranes in the Chemist's Toolbox. *Dalton Transactions* **2015**, *44*, 5939–5956.

(3)   Welch, A. J. Bis(Carboranes) and Their Derivatives; 2021; pp 163–195.

(4)   Jeans, R. J.; Chan, A. P. Y.; Riley, L. E.; Taylor, J.; Rosair, G. M.; Welch, A. J.; Sivaev, I. B. Arene–Ruthenium Complexes of 1,1′-Bis(*Ortho*-Carborane): Synthesis, Characterization, and Catalysis. *Inorg Chem* **2019**, *58*, 11751–11761.

(5)   Sivaev, I. B.; Bregadze, V. I. 1,1′-Bis(Ortho-Carborane)-Based Transition Metal Complexes. *Coord Chem Rev* **2019**, *392*, 146–176.

(6)   Chambrier, I.; Hughes, D. L.; Jeans, R. J.; Welch, A. J.; Budzelaar, P. H. M.; Bochmann, M. Do Gold(III) Complexes Form Hydrogen Bonds? An Exploration of Au[III] Dicarboranyl Chemistry. *Chemistry – A European Journal* **2020**, *26*, 939–947.

(7)   Martin, M. J.; Man, W. Y.; Rosair, G. M.; Welch, A. J. 1,1′-Bis(Ortho-Carborane) as a κ^2 Co-Ligand. *J Organomet Chem* **2015**, *798*, 36–40.

(8)   Yao, Z.-J.; Zhang, Y.-Y.; Jin, G.-X. Pseudo-Aromatic Bis-o-Carborane Iridium and Rhodium Complexes. *J Organomet Chem* **2015**, *798*, 274–277.

(9)   Kirlikovali, K. O.; Axtell, J. C.; Anderson, K.; Djurovich, P. I.; Rheingold, A. L.; Spokoyny, A. M. Fine-Tuning Electronic Properties of Luminescent Pt(II) Complexes via Vertex-Differentiated Coordination of Sterically Invariant Carborane-Based Ligands. *Organometallics* **2018**, *37*, 3122–3131.

(10)   Kirlikovali, K. O.; Axtell, J. C.; Gonzalez, A.; Phung, A. C.; Khan, S. I.; Spokoyny, A. M. Luminescent Metal Complexes Featuring Photophysically Innocent Boron Cluster Ligands. *Chem Sci* **2016**, *7*, 5132–5138.

(11)   Jeans, R. J.; Rosair, G. M.; Welch, A. J. *C,C′*-Ru to *C,B′*-Ru Isomerisation in Bis(Phosphine)Ru Complexes of [1,1′-Bis(*Ortho*-Carborane)]. *Chemical Communications* **2022**, *58*, 64–67.

(12)   Owen, D. A.; Hawthorne, M. F. Novel Chelated Biscarborane Transition Metal Complexes Formed through Carbon-Metal σ Bonds. *J Am Chem Soc* **1970**, *92*, 3194–3196.

(13)   Harwell, D. E.; McMillan, J.; Knobler, C. B.; Hawthorne, M. F. Structural Characterization of Representative d^7, d^8, and d^9 Transition Metal Complexes of Bis(*o*-Carborane). *Inorg Chem* **1997**, *36*, 5951–5955.

(14)   Mandal, D.; Rosair, G. M. Exploration of Bis(Nickelation) of 1,1′-Bis(o-Carborane). *Crystals (Basel)* **2020**, *11*, 16.

(15) Chan, A. P. Y.; Rosair, G. M.; Welch, A. J. Exopolyhedral Ligand Orientation Controls Diastereoisomer in Mixed-Metal Bis(Carboranes). *Molecules* **2020**, *25*, 519.

(16) Cui, C.-X.; Ren, S.; Qiu, Z.; Xie, Z. Synthesis of Carborane-Fused Carbo- and Heterocycles *via* Zirconacyclopentane Intermediates. *Dalton Transactions* **2018**, *47*, 2453–2459.

(17) Wong, Y. O.; Smith, M. D.; Peryshkov, D. v. Reversible Water Activation Driven by Contraction and Expansion of a 12-Vertex-Closo-12-Vertex-Nido Biscarborane Cluster. *Chemical Communications* **2016**, *52*, 12710–12713.

(18) Wong, Y. O.; Smith, M. D.; Peryshkov, D. v. Synthesis of the First Example of the 12-Vertex-*Closo*/12-Vertex-*Nido* Biscarborane Cluster by a Metal-Free B−H Activation at a Phosphorus(III) Center. *Chemistry - A European Journal* **2016**, *22*, 6764–6767.

(19) Yruegas, S.; Axtell, J. C.; Kirlikovali, K. O.; Spokoyny, A. M.; Martin, C. D. Synthesis of 9-Borafluorene Analogues Featuring a Three-Dimensional 1,1′-Bis(*o*-Carborane) Backbone. *Chemical Communications* **2019**, *55*, 2892–2895.

(20) Axtell, J. C.; Kirlikovali, K. O.; Dziedzic, R. M.; Gembicky, M.; Rheingold, A. L.; Spokoyny, A. M. Magnesium Reagents Featuring a 1,1′-Bis(*o*-carborane) Ligand Platform. *Eur J Inorg Chem* **2017**, *2017*, 4411–4416.

(21) Zhang, C.; Wang, J.; Lin, Z.; Ye, Q. Synthesis, Characterization, and Properties of Three-Dimensional Analogues of 9-Borafluorenes. *Inorg Chem* **2022**, *61*, 18275–18284.

(22) Riley, L. E.; Krämer, T.; McMullin, C. L.; Ellis, D.; Rosair, G. M.; Sivaev, I. B.; Welch, A. J. Large, Weakly Basic Bis(Carboranyl)Phosphines: An Experimental and Computational Study. *Dalton Transactions* **2017**, *46*, 5218–5228.

(23) Schroeder, H.; Papetti, S.; Alexander, R. P.; Sieckhaus, J. F.; Heying Theodore L. Icosahedral Carboranes. XI. Germanium and Tin Derivatives of o-, m-, and p-Carborane and Their Polymers. *Inorg Chem* **1969**, *8*, 2444–2449.

(24) Bregadze, V. I.; Dzhashiashvili, T. K.; Sadzhaya, D. N.; Petriashvili, M. v.; Ponomareva, O. B.; Shcherbina, T. M.; Kampel', V. Ts.; Kukushkina, L. B.; Rochev, V. Ya.; Godovikov, N. N. Carborane Derivatives with Boron-Tin Bond. *Bulletin of the Academy of Sciences of the USSR Division of Chemical Science* **1983**, *32*, 824–827.

(25) Zakharkin, L. I.; Bregadze, V. I.; Okhlobystin, O. Yu. Synthesis of Organoelement Derivatives of Barenes (Carboranes). *J Organomet Chem* **1965**, *4*, 211–216.

(26) Lee, J.-D.; Kim, S.-J.; Yoo, D.; Ko, J.; Cho, S.; Kang, S. O. Synthesis and Reactivity of Intramolecularly Stabilized Organotin Compounds Containing the C,N-Chelating *o*-Carboranylamino Ligand [*o*-C$_2$B$_{10}$H$_{10}$(CH$_2$NMe$_2$)-*C,N*]⁻ (Cab^{C,N}). X-Ray Structures of (Cab^{C,N})SnR$_2$X (R = Me, X = Cl; R = Ph, X = Cl), (Cab^{C,N})$_2$Hg, and [(Cab^{C,N})SnMe$_2$]$_2$. *Organometallics* **2000**, *19*, 1695–1703.

(27) Lee, T.; Lee, S. W.; Jang, H. G.; Kang, S. O.; Ko, J. Synthesis and Reactivity of Organotin Compounds Containing the C,P-Chelating *o*-Carboranylphosphino Ligand [*o*-

$C_2B_{10}H_{10}PPh_2$-*C,P*](Cab^{C,P}). X-Ray Structures of (Cab^{C,CH2P})SnMe$_2$Br, [(Cab^{C,P})SnMe$_2$]$_2$Pd, and [(Cab^{C,P})SnMe$_2$]Pd(PEt$_3$)Cl. *Organometallics* **2001**, *20*, 741–748.

(28) Gielen, M.; Kayser, F.; Zhidkova, O. B.; Kampel, V. Ts.; Bregadze, V. l.; de Vos, D.; Biesemans, M.; Mahieu, B.; Willem, R. Synthesis, Characterization and In Vitro Antitumour Activity of Novel Organotin Derivatives of 1,2- and 1,7-Dicarba-Closo-Dodecaboranes. *Met Based Drugs* **1995**, *2*, 37–42.

(29) Dostál, L.; Růžička, A.; Jambor, R. Synthesis of Me$_2$LSn(o-CH$_3$–C$_2$B$_{10}$H$_{10}$): Crystal Structure of Sn←O Intramolecularly Coordinated Organotin Compound Containing 1-Methyl-o-Carborane. *Inorganica Chim Acta* **2010**, *363*, 2051–2054.

(30) Lee, J.-D.; Kim, H.-S.; Han, W.-S.; Kang, S. O. Chiral Organotin Complexes Stabilized by C,N-Chelating Oxazolinyl-o-Carboranes. *J Organomet Chem* **2010**, *695*, 463–468.

(31) Nakamura, H.; Aoyagi, K.; Yamamoto, Y. *O*-Carborane as a Novel Protective Group for Aldehydes and Ketones. *J Org Chem* **1997**, *62*, 780–781.

(32) Nakamura, H.; Yamamoto, Y. Novel Addition and [3+2] Cycloaddition Reactions of Stannyl- and Silyl-Ortho-Carboranes to Carbonyl Compounds. *Collect Czechoslov Chem Commun* **1999**, *64*, 829–846.

(33) Lee, C.; Lee, J.; Lee, S. W.; Kang, S. O.; Ko, J. Synthesis and Reactivity of 1,2-Bis(Chlorodimethylgermyl)Carborane and 1,2-Bis(Bromodimethylstannyl)Carborane. *Inorg Chem* **2002**, *41*, 3084–3090.

(34) Batsanov, A. S.; Fox, M. A.; Hibbert, T. G.; Howard, J. A. K.; Kivekäs, R.; Laromaine, A.; Sillanpää, R.; Viñas, C.; Wade, K. Sulfur, Tin and Gold Derivatives of 1-(2′-Pyridyl)-Ortho-Carborane, 1-R-2-X-1,2-C$_2$B$_{10}$H$_{10}$ (R = 2′-Pyridyl, X = SH, SnMe$_3$ or AuPPh$_3$). *Dalton Trans.* **2004**, No. 22, 3822–3828.

(35) Dröse, P.; Hrib, C. G.; Edelmann, F. T. Carboranylamidinates. *J Am Chem Soc* **2010**, *132* (44), 15540–15541.

(36) Harmgarth, N.; Gräsing, D.; Dröse, P.; Hrib, C. G.; Jones, P. G.; Lorenz, V.; Hilfert, L.; Busse, S.; Edelmann, F. T. Novel Inorganic Heterocycles from Dimetalated Carboranylamidinates. *Dalton Trans.* **2014**, *43*, 5001–5013.

(37) Harmgarth, N.; Liebing, P.; Förster, A.; Hilfert, L.; Busse, S.; Edelmann, F. T. Spontaneous vs. Base-Induced Dehydrochlorination of Group 14 *Ortho*-Carboranylamidinates. *Eur J Inorg Chem* **2017**, *2017*, 4473–4479.

(38) Crujeiras, P.; Rodríguez-Rey, J. L.; Sousa-Pedrares, A. Coordinating Ability of the Iminophosphorane Group in *Ortho*-Carborane Derivatives. *Eur J Inorg Chem* **2017**, *2017*, 4653–4667.

(39) Neumann, W. P. Germylenes and Stannylenes. *Chem Rev* **1991**, *91*, 311–334.

(40)	Tokitoh, N.; Okazaki, R. Recent Topics in the Chemistry of Heavier Congeners of Carbenes. *Coord Chem Rev* **2000**, *210*, 251–277.

(41)	Product Subclass 7: Stannylenes. In *Category 1, Organometallics*; Moloney, M. G., Ed.; Georg Thieme Verlag: Stuttgart, 2003.

(42)	Ren, S.; Xie, Z. A Facile and Practical Synthetic Route to 1,1′-Bis(*o*-Carborane). *Organometallics* **2008**, *27*, 5167–5168.

(43)	Fulmer, G. R.; Miller, A. J. M.; Sherden, N. H.; Gottlieb, H. E.; Nudelman, A.; Stoltz, B. M.; Bercaw, J. E.; Goldberg, K. I. NMR Chemical Shifts of Trace Impurities: Common Laboratory Solvents, Organics, and Gases in Deuterated Solvents Relevant to the Organometallic Chemist. *Organometallics* **2010**, *29*, 2176–2179.

(44)	Kazakov, G. S.; Sivaev, I. B.; Suponitsky, K. Y.; Kirilin, A. D.; Bregadze, V. I.; Welch, A. J. Facile Synthesis of Closo-Nido Bis(Carborane) and Its Highly Regioselective Halogenation. *J Organomet Chem* **2016**, *805*, 1–5.

(45)	Popescu, A.-R.; Musteti, A. D.; Ferrer-Ugalde, A.; Viñas, C.; Núñez, R.; Teixidor, F. Influential Role of Ethereal Solvent on Organolithium Compounds: The Case of Carboranyllithium. *Chemistry - A European Journal* **2012**, *18*, 3174–3184.

(46)	Thomas, R. Ll.; Rosair, G. M.; Welch, A. J. Synthesis and Molecular Structure of Dicarbaboryl Ethenes and an Unexpected Dimetallated Derivative. *Chemical Communications* **1996**, 1327.

(47)	Wiesboeck, R. A.; Hawthorne, M. Frederick. Dicarbaundecaborane(13) and Derivatives. *J Am Chem Soc* **1964**, *86*, 1642–1643.

(48)	Hawthorne, M. F.; Young, D. C.; Garrett, P. M.; Owen, D. A.; Schwerin, S. G.; Tebbe, F. N.; Wegner, P. A. Preparation and Characterization of the (3)-1,2- and (3)-1,7-Dicarbadodecahydroundecaborate(-1) Ions. *J Am Chem Soc* **1968**, *90*, 862–868.

(49)	Hawthorne, M. F.; Owen, D. A.; Wiggins, J. W. Degradation of Biscarborane. *Inorg Chem* **1971**, *10*, 1304–1306.

(50)	Aleena, M. B.; Philip, R. M.; Anilkumar, G. Advances in Non-palladium-catalysed Stille Couplings. *Appl Organomet Chem* **2021**, *35*.

(51)	Yang, X.; Jiang, W.; Knobler, C. B.; Mortimer, M. D.; Hawthorne, M. F. The Synthesis and Structural Characterization of Carborane Oligomers Connected by Carbon-Carbon and Carbon-Boron Bonds between Icosahedra. *Inorganica Chim Acta* **1995**, *240*, 371–378.

(52)	Pyykkö, P.; Atsumi, M. Molecular Single-Bond Covalent Radii for Elements 1-118. *Chemistry - A European Journal* **2009**, *15*, 186–197.

(53)	Clegg, W.; Harrington, R. W. CCDC 2055793: Experimental Crystal Structure Determination. *CSD Communication* **2021**.

(54) Iwamoto, T.; Masuda, H.; Ishida, S.; Kabuto, C.; Kira, M. Addition of Stable Nitroxide Radical to Stable Divalent Compounds of Heavier Group 14 Elements. *J Am Chem Soc* **2003**, *125*, 9300–9301.

(55) Yan, C.; Li, Z.; Xiao, X.; Wei, N.; Lu, Q.; Kira, M. Reversible Stannylenoid Formation from the Corresponding Stannylene and Cesium Fluoride. *Angewandte Chemie International Edition* **2016**, *55*, 14784–14787.

(56) Schäfer, A.; Saak, W.; Haase, D.; Müller, T. Persistent Dialkyl(Silyl)Stannylium Ions. *J Am Chem Soc* **2011**, *133*, 14562–14565.

(57) Kira, M.; Yauchibara, R.; Hirano, R.; Kabuto, C.; Sakurai, H. Chemistry of Organosilicon Compounds. 287. Synthesis and X-Ray Structure of the First Dicoordinate Dialkylstannylene That Is Monomeric in the Solid State. *J Am Chem Soc* **1991**, *113*, 7785–7787.

(58) Saito, M.; Shiratake, M.; Tajima, T.; Guo, J. D.; Nagase, S. Synthesis and Structure of the Dithienostannole Anion. *J Organomet Chem* **2009**, *694*, 4056–4061.

(59) Kavara, A.; Kampf, J. W.; Banaszak Holl, M. M. Direct Formation of Propargyltin Compounds via C−H Activation. *Organometallics* **2008**, *27*, 2896–2897.

(60) Kavara, A.; Kheir, M. M.; Kampf, J. W.; Banaszak Holl, M. M. Aryl Halide Radical Clocks as Probes of Stannylene/Aryl Halide C–H Activation Rates. *J Inorg Organomet Polym Mater* **2014**, *24*, 250–257.

(61) Yan, C.; Xu, Z.; Xiao, X.-Q.; Li, Z.; Lu, Q.; Lai, G.; Kira, M. Reactions of an Isolable Dialkylstannylene with Carbon Disulfide and Related Heterocumulenes. *Organometallics* **2016**, *35*, 1323–1328.

(62) Kavara, A.; Cousineau, K. D.; Rohr, A. D.; Kampf, J. W.; Banaszak Holl, M. M. A Stannylene/Aryl Iodide Reagent for Allylic CH Activation and Double Bond Addition Chemistry. *Organometallics* **2008**, *27*, 1041–1043.

(63) Izod, K.; McFarlane, W.; Tyson, B. V.; Carr, I.; Clegg, W.; Harrington, R. W. Stabilization of a Dialkylstannylene by Unusual B−H···Sn γ-Agostic-Type Interactions. A Structural, Spectroscopic, and DFT Study. *Organometallics* **2006**, *25*, 1135–1143.

(64) Krebs, K. M.; Wiederkehr, J.; Schneider, J.; Schubert, H.; Eichele, K.; Wesemann, L. η³ - Allyl Coordination at Tin(II)-Reactivity towards Alkynes and Benzonitrile. *Angewandte Chemie International Edition* **2015**, *54*, 5502–5506.

(65) Veith, M.; Belot, C.; Huch, V.; Zimmer, M. Influence of the Solvent on the Formation of New Tin(II) Methoxides Containing Thienyl Substituents: Crystal Structure and NMR Investigations. *Z Anorg Allg Chem* **2009**, *635*, 942–948.

(66) Huang, M.; Kireenko, M. M.; Lermontova, E. Kh.; Churakov, A. V.; Oprunenko, Y. F.; Zaitsev, K. V.; Sorokin, D.; Harms, K.; Sundermeyer, J.; Zaitseva, G. S.; Karlov, S. S. Novel

Stannylenes Stabilized with Diethylenetriamido and Related Amido Ligands: Synthesis, Structure, and Chemical Properties. *Z Anorg Allg Chem* **2013**, *639*, 502–511.

(67)   Arii, H.; Matsuo, M.; Nakadate, F.; Mochida, K.; Kawashima, T. Coordination of a Chiral Tin(Ii) Cation Bearing a Bis(Oxazoline) Ligand with Tetrahydrofuran Derivatives. *Dalton Transactions* **2012**, *41*, 11195.

(68)   Eisler, D. J.; Chivers, T. Chalcogenide Derivatives of Imidotin Cage Complexes. *Chemistry - A European Journal* **2006**, *12*, 233–243.

(69)   Chorley, R. W.; Hitchock, P. B.; Jolly, B. S.; Lappert, M. F.; Lawless, G. A. Crystalline Binuclear Cis- and Trans-Chlorotin(II) Amides [Sn(μ-Cl)(NR$_2$)]$_2$, the *cis*-1a ⇌*trans*-1b Isomerisation for [NR$_2$= NCMe$_2$(CH$_2$)$_3$CMe$_2$], and the X-Ray Structures of 1a and of *trans*-[Sn(μ-Cl){N(SiMe$_3$)$_2$}]$_2$. *J. Chem. Soc., Chem. Commun.* **1991**, 1302–1303.

(70)   Peng, Y.; Fischer, R. C.; Merrill, W. A.; Fischer, J.; Pu, L.; Ellis, B. D.; Fettinger, J. C.; Herber, R. H.; Power, P. P. Substituent Effects in Ditetrel Alkyne Analogues: Multiple vs. Single Bonded Isomers. *Chem Sci* **2010**, *1* (4), 461.

(71)   Hitchcock, P. B.; Lappert, M. F.; Wang, Z.-X. A Contribution to 1-Azapentadienylmetal Chemistry: Si, Sn(II), Fe(II) and Co(II) Complexes. *J Organomet Chem* **2009**, *694*, 3762–3767.

(72)   Tang, Y.; Felix, A. M.; Zakharov, L. N.; Rheingold, A. L.; Kemp, R. A. Syntheses and Structural Characterization of a Monomeric Tin(II) Diamide and a Novel Chlorotin(II) Amide Trimer. *Inorg Chem* **2004**, *43*, 7239–7242.

(73)   Eichler, B. E.; Pu, L.; Stender, M.; Power, P. P. The Synthesis and Structure of Sterically Encumbered Terphenyl Tin(II) Halide Derivatives: Simultaneous Existence of Monomers and Dimers in the Crystalline Phase. *Polyhedron* **2001**, *20*, 551–556.

(74)   Eaborn, C.; Hitchcock, P. B.; Smith, J. D.; Sözerli, S. E. Synthesis and Crystal Structures of the Compounds [Sn{C(SiMe$_2$Ph)$_3$}Cl]$_2$, [Pb{C(SiMe$_3$)$_3$}Cl]$_3$, and [M{C(SiMe$_3$)$_2$(SiMe$_2$OMe)}Cl]$_2$ (M = Sn or Pb). *Organometallics* **1997**, *16*, 5653–5658.

(75)   Watson, I. C.; Ferguson, M. J.; Rivard, E. Zinc-Mediated Transmetalation as a Route to Anionic *N*-Heterocyclic Olefin Complexes in the p-Block. *Inorg Chem* **2021**, *60*, 18347–18359.

(76)   Keil, P. M.; Hadlington, T. J. Accessing Cationic Tetrylene-Nickel(0) Systems Featuring Donor–Acceptor E–Ni Triple Bonds (E = Ge, Sn). *Chemical Communications* **2022**, *58*, 3011–3014.

(77)   Khan, S.; Gopakumar, G.; Thiel, W.; Alcarazo, M. Stabilization of a Two-Coordinate [GeCl]$^+$ Cation by Simultaneous σ and π Donation from a Monodentate Carbodiphosphorane. *Angewandte Chemie International Edition* **2013**, *52*, 5644–5647.

(78)   Pu, L.; Phillips, A. D.; Richards, A. F.; Stender, M.; Simons, R. S.; Olmstead, M. M.; Power, P. P. Germanium and Tin Analogues of Alkynes and Their Reduction Products. *J Am Chem Soc* **2003**, *125*, 11626–11636.

(79)   Endo, Y.; Songkram, C.; Ohta, K.; Kaszynski, P.; Yamaguchi, K. Distorted Benzene Bearing Two Bulky Substituents on Adjacent Positions: Structure of 1,2-Bis(1,2-Dicarba-Closo-Dodecaboran-1-Yl)Benzene. *Tetrahedron Lett* **2005**, *46*, 699–702.

(80)   Endo, Y.; Songkram, C.; Ohta, K.; Yamaguchi, K. Synthesis of Distorted Molecules Based on Spatial Control with Icosahedral Carboranes. *J Organomet Chem* **2005**, *690*, 2750–2756.

(81)   Harder, R. A.; Hugh MacBride, J. A.; Rivers, G. P.; Yufit, D. S.; Goeta, A. E.; Howard, J. A. K.; Wade, K.; Fox, M. A. Studies on Bis(1′-Ortho-Carboranyl)Benzenes and Bis(1′-Ortho-Carboranyl)Biphenyls. *Tetrahedron* **2014**, *70*, 5182–5189.

(82)   Wrackmeyer, B. 119Sn-NMR Parameters; 1985; pp 73–186.

(83)   Otera, J. 119Sn Chemical Shifts in Five- and Six-Coordinate Organotin Chelates. *J Organomet Chem* **1981**, *221*, 57–61.

(84)   Mitchell, T. N. Carbon-13 NMR Investigations on Organotin Compounds. *J Organomet Chem* **1973**, *59*, 189–197.

(85)   Wrackmeyer, B. Long-Range Nuclear Spin-Spin Coupling between [11]B and ^{13}C, [29]Si or [119]Sn: A Promising Tool for Structural Assignment. *Polyhedron* **1986**, *5*, 1709–1721.

(86)   Abragam, A. *The Principles of Nuclear Magnetism*; Oxford University Press: Oxford, 1961.

(87)   Suzuki, M.; Kubo, R. Theoretical Calculation of N.M.R. Spectral Line Shapes. *Mol Phys* **1964**, *7*, 201–209.

(88)   Eichler, B. E.; Power, P. P. Characterization of the Sterically Encumbered Terphenyl-Substituted Species 2,6-Trip$_2$H$_3$C$_6$Šn−Sn(Me)$_2$C$_6$H$_3$-2,6-Trip$_2$, an Unsymmetric, Group 14 Element, Methylmethylene, Valence Isomer of an Alkene, Its Related Lithium Derivative 2,6-Trip$_2$H$_3$C$_6$(Me)$_2$Sn−Sn(Li)(Me)C$_6$H$_3$-2,6-Trip$_2$, and the Monomer Sn(t-Bu)C$_6$H$_3$-2,6-Trip$_2$ (Trip = C$_6$H$_2$-2,4,6-i-Pr$_3$). *Inorg Chem* **2000**, *39*, 5444–5449.

(89)   Kalsi, P. S. *Spectroscopy of Organic Compounds*; New age international, 2007.

CHAPTER 5

5.6 SUPPLEMENTARY INFORMATION

Table of Contents

X-ray Crystallography

Crystals of **1**, **2**, and **3** were removed from a Schlenk flask under a stream of nitrogen and immediately covered with a layer of hydrocarbon oil. A suitable crystal was selected, attached to a glass fiber on a copper pin and quickly placed in the cold N_2 stream on the diffractometer. Data was collected at 100 K on a Bruker APEX DUO diffractometer with Mo Kα radiation ($\lambda = 0.71073$ Å). Absorption corrections were applied using SADABS.[S1] The crystal structures were solved by direct methods and refined by full matrix least-squares procedures in SHELXTL.[S2] All non-H atoms were refined anisotropically.

Table S1. Selected X-ray Crystallographic data for **1-3**.

|	1	2	3
Formula	$C_{17}H_{58}B_{40}Cl_2O_2Sn_2$	$C_{10}H_{44}B_{40}Cl_4K_2Sn_2$	$C_{16}H_{50}B_{40}$
Fw	1035.31	1054.23	674.96
Color, habit	Colorless plate	Colorless shard	Yellow plate
Space group	$P\bar{1}$	$P2_1$	$C2/c$
A, å	11.86820(10)	12.7653(3)	31.509(4)
B, å	13.8376(2)	12.7550(3)	12.6857(17)
C, å	14.7426(2)	14.8445(4)	10.2461(13)
A, °	101.2593(7)	90	90
B, °	98.6642(6)	114.5093(11)	94.241(3)
Γ, °	92.6166(8)	90	90
V, å³	2340.40(5)	2199.22(10)	4084.3(9)
Z	2	2	4
Crystal size, mm³	0.219 x 0.179 x 0.080	0.464 x 0.401 x 0.280	0.410 x 0.239 x 0.118
D_{calc}, mg cm⁻³	1.469	1.592	1.098
Abs. M, mm⁻¹	9.700	1.586	0.047
2θ, °	3.098 to 69.471	1.753 to 30.753	2.593 to 25.249
R(int)	0.0330	R1 = 0.0243	0.0569
Obs. Reflns. [i>2σ(i)]	6881	13126	2642
Data/restraints/parameters	8069 / 22 / 595	13561 / 14 / 695	3705 / 14 / 369
R_1, obsd. Reflns.	0.0411	0.0255	0.0803

NMR Spectra

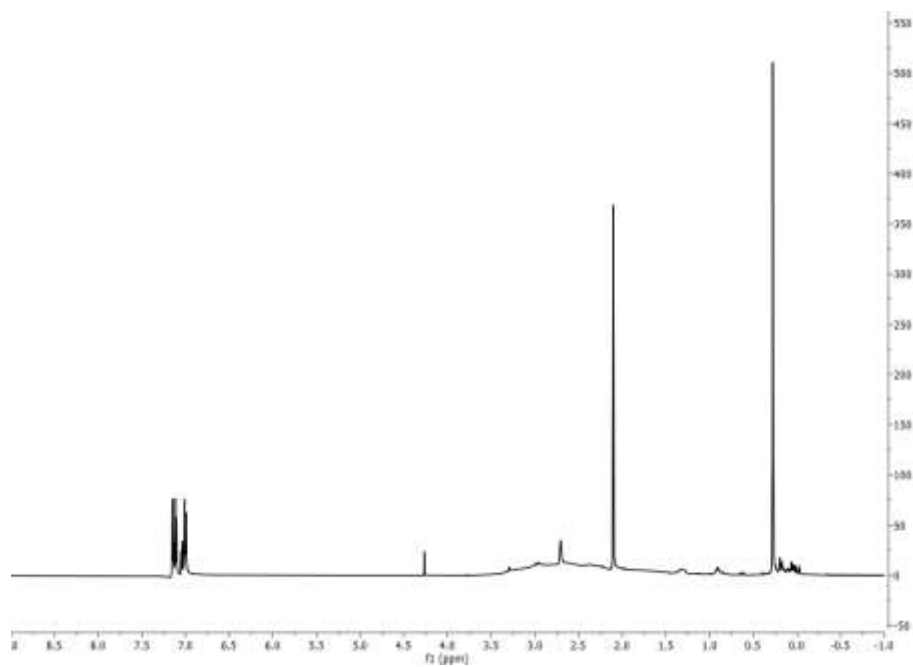**Figure S1**. ^{1}H NMR spectrum of **1** in C_6D_6 at 298 K.
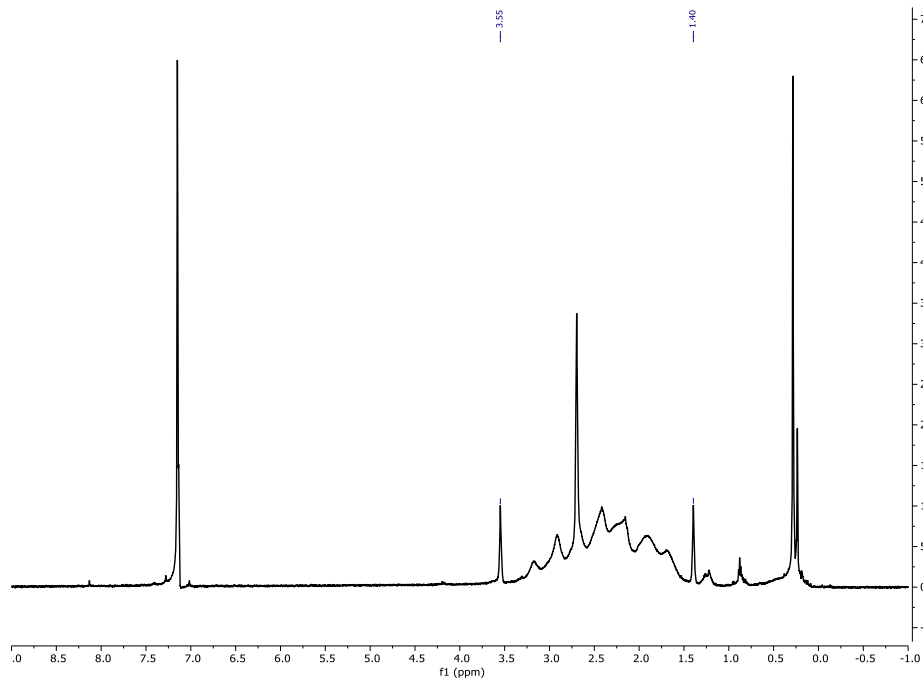
Note: δ 0.29: residual grease. δ 0.89, 1.24: residual hexanes. δ 7.15: residual benzene.

Figure S2. ^{11}B{^{1}H} NMR spectrum of **1** in C_6D_6 at 298 K.
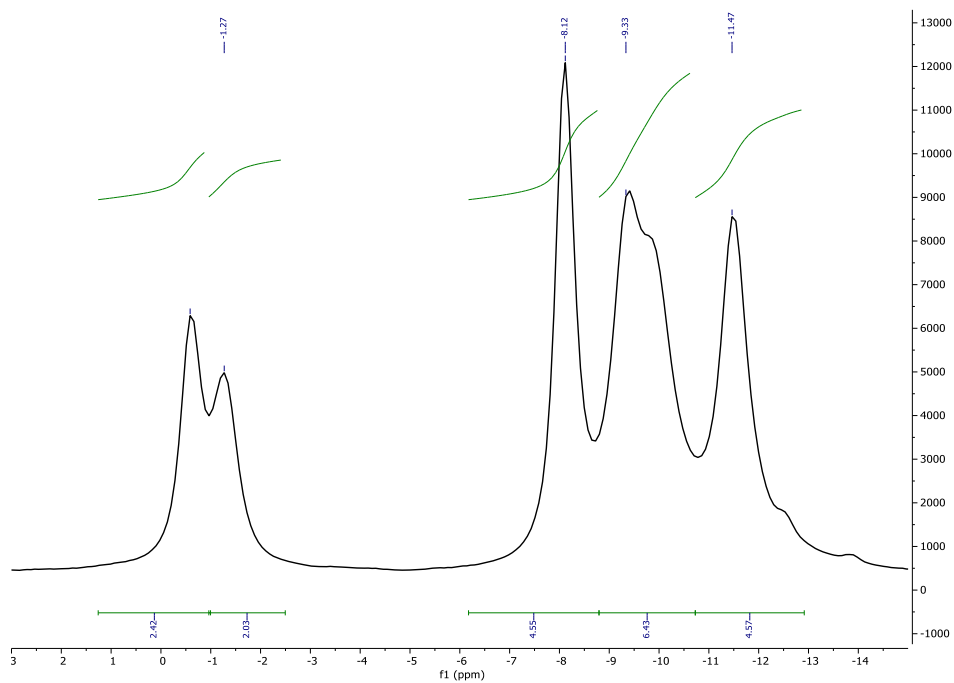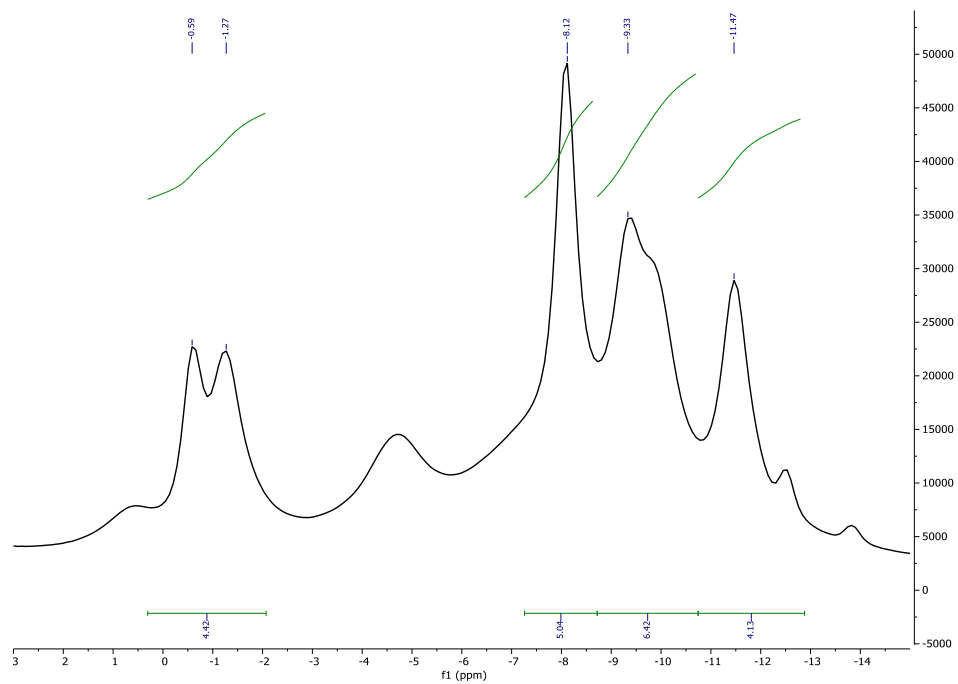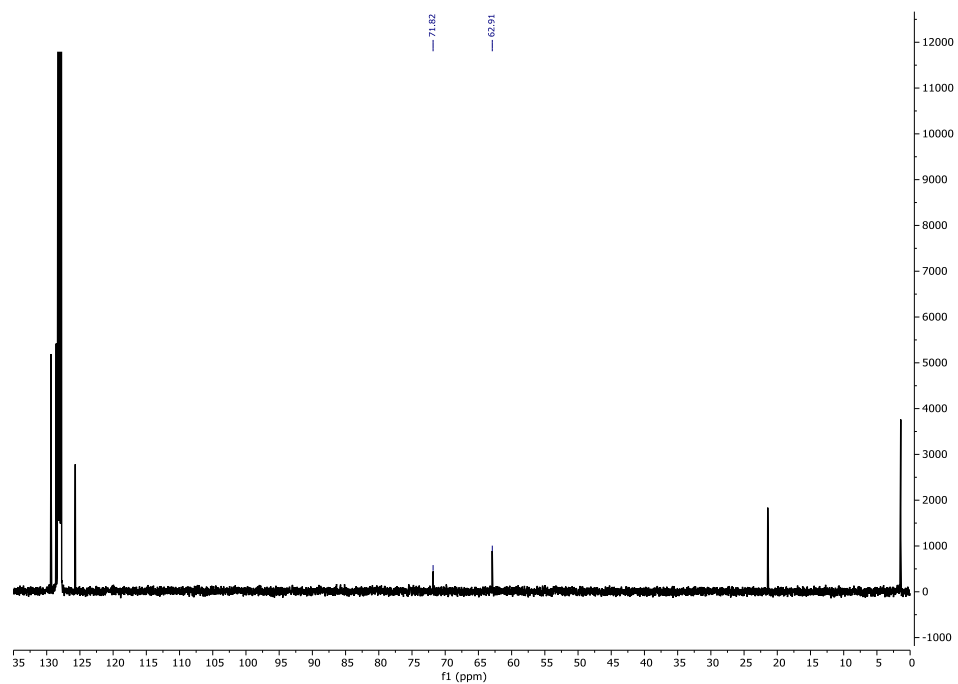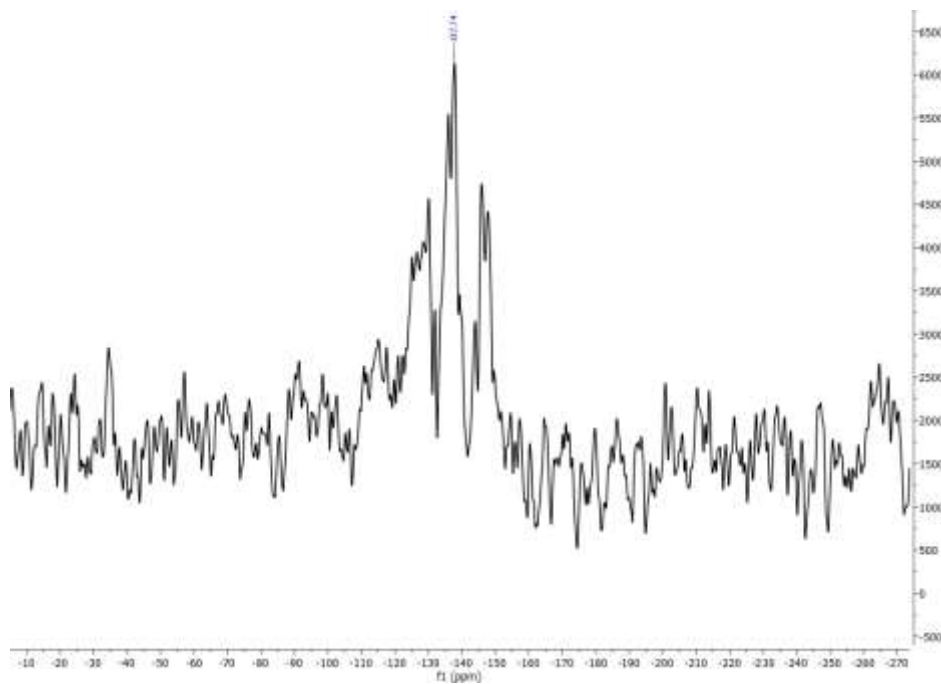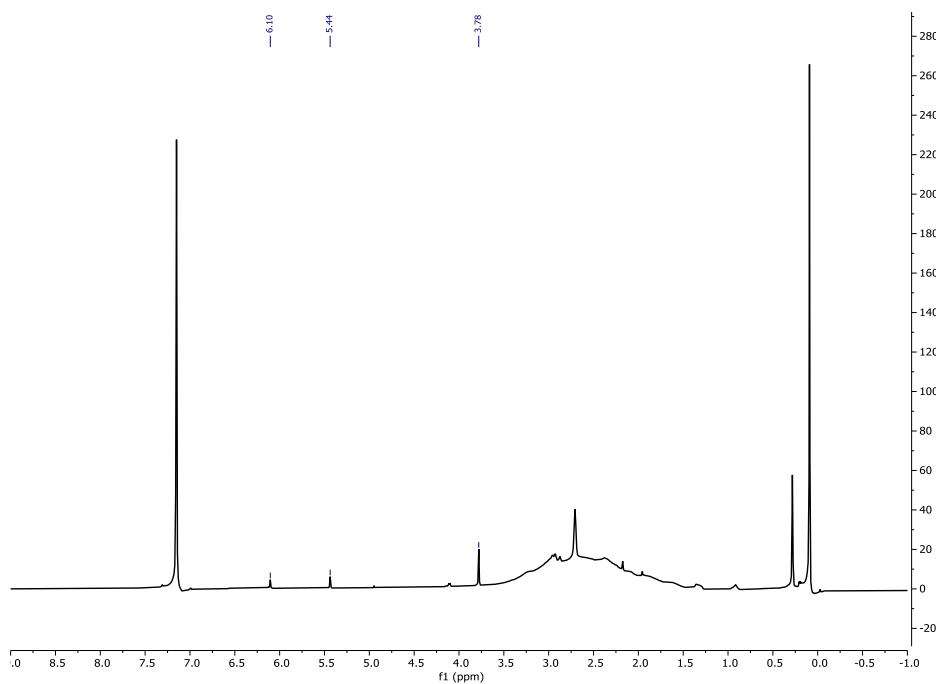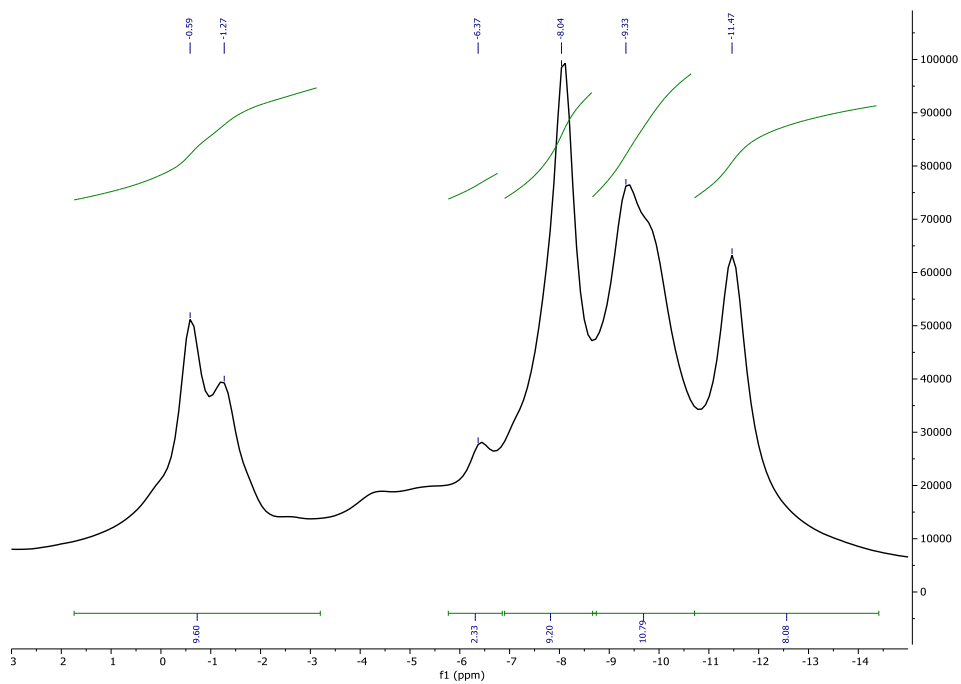
NMR Spectra

Figure S3. $^{13}C\{^1H\}$ NMR spectrum of **1** in C_6D_6 at 298 K.
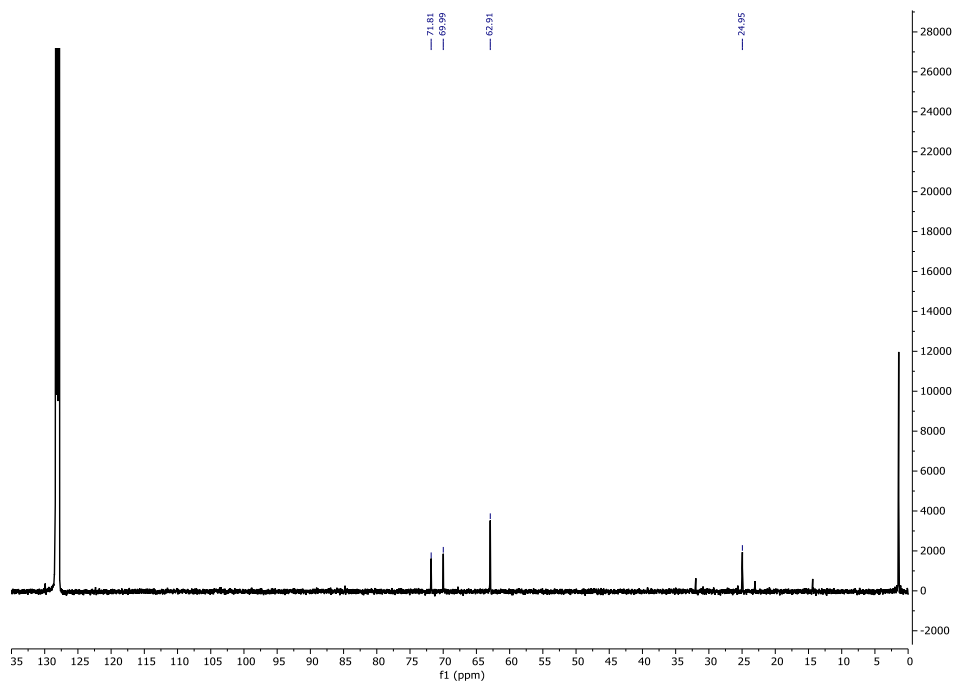
Note: δ 1.42: residual grease. δ 14.37, 23.06, 31.97: residual hexanes. δ 128.06: residual benzene.

Figure S4. ^1H NMR spectrum of **2** in C_6D_6 at 298 K.

Note: δ 0.29: residual grease. δ 2.10, 7.0 – 7.2: residual toluene. δ 4.27: residual dichloromethane.

NMR Spectra

Figure S5. $^{11}B\{^1H\}$ NMR spectrum of **2** in C_6D_6 at 298 K

Figure S6. $^{13}C\{^1H\}$ NMR spectrum of **2** in C_6D_6 at 298 K.

Note: δ 1.42: residual grease. δ 21.98, 126.23, 129.88: residual toluene.

NMR Spectra

Figure S7. ^{119}Sn$\{^1$H$\}$ NMR spectrum of **2** in C$_6$D$_6$ at 298 K.

Figure S8. ^{1}H NMR spectrum of **3** in C$_6$D$_6$ at 298 K.

Note: δ 0.09, 0.29: residual grease. δ 0.89, 1.24: residual hexanes. δ 7.15: residual benzene.

NMR Spectra

Figure S9. $^{11}B\{^1H\}$ NMR spectrum of **3** in C_6D_6 at 298 K.

Figure S10. $^{13}C\{^1H\}$ NMR spectrum of **3** in C_6D_6 at 298 K

Note: δ 1.42: residual grease. δ 128.06: residual benzene.

CHAPTER 5
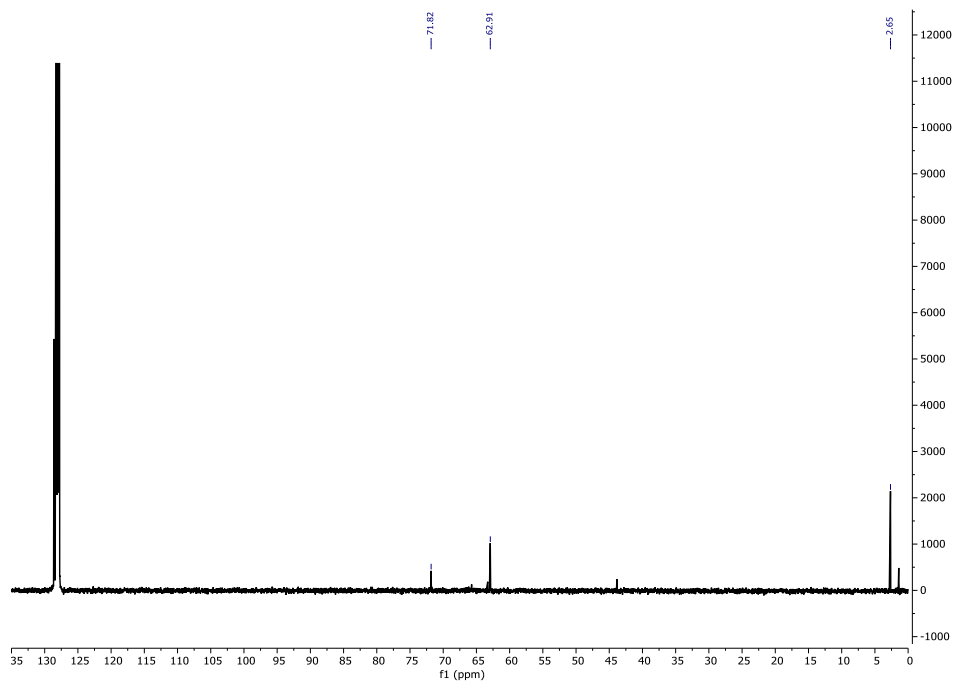
UV-vis Spectra

Figure S11. UV-vis spectrum of **1** in toluene at 298 K.

$(\mathbf{bc})Sn \cdot THF$, 4.20×10^{-4} µM
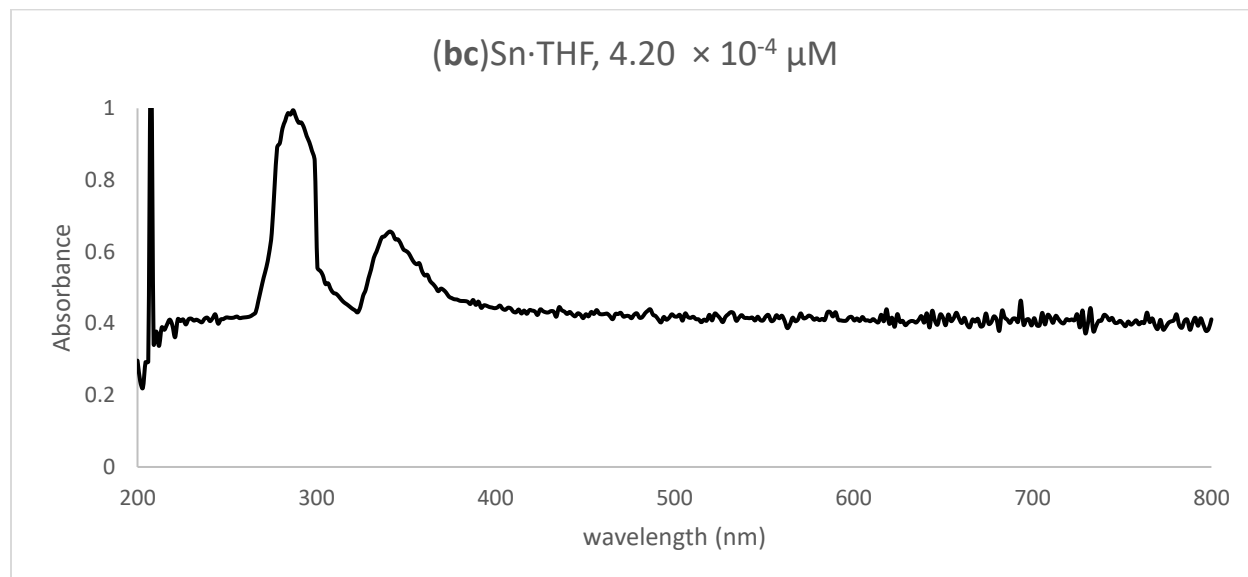
Figure S12. UV-vis spectrum of **2** in toluene at 298 K.

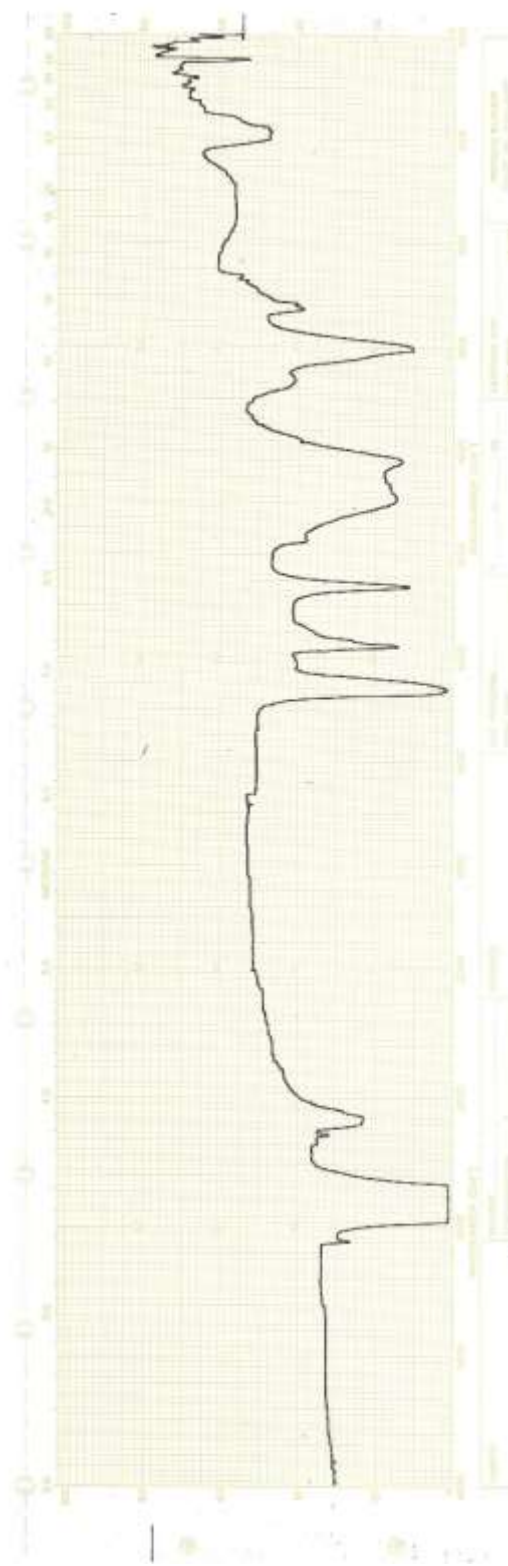$K_2[(\mathbf{bc})Sn]_2$, 5.95×10^{-4} µM
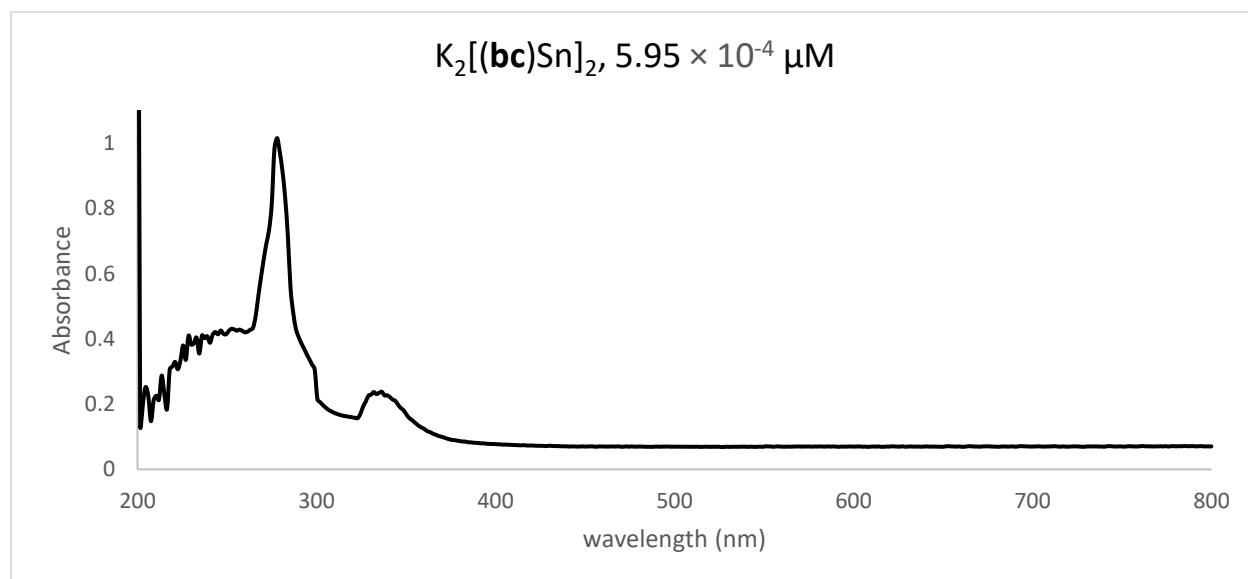
UV-vis Spectra
Figure S13. UV-vis spectra of **3** in toluene at 298 K.
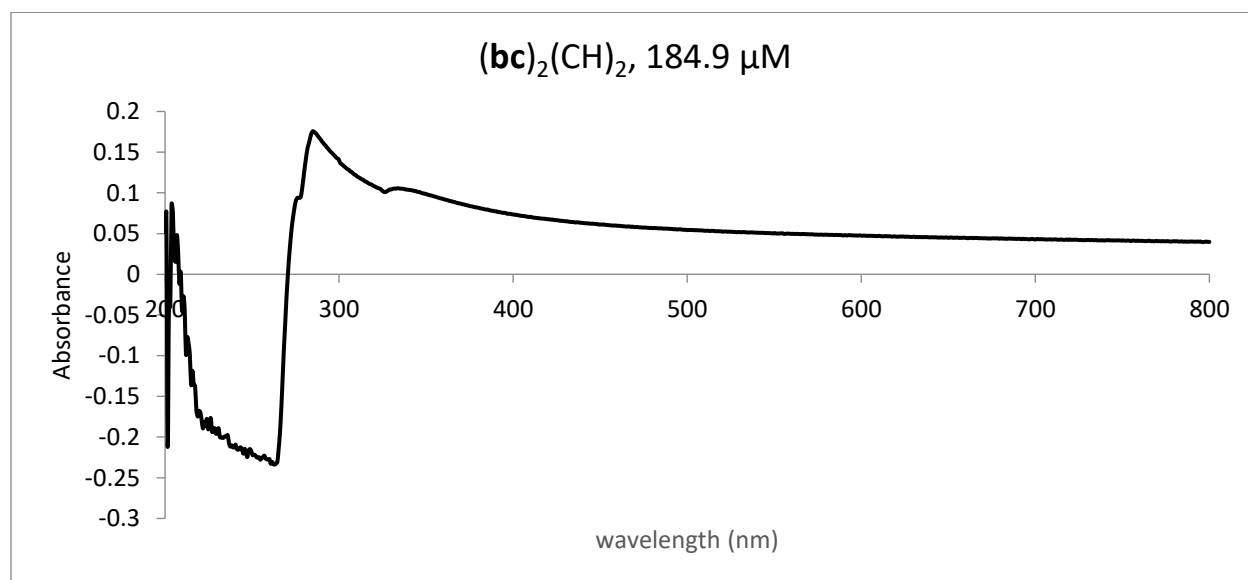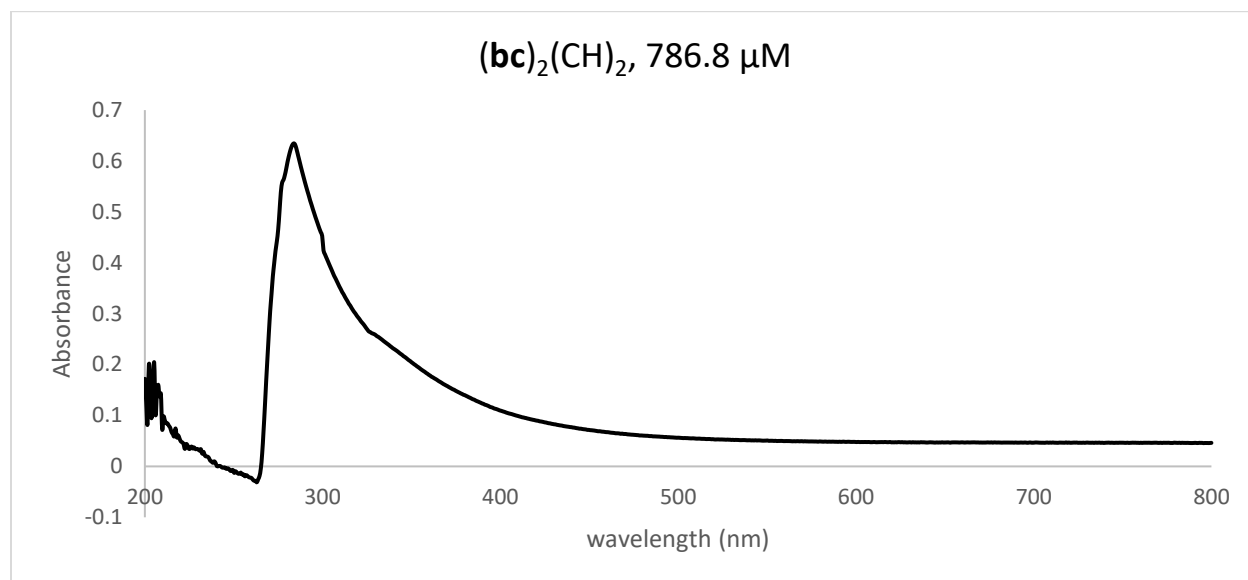
Note: A more dilute spectrum (bottom) is provided to clearly display the shoulder at 334 nm.
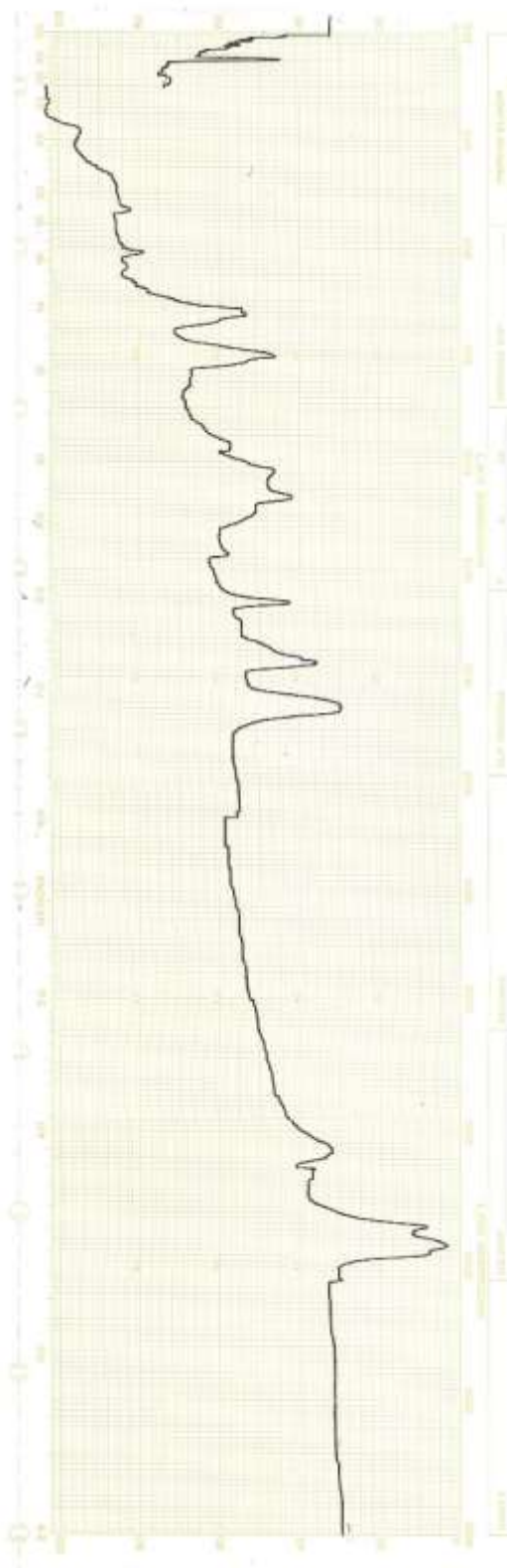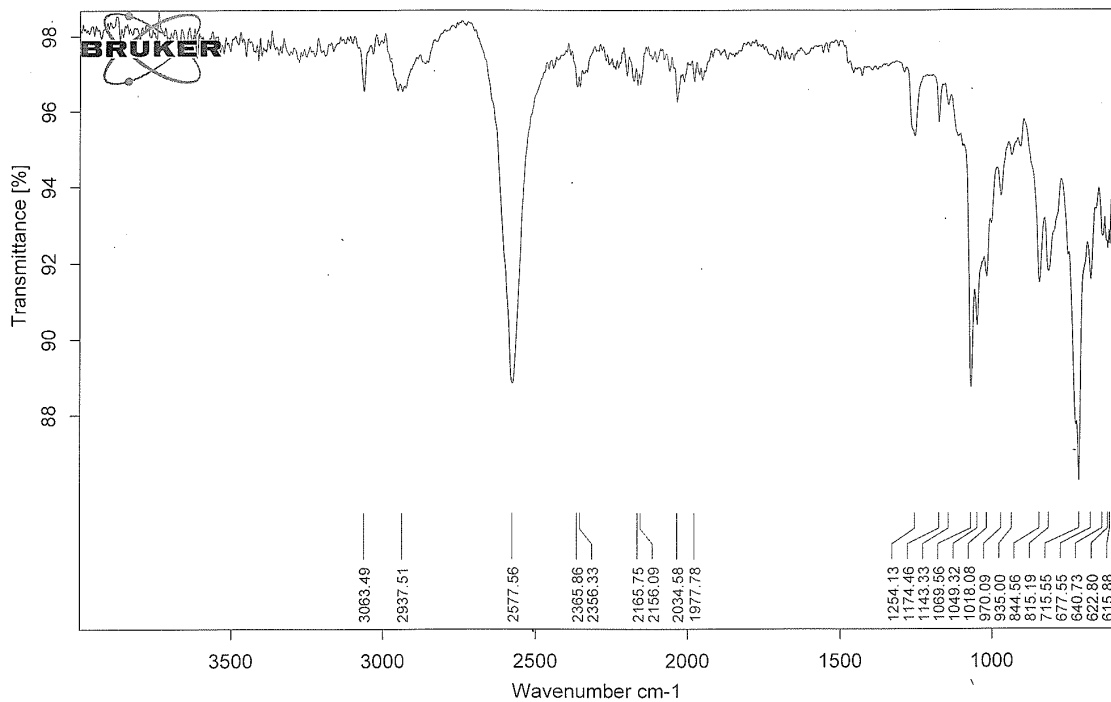
IR spectra

Figure S14. Infrared spectrum of **1**.

IR spectra
Figure S15. Infrared spectrum of **2**

IR spectra

Figure S16. Infrared spectrum of **3**

SI References

S1 Bruker, Bruker AXS Inc., Madison, Wisconsin, USA, **2001**

S2 G. M. Sheldrick, Acta Cryst. A 2015, 71, 3-8.

S3 Dolomanov, O. V.; Bourhis, L. J.; Gildea, R. J.; Howard, J. A. K.; Puschmann, H.; *OLEX2*: A complete structure solution, refinement and analysis program. J. Appl. Cryst, **2009**, *42*, 339-341.